

A new approach to analyzing solar coronal spectra and updated collisional ionization equilibrium calculations. II. Updated ionization rate coefficients

P. Bryans,¹ E. Landi,² and D. W. Savin¹

ABSTRACT

We have reanalyzed SUMER observations of a parcel of coronal gas using new collisional ionization equilibrium (CIE) calculations. These improved CIE fractional abundances were calculated using state-of-the-art electron-ion recombination data for K-shell, L-shell, Na-like, and Mg-like ions of all elements from H through Zn and, additionally, Al- through Ar-like ions of Fe. They also incorporate the latest recommended electron impact ionization data for all ions of H through Zn. Improved CIE calculations based on these recombination and ionization data are presented here. We have also developed a new systematic method for determining the average emission measure (EM) and electron temperature (T_e) of an isothermal plasma. With our new CIE data and our new approach for determining average EM and T_e , we have reanalyzed SUMER observations of the solar corona. We have compared our results with those of previous studies and found some significant differences for the derived EM and T_e . We have also calculated the enhancement of coronal elemental abundances compared to their photospheric abundances, using the SUMER observations themselves to determine the abundance enhancement factor for each of the emitting elements. Our observationally derived first ionization potential (FIP) factors are in reasonable agreement with the theoretical model of Laming (2008).

Subject headings: atomic data — atomic processes — plasmas — Sun: corona — Sun: UV radiation

1. Introduction

Investigating the dynamics of the solar corona is crucial if one is to understand fundamental solar and heliospheric physics. The corona also greatly influences the Sun-Earth

¹Columbia Astrophysics Laboratory, Columbia University, New York, NY 10027

²US Naval Research Laboratory, Space Science Division, 4555 Overlook Avenue, SW, Code 7600A, Washington, DC 20375

interaction, as it is from here that the solar wind originates. Explosive events in the corona can deposit up to 2×10^{16} g of ionized particles into the solar wind (Hundhausen 1993). These can have a profound effect on the Earth’s magnetosphere and ionosphere. Hence the investigation of the corona is of obvious importance.

Over the years there has been a significant amount of research invested in developing our understanding of the corona (reviewed by Aschwanden 2004 and Foukal 2004). However, gaps remain in our understanding of some of the most fundamental processes taking place in the corona. For example, the so-called coronal heating problem remains unsolved (Gudiksen & Norlund 2005; Klimchuk 2006) and we are still unable to explain the onset processes that cause solar flares and coronal mass ejections (Forbes 2000; Priest & Forbes 2002).

One of the most powerful tools for understanding the properties of the solar corona is spectroscopy (Tandberg-Hanssen & Emslie 1988; Foukal 2004). Analyzing the spectral emission of the corona can give the temperature and density of the plasma, as well as information on the complex plasma structures common in this region of the Sun’s atmosphere. One common approach to this end is to calculate the emission measure (*EM*) of the gas (e.g., Raymond & Doyle 1981).

The *EM* technique is particularly useful for studying the properties of the upper solar atmosphere. In this region, conditions are such that the plasma can often be described as low-density and in steady-state and the emitting region as constant in density and temperature. These relatively simple conditions allow one to neglect density effects and to assume all emission is from an isothermal plasma. For example, Landi et al. (2002) compared off-disk spectral observations of the solar corona with predictions from the CHIANTI version 3 atomic database (Dere et al. 1997, 2001). Landi et al. (2002) calculated the *EM* of the plasma based on the observed intensities using the atomic data assembled together in CHIANTI. From this, they also infer the electron temperature (T_e) of the emitting plasma. However, the power of this spectroscopic diagnostic can be limited by our understanding of the underlying atomic physics that produce the observed spectrum.

Reliable *EM* calculations require accurate fractional abundances for the ionization stages of the elements present in the plasma. For a plasma in collisional ionization equilibrium (CIE; sometimes also called coronal equilibrium), the atomic data needed for such a spectral analysis includes rate coefficients for electron-ion recombination and electron-impact ionization. These data directly affect the calculated ionic fractional abundances of the gas. The fractional abundances, in turn, are used to determine the *EM*. Hence the reliability of the CIE calculations is critical.

The recommended CIE calculations at the time of the work by Landi et al. (2002) were those of Mazzotta et al. (1998). Recently, however, state-of-the-art electron-ion recombination data have been published for K-shell, L-shell, and Na-like ions of all elements from H

through Zn (Badnell et al. 2003; Badnell 2006a,b,c; Gu 2003a,b, 2004). Based on these new recombination data, a significant update of the recommended CIE fractional abundances was published recently by Bryans et al. (2006, Paper I in this series). Since then additional recombination data have been published for Mg-like ions of H through Zn (Altun et al. 2007) and Al- through Ar-like ions of Fe (Badnell 2006d,e). Electron impact ionization (EII) data have also been updated recently by Suno & Kato (2006), Dere (2007), and Mattioli et al. (2007). Of these three, the recommended EII data of Dere (2007), which we adopt, provide the only complete available set of rate coefficients for all ions of H through Zn. Here we have updated the results of Bryans et al. (2006) using these new recombination and ionization data. One of the motivations behind this paper is to investigate the effects of the recent improvements in CIE calculations on solar observations.

Since the Landi et al. (2002) paper there have been other improved atomic data (e.g., the improvement of the model for N-like ions). These have been made available in a more recent CHIANTI release—version 5.2 (Landi et al. 2006). It is this version we use here.

We also investigate here the observed relative elemental abundances and the first ionization potential (FIP) effect. The FIP effect is the discrepancy between the coronal and photospheric elemental abundances, possibly explained by the ponderomotive force induced by the propagation of Alfvén waves through the chromosphere (Laming 2004, 2008). Elements with a FIP of below ~ 10 eV appear to have a coronal abundance that is enhanced by a factor of a few over their photospheric abundance (see, e.g., the review by Feldman & Laming 2000). Often, the FIP effect is accounted for by multiplying the abundance of the low-FIP elements by a single scaling factor (such as 3.5 as was done in Landi et al. 2002). In the present work, we investigate the reliability of this approach by quantifying the FIP effect based on the observations themselves. We determine the EM from the high-FIP element Ar and then scale the elemental abundances of the moderate- and low-FIP elements so that their derived EMs match that of Ar. We compare our derived abundances with those of a previous analysis of the same observation (Feldman et al. 1998) as well as with theoretical predictions (Laming 2008).

An important aspect of the present paper is the development of a sound mathematical method of determining the average EM and T_e of an isothermal plasma. Previous studies have done this in a less rigorous manner. Landi et al. (2002), for example, evaluate plots of EM versus T_e curves and give a “by eye” estimate of the average value of the EM and T_e and their associated errors. This method allows human bias to become important when deciding which curve crossings to include in the selection. In addition, it is unclear to what this “average” actually corresponds mathematically. The fact that the analysis is performed on graphs with logarithmic axes suggests that by-eye average is closer to the geometric mean than the arithmetic mean. Finally, no account is taken of the reliability of the atomic data used to calculate fractional abundances. Bryans et al. (2006) showed that CIE results are unreliable at temperatures where the ionic fractional abundances are less than 1%. Previous

studies have failed to account for this when using the CIE data in the *EM* analysis.

Taking the above four paragraphs into account, we have reanalyzed the observations of Landi et al. (2002). The rest of this paper is organized as follows: In Sec. 2 we give a description of the observing sequence, the observed lines and their categorizations by Landi et al. (2002). Section 3 defines the *EM* and explains the method we use to determine the plasma temperature from the observed line intensities. In Sec. 4 we review the recent developments in the understanding of dielectronic and radiative recombination and electron impact ionization, and the subsequent improvement in CIE calculations. We also present updated tables of these CIE calculations, which supersede those of Bryans et al. (2006). In Sec. 5 we describe our new approach for determining the *EM* and temperature of an isothermal plasma based on the observed spectral line intensities. Section 6 discusses our method of determining the elemental abundance enhancement factors due to the FIP effect. In Sec. 7 we present the results of our *EM* calculations for each of the categorizations introduced by Landi et al. (2002). Section 8 discusses the consequences of these results, in particular highlighting discrepancies between the results of this paper and those of Landi et al. (2002). In Sec. 9 we propose future observations needed to address some of the remaining issues raised by our results here. Concluding remarks are given in Sec. 10.

2. Observations

The spectrum analyzed by Landi et al. (2002), and revisited here, was detected using the Solar Ultraviolet Measurements of Emitted Radiation spectrometer (SUMER; Wilhelm et al. 1995) onboard the Solar and Heliospheric Observatory (SOHO). The observation spans over 5 hours, from 21:16 UT on 1996 November 21 to 02:28 UT November 22, and was collected in 61 spectral sections. The observing slit imaged at a height h of $1.03R_{\odot} \lesssim h \lesssim 1.3R_{\odot}$ above the western limb. The resulting spectrum covers the entire SUMER spectral range of 660–1500 Å. Landi et al. (2002) give a full description of the observation sequence and data reduction.

Table 1 lists the coronal lines identified in the spectrum and their corresponding transitions (reproduced from Landi et al. 2002). Known typos in the line assignment labels of Landi et al. (2002) have been corrected; these do not affect their reported results. Landi et al. estimate uncertainties on the extracted line intensities of 25–30%. Twelve of the emission lines observed in this run are omitted from the table here due to their being blended with other emission lines or having uncertain intensities. The remaining spectral lines are split into three distinct groups, labeled in the first column of Table 1 as:

I. Forbidden transitions within the ground configuration.

Ia. Non-N-like transitions.

Ib. N-like transitions.

II. Transitions between the ground and the first excited configuration:

- IIa. Allowed $2s-2p$ transitions in the Li-like isoelectronic sequence and allowed $3s-3p$ transitions in the Na-like isoelectronic sequence.
- IIb. Intercombination transitions in the Be-, B-, C-, and Mg-like isoelectronic sequences.

III. Transitions between the first and second excited configuration.

Within each group and subgroup we have derived the average T_e and EM . Categorizing the transitions in this way helps us to better identify any trends in the EM with respect to the transition type. Group I transitions have been further divided into non-N-like and N-like transitions. This separation was originally proposed by Landi et al. (2002) due to the poor agreement they found for the T_e derived within each of these transition types. This is discussed further in Secs. 6 and 8. The subdivision of transition Group II is to allow us to investigate a longstanding discrepancy between EMs derived using Li- and Na-like ions and those derived using other isoelectronic sequences (e.g., Dupree 1972; Feldman et al. 1998; Landi et al. 2002). We also discuss this further in Secs. 6 and 8.

3. Method of Calculating Temperature and Emission Measure

The intensity of an observed spectral line due to a transition from level j to level i in element X of ionization state $+m$ can be written as

$$I_{ji} = \frac{1}{4\pi d^2} \int_V G_{ji}(T_e, n_e) n_e^2 dV \quad (1)$$

where n_e is the electron density, V is the emitting volume along the line of sight, and d is the distance to the source. $G_{ji}(T_e, n_e)$ is the contribution function, which is defined as

$$G_{ji}(T_e, n_e) = \frac{n_j(X^{+m})}{n(X^{+m})} \frac{n(X^{+m})}{n(X)} \frac{n(X)}{n(H)} \frac{n(H)}{n_e} \frac{A_{ji}}{n_e} \quad (2)$$

where $n_j(X^{+m})/n(X^{+m})$ is the population of upper level j relative to all levels in X^{+m} , $n(X^{+m})/n(X)$ is the fractional abundance of ionization stage $+m$ relative to the sum of all ionization stages of X, $n(X)/n(H)$ is the abundance of element X relative to hydrogen, and $n(H)/n_e$ is the abundance of hydrogen relative to the electron density. A_{ji} is the spontaneous emission coefficient for the transition.

For the observation analyzed here, the emitting plasma was found to be isothermal by Feldman et al. (1999) and Landi et al. (2002). For the moment we assume this to be

correct but we revisit the validity of the isothermal assumption in Sec. 8.4. One can also make the assumption that the region emitting the observed line intensities is at a constant density. While the line-of-sight of the observation covers plasma where densities vary by orders of magnitude, the emission is dominated by a region with a small range of densities around the peak density. Only those emission lines that have a strong density sensitivity in this range will be affected by the density gradient (Lang et al. 1990). Feldman et al. (1999) inferred a density of $1.8 \times 10^8 \text{ cm}^{-3}$ for this observation. A density dependent study of the 74 lines observed here is beyond the scope of our paper. Here we use the inferred density of Feldman et al. (1999) in our analysis.

If we now assume that all the emission comes from the same parcel of gas of nearly constant temperature, T_c , and density, we can approximate

$$I_{ji} = \frac{G_{ji}(T_c, n_e)}{4\pi d^2} EM \quad (3)$$

where the emission measure EM is defined as

$$EM = \int n_e^2 dV \quad (4)$$

and can be evaluated from the observed line intensity as

$$EM = 4\pi d^2 \frac{I_{ji}}{G_{ji}(T_c, n_e)}. \quad (5)$$

This has the same value for all transitions if the constant temperature and density assumption is correct, which we label EM_c . Thus, from the observed line intensities, I_{ji} , and using accurate data for $G_{ji}(T_e, n_e)$, one can calculate the emission measure and electron temperature of the emitting region. This is done by plotting the EM against T_e . The resulting curves for each observed line should intersect at a common point yielding $[T_c, EM_c]$. But this depends on the assumption of constant temperature and density being correct and on the accuracy of the underlying atomic data. Here, one of the issues we are investigating is the effect on solar coronal observations of the newly calculated fractional abundances

$$f^m = \frac{n(\text{X}^{+m})}{n(\text{X})}. \quad (6)$$

The units used throughout this paper for EM and T_e are cm^{-3} and K, respectively. For ease of reading, we typically drop these units below.

4. Improved collisional ionization equilibrium (CIE) calculations

The plasma conditions of the solar upper atmosphere are often described as being optically-thin, low-density, dust-free, and in steady-state or quasi-steady-state. Under these

conditions the effects of any radiation field can be ignored, three-body collisions are unimportant, and the ionization balance of the gas is time-independent. This is commonly called CIE or coronal equilibrium. These conditions are not always the case in the solar upper atmosphere in the event of impulsive heating events but, given the inactivity and low density of the plasma analyzed here, they sufficiently describe the observed conditions. For a thorough discussion of plasma conditions where one must treat the time scales and density effects more carefully, we direct the reader to Summers et al. (2006).

In CIE, recombination is due primarily to dielectronic recombination (DR) and radiative recombination (RR). At the temperature of peak formation in CIE, DR dominates over RR for most ions. Ionization is primarily a result of electron impact ionization (EII). At temperatures low enough for both atoms and ions to exist, charge transfer (CT) can be both an important recombination and ionization process (Arnaud & Rothenflug 1985; Kingdon & Ferland 1996). CT is not expected to be important at solar coronal temperatures and is not included in the work of Mazzotta et al. (1998), Bryans et al. (2006), or the present paper. Considering all the ions and levels that need to be taken into account, it is clear that vast quantities of data are needed. Generating them to the accuracy required pushes atomic theoretical and experimental methods to the edge of what is currently achievable and often beyond. For this reason, the CIE data used by the solar physics and astrophysics communities have gone through numerous updates over the years as more reliable atomic data have become available.

4.1. Recombination rate coefficients

The DR and RR rate coefficients used to determine the CIE fractional abundances utilized by Landi et al. (2002) were those recommended by Mazzotta et al. (1998). However, there has been a significant improvement in the recombination rate coefficients since then. Badnell et al. (2003) and Badnell (2006a,b,c) have calculated DR and RR rate coefficients for all ionization stages from bare through Na-like for all elements from H through Zn and Gu (2003a,b, 2004) for a subset of these elements. The methods of Badnell and Gu are of comparable sophistication and their DR results for a given ion agree with one another typically to better than 35% at the electron temperatures where the CIE fractional abundance of that ion is $\geq 1\%$. The RR rate coefficients are in even better agreement, typically within 10% over this temperature range. These differences for the DR and RR rate coefficients do not appear to be systematic in any way (Bryans et al. 2006). For both DR and RR outside this temperature range, agreement between these two state-of-the-art theories can become significantly worse. The DR calculations have also been compared to experimental measurements, where they exist, and found to be in agreement to within 35% in the temperature range where the ion forms in CIE. For a fuller discussion of the agreement between recent theories and the agreement between theory and experiment, we direct the reader to

Bryans et al. (2006).

4.2. Electron impact ionization rate coefficients

There have also been recent attempts to improve the state of the EII rate coefficients used in CIE calculations. The most complete of these studies is that of Dere (2007), who produced recommended rate coefficients for all ionization stages of the elements H through Zn. These data are based on a combination of laboratory experiments and theoretical calculations. In addition, there have been works by Suno & Kato (2006) and Mattioli et al. (2007) that also address the issue of updating the EII database. These works are less complete than that of Dere (2007). Suno & Kato (2006) provides EII cross sections for all ionization stages of C. Mattioli et al. (2007) provides EII cross sections for all ionization stages of H through O plus Ne and a selection of other ions up to Ge.

Between these recent compilations there remain sizable differences in the EII rate coefficients for certain elements, often in the temperature range where an ion forms in CIE. For the ions important to the present work, differences between recent recommended rate coefficients of up to 50% are seen. Larger differences, of up to a factor of ~ 4 , are found for other ions not observed in this SUMER observation. In short, we do not see the uniform agreement between recommended sets of EII data as we do for the state-of-the-art DR and RR calculations.

Despite these outstanding issues regarding the accuracy of the various EII databases, we have used the compilation of Dere (2007) to calculate fractional CIE abundances. Of the recent EII compilations, the Dere database offers the most complete selection of rate coefficients. However, given the large differences between the Dere (2007) and Mattioli et al. (2007) results, we believe that further analysis of the EII database is required to resolve these differences.

4.3. Updated CIE calculations

The new recombination data of Badnell et al. (2003) and Badnell (2006a,b,c) motivated Bryans et al. (2006) to calculate new CIE fractional abundances. Their results show large differences from the Mazzotta et al. (1998) data for certain elements. Here we revise the work of Bryans et al. (2006) to include these newly recommended EII rate coefficients for all elements from H through Zn and some further updates to the DR and RR rate coefficients for selected ions.

We calculate CIE fractional abundances using the EII data of Dere (2007) for all ions of the elements H through Zn. We also include some corrections for Ca-like ions (K. P.

Dere 2007, private communication). The DR and RR rate coefficients used here are those of Bryans et al. (2006) but updated to include recent corrections to the fitting of some of the rate coefficients (Badnell 2006b). We also include recent DR work for Mg-like ions of H through Zn and for Al- through Ar-like ions of Fe (Altun et al. 2007; Badnell 2006b,d,e). The DR and RR data for all other ions are those of Mazzotta et al. (1998).

Here we provide electronic tables of the CIE fractional abundances for all elements from H through Zn calculated using these data (Tables 2–31). These tabulations are provided for a T_e range of 10^4 – 10^9 K. For ease of comparison with previous CIE fractional abundance calculations we present figures showing the present results along with those of Mazzotta et al. (1998) in Figs. 1–30, and the present results along with those of Bryans et al. (2006) in Figs. 31–60.

5. A new approach to derive average emission measures and temperatures

Using the method described in Sec. 3, the assumption of constant temperature and density, and our updated CIE results, we can calculate the EM curve for each of the observed spectral lines listed in Table 1. Due to oversimplifications of the plasma model, uncertainties in the observations, and errors in the atomic data, there is no common intersection of all EM curves at a single $[T_c, EM_c]$. So one must calculate the most likely EM and T_e of the plasma based on the range of values where the EM curves cross one another. To determine these values we have developed a mathematically more rigorous approach than has been used in the past for isothermal plasmas. Here we use the emission lines from Si to illustrate this new method. We calculate the EM curves using a constant electron density of 1.8×10^8 cm $^{-3}$ as was reported by Feldman et al. (1999) for the same source region.

Step 1 of our approach is to take the mean of all crossing points of the EM curves for a given group of lines. This can be seen in the left panel of Fig. 61. In this panel we have marked with an asterisk every crossing point of the EM curves shown.

The EM vs. T_e curves vary more slowly in log-log space than in linear space. Also, because of the shape of the curves, any outlying crossings are far more likely to occur at a higher EM than at a lower EM . Thus, those crossings that fall far from the preponderance skew the average always towards higher values of the EM . To avoid giving undue weight to these points we calculate the mean in log space, where $\langle \log_{10} EM \rangle \leq \log_{10} \langle EM \rangle$. This is equivalent to taking the geometric mean rather than the more common arithmetic mean. The log of the geometric mean EM is given by

$$\langle \log_{10} EM \rangle = \log_{10} \left(\prod_{i=1}^n EM_i \right)^{1/n} = \frac{1}{n} \sum_{i=1}^n \log_{10} EM_i \quad (7)$$

and its standard deviation by

$$\delta \langle \log_{10} EM \rangle = \sqrt{\frac{\sum_{i=1}^n (\log_{10} EM_i - \langle \log_{10} EM \rangle)^2}{n}} \quad (8)$$

where n is the number of crossing points over which the mean is being taken and EM_i is the value of EM at each of these crossings. By a similar argument the mean and standard deviation of T_e are calculated in the same way. From here on, unless otherwise stated, when we discuss the mean and standard deviation of the EM and T_e we are referring to the geometric mean and geometric standard deviation. In Fig. 61 the mean $\log_{10} EM$ and mean $\log_{10} T_e$ are shown as dashed lines and the standard deviations by dotted lines.

Step 2 eliminates the less physically probable crossings when two EM curves cross one another more than once. For any two curves we select only the crossing point that is closest, in the log EM -log T_e plane, to the mean calculated values of the EM and T_e from Step 1. In Step 2 we also exclude some additional unphysical crossing points. In all cases where there are multiple emission lines from a single ion, the EM curves are nearly parallel. Often, these curves nearly overlap with one another and can cross in one or more places. We attribute the crossings of these lines to errors in the effective line emission rate coefficients and/or issues with the observed line intensities. For this reason, we exclude these crossings from our calculation. For Si emission lines, such crossings are seen for Si VIII, X, and XI (Fig. 61). Using this reduced set of crossings we recalculate the mean and standard deviation of the EM and temperature. This plot is shown in the middle panel of Fig. 61.

In Step 3 we further reduce the dataset by considering only EM curves in the temperature range where $f^m \geq 0.01$. The reliability of all published CIE calculations is uncertain below this fractional abundance. Bryans et al. (2006) compared the results of CIE calculations using 2 different compilations of state-of-the-art DR and RR datasets. Agreement at peak abundance was found to be within 10% and within 50% when going to temperatures where the fractional abundance is 0.01. Outside this temperature range, for values of $f^m < 0.01$, the reliability of the CIE calculations grows significantly worse.

In the right panel of Fig. 61 we show the same EM curves as in the middle panel but only for the temperature range where $f^m \geq 0.01$. It is this mean EM and T_e after Step 3 that we consider the most likely EM and T_e for a given set of emission lines. Henceforth, when discussing the results after all three steps of our analysis, we refer to the EM and T_e as coming from the Geometric mean Emission Measure (GEM) method.

6. Coronal abundance enhancement factors

Our first step in determining the coronal abundance of the observed elements is to assume that the high-FIP elements Ne and Ar have the same abundance in the corona as they do in the photosphere. This follows the approach taken by Feldman et al. (1998). Using

the photospheric abundances of Feldman & Laming (2000; see Table 32) we have calculated the geometric mean EM from emission lines of Ne and Ar using the GEM method outlined in Sec. 5, giving $\langle \log_{10} EM_{\text{high-FIP}} \rangle$.

An objective of the present paper is to investigate the apparent abundance discrepancy of Li- and Na-like ions. Previous studies, such as those of Dupree (1972), Feldman et al. (1998), and Landi et al. (2002), have found the abundance of these ions to be greater than those of ions in other isoelectronic sequences. In order that this discrepancy does not affect our calculation of the FIP factors of each element we do not include any Li- or Na-like lines in the calculations of the FIP factors detailed below.

Landi et al. (2002) also reported a difference in T_e derived from N-like and non-N-like ions within Group I. However, unlike the Li- and Na-like abundance discrepancy, this has not been reported in the literature previously. If we adopt the uniform FIP factor of 3.5 used by Landi et al. (2002) for all high-FIP N-like and non-N-like ions and implement our GEM method we find no discrepancy in the T_e derived from N-like and non-N-like ions. This is discussed in more detail in Sec. 8. For these reasons, in this section we include both N-like and non-N-like ions in our analysis.

The results of the GEM analysis of the high-FIP elements can be seen in the upper left panel of Fig. 62. The exclusion of the Li- and Na-like ions results in only a single crossing remaining after the 3 steps—due to 2 emission lines from Ar XI and Ar XII. We use the value of the EM at this point as our reference value. Restricting the temperature range to that where the fractional abundance of an ion is greater than 1% limits us to this single crossing since the 2 Ne VII EM curves are below this limit at the T_e values where they cross the EM curves of Ar XI and Ar XII. It is not ideal that we are left with only a single crossing but we believe this represents an improvement over the work of Feldman et al. (1998). There they used only a single line, whereas here we use two. Additionally, the line they selected was Li-like O VI. As we have discussed above, and will also discuss in Sec. 8, there are several reasons to treat this line with suspicion. It is also worth noting that the crossing of the Ar lines results in $\log_{10} T_e = 6.24$. This is ~ 0.1 in the dex higher than the temperature derived from the other emission lines (see later in this section and Sec. 7). However, in the absence of additional non-Li- and Na-like emission from other high-FIP elements, we consider normalizing to this crossing of Ar lines to be the best approach to analyzing this particular observation.

We next separate all other emission lines by the element responsible for the emission and, again using the GEM method, calculate the mean EM of each of the low- and moderate-FIP elements individually using the photospheric elemental abundances as our starting value, giving $\langle \log_{10} EM_X \rangle$ for each element X. For each of these low- to moderate-FIP elements, we determine an “enhancement factor” f_X for the elemental abundance that will result in the same derived EM as found for the high-FIP element Ar. From Eqns. 2 and 5 we see that

the elemental abundance,

$$f(X) = \frac{n(X)}{n(H)}, \quad (9)$$

is inversely proportional to the EM of the emitting plasma so the f_X values can be calculated as

$$\log_{10} f_X = \langle \log_{10} EM_X \rangle - \langle \log_{10} EM_{\text{high-FIP}} \rangle \quad (10)$$

where

$$f_X = \frac{f(X)_{\text{corona}}}{f(X)_{\text{photosphere}}}. \quad (11)$$

For the emission from the elements Mg, Al, Si, S, and Fe we show the EM as a function of T_e in Fig. 62 where we have used our derived coronal elemental abundances. These are subject to the 3 steps of the GEM method but in this case we only show the last step. The derived elemental abundances are given in Table 32.

From Eq. 10, we estimate the absolute error in $\log_{10} f_X$ as the quadrature sum of the standard deviations of the EM from the high-FIP elements and the EM from the individual element X, i.e.,

$$\delta \langle \log_{10} f_X \rangle = \sqrt{\delta \langle \log_{10} EM_X \rangle^2 + \delta \langle \log_{10} EM_{\text{high-FIP}} \rangle^2} \quad (12)$$

However, since only a single crossing of Ar lines is used to determine the high-FIP EM , there is no error associated with $\log_{10} EM_{\text{high-FIP}}$ and the error in $\log_{10} f_X$ reduces to $\delta \langle \log_{10} EM_X \rangle$ and is thus probably an underestimate. Given our derived errors in $\langle \log_{10} EM \rangle$ presented in Sec. 7 we estimate $\langle \log_{10} EM_{\text{high-FIP}} \rangle$ is good to $\sim \pm 0.3$ in the dex. However, due to insufficient data, we do not attempt to assign an error to $\delta \langle \log_{10} EM_{\text{high-FIP}} \rangle$. Instead, we leave the errors in the FIP factors as they are, but note that they are likely underestimates.

With the Li- and Na-like lines omitted, we are left with only 2 emission lines from Na and Ca and a single emission line from K in this observation. Both Na emission lines are from the same charge state and their associated EM curves are therefore almost parallel. The same is true for the 2 emission lines from Ca. We thus have no crossing points of the EM curves over the T_e range considered for Na, K, and Ca. Also, as discussed in Sec. 8, we believe the emission from Li-like N v and O vi ions to be from a cooler region of plasma so we do not determine an average EM from the curves crossings of these elements.

To determine the FIP factors of Na, K and Ca we use their EM values at the T_e determined from those emission lines for which we have already calculated FIP factors. This mean T_e determination is shown in Fig. 63 where emission lines of Ne, Mg, Al, Si, S, Ar, and Fe have been considered (excluding Li- and Na-like ions). This gives a value of $\log_{10} T_e = 6.13 \pm 0.06$, at which value we calculate the EM of each of the Na, K and Ca lines. (For Na and Ca, for which we have 2 emission lines, we take the average value of the 2 EM values at $\log_{10} T_e = 6.13$.) We then determine a FIP factor for each of these elements

that will give the same EM as for the high-FIP element Ar. We estimate the absolute error in $\log_{10} f_X$ of these 3 elements by calculating their EM at the values of the extremes of the errors associated with T_e , i.e., the EM at $\log_{10} T_e = 6.07$ and $\log_{10} T_e = 6.19$.

Table 32 lists the enhancement factors, which are often called FIP factors or FIP biases, for all of the elements present in the observation. We also give the resulting coronal elemental abundances. The FIP factors are also shown in Fig. 64 alongside the results of Feldman et al. (1998). Note that Figs. 61–64 show the results when using the CIE fractional abundances of the present paper. We have repeated the analysis using the Mazzotta et al. (1998) CIE fractional abundances. We do not show figures of these results, but in Table 32 we list the FIP factors and coronal abundances determined when using these older CIE data.

7. Analysis by groups

Using our derived coronal abundances we calculate the EM and T_e of each of the line categorizations given in Sec. 2. Figures 65–73 show the GEM approach as applied to each of these groups. We also give the results in Table 33 listing the geometric mean and standard deviation of the EM and T_e after each step of the GEM method.

For the Group I and II categorizations we show their individual subcategorizations as well as the groups as a whole. In the case of Group IIb, the emission lines have been further subdivided by separating out the N V and O VI lines. This is because the EM curves from these lines do not match well with the others in this group. We elaborate on the possible reasons for this in Sec. 8. When we consider Group II as a whole, these lines are also excluded.

In addition to the division by groups we calculate the mean EM and T_e from every emission line (but again excluding the Li-like N V and O VI lines). This is done both including and excluding Li- and Na-like ions with the results shown in Figs. 74 and 75, respectively, and listed in Table 33. It should be noted that this is not simply the sum of all the crossings from the individual groups. It also includes crossings between lines from different groups and results in a total of 1428 and 872 crossings (including and excluding Li- and Na-like lines, respectively).

The results of our analysis, as given in Table 33, are shown in graphical form in Fig. 76 for the variation of $\log_{10} EM$ versus group and Fig. 77 for the variation of $\log_{10} T_e$ with group. The numbers in the data points in these figures are the number of crossings that were used to determine the average value and the errors shown are $\pm\delta\langle\log_{10} EM\rangle$ of the mean. The average and standard deviation of $\log_{10} EM$ and $\log_{10} T_e$ as determined from every emission line are shown for comparison as dashed and dotted lines, respectively. We show these values with and without Li- and Na-like ions included in the EM calculation (i.e., Figs. 74 and 75, respectively). The thick lines are the average and standard deviations when Li- and Na-like

ions are included (excluding N v and O vi) and the thin are when they are excluded.

8. Discussion

8.1. Updated CIE fractional abundances

One of the aims of the present paper is to investigate the effect of our new CIE fractional abundances on the *EM* analysis. But first we look at how the updated recombination and ionization data impact the fractional abundances themselves. Perhaps the most widely used recommended CIE fractional abundances are those of Mazzotta et al. (1998). Comparison of the current CIE fractional abundances with these are shown in Figs. 1–30. We also compare with the recently recommended CIE fractional abundances of Bryans et al. (2006) in Figs. 31–60. A comparison of the works of Mazzotta et al. (1998) and Bryans et al. (2006) was discussed in Bryans et al. (2006), showing the effects of the new DR and RR data on the Mazzotta et al. (1998) results.

We compare the current CIE results with those of Mazzotta et al. (1998) for temperatures where $f^m \geq 0.01$. As discussed in Bryans et al. (2006) and in Sec. 5, the reliability of the atomic data is uncertain below this abundance. Differences between the current CIE results and those of Mazzotta et al. (1998) are large for all elements other than H, He, and Li. Factors of typically at least 2 difference in abundance are found for at least one ionization stage of each of these elements. Differences are often much larger. We draw particular attention to the extremely large differences in abundance and peak formation temperature of Sc, Ti, V, Cr, Mn, Co, Ni, Cu, and Zn in the T_e range of 10^4 – 10^6 K. Differences for these elements can be up to a factor of 30. Such variation between the current results and those of Mazzotta et al. (1998) is a result of the new recombination and ionization rate coefficients being used here.

We also compare our present results with the more recent recommended CIE fractional abundances of Bryans et al. (2006). The DR and RR rate coefficients used in this work are largely the same as those used by Bryans et al. with the exception of the Mg-like ions of H through Zn, the Al- through Ar-like ions of Fe, and some corrections to the fitting of other ions. The most significant changes in atomic data bewteen this work and Bryans et al. (2006) is the introduction of the Dere (2007) EII rate coefficients. As expected, differences between the present results and those of Bryans et al. (2006) are not as large as those found between the present results and those of Mazzotta et al. (1998). However, large differences do remain. The differences highlighted above for Sc, Ti, V, Cr, Mn, Co, Ni, Cu, and Zn in the T_e range of 10^4 – 10^6 K are also present in the comparison with Bryans et al. For other elements, abundance differences of a factor a few are not uncommon. We attribute all these differences primarily to the EII rate coefficients.

In Secs. 8.2 and 8.4 we discuss the impact of these updated CIE calculations on the analysis of the present SUMER observation. However, only a selection of the ions discussed in this section are present in the SUMER observation. We recommend that the CIE fractional abundances provided here be used in all future analysis of astrophysical spectra until the next revision of the CIE fractional abundances is published.

8.2. Comparison with FIP factor observations

For this same SUMER observation, FIP factors were also determined by Feldman et al. (1998). The present results are shown in comparison to those of Feldman et al. in Fig. 64. They recommend a FIP factor of 1 for the high-FIP elements, a factor of 4 for the low-FIP elements, and a factor of somewhere between 1 and 2 for S. These results are the basis of the approach taken by Landi et al. (2002) who assumed a FIP factor of unity for the moderate- and high-FIP elements, S, O, N, Ar, and Ne, and a uniform factor of 3.5 for all of the low-FIP elements, K, Na, Al, Ca, Mg, Fe, and Si.

We believe our present results are more robust than those of Feldman et al. (1998). Firstly, our reference EM value is taken from the crossing of 2 Ar EM curves whereas Feldman et al. (1998) use the emission from a single Li-like O VI line as their reference value. This O VI line had an order of magnitude more counts than any other line in the dataset used by Feldman et al. and thus seems a natural reference emission line. However, given the apparent systematic abundance discrepancy of Li-like ions (which the authors acknowledge), the O VI line may not be the most reliable to use as an EM reference value.

Furthermore, in determining the FIP factor for each element we generally use more emission lines than Feldman et al. (1998). For most elements we have multiple emission lines, ranging from 3 lines for Fe to as many as 18 for Si. The only exceptions are the elements K, Na, and Ca as have already been discussed in Sec. 6. For K we only have 1 emission line and for Na and Ca we have 2. Feldman et al. (1998), however, use only 1 or 2 emission lines to determine the FIP factors for each of the elements they consider.

An additional source of unreliability in the Feldman et al. (1998) results lies in the method they use to estimate the plasma temperature. They use the crossing points of curves of FIP factors vs. T_e from different elements. They estimate $\log_{10} T_e = 6.13$ (the same value at which we ultimately arrive) but only calculate these FIP factor vs. T_e curves on a temperature grid of 0.1 in the log. From their figures it is reasonable to conclude that any value in the range of $\log_{10} T_e = 6.1$ to 6.2 would fit their data points. In which case, their reported FIP factors could range from ~ 1.5 to 11. However, Feldman & Laming (2000) estimate the error in these FIP factors to be of the order of 25% which seems to be a significant underestimate.

Of the low-FIP elements, we find rough agreement between our results and those of

Feldman et al. in the sense that the abundance of the low-FIP elements is enhanced over the high-FIP elements, though one should note that Feldman et al. did not ascribe errors to their results. The largest differences between our results and those of Feldman et al. occur for Na and Ca, where we find differences of a factor of 2.5 and 1.5 respectively. However, our results for these elements should be considered with some care since they are not determined from an average of crossing points but from the *EM* at a given T_e . The error bars on our results for Na and Ca are also relatively large and the Feldman et al. results lie within these errors. Our result for K (a FIP factor of 1.75) is in disagreement with the Feldman et al. conclusion that the low-FIP elements are best fitted with an enhancement factor of 4. However, it should be noted that Feldman et al. did not calculate the FIP factor for K itself and that our analysis uses only one line of K.

Finally, we compare the FIP factor results of our GEM method when we utilize the CIE fractional abundances of the present paper and those of Mazzotta et al. (1998). These results are given in Table 32. We find that the effect of our new CIE fractional abundances is largest for K, Ca, and Fe. In the case of K and Fe the differences in FIP factor are not within the estimated errors using our new CIE results. Naturally, these differences are also seen in the log of the inferred coronal abundances.

8.3. Comparison with FIP factor model

The FIP effect model of Laming (2004, 2008) allows an opportunity to quantitatively compare our derived coronal elemental abundances with those of theory. The Laming model builds on that of Schwadron et al. (1999) by explaining the FIP effect in terms of Alfvén waves in the chromosphere. These Alfvén waves drive a ponderomotive force on their reflection or transmission at the chromosphere-corona boundary which results in the elemental fractionation.

The extent of the FIP effect on each species is dependent on the upward energy flux of the Alfvén waves. Laming (2008) gives results for a number of wave energy fluxes and we compare these results with ours for wave energy fluxes of 2, 8 and 32 in units of $10^6 \text{ ergs cm}^{-2} \text{ s}^{-1}$. We show these comparisons in Fig. 78. Our results suggest that upward wave energy fluxes in this range best describe the solar conditions at the time of this particular SUMER observation. Our data generally fit the model well, with the exception of K. However, as has already been discussed in Sec. 6, our result for K should be considered less reliable than the other elements since we were limited to only a single K emission line in the SUMER observation.

It should also be noted that the low-FIP results of the present work were calculated relative to a high-FIP enhancement of 1, while in the Laming model the high-FIP elements do show a slight abundance variation dependent on their FIP value. If we were to normalize to the Ar FIP factor of the Laming (2008) model this would introduce a shift in our FIP

factors of somewhere between a factor of 0.88 to a factor of 1.77.

8.4. Groups

We have used the same group splitting as that used by Landi et al. (2002) and thus can compare directly with their results. Table 34 shows their results for the mean and “error” of $\log_{10} EM$ and $\log_{10} T_e$ for the various groups. However, unlike the present work, Landi et al. quotes the mean and the error as judged by eye as opposed to our GEM method. As our results demonstrate, they have considerably underestimated the uncertainty of their results.

The results of Landi et al. (2002) suggest a difference in the temperature derived from the subsets of Group I, with $\log_{10} T_e = 6.13 \pm 0.01$ and 6.17 ± 0.01 for Groups Ia and Ib, respectively. We do not see this difference in our analysis. In the present work, Groups Ia and Ib give $\log_{10} T_e = 6.16 \pm 0.07$ and 6.16 ± 0.05 , respectively. Within our error bars, we see no distinction between the N-like and non-N-like ions in this group. Using the same uniform low-FIP factor of 3.5 used by Landi et al. (2002) and the GEM method, the distinction remains unobserved as we find values of $\log_{10} T_e = 6.16 \pm 0.05$ and 6.17 ± 0.03 for Groups Ia and Ib, respectively. The temperatures derived from Groups IIa¹, IIb, and III agree reasonably well with those of Landi et al. (2002). We note that Landi et al. excluded the N v and O vi lines from their calculation of the Group IIa lines. When comparing with their results we also exclude these lines.

Figure 68 shows the EM curves for the lines in Group IIa. The largest discrepancies from the other lines in this group can be seen to come from the 2 pairs of N v and O vi lines. It is interesting to note that these lines are the lowest in temperature of peak formation of all the ions considered here (see Figs. 31–60 and Tables 2–31) and as a result the majority of the crossings from these lines are excluded in the right panel of Fig. 68 when we ignore fractional abundances below 0.01. This perhaps goes some way to highlight the need for care when using fractional abundances of such low values.

Given the disagreement with the other lines in Group IIa, and the lower formation temperature of N v and O vi compared to the other ions in the group, it is possible that the emission lines from these two ions originate from a different region of plasma. Thus, we have excluded the O vi and N v lines and recalculated the EM curves. Figure 69 shows this reduced set of EM curves. We have also done the same for the O and N lines on their own in Fig. 70. A much lower average temperature of $\log_{10} T_e = 5.44$ is derived from these curves. We do not give an estimated error on this value since the final result comes from a single crossing point and has no standard deviation. Given that the N v and O vi ions have lower formation temperatures than the other ions of this observation, this suggests that the source

¹Excluding the Li-like N v and O vi lines from Group IIa

of emission from these ions is from a different region of plasma with a lower temperature than that emitting the lines from other elements.

One of the questions that this paper seeks to address is the apparent discrepancy between the EM s derived from Li- and Na-like and that of all other ions. This has been identified previously (e.g., Dupree 1972; Feldman et al. 1998). All Li- and Na-like lines in this observation come from transitions between the ground and first excited configuration, i.e., our Group II. So we first investigate the difference between Li- and Na-like ions and all other ions within this group. Our results for the Li- and Na-like ions are shown in Fig. 69 (excluding N v and O vi) and can be compared to the EM from the other Group II ions shown in Fig. 71. Results are also given in Table 33. A comparison of our present results and those of Landi et al. (2002) can be seen in Table 34. The combination of using the most up-to-date atomic data, an improved method of arriving at the most likely EM and T_e , and a reanalysis of the FIP factors, has led to us finding no sign of any discrepancy between the emission of Li- and Na-like ions and all the other Group II ions. In the present case, the difference between the EM from Groups IIa¹ (excluding N v and O vi lines) and IIb is within the error bars on the EM of Group IIa¹.

In addition to the comparison of EM within Group II, we also compare the EM from the Li- and Na-like ions (Group IIa¹) with the EM derived from every other ion in the observation (i.e., those from Groups I, IIb, and III). The comparison between the EM s from the Li- and Na-like ions and all other ions is shown in Fig. 76. One can see that the EM from Li- and Na-like lines alone (point IIa¹) overlaps, within the errors, with the average determined excluding Li- and Na-like ions (thin dashed line). Thus, we find no statistically meaningful difference in the EM derived from Li- and Na-like ions and that from every other ion in the observation.

Given that we find fairly good agreement in EM and T_e between each of the group categories, our best estimate of the EM and T_e of the emitting plasma is found by applying our analysis method to every emission line (excluding the discrepant N v and O vi lines). These results are shown in Fig. 74 and give $\log_{10} EM = 42.98 \pm 0.29$ and $\log_{10} T_e = 6.12 \pm 0.07$. If, in addition to excluding the N v and O vi lines, we also exclude the Li- and Na-like lines then the calculated values become $\log_{10} EM = 43.02 \pm 0.29$ and $\log_{10} T_e = 6.13 \pm 0.06$ (see Fig. 75). Landi et al. estimate $\log_{10} EM = 43.20 \pm 0.15$ and $\log_{10} T_e = 6.13$ (no error given) for the plasma by combining results from Groups I and IIb. Our results agree, within our errors, with those of Landi et al. (2002). Our results have larger errors, which we believe to be more realistic due to our more rigorous method of calculating the mean and standard deviation of EM and T_e .

To investigate the effects of the updated CIE data on these results, we compare the EM and T_e derived for each group when utilizing the recommended CIE fractional abundances of the present paper and those of Mazzotta et al. (1998). These results are given in Table 34. While differences are found, they are all within the errors. It is interesting to note that the

large differences found in the FIP factors do not translate into differences on the same scale for the derived EM and T_e . Nonetheless, this would not necessarily be the case when applied to other observations, so we recommend the future use of the CIE fractional abundances presented here.

8.5. Other Issues

Despite an overall general agreement in the EM and T_e of each of the groups, there are a number of indications that the observed emission does not come from an isothermal plasma. We have already discussed the possibility that the Li-like N V and O VI lines come from a cooler region of gas. Even when these lines are removed from the Group IIa categorization, there remains a large scatter in the crossing points of the emission from Li- and Na-like ions (Fig. 69) suggesting the isothermal assumption is not entirely accurate. There is also some evidence of a low temperature component from Groups I and IIb (Figs. 67 and 71, respectively). It is also possible that the relatively large errors in EM and T_e are suggestive of a non-isothermal plasma. To determine whether the crossings that fall away from the average are indeed a product of the non-isothermal nature of the plasma, and not some error in the atomic data, one would have to perform a differential emission measure (DEM) analysis, which is beyond the scope of this paper.

A further possible source of error in our analysis is that the ionization balance was calculated using the zero-density approximation. This issue has been raised by Feldman & Laming (2000) in reference to Fe⁸⁺ emission. They claim that over half of the population can be in metastable levels at coronal densities, but there are no emission lines from Fe⁸⁺ in the observation analyzed in the present paper. The sensitivity of emission from Li-like ions has been investigated by Doyle et al. (2005). These authors found that the contribution function of emission from Li-like lines only becomes significantly affected on reaching densities $\geq 10^{11} \text{ cm}^{-3}$, orders of magnitude higher than the density of $1.8 \times 10^8 \text{ cm}^{-3}$ inferred by Feldman et al. (1999) for the observation analyzed here. We thus expect the zero-density approximation to be valid in the present case, but a full density-dependent analysis of every emission line in the observation would be required before one could answer this issue with complete certainty. Again, such a study is beyond the scope of this paper.

9. Proposals for future observations

Our work shows that SUMER observations can go a long way towards constraining FIP models such as those of Laming (2004, 2008). Even better constraints can be achieved through the simultaneous observation of lines from a number of additional charge states. More lines from high-FIP elements such as N, O, Ne, and Ar are required to better determine

the EM for these high-FIP elements, which can then be used to normalize the low-FIP elements. For N, O, and Ne, emission lines from H- and He-like stages need to be observed to avoid using Li-like ions. These charge states are predicted to be abundant for these elements at coronal temperatures. This may require simultaneous observations using separate, cross-calibrated spectrometers. For Ar, emission lines from the Ne-, F-, O-, and N-like ions would lie in the $6.0 \leq \log T_e \leq 6.2$ range typical of the corona. Additional line observations from elements such as Na, K, and Ca, for which we have few lines in the present observation, are also needed to better constrain their FIP factors.

10. Summary

This work has reanalyzed data from a SUMER coronal observation in an attempt to improve upon previous methods of analysis. We have given a brief review of and implemented state-of-the-art electron-ion recombination and ionization data. We have updated the CIE results of Bryans et al. (2006) by using recently published DR data for Mg-like ions of the elements from H through Zn and for Al- through Ar-like Fe ions, and have updated the EII data to those of Dere (2007) for all ions of H through Zn. We have also set out a new, mathematically rigorous, approach for determining the EM and T_e of an emitting plasma within the isothermal approximation. Using these new CIE data and our approach for determining the EM , we calculated the FIP factors of the observed elements.

Our assessment is generally in reasonable agreement with a previous study of the FIP factors (Feldman et al. 1998). Also, we are in reasonable agreement with the FIP-effect model of Laming (2008) using an Alfvén wave energy flux in the range $\sim 2\text{--}32 \times 10^6 \text{ erg cm}^{-2} \text{ s}^{-1}$. However, our results differ from those of Landi et al. (2002) in certain respects. The difference between the temperature derived using lines from non-N- and N-like ions is not evident when we apply our analysis technique. Also, the previously reported discrepancy between the EM derived from Li- and Na-like lines and the EM from all other lines (Groups I, IIb, and III) is not supported by our results, rather the two agree at the 1σ level.

Our best estimate of the EM and T_e of the emitting plasma of this observation is $\log_{10} EM = 42.98 \pm 0.29$ and $\log_{10} T_e = 6.12 \pm 0.07$ when we include all lines except those from N v and O vi, and $\log_{10} EM = 43.02 \pm 0.29$ and $\log_{10} T_e = 6.13 \pm 0.06$ when we additionally exclude all Li- and Na-like lines. There remains variation in the crossing points of the EM vs. T_e curves that are suggestive of errors in the atomic data, the observations, or the solar physics model used. However, from the results of the present work it is not possible to say where the source of these errors lie. Further improvements to the atomic database and new insight into the physical conditions of the upper solar atmosphere are needed before these questions can be answered. Given the evidence for regions of differing temperature, a DEM analysis might go some way to resolving the discrepancies found in the present paper.

We thank H. Bruhns, H. Kreckel, J. M. Laming, and M. Lestinsky for stimulating discussions. We also thank K. P. Dere for providing corrected versions of his EII rate coefficients and for discussions thereon. CHIANTI is a collaborative project involving the NRL (USA), RAL (UK), MSSL (UK), the Universities of Florence (Italy) and Cambridge (UK), and George Mason University (USA). P.B. and D.W.S. were supported in part by the NASA Solar and Heliospheric Physics Supporting Research and Technology program and the NASA Astronomy and Physics Research and Analysis Program. E.L. was supported by NASA grants NNG06EA14I and NNH06CD24 as well as other NASA grants.

REFERENCES

- Altun, Z., Yumak, A., Yavuz, I., Badnell, N. R., Loch, S. D., and Pindzola, M. S. 2007, *A&A*474, 1051
- Arnaud, M., & Rothenflug, R. 1985, *A&AS*, 60, 425
- Aschwanden, M. J. 2004, *Physics of the Solar Corona* (Chichester: Praxis Publishing)
- Badnell, N. R., et al. 2003, *A&A*, 406, 1151
- Badnell, N. R. 2006a, *ApJS*, 167, 334
- Badnell, N. R. 2006b, <http://amdpp.phys.strath.ac.uk/tamoc/DR/>
- Badnell, N. R. 2006c, <http://amdpp.phys.strath.ac.uk/tamoc/RR/>
- Badnell, N. R. 2006d, *J. Phys. B*, 39, 4825
- Badnell, N. R. 2006e, *ApJ*, 651, L73
- Bryans, P., Badnell, N. R., Gorczyca, T. W., Laming, J. M., Witthumsiri, W., & Savin, D. W. 2006, *ApJS*, 167, 343
- Dere, K. P., Landi, E., Mason, H. E., Monsignori Fossi, B. C., & Young, P. R. 1997, *A&AS*, 125, 149
- Dere, K. P., Landi, E., Del Zanna, G., & Young, P. R. 2001, *A&AS*, 134, 331
- Dere, K. P. 2007, *A&A*, 466, 771
- Doyle, J. G., Summers, H. P., & Bryans, P. 2005, *A&A*, 430, L29
- Dragoset, R. A., Musgrove, A., Clark, C. W., & Martin, W. C. 2001, <http://physics.nist.gov/PhysRefData/PerTable/index.html>
- Dupree, A. K. 1972, *ApJ*, 178, 527

- Feldman, U., & Laming, J. M. 2000, Phys. Scr., 61, 222
- Feldman, U., & Widing, K. G. 2003, Space Sci. Rev., 107, 665
- Feldman, U., Schühle, U., Widing, K. G., & Laming, J. M. 1998, ApJ, 505, 999
- Feldman, U., Doschek, G. A., Schühle, U., & Wilhelm, K. 1999, ApJ, 518, 500
- Forbes, T. G. 2000, Phil. Trans. Roy. Soc. A, 358, 711
- Foukal, P. V. 2004, Solar Astrophysics (2nd, Revised Edition; Weinheim: Wiley-VCH)
- Gu, M. F. 2003a, ApJ, 589, 1085
- Gu, M. F. 2003b, ApJ, 590, 1131
- Gu, M. F. 2004, ApJ, 153, 389
- Gudiksen, B. V., & Norlund, Å 2005 ApJ, 618, 1020
- Hundhausen, A. J. 1993, J. Geophys. Res., 98, 13177
- Kingdon, J. B., & Ferland, G. J. 1996, ApJS, 106, 205
- Klimchuk, J. A. 2006, Sol. Phys., 234, 41
- Laming, J. M. 2004, ApJ, 614, 1063
- Laming, J. M. 2008, ApJ, submitted
- Landi, E., Landini, M., Dere, K. P., Young, P. R., & Mason, H. E. 1999, A&AS, 135, 339
- Landi, E., Feldman, U., & Dere, K. P. 2002, ApJS, 139, 281
- Landi, E., et al. 2006, ApJS, 162, 261
- Lang, J., Mason, H. E., & McWhirter, R. W. P. 1990, Sol. Phys., 129, 31
- Lanzafame, A. C., Brooks, D. H., Lang, J., Summers, H. P., Thomas, R. J., & Thompson, A. M. 2002, A&A, 384, 242
- Mandrini, C. H., Démoulin, P., & Klimchuk, J. A. 2000, ApJ, 530, 999
- Mattioli, M., et al. 2007, J. Phys. B, 40, 3569
- Mazzotta, P., Mazzitelli, G., Colafrancesco, S., & Vittorio, N. 1998, A&AS, 133, 403
- Priest, E. R. & Forbes, T. G. 2002, A&A Rev., 10, 313
- Raymond, J. & Doyle, J. G. 1981, ApJ, 247, 686

- Schwadron, N. A., Fisk, L. A., & Zurbuchen, T. H. 1999, ApJ, 521, 859
- Summers, H. P., et al. 2006, Plasma Phys. Contr. Fusion, 48, 263
- Suno, H., & Kato, T. 2006, ADNDT, 92, 407
- Tandberg-Hanssen, E. & Emslie, A. G. 1988, The Physics of Solar Flares (Cambridge: Cambridge University Press)
- Wilhelm, K., et al. 1995, Sol. Phys., 170, 75
- Zirker, J. B. 1993, Sol. Phys., 148, 43

Table 1. Emission lines and intensities used in the present study

Group	Ion	Sequence	Wavelength (Å)	Transition	Intensity (ergs cm ⁻² s ⁻¹ sr ⁻¹)
IIa	N v	Li	1238.82	$2s^2 S_{1/2} - 2p^2 P_{3/2}$	2.520
IIa	N v	Li	1242.80	$2s^2 S_{1/2} - 2p^2 P_{1/2}$	1.420
IIa	O vi	Li	1031.91	$2s^2 S_{1/2} - 2p^2 P_{3/2}$	63.000
IIa	O vi	Li	1037.62	$2s^2 S_{1/2} - 2p^2 P_{1/2}$	28.500
IIa	Ne viii	Li	770.41	$2s^2 S_{1/2} - 2p^2 P_{3/2}$	30.700
IIa	Ne viii	Li	780.32	$2s^2 S_{1/2} - 2p^2 P_{1/2}$	14.200
IIb	Ne vii	Be	895.17	$2s^2 1S_0 - 2s2p^3 P_1$	0.132
III	Ne vii	Be	973.33	$2s2p^1 P_1 - 2p^2 1D_2$	0.070
IIa	Na ix	Li	681.72	$2s^2 S_{1/2} - 2p^2 P_{3/2}$	4.515
IIa	Na ix	Li	694.13	$2s^2 S_{1/2} - 2p^2 P_{1/2}$	2.600
IIb	Na viii	Be	789.78	$2s^2 1S_0 - 2s2p^3 P_1$	0.074
III	Na viii	Be	847.91	$2s2p^1 P_1 - 2p^2 1D_2$	0.058
IIa	Mg x	Li	609.79	$2s^2 S_{1/2} - 2p^2 P_{3/2}$	153.000
IIa	Mg x	Li	624.94	$2s^2 S_{1/2} - 2p^2 P_{1/2}$	91.700
IIb	Mg ix	Be	693.98	$2s^2 1S_0 - 2s2p^3 P_2$	0.898
IIb	Mg ix	Be	706.06	$2s^2 1S_0 - 2s2p^3 P_1$	8.160
III	Mg ix	Be	749.55	$2s2p^1 P_1 - 2p^2 1D_2$	1.490
IIb	Mg viii	B	762.66	$2s^2 2p^2 P_{1/2} - 2s2p^2 4P_{3/2}$	0.047
IIb	Mg viii	B	769.38	$2s^2 2p^2 P_{1/2} - 2s2p^2 4P_{1/2}$	0.152
IIb	Mg viii	B	772.28	$2s^2 2p^2 P_{3/2} - 2s2p^2 4P_{5/2}$	0.670
IIb	Mg viii	B	782.36	$2s^2 2p^2 P_{3/2} - 2s2p^2 4P_{3/2}$	0.357
IIb	Mg viii	B	789.43	$2s^2 2p^2 P_{3/2} - 2s2p^2 4P_{1/2}$	0.099
IIb	Mg vii	C	868.11	$2s^2 2p^2 3P_2 - 2s2p^3 5S_2$	0.048
IIa	Al xi	Li	549.98	$2s^2 S_{1/2} - 2p^2 P_{3/2}$	7.820
IIa	Al xi	Li	568.18	$2s^2 S_{1/2} - 2p^2 P_{1/2}$	5.050
IIb	Al x	Be	637.76	$2s^2 1S_0 - 2s2p^3 P_1$	2.070
III	Al x	Be	670.01	$2s2p^1 P_1 - 2p^2 1D_2$	0.265
IIb	Al ix	B	688.25	$2s^2 2p^2 P_{1/2} - 2s2p^2 4P_{1/2}$	0.076
IIb	Al ix	B	691.54	$2s^2 2p^2 P_{3/2} - 2s2p^2 4P_{5/2}$	0.441
IIb	Al ix	B	703.65	$2s^2 2p^2 P_{3/2} - 2s2p^2 4P_{3/2}$	0.205
IIb	Al ix	B	712.23	$2s^2 2p^2 P_{3/2} - 2s2p^2 4P_{1/2}$	0.058
IIb	Al viii	C	756.70	$2s^2 2p^2 3P_1 - 2s2p^3 5S_2$	0.036

Table 1—Continued

Group	Ion	Sequence	Wavelength (Å)	Transition	Intensity (ergs cm ⁻² s ⁻¹ sr ⁻¹)
IIb	Al VIII	C	772.54	$2s^2 2p^2 {}^3P_2 - 2s2p^3 {}^5S_2$	0.055
Ib	Al VII	N	1053.84	$2s^2 2p^3 {}^4S_{3/2} - 2s^2 2p^3 {}^2P_{3/2}$	0.017
Ia	Al VIII	C	1057.85	$2s^2 2p^2 {}^3P_1 - 2s^2 2p^2 {}^1S_0$	0.036
IIa	Si XII	Li	499.40	$2s^2 {}^2S_{1/2} - 2p^2 {}^2P_{3/2}$	19.200
IIa	Si XII	Li	520.67	$2s^2 {}^2S_{1/2} - 2p^2 {}^2P_{1/2}$	9.160
III	Si X	B	551.18	$2s2p^2 {}^2P_{3/2} - 2p^3 {}^2D_{5/2}$	0.200
IIb	Si XI	Be	564.02	$2s^2 {}^1S_0 - 2s2p^3 {}^3P_2$	1.110
IIb	Si XI	Be	580.91	$2s^2 {}^1S_0 - 2s2p^3 {}^3P_1$	16.000
III	Si XI	Be	604.15	$2s2p^1 {}^1P_1 - 2p^2 {}^1D_2$	1.840
IIb	Si X	B	611.60	$2s^2 2p^2 {}^2P_{1/2} - 2s2p^2 {}^4P_{3/2}$	0.553
IIb	Si X	B	624.70	$2s^2 2p^2 {}^2P_{3/2} - 2s2p^2 {}^4P_{5/2}$	6.970
IIb	Si X	B	638.94	$2s^2 2p^2 {}^2P_{3/2} - 2s2p^2 {}^4P_{3/2}$	5.210
IIb	Si X	B	649.19	$2s^2 2p^2 {}^2P_{3/2} - 2s2p^2 {}^4P_{1/2}$	1.510
IIb	Si IX	C	676.50	$2s^2 2p^2 {}^3P_1 - 2s2p^3 {}^5S_2$	1.560
IIb	Si IX	C	694.70	$2s^2 2p^2 {}^3P_2 - 2s2p^3 {}^5S_2$	3.550
Ib	Si VIII	N	944.38	$2s^2 2p^3 {}^4S_{3/2} - 2s^2 2p^3 {}^2P_{3/2}$	2.030
Ib	Si VIII	N	949.22	$2s^2 2p^3 {}^4S_{3/2} - 2s^2 2p^3 {}^2P_{1/2}$	0.870
Ia	Si IX	C	950.14	$2s^2 2p^2 {}^3P_1 - 2s^2 2p^2 {}^1S_0$	1.920
Ia	Si VII	O	1049.22	$2s^2 2p^4 {}^3P_1 - 2s^2 2p^4 {}^1S_0$	0.045
Ib	Si VIII	N	1440.49	$2s^2 2p^3 {}^4S_{3/2} - 2s^2 2p^3 {}^2D_{5/2}$	0.176
Ib	Si VIII	N	1445.76	$2s^2 2p^3 {}^4S_{3/2} - 2s^2 2p^3 {}^2D_{3/2}$	2.090
IIb	S XI	C	552.12	$2s^2 2p^2 {}^3P_1 - 2s2p^3 {}^5S_2$	0.190
IIb	S XI	C	574.89	$2s^2 2p^2 {}^3P_2 - 2s2p^3 {}^5S_2$	0.470
Ib	S X	N	776.25	$2s^2 2p^3 {}^4S_{3/2} - 2s^2 2p^3 {}^2P_{3/2}$	1.910
Ia	S XI	C	782.96	$2s^2 2p^2 {}^3P_1 - 2s^2 2p^2 {}^1S_0$	0.4005
Ib	S X	N	787.56	$2s^2 2p^3 {}^4S_{3/2} - 2s^2 2p^3 {}^2P_{1/2}$	0.946
Ia	S IX	O	871.73	$2s^2 2p^4 {}^3P_1 - 2s^2 2p^4 {}^1S_0$	0.440
Ib	S X	N	1196.26	$2s^2 2p^3 {}^4S_{3/2} - 2s^2 2p^3 {}^2D_{5/2}$	1.590
Ib	S X	N	1212.93	$2s^2 2p^3 {}^4S_{3/2} - 2s^2 2p^3 {}^2D_{3/2}$	3.410
IIa	Ar VIII	Na	700.25	$3s^2 {}^2S_{1/2} - 3p^2 {}^2P_{3/2}$	0.635
IIa	Ar VIII	Na	713.81	$3s^2 {}^2S_{1/2} - 3p^2 {}^2P_{1/2}$	0.310
Ib	Ar XII	N	1018.89	$2s^2 2p^3 {}^4S_{3/2} - 2s^2 2p^3 {}^2D_{5/2}$	0.274

Table 1—Continued

Group	Ion	Sequence	Wavelength (Å)	Transition	Intensity (ergs cm ⁻² s ⁻¹ sr ⁻¹)
Ib	Ar XII	N	1054.57	$2s^2 2p^3 {}^4S_{3/2} - 2s^2 2p^3 {}^2D_{3/2}$	0.056
Ia	Ar XI	O	1392.11	$2s^2 2p^4 {}^3P_2 - 2s^2 2p^4 {}^1D_2$	0.134
IIa	K IX	Na	636.29	$3s {}^2S_{1/2} - 3p {}^2P_{1/2}$	0.133
IIa	Ca X	Na	557.76	$3s {}^2S_{1/2} - 3p {}^2P_{3/2}$	8.000
IIa	Ca X	Na	574.00	$3s {}^2S_{1/2} - 3p {}^2P_{1/2}$	4.880
IIb	Ca IX	Mg	691.41	$3s^2 {}^1S_0 - 3s 3p {}^3P_1$	0.109
III	Ca IX	Mg	821.23	$3s 3p {}^1P_1 - 3p^2 {}^1D_2$	0.048
Ia	Fe XII	P	1242.00	$3s^2 3p^3 {}^4S_{3/2} - 3s^2 3p^3 {}^2P_{3/2}$	11.840
Ia	Fe XII	P	1349.36	$3s^2 3p^3 {}^4S_{3/2} - 3s^2 3p^3 {}^2P_{1/2}$	5.353
Ia	Fe XI	S	1467.06	$3s^2 3p^4 {}^3P_1 - 3s^2 3p^4 {}^1S_0$	3.390

Note. — We list here the all the emission lines of the SUMER 1996 November 21 21:16 UT to 1996 November 22 02:28 UT observation that are used in the analysis here. This table is reproduced from Landi et al. (2002) with known transition assignment errors corrected. Lines that are blended or have uncertain intensities have also been omitted.

Table 2. Hydrogen CIE Fractional Abundances

$\log(T)$	H^{0+}	H^{1+}
4.00	0.001	2.751
4.10	0.026	1.240
4.20	0.318	0.285
4.30	1.089	0.037
4.40	1.895	0.006
4.50	2.584	0.001
4.60	3.162	0.000
4.70	3.649	0.000
4.80	4.064	0.000
4.90	4.420	0.000
5.00	4.730	0.000
5.10	5.002	0.000
5.20	5.244	0.000
5.30	5.461	0.000
5.40	5.658	0.000
5.50	5.838	0.000
5.60	6.005	0.000
5.70	6.160	0.000
5.80	6.306	0.000
5.90	6.445	0.000
6.00	6.577	0.000
6.10	6.703	0.000
6.20	6.824	0.000
6.30	6.942	0.000
6.40	7.056	0.000
6.50	7.168	0.000
6.60	7.277	0.000
6.70	7.384	0.000
6.80	7.490	0.000
6.90	7.594	0.000
7.00	7.699	0.000
7.10	7.803	0.000
7.20	7.906	0.000
7.30	8.010	0.000
7.40	8.113	0.000
7.50	8.216	0.000
7.60	8.318	0.000
7.70	8.421	0.000
7.80	8.524	0.000
7.90	8.627	0.000
8.00	8.731	0.000
8.10	8.835	0.000
8.20	8.939	0.000
8.30	9.043	0.000
8.40	9.148	0.000
8.50	9.253	0.000
8.60	9.358	0.000
8.70	9.463	0.000
8.80	9.569	0.000
8.90	9.675	0.000
9.00	9.780	0.000

Note. — Calculated
 $-\log_{10}$ of the fractional
abundance for all ionization
stages of hydrogen. We use
the RR rate coefficients of
Badnell (2006c) and the
EII rate coefficients of Dere
(2007).

Table 3. Helium CIE Fractional Abundances

$\log(T)$	He^{0+}	He^{1+}	He^{2+}
4.00	0.000	8.813	15.000
4.10	0.000	6.135	15.000
4.20	0.000	3.980	15.000
4.30	0.003	2.240	13.153
4.40	0.061	0.885	8.981
4.50	0.496	0.167	5.896
4.60	1.295	0.023	3.845
4.70	2.043	0.006	2.288
4.80	2.650	0.040	1.071
4.90	3.265	0.295	0.307
5.00	4.052	0.884	0.061
5.10	4.827	1.527	0.013
5.20	5.511	2.092	0.004
5.30	6.116	2.571	0.001
5.40	6.658	2.979	0.000
5.50	7.150	3.329	0.000
5.60	7.603	3.633	0.000
5.70	8.022	3.899	0.000
5.80	8.413	4.135	0.000
5.90	8.779	4.346	0.000
6.00	9.125	4.538	0.000
6.10	9.452	4.713	0.000
6.20	9.764	4.874	0.000
6.30	10.061	5.023	0.000
6.40	10.346	5.164	0.000
6.50	10.621	5.296	0.000
6.60	10.886	5.422	0.000
6.70	11.143	5.542	0.000
6.80	11.392	5.658	0.000
6.90	11.636	5.770	0.000
7.00	11.874	5.880	0.000
7.10	12.109	5.988	0.000
7.20	12.341	6.095	0.000
7.30	12.570	6.201	0.000
7.40	12.796	6.306	0.000
7.50	13.020	6.410	0.000
7.60	13.242	6.514	0.000
7.70	13.462	6.617	0.000
7.80	13.681	6.721	0.000
7.90	13.899	6.824	0.000
8.00	14.115	6.927	0.000
8.10	14.332	7.030	0.000
8.20	14.547	7.133	0.000
8.30	14.762	7.237	0.000
8.40	14.977	7.340	0.000
8.50	15.000	7.445	0.000
8.60	15.000	7.549	0.000
8.70	15.000	7.653	0.000
8.80	15.000	7.758	0.000
8.90	15.000	7.863	0.000
9.00	15.000	7.968	0.000

Note. — Same as Table 2 but for helium and additionally using the DR rate coefficients of Badnell (2006b). Fractional abundances are cut off at 10^{-15} . For ease of machine readability, values less than 10^{-15} are given $-\log_{10}$ values of 15.

Table 4. Lithium CIE Fractional Abundances

$\log(T)$	Li^{0+}	Li^{1+}	Li^{2+}	Li^{3+}
4.00	2.408	0.002	15.000	15.000
4.10	3.095	0.000	15.000	15.000
4.20	3.667	0.000	15.000	15.000
4.30	4.147	0.000	14.841	15.000
4.40	4.553	0.000	12.035	15.000
4.50	4.897	0.000	9.228	15.000
4.60	5.192	0.000	6.625	15.000
4.70	5.445	0.000	4.531	14.616
4.80	5.663	0.001	2.841	10.276
4.90	5.861	0.014	1.486	6.790
5.00	6.141	0.157	0.517	4.106
5.10	6.694	0.644	0.115	2.317
5.20	7.294	1.253	0.060	1.137
5.30	7.857	1.868	0.234	0.395
5.40	8.542	2.609	0.691	0.100
5.50	9.263	3.367	1.237	0.026
5.60	9.936	4.050	1.735	0.008
5.70	10.558	4.654	2.163	0.003
5.80	11.139	5.195	2.531	0.001
5.90	11.689	5.685	2.849	0.001
6.00	12.210	6.132	3.127	0.000
6.10	12.706	6.545	3.371	0.000
6.20	13.179	6.929	3.589	0.000
6.30	13.631	7.287	3.784	0.000
6.40	14.066	7.624	3.960	0.000
6.50	14.486	7.944	4.122	0.000
6.60	14.894	8.248	4.272	0.000
6.70	15.000	8.538	4.410	0.000
6.80	15.000	8.815	4.539	0.000
6.90	15.000	9.081	4.659	0.000
7.00	15.000	9.338	4.773	0.000
7.10	15.000	9.587	4.883	0.000
7.20	15.000	9.832	4.990	0.000
7.30	15.000	10.072	5.097	0.000
7.40	15.000	10.308	5.202	0.000
7.50	15.000	10.541	5.306	0.000
7.60	15.000	10.771	5.409	0.000
7.70	15.000	10.997	5.512	0.000
7.80	15.000	11.221	5.613	0.000
7.90	15.000	11.443	5.714	0.000
8.00	15.000	11.664	5.815	0.000
8.10	15.000	11.883	5.916	0.000
8.20	15.000	12.101	6.017	0.000
8.30	15.000	12.319	6.119	0.000
8.40	15.000	12.536	6.221	0.000
8.50	15.000	12.752	6.324	0.000
8.60	15.000	12.968	6.427	0.000
8.70	15.000	13.184	6.530	0.000
8.80	15.000	13.399	6.634	0.000
8.90	15.000	13.615	6.738	0.000
9.00	15.000	13.830	6.843	0.000

Note. — Same as Table 3 but for lithium.

Table 5. Beryllium CIE Fractional Abundances

log(T)	Be ⁰⁺	Be ¹⁺	Be ²⁺	Be ³⁺	Be ⁴⁺
4.00	0.021	1.335	6.887	15.000	15.000
4.10	0.114	0.637	4.177	15.000	15.000
4.20	0.379	0.240	2.156	15.000	15.000
4.30	0.865	0.161	0.762	15.000	15.000
4.40	1.797	0.603	0.134	15.000	15.000
4.50	2.987	1.363	0.020	15.000	15.000
4.60	4.072	2.065	0.004	15.000	15.000
4.70	5.007	2.656	0.001	12.940	15.000
4.80	5.812	3.149	0.000	10.076	15.000
4.90	6.513	3.564	0.000	7.419	15.000
5.00	7.127	3.914	0.000	5.280	14.466
5.10	7.671	4.212	0.000	3.552	10.362
5.20	8.149	4.461	0.003	2.155	7.053
5.30	8.577	4.673	0.040	1.058	4.411
5.40	9.064	4.957	0.248	0.365	2.467
5.50	9.683	5.384	0.688	0.134	1.217
5.60	10.367	5.887	1.239	0.220	0.469
5.70	11.187	6.535	1.927	0.578	0.140
5.80	12.066	7.250	2.658	1.048	0.042
5.90	12.909	7.938	3.334	1.496	0.014
6.00	13.698	8.576	3.936	1.888	0.006
6.10	14.437	9.170	4.473	2.226	0.003
6.20	15.000	9.726	4.956	2.519	0.001
6.30	15.000	10.249	5.394	2.775	0.001
6.40	15.000	10.745	5.795	3.001	0.000
6.50	15.000	11.215	6.164	3.202	0.000
6.60	15.000	11.664	6.506	3.385	0.000
6.70	15.000	12.093	6.827	3.551	0.000
6.80	15.000	12.505	7.128	3.703	0.000
6.90	15.000	12.902	7.412	3.846	0.000
7.00	15.000	13.287	7.684	3.979	0.000
7.10	15.000	13.660	7.944	4.105	0.000
7.20	15.000	14.024	8.194	4.225	0.000
7.30	15.000	14.380	8.436	4.339	0.000
7.40	15.000	14.730	8.673	4.449	0.000
7.50	15.000	15.000	8.904	4.556	0.000
7.60	15.000	15.000	9.132	4.660	0.000
7.70	15.000	15.000	9.357	4.764	0.000
7.80	15.000	15.000	9.580	4.867	0.000
7.90	15.000	15.000	9.800	4.970	0.000
8.00	15.000	15.000	10.018	5.072	0.000
8.10	15.000	15.000	10.235	5.174	0.000
8.20	15.000	15.000	10.451	5.275	0.000
8.30	15.000	15.000	10.666	5.377	0.000
8.40	15.000	15.000	10.881	5.478	0.000
8.50	15.000	15.000	11.095	5.579	0.000
8.60	15.000	15.000	11.310	5.681	0.000
8.70	15.000	15.000	11.524	5.783	0.000
8.80	15.000	15.000	11.739	5.886	0.000
8.90	15.000	15.000	11.953	5.989	0.000
9.00	15.000	15.000	12.168	6.092	0.000

Note. — Same as Table 3 but for beryllium.

Table 6. Boron CIE Fractional Abundances

$\log(T)$	B^{0+}	B^{1+}	B^{2+}	B^{3+}	B^{4+}	B^{5+}
4.00	0.382	0.233	9.957	15.000	15.000	15.000
4.10	1.029	0.043	7.367	15.000	15.000	15.000
4.20	1.516	0.013	5.445	14.843	15.000	15.000
4.30	1.822	0.007	3.913	10.708	15.000	15.000
4.40	2.052	0.005	2.668	7.368	15.000	15.000
4.50	2.265	0.012	1.653	4.664	15.000	15.000
4.60	2.518	0.068	0.859	2.503	15.000	15.000
4.70	2.964	0.318	0.397	0.930	15.000	15.000
4.80	3.929	1.088	0.565	0.190	15.000	15.000
4.90	5.229	2.193	1.154	0.035	13.989	15.000
5.00	6.458	3.228	1.743	0.008	11.241	15.000
5.10	7.546	4.124	2.249	0.002	8.543	15.000
5.20	8.508	4.897	2.677	0.001	6.275	15.000
5.30	9.365	5.568	3.037	0.000	4.446	11.514
5.40	10.127	6.148	3.337	0.001	2.965	8.145
5.50	10.791	6.635	3.566	0.008	1.772	5.428
5.60	11.371	7.043	3.736	0.063	0.869	3.289
5.70	11.980	7.486	3.957	0.273	0.347	1.761
5.80	12.702	8.046	4.310	0.662	0.206	0.796
5.90	13.574	8.762	4.831	1.216	0.375	0.286
6.00	14.572	9.609	5.496	1.889	0.744	0.093
6.10	15.000	10.469	6.186	2.559	1.154	0.033
6.20	15.000	11.288	6.842	3.170	1.531	0.013
6.30	15.000	12.056	7.456	3.718	1.861	0.006
6.40	15.000	12.780	8.033	4.212	2.150	0.003
6.50	15.000	13.465	8.575	4.659	2.403	0.002
6.60	15.000	14.116	9.088	5.067	2.627	0.001
6.70	15.000	14.735	9.574	5.442	2.827	0.001
6.80	15.000	15.000	10.038	5.790	3.008	0.000
6.90	15.000	15.000	10.481	6.114	3.173	0.000
7.00	15.000	15.000	10.905	6.418	3.325	0.000
7.10	15.000	15.000	11.312	6.705	3.466	0.000
7.20	15.000	15.000	11.706	6.978	3.599	0.000
7.30	15.000	15.000	12.088	7.239	3.725	0.000
7.40	15.000	15.000	12.459	7.490	3.844	0.000
7.50	15.000	15.000	12.822	7.733	3.958	0.000
7.60	15.000	15.000	13.178	7.970	4.068	0.000
7.70	15.000	15.000	13.529	8.201	4.174	0.000
7.80	15.000	15.000	13.874	8.429	4.279	0.000
7.90	15.000	15.000	14.216	8.654	4.382	0.000
8.00	15.000	15.000	14.554	8.877	4.486	0.000
8.10	15.000	15.000	14.889	9.097	4.588	0.000
8.20	15.000	15.000	15.000	9.315	4.691	0.000
8.30	15.000	15.000	15.000	9.532	4.792	0.000
8.40	15.000	15.000	15.000	9.747	4.894	0.000
8.50	15.000	15.000	15.000	9.962	4.995	0.000
8.60	15.000	15.000	15.000	10.176	5.096	0.000
8.70	15.000	15.000	15.000	10.390	5.198	0.000
8.80	15.000	15.000	15.000	10.604	5.300	0.000
8.90	15.000	15.000	15.000	10.819	5.402	0.000
9.00	15.000	15.000	15.000	11.033	5.504	0.000

Note. — Same as Table 3 but for boron.

Table 7. Carbon CIE Fractional Abundances

log(T)	C ⁰⁺	C ¹⁺	C ²⁺	C ³⁺	C ⁴⁺	C ⁵⁺	C ⁶⁺
4.00	0.014	1.487	10.947	15.000	15.000	15.000	15.000
4.10	0.203	0.428	7.258	15.000	15.000	15.000	15.000
4.20	0.795	0.076	4.809	15.000	15.000	15.000	15.000
4.30	1.369	0.019	3.125	13.250	15.000	15.000	15.000
4.40	1.768	0.013	1.918	9.615	15.000	15.000	15.000
4.50	2.099	0.043	1.068	6.842	14.727	15.000	15.000
4.60	2.476	0.164	0.508	4.733	10.382	15.000	15.000
4.70	2.970	0.423	0.207	3.170	7.020	15.000	15.000
4.80	3.546	0.778	0.085	2.010	4.404	15.000	15.000
4.90	4.158	1.177	0.068	1.131	2.346	15.000	15.000
5.00	4.905	1.717	0.241	0.583	0.836	15.000	15.000
5.10	6.158	2.769	0.965	0.696	0.162	13.909	15.000
5.20	7.692	4.106	2.006	1.214	0.032	10.883	15.000
5.30	9.120	5.342	2.971	1.730	0.009	8.174	15.000
5.40	10.396	6.429	3.808	2.174	0.003	6.010	14.630
5.50	11.535	7.383	4.530	2.550	0.001	4.269	10.752
5.60	12.549	8.217	5.147	2.859	0.001	2.864	7.625
5.70	13.434	8.927	5.655	3.089	0.008	1.739	5.108
5.80	14.211	9.533	6.070	3.254	0.060	0.895	3.135
5.90	14.984	10.139	6.495	3.453	0.238	0.395	1.715
6.00	15.000	10.838	7.020	3.773	0.578	0.238	0.803
6.10	15.000	11.677	7.693	4.260	1.081	0.369	0.310
6.20	15.000	12.629	8.485	4.882	1.699	0.688	0.111
6.30	15.000	13.591	9.294	5.534	2.325	1.055	0.042
6.40	15.000	14.512	10.067	6.162	2.904	1.401	0.018
6.50	15.000	15.000	10.796	6.753	3.428	1.707	0.009
6.60	15.000	15.000	11.486	7.309	3.902	1.977	0.005
6.70	15.000	15.000	12.141	7.835	4.336	2.215	0.003
6.80	15.000	15.000	12.768	8.335	4.734	2.427	0.002
6.90	15.000	15.000	13.370	8.812	5.102	2.617	0.001
7.00	15.000	15.000	13.951	9.268	5.446	2.791	0.001
7.10	15.000	15.000	14.512	9.707	5.770	2.950	0.000
7.20	15.000	15.000	15.000	10.131	6.076	3.099	0.000
7.30	15.000	15.000	15.000	10.541	6.367	3.239	0.000
7.40	15.000	15.000	15.000	10.940	6.647	3.373	0.000
7.50	15.000	15.000	15.000	11.330	6.918	3.502	0.000
7.60	15.000	15.000	15.000	11.712	7.182	3.629	0.000
7.70	15.000	15.000	15.000	12.089	7.440	3.753	0.000
7.80	15.000	15.000	15.000	12.462	7.695	3.878	0.000
7.90	15.000	15.000	15.000	12.832	7.947	4.002	0.000
8.00	15.000	15.000	15.000	13.200	8.199	4.128	0.000
8.10	15.000	15.000	15.000	13.568	8.450	4.257	0.000
8.20	15.000	15.000	15.000	13.935	8.702	4.388	0.000
8.30	15.000	15.000	15.000	14.304	8.956	4.523	0.000
8.40	15.000	15.000	15.000	14.673	9.211	4.661	0.000
8.50	15.000	15.000	15.000	15.000	9.470	4.804	0.000
8.60	15.000	15.000	15.000	15.000	9.731	4.951	0.000
8.70	15.000	15.000	15.000	15.000	9.996	5.102	0.000
8.80	15.000	15.000	15.000	15.000	10.265	5.258	0.000
8.90	15.000	15.000	15.000	15.000	10.537	5.419	0.000
9.00	15.000	15.000	15.000	15.000	10.813	5.584	0.000

Note. — Same as Table 3 but for carbon.

Table 8. Nitrogen CIE Fractional Abundances

log(T)	N ⁰⁺	N ¹⁺	N ²⁺	N ³⁺	N ⁴⁺	N ⁵⁺	N ⁶⁺	N ⁷⁺
4.00	0.000	3.390	14.613	15.000	15.000	15.000	15.000	15.000
4.10	0.008	1.746	10.223	15.000	15.000	15.000	15.000	15.000
4.20	0.140	0.559	6.507	15.000	15.000	15.000	15.000	15.000
4.30	0.680	0.102	4.089	13.747	15.000	15.000	15.000	15.000
4.40	1.290	0.024	2.554	9.663	15.000	15.000	15.000	15.000
4.50	1.758	0.023	1.476	6.596	15.000	15.000	15.000	15.000
4.60	2.180	0.095	0.722	4.316	12.687	15.000	15.000	15.000
4.70	2.690	0.318	0.288	2.706	9.065	15.000	15.000	15.000
4.80	3.304	0.681	0.116	1.605	6.337	11.980	15.000	15.000
4.90	3.974	1.121	0.107	0.844	4.249	8.163	15.000	15.000
5.00	4.725	1.655	0.259	0.372	2.685	5.202	15.000	15.000
5.10	5.580	2.302	0.571	0.156	1.565	2.948	15.000	15.000
5.20	6.535	3.054	1.023	0.157	0.811	1.269	15.000	15.000
5.30	7.836	4.156	1.854	0.595	0.612	0.312	12.862	15.000
5.40	9.546	5.672	3.118	1.513	0.988	0.063	9.758	15.000
5.50	11.219	7.154	4.366	2.452	1.462	0.017	7.312	15.000
5.60	12.731	8.480	5.471	3.279	1.886	0.006	5.370	12.795
5.70	14.087	9.655	6.436	3.990	2.244	0.003	3.809	9.381
5.80	15.000	10.686	7.268	4.587	2.529	0.003	2.550	6.627
5.90	15.000	11.569	7.960	5.062	2.725	0.013	1.553	4.418
6.00	15.000	12.343	8.552	5.450	2.864	0.072	0.825	2.705
6.10	15.000	13.118	9.150	5.858	3.047	0.243	0.404	1.476
6.20	15.000	13.984	9.848	6.376	3.364	0.566	0.281	0.689
6.30	15.000	14.988	10.690	7.049	3.855	1.052	0.419	0.275
6.40	15.000	15.000	11.624	7.823	4.464	1.635	0.712	0.106
6.50	15.000	15.000	12.558	8.605	5.095	2.220	1.040	0.044
6.60	15.000	15.000	13.453	9.354	5.702	2.762	1.349	0.021
6.70	15.000	15.000	14.303	10.064	6.277	3.257	1.627	0.011
6.80	15.000	15.000	15.000	10.737	6.819	3.707	1.873	0.006
6.90	15.000	15.000	15.000	11.379	7.334	4.121	2.092	0.004
7.00	15.000	15.000	15.000	11.994	7.823	4.502	2.288	0.002
7.10	15.000	15.000	15.000	12.586	8.290	4.856	2.467	0.001
7.20	15.000	15.000	15.000	13.157	8.739	5.188	2.630	0.001
7.30	15.000	15.000	15.000	13.711	9.170	5.501	2.782	0.001
7.40	15.000	15.000	15.000	14.248	9.587	5.798	2.925	0.001
7.50	15.000	15.000	15.000	14.773	9.991	6.082	3.061	0.000
7.60	15.000	15.000	15.000	15.000	10.385	6.356	3.191	0.000
7.70	15.000	15.000	15.000	15.000	10.771	6.622	3.318	0.000
7.80	15.000	15.000	15.000	15.000	11.150	6.882	3.443	0.000
7.90	15.000	15.000	15.000	15.000	11.524	7.137	3.568	0.000
8.00	15.000	15.000	15.000	15.000	11.895	7.390	3.692	0.000
8.10	15.000	15.000	15.000	15.000	12.264	7.641	3.818	0.000
8.20	15.000	15.000	15.000	15.000	12.631	7.892	3.945	0.000
8.30	15.000	15.000	15.000	15.000	12.998	8.143	4.076	0.000
8.40	15.000	15.000	15.000	15.000	13.366	8.395	4.209	0.000
8.50	15.000	15.000	15.000	15.000	13.735	8.649	4.346	0.000
8.60	15.000	15.000	15.000	15.000	14.106	8.906	4.487	0.000
8.70	15.000	15.000	15.000	15.000	14.479	9.166	4.633	0.000
8.80	15.000	15.000	15.000	15.000	14.855	9.429	4.783	0.000
8.90	15.000	15.000	15.000	15.000	15.000	9.696	4.937	0.000
9.00	15.000	15.000	15.000	15.000	15.000	9.966	5.096	0.000

Note. — Same as Table 3 but for nitrogen.

Table 9. Oxygen CIE Fractional Abundances

log(T)	O ⁰⁺	O ¹⁺	O ²⁺	O ³⁺	O ⁴⁺	O ⁵⁺	O ⁶⁺	O ⁷⁺	O ⁸⁺
4.00	0.000	2.959	15.000	15.000	15.000	15.000	15.000	15.000	15.000
4.10	0.017	1.409	12.192	15.000	15.000	15.000	15.000	15.000	15.000
4.20	0.244	0.367	8.276	15.000	15.000	15.000	15.000	15.000	15.000
4.30	0.910	0.057	5.558	15.000	15.000	15.000	15.000	15.000	15.000
4.40	1.510	0.014	3.616	11.944	15.000	15.000	15.000	15.000	15.000
4.50	1.890	0.009	2.183	8.206	15.000	15.000	15.000	15.000	15.000
4.60	2.188	0.033	1.173	5.441	13.325	15.000	15.000	15.000	15.000
4.70	2.550	0.158	0.521	3.452	9.310	15.000	15.000	15.000	15.000
4.80	3.070	0.453	0.195	2.077	6.346	14.286	15.000	15.000	15.000
4.90	3.714	0.876	0.100	1.135	4.149	10.184	15.000	15.000	15.000
5.00	4.459	1.404	0.183	0.521	2.527	7.014	12.023	15.000	15.000
5.10	5.341	2.069	0.460	0.218	1.402	4.623	8.080	15.000	15.000
5.20	6.346	2.862	0.907	0.178	0.680	2.860	5.061	15.000	15.000
5.30	7.468	3.774	1.507	0.362	0.294	1.611	2.790	15.000	15.000
5.40	8.727	4.828	2.278	0.773	0.219	0.816	1.160	14.593	15.000
5.50	10.345	6.245	3.434	1.612	0.640	0.632	0.290	10.978	15.000
5.60	12.288	7.993	4.940	2.834	1.497	0.976	0.065	8.208	15.000
5.70	14.153	9.668	6.389	4.025	2.365	1.404	0.019	6.116	14.110
5.80	15.000	11.174	7.681	5.080	3.130	1.788	0.007	4.454	10.530
5.90	15.000	12.511	8.816	5.995	3.782	2.106	0.004	3.117	7.646
6.00	15.000	13.682	9.793	6.765	4.310	2.340	0.006	2.047	5.323
6.10	15.000	14.696	10.622	7.399	4.720	2.489	0.029	1.221	3.479
6.20	15.000	15.000	11.377	7.969	5.081	2.619	0.115	0.655	2.080
6.30	15.000	15.000	12.164	8.578	5.496	2.830	0.315	0.361	1.100
6.40	15.000	15.000	13.061	9.307	6.041	3.197	0.669	0.329	0.500
6.50	15.000	15.000	14.082	10.165	6.728	3.724	1.168	0.510	0.206
6.60	15.000	15.000	15.000	11.076	7.478	4.329	1.724	0.791	0.087
6.70	15.000	15.000	15.000	11.972	8.220	4.936	2.265	1.086	0.040
6.80	15.000	15.000	15.000	12.828	8.932	5.518	2.767	1.360	0.020
6.90	15.000	15.000	15.000	13.646	9.609	6.070	3.226	1.607	0.011
7.00	15.000	15.000	15.000	14.427	10.256	6.593	3.647	1.828	0.007
7.10	15.000	15.000	15.000	15.000	10.875	7.090	4.035	2.027	0.004
7.20	15.000	15.000	15.000	15.000	11.471	7.564	4.395	2.208	0.003
7.30	15.000	15.000	15.000	15.000	12.047	8.017	4.732	2.373	0.002
7.40	15.000	15.000	15.000	15.000	12.603	8.453	5.049	2.527	0.001
7.50	15.000	15.000	15.000	15.000	13.144	8.873	5.349	2.671	0.001
7.60	15.000	15.000	15.000	15.000	13.671	9.279	5.635	2.807	0.001
7.70	15.000	15.000	15.000	15.000	14.186	9.675	5.910	2.939	0.001
7.80	15.000	15.000	15.000	15.000	14.691	10.062	6.177	3.066	0.000
7.90	15.000	15.000	15.000	15.000	15.000	10.442	6.437	3.191	0.000
8.00	15.000	15.000	15.000	15.000	15.000	10.816	6.692	3.316	0.000
8.10	15.000	15.000	15.000	15.000	15.000	11.187	6.945	3.440	0.000
8.20	15.000	15.000	15.000	15.000	15.000	11.555	7.195	3.565	0.000
8.30	15.000	15.000	15.000	15.000	15.000	11.922	7.445	3.693	0.000
8.40	15.000	15.000	15.000	15.000	15.000	12.288	7.695	3.822	0.000
8.50	15.000	15.000	15.000	15.000	15.000	12.655	7.947	3.955	0.000
8.60	15.000	15.000	15.000	15.000	15.000	13.023	8.200	4.092	0.000
8.70	15.000	15.000	15.000	15.000	15.000	13.392	8.455	4.232	0.000
8.80	15.000	15.000	15.000	15.000	15.000	13.764	8.714	4.377	0.000
8.90	15.000	15.000	15.000	15.000	15.000	14.139	8.975	4.526	0.000
9.00	15.000	15.000	15.000	15.000	15.000	14.517	9.241	4.680	0.000

Note. — Same as Table 3 but for oxygen.

Table 10. Fluorine CIE Fractional Abundances

$\log(T)$	F^{0+}	F^{1+}	F^{2+}	F^{3+}	F^{4+}	F^{5+}	F^{6+}	F^{7+}	F^{8+}	F^{9+}
4.00	0.000	4.765	15.000	15.000	15.000	15.000	15.000	15.000	15.000	15.000
4.10	0.001	2.820	13.944	15.000	15.000	15.000	15.000	15.000	15.000	15.000
4.20	0.024	1.268	9.524	15.000	15.000	15.000	15.000	15.000	15.000	15.000
4.30	0.315	0.288	6.129	15.000	15.000	15.000	15.000	15.000	15.000	15.000
4.40	1.052	0.040	3.951	13.757	15.000	15.000	15.000	15.000	15.000	15.000
4.50	1.673	0.011	2.429	9.568	15.000	15.000	15.000	15.000	15.000	15.000
4.60	2.046	0.024	1.354	6.422	15.000	15.000	15.000	15.000	15.000	15.000
4.70	2.364	0.112	0.653	4.134	10.748	15.000	15.000	15.000	15.000	15.000
4.80	2.791	0.341	0.268	2.527	7.363	15.000	15.000	15.000	15.000	15.000
4.90	3.344	0.701	0.118	1.414	4.858	10.657	15.000	15.000	15.000	15.000
5.00	4.009	1.169	0.146	0.665	3.001	7.297	14.277	15.000	15.000	15.000
5.10	4.834	1.793	0.380	0.262	1.700	4.786	10.056	15.000	15.000	15.000
5.20	5.816	2.569	0.806	0.155	0.855	2.953	6.831	10.942	15.000	15.000
5.30	6.927	3.474	1.391	0.288	0.375	1.659	4.394	7.175	15.000	15.000
5.40	8.170	4.512	2.135	0.642	0.215	0.818	2.613	4.313	15.000	15.000
5.50	9.544	5.684	3.034	1.201	0.337	0.368	1.383	2.201	15.000	15.000
5.60	11.126	7.067	4.163	2.028	0.789	0.332	0.697	0.791	12.007	15.000
5.70	13.118	8.867	5.725	3.318	1.751	0.875	0.694	0.190	8.800	15.000
5.80	15.000	10.817	7.452	4.796	2.938	1.698	1.053	0.050	6.567	14.817
5.90	15.000	12.620	9.045	6.159	4.040	2.479	1.435	0.018	4.846	11.168
6.00	15.000	14.234	10.460	7.359	5.001	3.154	1.764	0.008	3.472	8.239
6.10	15.000	15.000	11.696	8.393	5.814	3.710	2.017	0.006	2.371	5.879
6.20	15.000	15.000	12.762	9.268	6.484	4.146	2.184	0.017	1.507	3.992
6.30	15.000	15.000	13.712	10.036	7.058	4.505	2.309	0.066	0.877	2.524
6.40	15.000	15.000	14.639	10.790	7.629	4.877	2.476	0.198	0.486	1.444
6.50	15.000	15.000	15.000	11.615	8.280	5.345	2.764	0.459	0.336	0.724
6.60	15.000	15.000	15.000	12.561	9.059	5.952	3.214	0.870	0.411	0.322
6.70	15.000	15.000	15.000	13.587	9.926	6.658	3.777	1.379	0.631	0.140
6.80	15.000	15.000	15.000	14.619	10.806	7.385	4.370	1.903	0.899	0.065
6.90	15.000	15.000	15.000	15.000	11.660	8.092	4.951	2.400	1.162	0.033
7.00	15.000	15.000	15.000	15.000	12.479	8.770	5.505	2.860	1.404	0.018
7.10	15.000	15.000	15.000	15.000	13.264	9.419	6.030	3.283	1.623	0.011
7.20	15.000	15.000	15.000	15.000	14.018	10.041	6.530	3.673	1.821	0.007
7.30	15.000	15.000	15.000	15.000	14.745	10.638	7.006	4.034	2.001	0.004
7.40	15.000	15.000	15.000	15.000	15.000	11.215	7.461	4.372	2.166	0.003
7.50	15.000	15.000	15.000	15.000	15.000	11.774	7.898	4.690	2.319	0.002
7.60	15.000	15.000	15.000	15.000	15.000	12.315	8.318	4.991	2.463	0.002
7.70	15.000	15.000	15.000	15.000	15.000	12.843	8.726	5.277	2.600	0.001
7.80	15.000	15.000	15.000	15.000	15.000	13.358	9.121	5.552	2.731	0.001
7.90	15.000	15.000	15.000	15.000	15.000	13.863	9.508	5.819	2.859	0.001
8.00	15.000	15.000	15.000	15.000	15.000	14.360	9.887	6.078	2.984	0.000
8.10	15.000	15.000	15.000	15.000	15.000	14.851	10.261	6.333	3.108	0.000
8.20	15.000	15.000	15.000	15.000	15.000	15.000	10.631	6.585	3.233	0.000
8.30	15.000	15.000	15.000	15.000	15.000	15.000	10.998	6.835	3.358	0.000
8.40	15.000	15.000	15.000	15.000	15.000	15.000	11.364	7.084	3.485	0.000
8.50	15.000	15.000	15.000	15.000	15.000	15.000	11.729	7.333	3.615	0.000
8.60	15.000	15.000	15.000	15.000	15.000	15.000	12.095	7.583	3.748	0.000
8.70	15.000	15.000	15.000	15.000	15.000	15.000	12.461	7.836	3.884	0.000
8.80	15.000	15.000	15.000	15.000	15.000	15.000	12.830	8.090	4.024	0.000
8.90	15.000	15.000	15.000	15.000	15.000	15.000	13.201	8.348	4.169	0.000
9.00	15.000	15.000	15.000	15.000	15.000	15.000	13.575	8.609	4.318	0.000

Note. — Same as Table 3 but for fluorine.

Table 11. Neon CIE Fractional Abundances

log(T)	Ne ⁰⁺	Ne ¹⁺	Ne ²⁺	Ne ³⁺	Ne ⁴⁺	Ne ⁵⁺	Ne ⁶⁺	Ne ⁷⁺	Ne ⁸⁺	Ne ⁹⁺	Ne ¹⁰⁺
4.00	0.000	7.324	15.000	15.000	15.000	15.000	15.000	15.000	15.000	15.000	15.000
4.10	0.000	4.891	15.000	15.000	15.000	15.000	15.000	15.000	15.000	15.000	15.000
4.20	0.001	2.918	12.845	15.000	15.000	15.000	15.000	15.000	15.000	15.000	15.000
4.30	0.021	1.330	8.442	15.000	15.000	15.000	15.000	15.000	15.000	15.000	15.000
4.40	0.303	0.299	5.146	15.000	15.000	15.000	15.000	15.000	15.000	15.000	15.000
4.50	1.090	0.037	3.079	10.508	15.000	15.000	15.000	15.000	15.000	15.000	15.000
4.60	1.800	0.016	1.686	6.961	15.000	15.000	15.000	15.000	15.000	15.000	15.000
4.70	2.261	0.081	0.784	4.411	11.839	15.000	15.000	15.000	15.000	15.000	15.000
4.80	2.705	0.296	0.310	2.689	8.104	15.000	15.000	15.000	15.000	15.000	15.000
4.90	3.249	0.652	0.126	1.538	5.395	11.656	15.000	15.000	15.000	15.000	15.000
5.00	3.888	1.106	0.126	0.760	3.391	8.010	14.847	15.000	15.000	15.000	15.000
5.10	4.668	1.695	0.319	0.310	1.955	5.264	10.426	15.000	15.000	15.000	15.000
5.20	5.607	2.435	0.705	0.156	0.996	3.246	7.056	12.781	15.000	15.000	15.000
5.30	6.690	3.314	1.263	0.254	0.429	1.815	4.523	8.788	13.291	15.000	15.000
5.40	7.927	4.345	1.999	0.595	0.218	0.891	2.695	5.766	8.907	15.000	15.000
5.50	9.306	5.520	2.899	1.151	0.311	0.394	1.447	3.538	5.573	15.000	15.000
5.60	10.819	6.830	3.953	1.902	0.668	0.257	0.683	1.965	3.098	15.000	15.000
5.70	12.486	8.300	5.182	2.858	1.285	0.456	0.353	0.963	1.356	12.638	15.000
5.80	14.471	10.094	6.748	4.176	2.305	1.118	0.564	0.614	0.396	9.086	15.000
5.90	15.000	12.195	8.634	5.831	3.694	2.195	1.252	0.829	0.103	6.710	14.965
6.00	15.000	14.232	10.465	7.448	5.068	3.292	2.010	1.184	0.034	4.963	11.325
6.10	15.000	15.000	12.114	8.895	6.292	4.267	2.686	1.511	0.015	3.589	8.423
6.20	15.000	15.000	13.570	10.159	7.349	5.096	3.248	1.770	0.009	2.493	6.089
6.30	15.000	15.000	14.844	11.250	8.246	5.782	3.694	1.949	0.015	1.630	4.220
6.40	15.000	15.000	15.000	12.213	9.025	6.365	4.057	2.080	0.052	0.987	2.754
6.50	15.000	15.000	15.000	13.130	9.768	6.923	4.415	2.234	0.155	0.565	1.654
6.60	15.000	15.000	15.000	14.083	10.555	7.535	4.842	2.484	0.365	0.361	0.888
6.70	15.000	15.000	15.000	15.000	11.442	8.255	5.390	2.876	0.709	0.369	0.426
6.80	15.000	15.000	15.000	15.000	12.418	9.071	6.045	3.390	1.161	0.534	0.195
6.90	15.000	15.000	15.000	15.000	13.419	9.920	6.741	3.953	1.650	0.770	0.093
7.00	15.000	15.000	15.000	15.000	14.401	10.756	7.430	4.515	2.125	1.017	0.048
7.10	15.000	15.000	15.000	15.000	15.000	11.563	8.095	5.056	2.569	1.250	0.026
7.20	15.000	15.000	15.000	15.000	15.000	12.339	8.734	5.572	2.980	1.463	0.016
7.30	15.000	15.000	15.000	15.000	15.000	13.086	9.348	6.063	3.360	1.657	0.010
7.40	15.000	15.000	15.000	15.000	15.000	13.807	9.939	6.532	3.714	1.835	0.006
7.50	15.000	15.000	15.000	15.000	14.506	10.512	6.982	4.046	1.998	0.004	
7.60	15.000	15.000	15.000	15.000	15.000	11.067	7.415	4.360	2.150	0.003	
7.70	15.000	15.000	15.000	15.000	15.000	11.608	7.835	4.659	2.293	0.002	
7.80	15.000	15.000	15.000	15.000	15.000	12.137	8.244	4.947	2.429	0.002	
7.90	15.000	15.000	15.000	15.000	15.000	12.657	8.643	5.226	2.560	0.001	
8.00	15.000	15.000	15.000	15.000	15.000	13.168	9.036	5.498	2.687	0.001	
8.10	15.000	15.000	15.000	15.000	15.000	13.674	9.424	5.767	2.812	0.001	
8.20	15.000	15.000	15.000	15.000	15.000	14.177	9.809	6.034	2.936	0.001	
8.30	15.000	15.000	15.000	15.000	15.000	14.677	10.194	6.300	3.061	0.000	
8.40	15.000	15.000	15.000	15.000	15.000	15.000	10.579	6.569	3.186	0.000	
8.50	15.000	15.000	15.000	15.000	15.000	15.000	10.967	6.840	3.313	0.000	
8.60	15.000	15.000	15.000	15.000	15.000	15.000	11.358	7.115	3.443	0.000	
8.70	15.000	15.000	15.000	15.000	15.000	15.000	11.754	7.396	3.576	0.000	
8.80	15.000	15.000	15.000	15.000	15.000	15.000	12.155	7.684	3.713	0.000	
8.90	15.000	15.000	15.000	15.000	15.000	15.000	12.563	7.979	3.853	0.000	
9.00	15.000	15.000	15.000	15.000	15.000	15.000	12.979	8.281	3.998	0.000	

Note. — Same as Table 3 but for neon.

Table 12. Sodium CIE Fractional Abundances

log(T)	Na ⁰⁺	Na ¹⁺	Na ²⁺	Na ³⁺	Na ⁴⁺	Na ⁵⁺	Na ⁶⁺	Na ⁷⁺	Na ⁸⁺	Na ⁹⁺	Na ¹⁰⁺	Na ¹¹⁺
4.00	3.201	0.000	15.000	15.000	15.000	15.000	15.000	15.000	15.000	15.000	15.000	15.000
4.10	3.873	0.000	14.221	15.000	15.000	15.000	15.000	15.000	15.000	15.000	15.000	15.000
4.20	4.435	0.000	11.417	15.000	15.000	15.000	15.000	15.000	15.000	15.000	15.000	15.000
4.30	4.908	0.000	8.613	15.000	15.000	15.000	15.000	15.000	15.000	15.000	15.000	15.000
4.40	5.310	0.000	6.012	15.000	15.000	15.000	15.000	15.000	15.000	15.000	15.000	15.000
4.50	5.652	0.000	3.918	12.315	15.000	15.000	15.000	15.000	15.000	15.000	15.000	15.000
4.60	5.931	0.002	2.243	8.194	15.000	15.000	15.000	15.000	15.000	15.000	15.000	15.000
4.70	6.126	0.046	1.000	5.061	13.104	15.000	15.000	15.000	15.000	15.000	15.000	15.000
4.80	6.326	0.278	0.326	2.966	8.923	15.000	15.000	15.000	15.000	15.000	15.000	15.000
4.90	6.599	0.691	0.111	1.670	5.999	13.108	15.000	15.000	15.000	15.000	15.000	15.000
5.00	6.932	1.165	0.108	0.819	3.862	9.126	15.000	15.000	15.000	15.000	15.000	15.000
5.10	7.417	1.752	0.298	0.324	2.329	6.130	11.815	15.000	15.000	15.000	15.000	15.000
5.20	8.082	2.476	0.675	0.135	1.286	3.912	8.144	14.045	15.000	15.000	15.000	15.000
5.30	8.883	3.298	1.185	0.167	0.606	2.277	5.328	9.781	15.000	15.000	15.000	15.000
5.40	9.852	4.256	1.854	0.427	0.266	1.155	3.239	6.508	11.002	15.000	15.000	15.000
5.50	11.015	5.382	2.713	0.927	0.260	0.504	1.789	4.083	7.360	10.682	15.000	15.000
5.60	12.361	6.671	3.750	1.646	0.546	0.255	0.878	2.363	4.642	6.862	15.000	15.000
5.70	13.864	8.100	4.941	2.550	1.079	0.337	0.409	1.216	2.675	3.995	15.000	15.000
5.80	15.000	9.682	6.297	3.644	1.848	0.721	0.329	0.568	1.348	1.930	13.055	15.000
5.90	15.000	11.538	7.936	5.043	2.960	1.498	0.710	0.465	0.682	0.655	9.254	15.000
6.00	15.000	13.777	9.970	6.852	4.512	2.755	1.624	0.964	0.708	0.174	6.743	14.810
6.10	15.000	15.000	12.047	8.720	6.144	4.123	2.689	1.670	1.012	0.056	4.988	11.231
6.20	15.000	15.000	13.945	10.421	7.630	5.368	3.664	2.330	1.325	0.023	3.635	8.405
6.30	15.000	15.000	15.000	11.923	8.932	6.448	4.500	2.887	1.580	0.013	2.561	6.137
6.40	15.000	15.000	15.000	13.232	10.054	7.365	5.194	3.331	1.761	0.016	1.715	4.319
6.50	15.000	15.000	15.000	14.394	11.039	8.158	5.781	3.694	1.895	0.045	1.076	2.884
6.60	15.000	15.000	15.000	15.000	11.960	8.898	6.330	4.041	2.043	0.128	0.638	1.790
6.70	15.000	15.000	15.000	15.000	12.897	9.664	6.915	4.441	2.271	0.303	0.399	1.006
6.80	15.000	15.000	15.000	15.000	13.910	10.515	7.595	4.951	2.627	0.602	0.358	0.509
6.90	15.000	15.000	15.000	15.000	15.000	11.455	8.373	5.570	3.106	1.013	0.479	0.244
7.00	15.000	15.000	15.000	15.000	15.000	12.432	9.195	6.242	3.647	1.473	0.684	0.120
7.10	15.000	15.000	15.000	15.000	15.000	13.399	10.014	6.919	4.197	1.931	0.911	0.063
7.20	15.000	15.000	15.000	15.000	15.000	14.338	10.809	7.577	4.730	2.364	1.132	0.035
7.30	15.000	15.000	15.000	15.000	15.000	15.000	11.576	8.211	5.240	2.767	1.338	0.021
7.40	15.000	15.000	15.000	15.000	15.000	15.000	12.316	8.822	5.728	3.142	1.527	0.013
7.50	15.000	15.000	15.000	15.000	15.000	13.032	9.410	6.193	3.491	1.700	0.009	
7.60	15.000	15.000	15.000	15.000	15.000	13.727	9.980	6.640	3.819	1.861	0.006	
7.70	15.000	15.000	15.000	15.000	15.000	14.404	10.533	7.071	4.130	2.010	0.004	
7.80	15.000	15.000	15.000	15.000	15.000	15.000	15.000	11.072	7.488	4.427	2.151	0.003
7.90	15.000	15.000	15.000	15.000	15.000	15.000	15.000	11.599	7.894	4.712	2.286	0.002
8.00	15.000	15.000	15.000	15.000	15.000	15.000	15.000	12.116	8.291	4.989	2.416	0.002
8.10	15.000	15.000	15.000	15.000	15.000	15.000	15.000	12.625	8.682	5.259	2.543	0.001
8.20	15.000	15.000	15.000	15.000	15.000	15.000	15.000	13.129	9.068	5.527	2.667	0.001
8.30	15.000	15.000	15.000	15.000	15.000	15.000	15.000	13.630	9.451	5.792	2.792	0.001
8.40	15.000	15.000	15.000	15.000	15.000	15.000	15.000	14.130	9.834	6.058	2.916	0.001
8.50	15.000	15.000	15.000	15.000	15.000	15.000	15.000	14.630	10.219	6.325	3.042	0.000
8.60	15.000	15.000	15.000	15.000	15.000	15.000	15.000	15.000	10.605	6.596	3.169	0.000
8.70	15.000	15.000	15.000	15.000	15.000	15.000	15.000	15.000	10.995	6.871	3.300	0.000
8.80	15.000	15.000	15.000	15.000	15.000	15.000	15.000	15.000	11.391	7.152	3.433	0.000
8.90	15.000	15.000	15.000	15.000	15.000	15.000	15.000	15.000	11.792	7.440	3.571	0.000
9.00	15.000	15.000	15.000	15.000	15.000	15.000	15.000	15.000	12.200	7.735	3.712	0.000

Note. — Same as Table 3 but for sodium.

Table 13. Magnesium CIE Fractional Abundances

log(T)	Mg ⁰⁺	Mg ¹⁺	Mg ²⁺	Mg ³⁺	Mg ⁴⁺	Mg ⁵⁺	Mg ⁶⁺	Mg ⁷⁺	Mg ⁸⁺	Mg ⁹⁺	Mg ¹⁰⁺	Mg ¹¹⁺	Mg ¹²⁺
4.00	0.272	0.333	4.014	15.000	15.000	15.000	15.000	15.000	15.000	15.000	15.000	15.000	15.000
4.10	0.616	0.125	2.118	15.000	15.000	15.000	15.000	15.000	15.000	15.000	15.000	15.000	15.000
4.20	1.093	0.129	0.754	15.000	15.000	15.000	15.000	15.000	15.000	15.000	15.000	15.000	15.000
4.30	1.991	0.614	0.127	15.000	15.000	15.000	15.000	15.000	15.000	15.000	15.000	15.000	15.000
4.40	3.156	1.413	0.017	12.784	15.000	15.000	15.000	15.000	15.000	15.000	15.000	15.000	15.000
4.50	4.215	2.146	0.003	9.795	15.000	15.000	15.000	15.000	15.000	15.000	15.000	15.000	15.000
4.60	5.125	2.761	0.001	7.040	15.000	15.000	15.000	15.000	15.000	15.000	15.000	15.000	15.000
4.70	5.904	3.273	0.000	4.844	13.296	15.000	15.000	15.000	15.000	15.000	15.000	15.000	15.000
4.80	6.567	3.689	0.000	3.124	9.250	15.000	15.000	15.000	15.000	15.000	15.000	15.000	15.000
4.90	7.097	3.992	0.006	1.836	6.171	13.637	15.000	15.000	15.000	15.000	15.000	15.000	15.000
5.00	7.488	4.171	0.054	0.930	3.891	9.485	15.000	15.000	15.000	15.000	15.000	15.000	15.000
5.10	7.864	4.350	0.236	0.383	2.268	6.370	12.364	15.000	15.000	15.000	15.000	15.000	15.000
5.20	8.367	4.668	0.603	0.164	1.185	4.080	8.509	14.650	15.000	15.000	15.000	15.000	15.000
5.30	9.034	5.161	1.133	0.207	0.520	2.424	5.592	10.209	15.000	15.000	15.000	15.000	15.000
5.40	9.892	5.852	1.832	0.489	0.214	1.298	3.440	6.820	11.419	15.000	15.000	15.000	15.000
5.50	10.919	6.721	2.677	0.970	0.201	0.604	1.907	4.276	7.679	12.197	15.000	15.000	15.000
5.60	12.125	7.777	3.681	1.652	0.461	0.296	0.914	2.454	4.872	8.185	11.548	15.000	15.000
5.70	13.533	9.039	4.868	2.548	0.990	0.351	0.405	1.264	2.866	5.193	7.480	15.000	15.000
5.80	15.000	10.487	6.220	3.633	1.754	0.711	0.299	0.594	1.517	3.036	4.444	15.000	15.000
5.90	15.000	12.108	7.732	4.898	2.730	1.342	0.537	0.360	0.714	1.569	2.255	12.993	15.000
6.00	15.000	13.985	9.487	6.423	3.994	2.302	1.158	0.583	0.456	0.761	0.851	9.171	15.000
6.10	15.000	15.000	11.615	8.334	5.665	3.703	2.262	1.343	0.806	0.651	0.244	6.620	14.358
6.20	15.000	15.000	13.847	10.360	7.468	5.262	3.556	2.335	1.445	0.899	0.079	4.887	10.894
6.30	15.000	15.000	15.000	12.238	9.138	6.710	4.763	3.273	2.073	1.191	0.033	3.575	8.182
6.40	15.000	15.000	15.000	13.913	10.618	7.983	5.816	4.083	2.609	1.434	0.019	2.541	6.013
6.50	15.000	15.000	15.000	15.000	11.912	9.085	6.715	4.760	3.041	1.611	0.020	1.728	4.274
6.60	15.000	15.000	15.000	15.000	13.064	10.057	7.495	5.335	3.397	1.746	0.044	1.110	2.898
6.70	15.000	15.000	15.000	15.000	14.144	10.965	8.224	5.873	3.737	1.894	0.118	0.677	1.838
6.80	15.000	15.000	15.000	15.000	11.884	8.973	6.442	4.124	2.113	0.274	0.427	1.067	
6.90	15.000	15.000	15.000	15.000	12.871	9.799	7.098	4.612	2.450	0.544	0.360	0.562	
7.00	15.000	15.000	15.000	15.000	15.000	13.938	10.711	7.848	5.205	2.904	0.921	0.450	0.281
7.10	15.000	15.000	15.000	15.000	15.000	15.000	11.667	8.649	5.858	3.425	1.355	0.629	0.142
7.20	15.000	15.000	15.000	15.000	15.000	15.000	12.620	9.453	6.521	3.960	1.794	0.838	0.076
7.30	15.000	15.000	15.000	15.000	15.000	15.000	13.549	10.239	7.171	4.484	2.214	1.046	0.044
7.40	15.000	15.000	15.000	15.000	15.000	14.448	10.999	7.798	4.987	2.607	1.242	0.027	
7.50	15.000	15.000	15.000	15.000	15.000	15.000	11.734	8.404	5.468	2.973	1.424	0.017	
7.60	15.000	15.000	15.000	15.000	15.000	15.000	12.445	8.988	5.928	3.317	1.592	0.011	
7.70	15.000	15.000	15.000	15.000	15.000	15.000	13.136	9.554	6.371	3.639	1.749	0.008	
7.80	15.000	15.000	15.000	15.000	15.000	15.000	13.809	10.103	6.797	3.946	1.896	0.006	
7.90	15.000	15.000	15.000	15.000	15.000	15.000	14.465	10.639	7.211	4.238	2.035	0.004	
8.00	15.000	15.000	15.000	15.000	15.000	15.000	15.000	11.162	7.613	4.520	2.168	0.003	
8.10	15.000	15.000	15.000	15.000	15.000	15.000	15.000	11.676	8.007	4.794	2.296	0.002	
8.20	15.000	15.000	15.000	15.000	15.000	15.000	15.000	12.183	8.395	5.063	2.422	0.002	
8.30	15.000	15.000	15.000	15.000	15.000	15.000	15.000	12.685	8.779	5.328	2.547	0.001	
8.40	15.000	15.000	15.000	15.000	15.000	15.000	15.000	13.184	9.160	5.592	2.670	0.001	
8.50	15.000	15.000	15.000	15.000	15.000	15.000	15.000	13.682	9.542	5.857	2.795	0.001	
8.60	15.000	15.000	15.000	15.000	15.000	15.000	15.000	14.181	9.925	6.124	2.921	0.001	
8.70	15.000	15.000	15.000	15.000	15.000	15.000	15.000	14.682	10.311	6.395	3.049	0.000	
8.80	15.000	15.000	15.000	15.000	15.000	15.000	15.000	15.000	10.701	6.670	3.180	0.000	
8.90	15.000	15.000	15.000	15.000	15.000	15.000	15.000	15.000	11.096	6.952	3.315	0.000	
9.00	15.000	15.000	15.000	15.000	15.000	15.000	15.000	15.000	11.497	7.240	3.453	0.000	

Note. — Same as Table 3 but for magnesium.

Table 20. Potassium CIE Fractional Abundances

Table 20—Continued

log(T)	K ¹⁰⁺	K ¹¹⁺	K ¹²⁺	K ¹³⁺	K ¹⁴⁺	K ¹⁵⁺	K ¹⁶⁺	K ¹⁷⁺	K ¹⁸⁺	K ¹⁹⁺
4.00	15.000	15.000	15.000	15.000	15.000	15.000	15.000	15.000	15.000	15.000
4.10	15.000	15.000	15.000	15.000	15.000	15.000	15.000	15.000	15.000	15.000
4.20	15.000	15.000	15.000	15.000	15.000	15.000	15.000	15.000	15.000	15.000
4.30	15.000	15.000	15.000	15.000	15.000	15.000	15.000	15.000	15.000	15.000
4.40	15.000	15.000	15.000	15.000	15.000	15.000	15.000	15.000	15.000	15.000
4.50	15.000	15.000	15.000	15.000	15.000	15.000	15.000	15.000	15.000	15.000
4.60	15.000	15.000	15.000	15.000	15.000	15.000	15.000	15.000	15.000	15.000
4.70	15.000	15.000	15.000	15.000	15.000	15.000	15.000	15.000	15.000	15.000
4.80	15.000	15.000	15.000	15.000	15.000	15.000	15.000	15.000	15.000	15.000
4.90	15.000	15.000	15.000	15.000	15.000	15.000	15.000	15.000	15.000	15.000
5.00	15.000	15.000	15.000	15.000	15.000	15.000	15.000	15.000	15.000	15.000
5.10	15.000	15.000	15.000	15.000	15.000	15.000	15.000	15.000	15.000	15.000
5.20	15.000	15.000	15.000	15.000	15.000	15.000	15.000	15.000	15.000	15.000
5.30	15.000	15.000	15.000	15.000	15.000	15.000	15.000	15.000	15.000	15.000
5.40	15.000	15.000	15.000	15.000	15.000	15.000	15.000	15.000	15.000	15.000
5.50	10.821	15.000	15.000	15.000	15.000	15.000	15.000	15.000	15.000	15.000
5.60	6.966	13.130	15.000	15.000	15.000	15.000	15.000	15.000	15.000	15.000
5.70	4.287	8.918	14.684	15.000	15.000	15.000	15.000	15.000	15.000	15.000
5.80	2.749	6.155	10.516	15.000	15.000	15.000	15.000	15.000	15.000	15.000
5.90	1.820	4.253	7.482	11.366	15.000	15.000	15.000	15.000	15.000	15.000
6.00	1.167	2.830	5.156	8.023	11.557	15.000	15.000	15.000	15.000	15.000
6.10	0.710	1.764	3.373	5.431	8.047	11.190	14.806	15.000	15.000	15.000
6.20	0.447	1.009	2.044	3.459	5.340	7.646	10.342	13.069	15.000	15.000
6.30	0.409	0.562	1.131	2.027	3.316	4.936	6.887	8.819	15.000	15.000
6.40	0.638	0.441	0.620	1.088	1.891	2.947	4.292	5.568	15.000	15.000
6.50	1.159	0.654	0.498	0.603	1.000	1.585	2.431	3.164	10.675	15.000
6.60	2.008	1.225	0.776	0.566	0.614	0.802	1.230	1.509	7.390	14.178
6.70	3.267	2.232	1.519	1.029	0.773	0.619	0.689	0.591	5.156	10.543
6.80	4.827	3.557	2.605	1.864	1.336	0.884	0.644	0.237	3.735	7.988
6.90	6.399	4.912	3.740	2.770	1.997	1.279	0.770	0.117	2.753	6.080
7.00	7.861	6.171	4.795	3.614	2.617	1.663	0.916	0.073	2.012	4.580
7.10	9.207	7.325	5.758	4.381	3.177	2.010	1.054	0.063	1.437	3.378
7.20	10.467	8.404	6.657	5.097	3.699	2.339	1.197	0.083	0.994	2.414
7.30	11.684	9.448	7.531	5.796	4.217	2.679	1.369	0.144	0.669	1.653
7.40	12.897	10.497	8.417	6.518	4.766	3.064	1.597	0.264	0.462	1.076
7.50	14.135	11.578	9.343	7.286	5.372	3.514	1.900	0.458	0.372	0.670
7.60	15.000	12.698	10.313	8.105	6.035	4.029	2.275	0.720	0.384	0.408
7.70	15.000	13.837	11.308	8.956	6.735	4.588	2.698	1.028	0.466	0.250
7.80	15.000	14.975	12.306	9.813	7.449	5.165	3.141	1.354	0.586	0.157
7.90	15.000	15.000	13.291	10.662	8.158	5.741	3.587	1.680	0.723	0.103
8.00	15.000	15.000	14.256	11.494	8.855	6.308	4.024	1.998	0.864	0.069
8.10	15.000	15.000	15.000	12.307	9.536	6.861	4.451	2.304	1.003	0.048
8.20	15.000	15.000	15.000	13.101	10.201	7.401	4.866	2.598	1.139	0.034
8.30	15.000	15.000	15.000	13.879	10.852	7.929	5.270	2.882	1.272	0.024
8.40	15.000	15.000	15.000	14.641	11.491	8.446	5.665	3.159	1.402	0.018
8.50	15.000	15.000	15.000	15.000	12.119	8.955	6.053	3.429	1.529	0.013
8.60	15.000	15.000	15.000	15.000	12.741	9.458	6.437	3.697	1.656	0.010
8.70	15.000	15.000	15.000	15.000	13.356	9.957	6.818	3.962	1.782	0.007
8.80	15.000	15.000	15.000	15.000	13.969	10.455	7.199	4.229	1.910	0.005
8.90	15.000	15.000	15.000	15.000	14.582	10.953	7.582	4.498	2.039	0.004
9.00	15.000	15.000	15.000	15.000	15.000	11.453	7.967	4.770	2.170	0.003

Note. — Same as Table 15 but for potassium.

Table 21. Calcium CIE Fractional Abundances

Table 21—Continued

log(T)	Ca ¹¹⁺	Ca ¹²⁺	Ca ¹³⁺	Ca ¹⁴⁺	Ca ¹⁵⁺	Ca ¹⁶⁺	Ca ¹⁷⁺	Ca ¹⁸⁺	Ca ¹⁹⁺	Ca ²⁰⁺
4.00	15.000	15.000	15.000	15.000	15.000	15.000	15.000	15.000	15.000	15.000
4.10	15.000	15.000	15.000	15.000	15.000	15.000	15.000	15.000	15.000	15.000
4.20	15.000	15.000	15.000	15.000	15.000	15.000	15.000	15.000	15.000	15.000
4.30	15.000	15.000	15.000	15.000	15.000	15.000	15.000	15.000	15.000	15.000
4.40	15.000	15.000	15.000	15.000	15.000	15.000	15.000	15.000	15.000	15.000
4.50	15.000	15.000	15.000	15.000	15.000	15.000	15.000	15.000	15.000	15.000
4.60	15.000	15.000	15.000	15.000	15.000	15.000	15.000	15.000	15.000	15.000
4.70	15.000	15.000	15.000	15.000	15.000	15.000	15.000	15.000	15.000	15.000
4.80	15.000	15.000	15.000	15.000	15.000	15.000	15.000	15.000	15.000	15.000
4.90	15.000	15.000	15.000	15.000	15.000	15.000	15.000	15.000	15.000	15.000
5.00	15.000	15.000	15.000	15.000	15.000	15.000	15.000	15.000	15.000	15.000
5.10	15.000	15.000	15.000	15.000	15.000	15.000	15.000	15.000	15.000	15.000
5.20	15.000	15.000	15.000	15.000	15.000	15.000	15.000	15.000	15.000	15.000
5.30	15.000	15.000	15.000	15.000	15.000	15.000	15.000	15.000	15.000	15.000
5.40	11.544	15.000	15.000	15.000	15.000	15.000	15.000	15.000	15.000	15.000
5.50	7.713	15.000	15.000	15.000	15.000	15.000	15.000	15.000	15.000	15.000
5.60	4.671	10.899	15.000	15.000	15.000	15.000	15.000	15.000	15.000	15.000
5.70	2.354	7.006	12.708	15.000	15.000	15.000	15.000	15.000	15.000	15.000
5.80	0.847	4.254	8.535	13.807	15.000	15.000	15.000	15.000	15.000	15.000
5.90	0.245	2.674	5.826	9.807	14.462	15.000	15.000	15.000	15.000	15.000
6.00	0.102	1.769	4.029	6.975	10.477	14.681	15.000	15.000	15.000	15.000
6.10	0.083	1.151	2.707	4.828	7.412	10.588	14.322	15.000	15.000	15.000
6.20	0.134	0.719	1.714	3.181	5.035	7.386	10.187	13.397	15.000	15.000
6.30	0.283	0.466	1.002	1.943	3.215	4.902	6.942	9.324	11.723	15.000
6.40	0.590	0.427	0.577	1.086	1.882	3.029	4.445	6.158	7.837	15.000
6.50	1.123	0.655	0.470	0.614	1.011	1.711	2.612	3.775	4.860	13.344
6.60	1.931	1.188	0.705	0.533	0.588	0.910	1.378	2.084	2.673	9.357
6.70	3.073	2.080	1.329	0.876	0.632	0.626	0.723	1.042	1.217	6.449
6.80	4.618	3.393	2.397	1.690	1.179	0.884	0.660	0.645	0.478	4.534
6.90	6.373	4.934	3.709	2.771	2.018	1.463	0.957	0.652	0.207	3.311
7.00	8.084	6.444	5.007	3.856	2.881	2.091	1.334	0.776	0.112	2.445
7.10	9.675	7.846	6.210	4.861	3.681	2.674	1.694	0.913	0.076	1.784
7.20	11.154	9.147	7.322	5.788	4.417	3.210	2.027	1.048	0.073	1.270
7.30	12.556	10.381	8.378	6.667	5.117	3.721	2.354	1.198	0.101	0.877
7.40	13.921	11.586	9.413	7.535	5.815	4.243	2.704	1.385	0.175	0.595
7.50	15.000	12.796	10.462	8.425	6.543	4.803	3.104	1.633	0.311	0.426
7.60	15.000	14.034	11.545	9.354	7.318	5.418	3.568	1.952	0.517	0.365
7.70	15.000	15.000	12.659	10.321	8.136	6.083	4.088	2.334	0.783	0.394
7.80	15.000	15.000	13.785	11.306	8.978	6.778	4.643	2.753	1.085	0.480
7.90	15.000	15.000	14.905	12.288	9.821	7.480	5.210	3.187	1.399	0.598
8.00	15.000	15.000	15.000	13.256	10.655	8.175	5.774	3.621	1.713	0.730
8.10	15.000	15.000	15.000	14.204	11.471	8.858	6.328	4.048	2.019	0.865
8.20	15.000	15.000	15.000	15.000	12.271	9.527	6.870	4.464	2.314	0.999
8.30	15.000	15.000	15.000	15.000	13.053	10.181	7.400	4.869	2.600	1.131
8.40	15.000	15.000	15.000	15.000	13.819	10.823	7.919	5.266	2.877	1.260
8.50	15.000	15.000	15.000	15.000	14.572	11.453	8.429	5.655	3.148	1.387
8.60	15.000	15.000	15.000	15.000	15.000	12.075	8.932	6.038	3.415	1.513
8.70	15.000	15.000	15.000	15.000	15.000	12.691	9.431	6.419	3.680	1.639
8.80	15.000	15.000	15.000	15.000	15.000	13.303	9.927	6.798	3.945	1.766
8.90	15.000	15.000	15.000	15.000	15.000	13.914	10.423	7.178	4.212	1.893
9.00	15.000	15.000	15.000	15.000	15.000	14.525	10.921	7.561	4.482	2.023

Note. — Same as Table 15 but for calcium.

Table 22. Scandium CIE Fractional Abundances

Table 22—Continued

$\log(T)$	Sc ¹¹⁺	Sc ¹²⁺	Sc ¹³⁺	Sc ¹⁴⁺	Sc ¹⁵⁺	Sc ¹⁶⁺	Sc ¹⁷⁺	Sc ¹⁸⁺	Sc ¹⁹⁺	Sc ²⁰⁺	Sc ²¹⁺
4.00	15.000	15.000	15.000	15.000	15.000	15.000	15.000	15.000	15.000	15.000	15.000
4.10	15.000	15.000	15.000	15.000	15.000	15.000	15.000	15.000	15.000	15.000	15.000
4.20	15.000	15.000	15.000	15.000	15.000	15.000	15.000	15.000	15.000	15.000	15.000
4.30	15.000	15.000	15.000	15.000	15.000	15.000	15.000	15.000	15.000	15.000	15.000
4.40	15.000	15.000	15.000	15.000	15.000	15.000	15.000	15.000	15.000	15.000	15.000
4.50	15.000	15.000	15.000	15.000	15.000	15.000	15.000	15.000	15.000	15.000	15.000
4.60	15.000	15.000	15.000	15.000	15.000	15.000	15.000	15.000	15.000	15.000	15.000
4.70	15.000	15.000	15.000	15.000	15.000	15.000	15.000	15.000	15.000	15.000	15.000
4.80	15.000	15.000	15.000	15.000	15.000	15.000	15.000	15.000	15.000	15.000	15.000
4.90	15.000	15.000	15.000	15.000	15.000	15.000	15.000	15.000	15.000	15.000	15.000
5.00	15.000	15.000	15.000	15.000	15.000	15.000	15.000	15.000	15.000	15.000	15.000
5.10	15.000	15.000	15.000	15.000	15.000	15.000	15.000	15.000	15.000	15.000	15.000
5.20	15.000	15.000	15.000	15.000	15.000	15.000	15.000	15.000	15.000	15.000	15.000
5.30	15.000	15.000	15.000	15.000	15.000	15.000	15.000	15.000	15.000	15.000	15.000
5.40	15.000	15.000	15.000	15.000	15.000	15.000	15.000	15.000	15.000	15.000	15.000
5.50	11.859	15.000	15.000	15.000	15.000	15.000	15.000	15.000	15.000	15.000	15.000
5.60	7.871	15.000	15.000	15.000	15.000	15.000	15.000	15.000	15.000	15.000	15.000
5.70	4.764	10.536	15.000	15.000	15.000	15.000	15.000	15.000	15.000	15.000	15.000
5.80	2.420	6.733	11.937	15.000	15.000	15.000	15.000	15.000	15.000	15.000	15.000
5.90	0.894	4.057	7.959	12.744	15.000	15.000	15.000	15.000	15.000	15.000	15.000
6.00	0.274	2.540	5.407	9.008	13.222	15.000	15.000	15.000	15.000	15.000	15.000
6.10	0.121	1.687	3.740	6.399	9.566	13.314	15.000	15.000	15.000	15.000	15.000
6.20	0.097	1.110	2.520	4.433	6.768	9.590	12.896	15.000	15.000	15.000	15.000
6.30	0.147	0.707	1.601	2.922	4.593	6.674	9.138	11.956	14.832	15.000	15.000
6.40	0.297	0.476	0.943	1.783	2.920	4.402	6.180	8.259	10.347	15.000	15.000
6.50	0.610	0.457	0.563	1.002	1.697	2.689	3.902	5.379	6.818	15.000	15.000
6.60	1.155	0.706	0.498	0.594	0.916	1.498	2.240	3.221	4.121	11.637	15.000
6.70	1.989	1.275	0.787	0.583	0.581	0.811	1.156	1.721	2.171	8.091	14.859
6.80	3.195	2.236	1.496	1.025	0.737	0.659	0.662	0.872	0.947	5.577	10.982
6.90	4.778	3.594	2.623	1.910	1.365	1.013	0.717	0.619	0.384	3.970	8.268
7.00	6.483	5.089	3.906	2.972	2.194	1.594	1.033	0.667	0.182	2.921	6.316
7.10	8.118	6.527	5.147	4.008	3.015	2.190	1.392	0.789	0.107	2.158	4.813
7.20	9.640	7.864	6.298	4.969	3.778	2.743	1.733	0.920	0.080	1.571	3.615
7.30	11.067	9.117	7.376	5.867	4.490	3.262	2.058	1.057	0.084	1.115	2.650
7.40	12.434	10.319	8.412	6.733	5.181	3.770	2.389	1.216	0.124	0.769	1.877
7.50	13.778	11.506	9.440	7.599	5.880	4.297	2.751	1.420	0.213	0.531	1.276
7.60	15.000	12.706	10.488	8.492	6.615	4.868	3.166	1.687	0.365	0.398	0.832
7.70	15.000	13.932	11.568	9.424	7.395	5.491	3.641	2.020	0.582	0.364	0.529
7.80	15.000	15.000	12.672	10.385	8.209	6.156	4.164	2.405	0.850	0.407	0.335
7.90	15.000	15.000	13.782	11.356	9.040	6.843	4.713	2.821	1.145	0.497	0.216
8.00	15.000	15.000	14.883	12.322	9.869	7.533	5.270	3.246	1.450	0.614	0.142
8.10	15.000	15.000	15.000	13.273	10.687	8.215	5.822	3.669	1.753	0.741	0.097
8.20	15.000	15.000	15.000	14.206	11.490	8.886	6.365	4.085	2.048	0.871	0.067
8.30	15.000	15.000	15.000	15.000	12.276	9.543	6.897	4.492	2.335	1.001	0.048
8.40	15.000	15.000	15.000	15.000	13.047	10.188	7.419	4.890	2.613	1.130	0.035
8.50	15.000	15.000	15.000	15.000	13.803	10.821	7.930	5.280	2.885	1.257	0.025
8.60	15.000	15.000	15.000	15.000	14.548	11.445	8.435	5.665	3.153	1.383	0.019
8.70	15.000	15.000	15.000	15.000	15.000	12.062	8.934	6.045	3.418	1.509	0.014
8.80	15.000	15.000	15.000	15.000	15.000	12.674	9.430	6.424	3.682	1.635	0.010
8.90	15.000	15.000	15.000	15.000	15.000	13.285	9.926	6.803	3.948	1.763	0.008
9.00	15.000	15.000	15.000	15.000	15.000	13.895	10.422	7.185	4.217	1.893	0.006

Note. — Same as Table 15 but for scandium.

Table 23. Titanium CIE Fractional Abundances

Table 23—Continued

log(T)	Ti ¹²⁺	Ti ¹³⁺	Ti ¹⁴⁺	Ti ¹⁵⁺	Ti ¹⁶⁺	Ti ¹⁷⁺	Ti ¹⁸⁺	Ti ¹⁹⁺	Ti ²⁰⁺	Ti ²¹⁺	Ti ²²⁺
4.00	15.000	15.000	15.000	15.000	15.000	15.000	15.000	15.000	15.000	15.000	15.000
4.10	15.000	15.000	15.000	15.000	15.000	15.000	15.000	15.000	15.000	15.000	15.000
4.20	15.000	15.000	15.000	15.000	15.000	15.000	15.000	15.000	15.000	15.000	15.000
4.30	15.000	15.000	15.000	15.000	15.000	15.000	15.000	15.000	15.000	15.000	15.000
4.40	15.000	15.000	15.000	15.000	15.000	15.000	15.000	15.000	15.000	15.000	15.000
4.50	15.000	15.000	15.000	15.000	15.000	15.000	15.000	15.000	15.000	15.000	15.000
4.60	15.000	15.000	15.000	15.000	15.000	15.000	15.000	15.000	15.000	15.000	15.000
4.70	15.000	15.000	15.000	15.000	15.000	15.000	15.000	15.000	15.000	15.000	15.000
4.80	15.000	15.000	15.000	15.000	15.000	15.000	15.000	15.000	15.000	15.000	15.000
4.90	15.000	15.000	15.000	15.000	15.000	15.000	15.000	15.000	15.000	15.000	15.000
5.00	15.000	15.000	15.000	15.000	15.000	15.000	15.000	15.000	15.000	15.000	15.000
5.10	15.000	15.000	15.000	15.000	15.000	15.000	15.000	15.000	15.000	15.000	15.000
5.20	15.000	15.000	15.000	15.000	15.000	15.000	15.000	15.000	15.000	15.000	15.000
5.30	15.000	15.000	15.000	15.000	15.000	15.000	15.000	15.000	15.000	15.000	15.000
5.40	15.000	15.000	15.000	15.000	15.000	15.000	15.000	15.000	15.000	15.000	15.000
5.50	15.000	15.000	15.000	15.000	15.000	15.000	15.000	15.000	15.000	15.000	15.000
5.60	11.788	15.000	15.000	15.000	15.000	15.000	15.000	15.000	15.000	15.000	15.000
5.70	7.638	14.578	15.000	15.000	15.000	15.000	15.000	15.000	15.000	15.000	15.000
5.80	4.538	9.791	15.000	15.000	15.000	15.000	15.000	15.000	15.000	15.000	15.000
5.90	2.271	6.193	10.907	15.000	15.000	15.000	15.000	15.000	15.000	15.000	15.000
6.00	0.830	3.713	7.240	11.509	15.000	15.000	15.000	15.000	15.000	15.000	15.000
6.10	0.270	2.345	4.938	8.148	11.943	15.000	15.000	15.000	15.000	15.000	15.000
6.20	0.130	1.572	3.431	5.804	8.655	12.012	15.000	15.000	15.000	15.000	15.000
6.30	0.110	1.044	2.320	4.026	6.127	8.650	11.562	14.835	15.000	15.000	15.000
6.40	0.165	0.676	1.478	2.648	4.147	6.001	8.157	10.619	13.123	15.000	15.000
6.50	0.324	0.474	0.879	1.608	2.616	3.926	5.462	7.266	9.064	15.000	15.000
6.60	0.653	0.487	0.550	0.907	1.503	2.363	3.387	4.651	5.865	14.241	15.000
6.70	1.227	0.777	0.540	0.575	0.819	1.297	1.892	2.705	3.432	10.063	15.000
6.80	2.117	1.410	0.904	0.655	0.591	0.738	0.965	1.397	1.717	6.938	12.943
6.90	3.413	2.469	1.720	1.215	0.876	0.732	0.640	0.743	0.725	4.804	9.606
7.00	5.030	3.866	2.894	2.157	1.569	1.163	0.791	0.607	0.313	3.466	7.287
7.10	6.691	5.323	4.145	3.194	2.379	1.735	1.114	0.679	0.162	2.564	5.584
7.20	8.266	6.706	5.336	4.187	3.162	2.300	1.456	0.799	0.104	1.893	4.253
7.30	9.740	7.999	6.448	5.114	3.894	2.829	1.783	0.928	0.086	1.373	3.185
7.40	11.135	9.225	7.503	5.994	4.589	3.336	2.105	1.072	0.100	0.970	2.323
7.50	12.487	10.415	8.530	6.855	5.277	3.846	2.444	1.247	0.153	0.671	1.637
7.60	13.825	11.600	9.559	7.725	5.983	4.384	2.821	1.471	0.259	0.474	1.109
7.70	15.000	12.802	10.611	8.626	6.726	4.967	3.253	1.757	0.427	0.377	0.726
7.80	15.000	14.026	11.691	9.560	7.510	5.598	3.739	2.103	0.653	0.367	0.468
7.90	15.000	15.000	12.788	10.515	8.320	6.262	4.264	2.491	0.922	0.422	0.302
8.00	15.000	15.000	13.885	11.475	9.140	6.940	4.807	2.901	1.211	0.516	0.199
8.10	15.000	15.000	14.969	12.426	9.955	7.618	5.353	3.318	1.506	0.631	0.134
8.20	15.000	15.000	15.000	13.362	10.759	8.288	5.894	3.731	1.798	0.755	0.093
8.30	15.000	15.000	15.000	14.280	11.547	8.947	6.426	4.137	2.084	0.881	0.065
8.40	15.000	15.000	15.000	15.000	12.321	9.593	6.948	4.536	2.363	1.008	0.047
8.50	15.000	15.000	15.000	15.000	13.081	10.228	7.461	4.926	2.636	1.135	0.034
8.60	15.000	15.000	15.000	15.000	13.828	10.854	7.967	5.311	2.904	1.260	0.025
8.70	15.000	15.000	15.000	15.000	14.566	11.472	8.466	5.692	3.169	1.386	0.019
8.80	15.000	15.000	15.000	15.000	15.000	12.085	8.962	6.070	3.433	1.512	0.014
8.90	15.000	15.000	15.000	15.000	15.000	12.695	9.457	6.449	3.698	1.640	0.010
9.00	15.000	15.000	15.000	15.000	15.000	13.304	9.952	6.829	3.966	1.770	0.007

Note. — Same as Table 15 but for titanium.

Table 24. Vanadium CIE Fractional Abundances

Table 24—Continued

log(T)	V ¹²⁺	V ¹³⁺	V ¹⁴⁺	V ¹⁵⁺	V ¹⁶⁺	V ¹⁷⁺	V ¹⁸⁺	V ¹⁹⁺	V ²⁰⁺	V ²¹⁺	V ²²⁺	V ²³⁺
4.00	15.000	15.000	15.000	15.000	15.000	15.000	15.000	15.000	15.000	15.000	15.000	15.000
4.10	15.000	15.000	15.000	15.000	15.000	15.000	15.000	15.000	15.000	15.000	15.000	15.000
4.20	15.000	15.000	15.000	15.000	15.000	15.000	15.000	15.000	15.000	15.000	15.000	15.000
4.30	15.000	15.000	15.000	15.000	15.000	15.000	15.000	15.000	15.000	15.000	15.000	15.000
4.40	15.000	15.000	15.000	15.000	15.000	15.000	15.000	15.000	15.000	15.000	15.000	15.000
4.50	15.000	15.000	15.000	15.000	15.000	15.000	15.000	15.000	15.000	15.000	15.000	15.000
4.60	15.000	15.000	15.000	15.000	15.000	15.000	15.000	15.000	15.000	15.000	15.000	15.000
4.70	15.000	15.000	15.000	15.000	15.000	15.000	15.000	15.000	15.000	15.000	15.000	15.000
4.80	15.000	15.000	15.000	15.000	15.000	15.000	15.000	15.000	15.000	15.000	15.000	15.000
4.90	15.000	15.000	15.000	15.000	15.000	15.000	15.000	15.000	15.000	15.000	15.000	15.000
5.00	15.000	15.000	15.000	15.000	15.000	15.000	15.000	15.000	15.000	15.000	15.000	15.000
5.10	15.000	15.000	15.000	15.000	15.000	15.000	15.000	15.000	15.000	15.000	15.000	15.000
5.20	15.000	15.000	15.000	15.000	15.000	15.000	15.000	15.000	15.000	15.000	15.000	15.000
5.30	15.000	15.000	15.000	15.000	15.000	15.000	15.000	15.000	15.000	15.000	15.000	15.000
5.40	15.000	15.000	15.000	15.000	15.000	15.000	15.000	15.000	15.000	15.000	15.000	15.000
5.50	15.000	15.000	15.000	15.000	15.000	15.000	15.000	15.000	15.000	15.000	15.000	15.000
5.60	13.026	15.000	15.000	15.000	15.000	15.000	15.000	15.000	15.000	15.000	15.000	15.000
5.70	8.996	11.185	15.000	15.000	15.000	15.000	15.000	15.000	15.000	15.000	15.000	15.000
5.80	5.865	7.228	13.481	15.000	15.000	15.000	15.000	15.000	15.000	15.000	15.000	15.000
5.90	3.502	4.212	8.940	14.534	15.000	15.000	15.000	15.000	15.000	15.000	15.000	15.000
6.00	1.788	2.017	5.551	9.792	14.787	15.000	15.000	15.000	15.000	15.000	15.000	15.000
6.10	0.833	0.710	3.316	6.484	10.289	14.728	15.000	15.000	15.000	15.000	15.000	15.000
6.20	0.646	0.252	2.135	4.463	7.321	10.701	14.598	15.000	15.000	15.000	15.000	15.000
6.30	0.754	0.136	1.444	3.111	5.220	7.756	10.727	14.097	15.000	15.000	15.000	15.000
6.40	0.940	0.124	0.963	2.101	3.612	5.475	7.701	10.243	13.100	15.000	15.000	15.000
6.50	1.187	0.189	0.633	1.335	2.361	3.678	5.304	7.169	9.306	11.467	15.000	15.000
6.60	1.537	0.368	0.469	0.801	1.422	2.289	3.421	4.729	6.278	7.807	15.000	15.000
6.70	2.063	0.728	0.527	0.537	0.811	1.297	2.015	2.859	3.921	4.925	12.288	15.000
6.80	2.848	1.352	0.877	0.602	0.573	0.728	1.092	1.543	2.195	2.761	8.588	15.000
6.90	3.985	2.330	1.607	1.075	0.775	0.638	0.692	0.804	1.106	1.304	5.890	11.207
7.00	5.538	3.726	2.774	2.007	1.463	1.064	0.842	0.657	0.655	0.550	4.129	8.385
7.10	7.315	5.349	4.184	3.201	2.433	1.796	1.325	0.878	0.609	0.257	3.018	6.408
7.20	9.076	6.958	5.594	4.411	3.437	2.581	1.883	1.201	0.697	0.146	2.241	4.919
7.30	10.744	8.476	6.925	5.555	4.388	3.330	2.422	1.529	0.817	0.102	1.652	3.741
7.40	12.321	9.906	8.179	6.632	5.285	4.037	2.935	1.849	0.950	0.093	1.193	2.791
7.50	13.833	11.273	9.381	7.665	6.147	4.721	3.436	2.173	1.103	0.119	0.840	2.025
7.60	15.000	12.609	10.559	8.684	7.004	5.408	3.951	2.523	1.295	0.188	0.586	1.420
7.70	15.000	13.941	11.741	9.713	7.877	6.121	4.500	2.916	1.539	0.312	0.429	0.961
7.80	15.000	15.000	12.940	10.765	8.781	6.871	5.094	3.363	1.842	0.495	0.364	0.634
7.90	15.000	15.000	14.157	11.840	9.712	7.655	5.728	3.855	2.197	0.729	0.375	0.414
8.00	15.000	15.000	15.000	12.925	10.658	8.458	6.388	4.378	2.585	0.996	0.440	0.273
8.10	15.000	15.000	15.000	14.005	11.603	9.266	7.057	4.913	2.989	1.279	0.537	0.183
8.20	15.000	15.000	15.000	15.000	12.538	10.067	7.723	5.449	3.397	1.565	0.650	0.126
8.30	15.000	15.000	15.000	15.000	13.457	10.856	8.380	5.980	3.800	1.848	0.771	0.088
8.40	15.000	15.000	15.000	15.000	14.360	11.632	9.028	6.502	4.198	2.126	0.894	0.063
8.50	15.000	15.000	15.000	15.000	15.000	12.393	9.664	7.015	4.589	2.398	1.019	0.046
8.60	15.000	15.000	15.000	15.000	15.000	13.143	10.291	7.521	4.974	2.666	1.144	0.033
8.70	15.000	15.000	15.000	15.000	15.000	13.883	10.909	8.021	5.354	2.931	1.269	0.025
8.80	15.000	15.000	15.000	15.000	15.000	14.615	11.523	8.517	5.732	3.195	1.395	0.018
8.90	15.000	15.000	15.000	15.000	15.000	15.000	12.133	9.011	6.110	3.459	1.523	0.013
9.00	15.000	15.000	15.000	15.000	15.000	15.000	12.741	9.505	6.489	3.726	1.652	0.010

Note. — Same as Table 15 but for vanadium.

Table 25. Chromium CIE Fractional Abundances

Table 25—Continued

log(T)	Cr ¹³⁺	Cr ¹⁴⁺	Cr ¹⁵⁺	Cr ¹⁶⁺	Cr ¹⁷⁺	Cr ¹⁸⁺	Cr ¹⁹⁺	Cr ²⁰⁺	Cr ²¹⁺	Cr ²²⁺	Cr ²³⁺	Cr ²⁴⁺
4.00	15.000	15.000	15.000	15.000	15.000	15.000	15.000	15.000	15.000	15.000	15.000	15.000
4.10	15.000	15.000	15.000	15.000	15.000	15.000	15.000	15.000	15.000	15.000	15.000	15.000
4.20	15.000	15.000	15.000	15.000	15.000	15.000	15.000	15.000	15.000	15.000	15.000	15.000
4.30	15.000	15.000	15.000	15.000	15.000	15.000	15.000	15.000	15.000	15.000	15.000	15.000
4.40	15.000	15.000	15.000	15.000	15.000	15.000	15.000	15.000	15.000	15.000	15.000	15.000
4.50	15.000	15.000	15.000	15.000	15.000	15.000	15.000	15.000	15.000	15.000	15.000	15.000
4.60	15.000	15.000	15.000	15.000	15.000	15.000	15.000	15.000	15.000	15.000	15.000	15.000
4.70	15.000	15.000	15.000	15.000	15.000	15.000	15.000	15.000	15.000	15.000	15.000	15.000
4.80	15.000	15.000	15.000	15.000	15.000	15.000	15.000	15.000	15.000	15.000	15.000	15.000
4.90	15.000	15.000	15.000	15.000	15.000	15.000	15.000	15.000	15.000	15.000	15.000	15.000
5.00	15.000	15.000	15.000	15.000	15.000	15.000	15.000	15.000	15.000	15.000	15.000	15.000
5.10	15.000	15.000	15.000	15.000	15.000	15.000	15.000	15.000	15.000	15.000	15.000	15.000
5.20	15.000	15.000	15.000	15.000	15.000	15.000	15.000	15.000	15.000	15.000	15.000	15.000
5.30	15.000	15.000	15.000	15.000	15.000	15.000	15.000	15.000	15.000	15.000	15.000	15.000
5.40	15.000	15.000	15.000	15.000	15.000	15.000	15.000	15.000	15.000	15.000	15.000	15.000
5.50	15.000	15.000	15.000	15.000	15.000	15.000	15.000	15.000	15.000	15.000	15.000	15.000
5.60	15.000	15.000	15.000	15.000	15.000	15.000	15.000	15.000	15.000	15.000	15.000	15.000
5.70	12.294	15.000	15.000	15.000	15.000	15.000	15.000	15.000	15.000	15.000	15.000	15.000
5.80	8.285	10.222	15.000	15.000	15.000	15.000	15.000	15.000	15.000	15.000	15.000	15.000
5.90	5.200	6.382	11.932	15.000	15.000	15.000	15.000	15.000	15.000	15.000	15.000	15.000
6.00	2.983	3.587	7.785	12.827	15.000	15.000	15.000	15.000	15.000	15.000	15.000	15.000
6.10	1.478	1.660	4.804	8.646	13.087	15.000	15.000	15.000	15.000	15.000	15.000	15.000
6.20	0.727	0.594	2.921	5.819	9.204	13.075	15.000	15.000	15.000	15.000	15.000	15.000
6.30	0.623	0.240	1.923	4.079	6.625	9.570	13.016	15.000	15.000	15.000	15.000	15.000
6.40	0.741	0.144	1.308	2.873	4.752	6.957	9.581	12.501	15.000	15.000	15.000	15.000
6.50	0.931	0.142	0.874	1.955	3.296	4.906	6.867	9.054	11.535	14.066	15.000	15.000
6.60	1.186	0.218	0.581	1.257	2.153	3.275	4.694	6.281	8.122	9.971	15.000	15.000
6.70	1.549	0.412	0.451	0.777	1.296	2.008	2.977	4.067	5.381	6.665	14.783	15.000
6.80	2.099	0.796	0.546	0.566	0.758	1.117	1.704	2.375	3.250	4.061	10.514	15.000
6.90	2.943	1.479	0.967	0.712	0.614	0.665	0.921	1.233	1.733	2.151	7.257	13.101
7.00	4.197	2.575	1.823	1.319	0.960	0.735	0.699	0.699	0.877	0.965	4.980	9.679
7.10	5.837	4.059	3.085	2.354	1.757	1.283	0.985	0.710	0.605	0.423	3.551	7.317
7.20	7.599	5.667	4.487	3.545	2.730	2.028	1.493	0.972	0.620	0.217	2.624	5.624
7.30	9.308	7.225	5.851	4.713	3.695	2.784	2.031	1.290	0.718	0.134	1.951	4.320
7.40	10.928	8.695	7.140	5.817	4.610	3.503	2.548	1.608	0.840	0.102	1.433	3.277
7.50	12.471	10.091	8.365	6.868	5.481	4.191	3.048	1.925	0.979	0.105	1.030	2.434
7.60	13.963	11.439	9.552	7.889	6.333	4.869	3.549	2.256	1.146	0.145	0.725	1.756
7.70	15.000	12.767	10.726	8.905	7.187	5.560	4.072	2.619	1.356	0.231	0.514	1.226
7.80	15.000	14.096	11.908	9.935	8.064	6.280	4.632	3.029	1.620	0.372	0.395	0.831
7.90	15.000	15.000	13.107	10.988	8.969	7.035	5.235	3.488	1.938	0.568	0.359	0.552
8.00	15.000	15.000	14.318	12.058	9.896	7.818	5.872	3.985	2.299	0.807	0.388	0.367
8.10	15.000	15.000	15.000	13.131	10.831	8.613	6.526	4.504	2.686	1.072	0.461	0.246
8.20	15.000	15.000	15.000	14.196	11.762	9.409	7.185	5.031	3.084	1.348	0.560	0.168
8.30	15.000	15.000	15.000	15.000	12.682	10.197	7.840	5.558	3.483	1.627	0.672	0.117
8.40	15.000	15.000	15.000	15.000	13.587	10.973	8.487	6.078	3.878	1.902	0.791	0.083
8.50	15.000	15.000	15.000	15.000	14.476	11.736	9.124	6.592	4.268	2.174	0.913	0.060
8.60	15.000	15.000	15.000	15.000	15.000	12.488	9.752	7.098	4.652	2.441	1.036	0.044
8.70	15.000	15.000	15.000	15.000	15.000	13.229	10.371	7.598	5.033	2.706	1.160	0.032
8.80	15.000	15.000	15.000	15.000	15.000	13.963	10.985	8.093	5.411	2.969	1.286	0.024
8.90	15.000	15.000	15.000	15.000	15.000	14.690	11.595	8.587	5.787	3.233	1.413	0.017
9.00	15.000	15.000	15.000	15.000	15.000	15.000	12.203	9.080	6.165	3.498	1.542	0.013

Note. — Same as Table 15 but for chromium.

Table 26. Manganese CIE Fractional Abundances

Table 26—Continued

log(T)	Mn ¹³⁺	Mn ¹⁴⁺	Mn ¹⁵⁺	Mn ¹⁶⁺	Mn ¹⁷⁺	Mn ¹⁸⁺	Mn ¹⁹⁺	Mn ²⁰⁺	Mn ²¹⁺	Mn ²²⁺	Mn ²³⁺	Mn ²⁴⁺	Mn ²⁵⁺
4.00	15.000	15.000	15.000	15.000	15.000	15.000	15.000	15.000	15.000	15.000	15.000	15.000	15.000
4.10	15.000	15.000	15.000	15.000	15.000	15.000	15.000	15.000	15.000	15.000	15.000	15.000	15.000
4.20	15.000	15.000	15.000	15.000	15.000	15.000	15.000	15.000	15.000	15.000	15.000	15.000	15.000
4.30	15.000	15.000	15.000	15.000	15.000	15.000	15.000	15.000	15.000	15.000	15.000	15.000	15.000
4.40	15.000	15.000	15.000	15.000	15.000	15.000	15.000	15.000	15.000	15.000	15.000	15.000	15.000
4.50	15.000	15.000	15.000	15.000	15.000	15.000	15.000	15.000	15.000	15.000	15.000	15.000	15.000
4.60	15.000	15.000	15.000	15.000	15.000	15.000	15.000	15.000	15.000	15.000	15.000	15.000	15.000
4.70	15.000	15.000	15.000	15.000	15.000	15.000	15.000	15.000	15.000	15.000	15.000	15.000	15.000
4.80	15.000	15.000	15.000	15.000	15.000	15.000	15.000	15.000	15.000	15.000	15.000	15.000	15.000
4.90	15.000	15.000	15.000	15.000	15.000	15.000	15.000	15.000	15.000	15.000	15.000	15.000	15.000
5.00	15.000	15.000	15.000	15.000	15.000	15.000	15.000	15.000	15.000	15.000	15.000	15.000	15.000
5.10	15.000	15.000	15.000	15.000	15.000	15.000	15.000	15.000	15.000	15.000	15.000	15.000	15.000
5.20	15.000	15.000	15.000	15.000	15.000	15.000	15.000	15.000	15.000	15.000	15.000	15.000	15.000
5.30	15.000	15.000	15.000	15.000	15.000	15.000	15.000	15.000	15.000	15.000	15.000	15.000	15.000
5.40	15.000	15.000	15.000	15.000	15.000	15.000	15.000	15.000	15.000	15.000	15.000	15.000	15.000
5.50	15.000	15.000	15.000	15.000	15.000	15.000	15.000	15.000	15.000	15.000	15.000	15.000	15.000
5.60	15.000	15.000	15.000	15.000	15.000	15.000	15.000	15.000	15.000	15.000	15.000	15.000	15.000
5.70	12.102	15.000	15.000	15.000	15.000	15.000	15.000	15.000	15.000	15.000	15.000	15.000	15.000
5.80	8.346	11.474	14.014	15.000	15.000	15.000	15.000	15.000	15.000	15.000	15.000	15.000	15.000
5.90	5.376	7.676	9.365	15.000	15.000	15.000	15.000	15.000	15.000	15.000	15.000	15.000	15.000
6.00	3.170	4.756	5.772	10.716	15.000	15.000	15.000	15.000	15.000	15.000	15.000	15.000	15.000
6.10	1.681	2.649	3.167	6.915	11.360	15.000	15.000	15.000	15.000	15.000	15.000	15.000	15.000
6.20	0.813	1.253	1.408	4.224	7.614	11.506	15.000	15.000	15.000	15.000	15.000	15.000	15.000
6.30	0.646	0.644	0.522	2.609	5.168	8.133	11.544	15.000	15.000	15.000	15.000	15.000	15.000
6.40	0.958	0.592	0.240	1.745	3.648	5.876	8.465	11.443	14.765	15.000	15.000	15.000	15.000
6.50	1.377	0.714	0.161	1.189	2.561	4.200	6.130	8.387	10.913	13.744	15.000	15.000	15.000
6.60	1.817	0.906	0.168	0.794	1.727	2.882	4.277	5.950	7.825	9.963	12.136	15.000	15.000
6.70	2.298	1.175	0.264	0.541	1.100	1.850	2.800	3.991	5.330	6.900	8.465	15.000	15.000
6.80	2.883	1.572	0.494	0.463	0.696	1.097	1.669	2.454	3.345	4.442	5.502	12.597	15.000
6.90	3.671	2.188	0.947	0.640	0.583	0.678	0.921	1.358	1.867	2.565	3.202	8.842	15.000
7.00	4.791	3.148	1.748	1.190	0.872	0.693	0.645	0.775	0.954	1.309	1.593	6.054	11.205
7.10	6.341	4.546	2.991	2.201	1.645	1.218	0.908	0.766	0.655	0.712	0.701	4.205	8.353
7.20	8.176	6.234	4.526	3.522	2.746	2.092	1.545	1.156	0.789	0.585	0.330	3.055	6.383
7.30	10.040	7.955	6.097	4.894	3.914	3.050	2.285	1.670	1.073	0.639	0.185	2.274	4.926
7.40	11.830	9.605	7.599	6.209	5.039	3.979	3.012	2.189	1.385	0.746	0.124	1.690	3.782
7.50	13.535	11.173	9.021	7.455	6.106	4.863	3.706	2.691	1.697	0.872	0.106	1.236	2.860
7.60	15.000	12.678	10.384	8.652	7.133	5.715	4.381	3.184	2.015	1.021	0.121	0.885	2.113
7.70	15.000	14.145	11.711	9.822	8.141	6.559	5.056	3.688	2.355	1.203	0.177	0.626	1.517
7.80	15.000	15.000	13.027	10.989	9.153	7.414	5.751	4.221	2.733	1.432	0.281	0.456	1.056
7.90	15.000	15.000	14.348	12.166	10.183	8.293	6.478	4.792	3.158	1.713	0.440	0.371	0.718
8.00	15.000	15.000	15.000	13.359	11.232	9.197	7.235	5.402	3.625	2.043	0.647	0.361	0.483
8.10	15.000	15.000	15.000	14.557	12.291	10.117	8.014	6.037	4.124	2.407	0.889	0.404	0.325
8.20	15.000	15.000	15.000	15.000	13.349	11.039	8.799	6.684	4.638	2.791	1.150	0.484	0.222
8.30	15.000	15.000	15.000	14.397	11.955	9.582	7.333	5.157	3.182	1.420	0.584	0.155	
8.40	15.000	15.000	15.000	15.000	15.000	12.859	10.357	7.977	5.674	3.573	1.691	0.695	0.109
8.50	15.000	15.000	15.000	15.000	15.000	13.749	11.120	8.613	6.186	3.961	1.960	0.813	0.078
8.60	15.000	15.000	15.000	15.000	15.000	14.626	11.873	9.241	6.691	4.344	2.226	0.933	0.057
8.70	15.000	15.000	15.000	15.000	15.000	15.000	12.615	9.861	7.190	4.724	2.490	1.056	0.042
8.80	15.000	15.000	15.000	15.000	15.000	15.000	13.349	10.474	7.686	5.101	2.753	1.180	0.030
8.90	15.000	15.000	15.000	15.000	15.000	15.000	14.076	11.084	8.178	5.477	3.015	1.307	0.022
9.00	15.000	15.000	15.000	15.000	15.000	15.000	14.800	11.691	8.670	5.854	3.280	1.435	0.016

Note. — Same as Table 15 but for manganese.

Table 27. Iron CIE Fractional Abundances

Table 27—Continued

log(T)	Fe ¹⁴⁺	Fe ¹⁵⁺	Fe ¹⁶⁺	Fe ¹⁷⁺	Fe ¹⁸⁺	Fe ¹⁹⁺	Fe ²⁰⁺	Fe ²¹⁺	Fe ²²⁺	Fe ²³⁺	Fe ²⁴⁺	Fe ²⁵⁺	Fe ²⁶⁺
4.00	15.000	15.000	15.000	15.000	15.000	15.000	15.000	15.000	15.000	15.000	15.000	15.000	15.000
4.10	15.000	15.000	15.000	15.000	15.000	15.000	15.000	15.000	15.000	15.000	15.000	15.000	15.000
4.20	15.000	15.000	15.000	15.000	15.000	15.000	15.000	15.000	15.000	15.000	15.000	15.000	15.000
4.30	15.000	15.000	15.000	15.000	15.000	15.000	15.000	15.000	15.000	15.000	15.000	15.000	15.000
4.40	15.000	15.000	15.000	15.000	15.000	15.000	15.000	15.000	15.000	15.000	15.000	15.000	15.000
4.50	15.000	15.000	15.000	15.000	15.000	15.000	15.000	15.000	15.000	15.000	15.000	15.000	15.000
4.60	15.000	15.000	15.000	15.000	15.000	15.000	15.000	15.000	15.000	15.000	15.000	15.000	15.000
4.70	15.000	15.000	15.000	15.000	15.000	15.000	15.000	15.000	15.000	15.000	15.000	15.000	15.000
4.80	15.000	15.000	15.000	15.000	15.000	15.000	15.000	15.000	15.000	15.000	15.000	15.000	15.000
4.90	15.000	15.000	15.000	15.000	15.000	15.000	15.000	15.000	15.000	15.000	15.000	15.000	15.000
5.00	15.000	15.000	15.000	15.000	15.000	15.000	15.000	15.000	15.000	15.000	15.000	15.000	15.000
5.10	15.000	15.000	15.000	15.000	15.000	15.000	15.000	15.000	15.000	15.000	15.000	15.000	15.000
5.20	15.000	15.000	15.000	15.000	15.000	15.000	15.000	15.000	15.000	15.000	15.000	15.000	15.000
5.30	15.000	15.000	15.000	15.000	15.000	15.000	15.000	15.000	15.000	15.000	15.000	15.000	15.000
5.40	15.000	15.000	15.000	15.000	15.000	15.000	15.000	15.000	15.000	15.000	15.000	15.000	15.000
5.50	15.000	15.000	15.000	15.000	15.000	15.000	15.000	15.000	15.000	15.000	15.000	15.000	15.000
5.60	15.000	15.000	15.000	15.000	15.000	15.000	15.000	15.000	15.000	15.000	15.000	15.000	15.000
5.70	15.000	15.000	15.000	15.000	15.000	15.000	15.000	15.000	15.000	15.000	15.000	15.000	15.000
5.80	12.579	15.000	15.000	15.000	15.000	15.000	15.000	15.000	15.000	15.000	15.000	15.000	15.000
5.90	8.713	11.489	13.683	15.000	15.000	15.000	15.000	15.000	15.000	15.000	15.000	15.000	15.000
6.00	5.597	7.595	9.022	14.711	15.000	15.000	15.000	15.000	15.000	15.000	15.000	15.000	15.000
6.10	3.191	4.516	5.355	9.701	14.791	15.000	15.000	15.000	15.000	15.000	15.000	15.000	15.000
6.20	1.528	2.276	2.684	5.984	9.901	14.395	15.000	15.000	15.000	15.000	15.000	15.000	15.000
6.30	0.710	0.974	1.058	3.542	6.535	9.992	13.851	15.000	15.000	15.000	15.000	15.000	15.000
6.40	0.714	0.582	0.408	2.247	4.511	7.146	10.104	13.495	15.000	15.000	15.000	15.000	15.000
6.50	1.061	0.608	0.214	1.530	3.209	5.189	7.426	10.029	12.901	15.000	15.000	15.000	15.000
6.60	1.470	0.751	0.163	1.043	2.242	3.689	5.343	7.308	9.477	11.930	14.428	15.000	15.000
6.70	1.903	0.961	0.193	0.699	1.494	2.499	3.672	5.114	6.705	8.543	10.391	15.000	15.000
6.80	2.397	1.259	0.320	0.500	0.945	1.574	2.341	3.346	4.457	5.788	7.095	14.852	15.000
6.90	3.023	1.707	0.604	0.492	0.630	0.932	1.350	1.981	2.687	3.591	4.448	10.635	15.000
7.00	3.896	2.417	1.153	0.779	0.642	0.653	0.765	1.071	1.428	1.968	2.447	7.365	12.979
7.10	5.162	3.527	2.107	1.491	1.105	0.854	0.693	0.713	0.765	0.990	1.152	5.041	9.578
7.20	6.834	5.050	3.476	2.638	2.023	1.535	1.126	0.888	0.671	0.621	0.521	3.572	7.230
7.30	8.674	6.746	5.019	3.975	3.149	2.442	1.807	1.335	0.878	0.585	0.269	2.635	5.571
7.40	10.489	8.419	6.543	5.306	4.283	3.373	2.531	1.844	1.170	0.661	0.164	1.968	4.308
7.50	12.225	10.017	7.995	6.576	5.369	4.269	3.233	2.346	1.476	0.774	0.120	1.459	3.301
7.60	13.889	11.544	9.378	7.789	6.407	5.129	3.910	2.838	1.787	0.909	0.114	1.062	2.486
7.70	15.000	13.021	10.714	8.964	7.417	5.969	4.579	3.331	2.112	1.071	0.144	0.759	1.827
7.80	15.000	14.471	12.026	10.124	8.418	6.810	5.256	3.843	2.465	1.272	0.217	0.543	1.305
7.90	15.000	15.000	13.333	11.285	9.428	7.666	5.957	4.386	2.859	1.520	0.339	0.412	0.909
8.00	15.000	15.000	14.645	12.458	10.456	8.546	6.689	4.967	3.296	1.817	0.512	0.359	0.621
8.10	15.000	15.000	15.000	13.641	11.498	9.447	7.446	5.579	3.769	2.155	0.727	0.369	0.423
8.20	15.000	15.000	15.000	14.825	12.545	10.356	8.218	6.211	4.267	2.520	0.970	0.424	0.289
8.30	15.000	15.000	15.000	15.000	13.588	11.265	8.992	6.850	4.775	2.900	1.228	0.509	0.201
8.40	15.000	15.000	15.000	15.000	14.620	12.167	9.763	7.489	5.286	3.284	1.492	0.610	0.141
8.50	15.000	15.000	15.000	15.000	15.000	13.057	10.525	8.123	5.795	3.668	1.757	0.721	0.101
8.60	15.000	15.000	15.000	15.000	15.000	13.934	11.277	8.749	6.298	4.049	2.021	0.838	0.073
8.70	15.000	15.000	15.000	15.000	15.000	14.798	12.019	9.369	6.797	4.427	2.283	0.958	0.053
8.80	15.000	15.000	15.000	15.000	15.000	15.000	12.753	9.982	7.291	4.803	2.544	1.081	0.039
8.90	15.000	15.000	15.000	15.000	15.000	15.000	13.481	10.591	7.783	5.177	2.806	1.206	0.029
9.00	15.000	15.000	15.000	15.000	15.000	15.000	14.205	11.198	8.274	5.553	3.070	1.334	0.021

Note. — Same as Table 15 but for iron.

Table 28. Cobalt CIE Fractional Abundances

Table 28—Continued

$\log(T)$	Co^{14+}	Co^{15+}	Co^{16+}	Co^{17+}	Co^{18+}	Co^{19+}	Co^{20+}	Co^{21+}	Co^{22+}	Co^{23+}	Co^{24+}	Co^{25+}	Co^{26+}	Co^{27+}
4.00	15.000	15.000	15.000	15.000	15.000	15.000	15.000	15.000	15.000	15.000	15.000	15.000	15.000	15.000
4.10	15.000	15.000	15.000	15.000	15.000	15.000	15.000	15.000	15.000	15.000	15.000	15.000	15.000	15.000
4.20	15.000	15.000	15.000	15.000	15.000	15.000	15.000	15.000	15.000	15.000	15.000	15.000	15.000	15.000
4.30	15.000	15.000	15.000	15.000	15.000	15.000	15.000	15.000	15.000	15.000	15.000	15.000	15.000	15.000
4.40	15.000	15.000	15.000	15.000	15.000	15.000	15.000	15.000	15.000	15.000	15.000	15.000	15.000	15.000
4.50	15.000	15.000	15.000	15.000	15.000	15.000	15.000	15.000	15.000	15.000	15.000	15.000	15.000	15.000
4.60	15.000	15.000	15.000	15.000	15.000	15.000	15.000	15.000	15.000	15.000	15.000	15.000	15.000	15.000
4.70	15.000	15.000	15.000	15.000	15.000	15.000	15.000	15.000	15.000	15.000	15.000	15.000	15.000	15.000
4.80	15.000	15.000	15.000	15.000	15.000	15.000	15.000	15.000	15.000	15.000	15.000	15.000	15.000	15.000
4.90	15.000	15.000	15.000	15.000	15.000	15.000	15.000	15.000	15.000	15.000	15.000	15.000	15.000	15.000
5.00	15.000	15.000	15.000	15.000	15.000	15.000	15.000	15.000	15.000	15.000	15.000	15.000	15.000	15.000
5.10	15.000	15.000	15.000	15.000	15.000	15.000	15.000	15.000	15.000	15.000	15.000	15.000	15.000	15.000
5.20	15.000	15.000	15.000	15.000	15.000	15.000	15.000	15.000	15.000	15.000	15.000	15.000	15.000	15.000
5.30	15.000	15.000	15.000	15.000	15.000	15.000	15.000	15.000	15.000	15.000	15.000	15.000	15.000	15.000
5.40	15.000	15.000	15.000	15.000	15.000	15.000	15.000	15.000	15.000	15.000	15.000	15.000	15.000	15.000
5.50	15.000	15.000	15.000	15.000	15.000	15.000	15.000	15.000	15.000	15.000	15.000	15.000	15.000	15.000
5.60	15.000	15.000	15.000	15.000	15.000	15.000	15.000	15.000	15.000	15.000	15.000	15.000	15.000	15.000
5.70	15.000	15.000	15.000	15.000	15.000	15.000	15.000	15.000	15.000	15.000	15.000	15.000	15.000	15.000
5.80	11.152	14.747	15.000	15.000	15.000	15.000	15.000	15.000	15.000	15.000	15.000	15.000	15.000	15.000
5.90	7.711	10.445	13.727	15.000	15.000	15.000	15.000	15.000	15.000	15.000	15.000	15.000	15.000	15.000
6.00	4.980	6.987	9.424	11.284	15.000	15.000	15.000	15.000	15.000	15.000	15.000	15.000	15.000	15.000
6.10	2.941	4.324	6.030	7.215	12.209	15.000	15.000	15.000	15.000	15.000	15.000	15.000	15.000	15.000
6.20	1.589	2.431	3.510	4.190	8.011	12.479	15.000	15.000	15.000	15.000	15.000	15.000	15.000	15.000
6.30	0.820	1.188	1.739	2.045	4.950	8.389	12.278	15.000	15.000	15.000	15.000	15.000	15.000	15.000
6.40	0.700	0.659	0.775	0.790	2.975	5.602	8.592	11.964	15.000	15.000	15.000	15.000	15.000	15.000
6.50	1.193	0.800	0.560	0.336	1.944	3.926	6.201	8.780	11.694	14.924	15.000	15.000	15.000	15.000
6.60	1.859	1.162	0.631	0.199	1.333	2.791	4.489	6.430	8.657	11.128	13.878	15.000	15.000	15.000
6.70	2.528	1.567	0.794	0.173	0.905	1.926	3.150	4.570	6.236	8.086	10.177	12.312	15.000	15.000
6.80	3.202	2.010	1.027	0.230	0.614	1.262	2.086	3.071	4.271	5.608	7.156	8.714	15.000	15.000
6.90	3.936	2.537	1.368	0.402	0.478	0.801	1.279	1.893	2.699	3.603	4.697	5.775	12.523	15.000
7.00	4.824	3.236	1.896	0.768	0.568	0.601	0.774	1.064	1.529	2.064	2.773	3.448	8.833	14.920
7.10	6.008	4.245	2.745	1.459	1.007	0.779	0.680	0.682	0.848	1.062	1.440	1.776	6.055	10.989
7.20	7.612	5.686	4.034	2.592	1.909	1.443	1.097	0.841	0.738	0.670	0.759	0.812	4.193	8.188
7.30	9.524	7.442	5.643	4.048	3.151	2.466	1.894	1.403	1.058	0.739	0.574	0.392	3.039	6.264
7.40	11.491	9.260	7.317	5.572	4.477	3.588	2.808	2.100	1.533	0.989	0.601	0.220	2.266	4.856
7.50	13.398	11.023	8.940	7.047	5.765	4.687	3.712	2.804	2.032	1.284	0.695	0.146	1.694	3.756
7.60	15.000	12.711	10.491	8.453	6.996	5.739	4.581	3.485	2.523	1.589	0.818	0.118	1.251	2.870
7.70	15.000	14.338	11.982	9.803	8.181	6.754	5.423	4.152	3.010	1.903	0.964	0.127	0.907	2.150
7.80	15.000	15.000	13.436	11.117	9.339	7.750	6.256	4.818	3.507	2.238	1.142	0.173	0.650	1.572
7.90	15.000	15.000	14.870	12.415	10.489	8.747	7.096	5.499	4.028	2.606	1.362	0.265	0.476	1.120
8.00	15.000	15.000	15.000	13.712	11.645	9.755	7.955	6.206	4.583	3.014	1.628	0.405	0.381	0.781
8.10	15.000	15.000	15.000	15.000	12.811	10.779	8.835	6.941	5.170	3.462	1.938	0.591	0.355	0.538
8.20	15.000	15.000	15.000	15.000	13.983	11.812	9.729	7.695	5.783	3.939	2.282	0.811	0.382	0.371
8.30	15.000	15.000	15.000	15.000	15.000	12.846	10.628	8.459	6.410	4.433	2.647	1.054	0.447	0.258
8.40	15.000	15.000	15.000	15.000	15.000	13.873	11.524	9.223	7.041	4.936	3.022	1.309	0.536	0.181
8.50	15.000	15.000	15.000	15.000	15.000	14.889	12.411	9.981	7.670	5.438	3.400	1.567	0.639	0.129
8.60	15.000	15.000	15.000	15.000	15.000	15.000	13.287	10.732	8.294	5.939	3.777	1.827	0.750	0.093
8.70	15.000	15.000	15.000	15.000	15.000	15.000	14.152	11.473	8.912	6.435	4.153	2.087	0.867	0.068
8.80	15.000	15.000	15.000	15.000	15.000	15.000	15.000	12.207	9.525	6.928	4.527	2.347	0.987	0.049
8.90	15.000	15.000	15.000	15.000	15.000	15.000	15.000	12.934	10.133	7.418	4.900	2.607	1.111	0.036
9.00	15.000	15.000	15.000	15.000	15.000	15.000	15.000	13.657	10.738	7.907	5.274	2.869	1.237	0.027

Note. — Same as Table 15 but for cobalt.

Table 29. Nickel CIE Fractional Abundances

Table 29—Continued

log(T)	Ni ¹⁴⁺	Ni ¹⁵⁺	Ni ¹⁶⁺	Ni ¹⁷⁺	Ni ¹⁸⁺	Ni ¹⁹⁺	Ni ²⁰⁺	Ni ²¹⁺	Ni ²²⁺	Ni ²³⁺	Ni ²⁴⁺	Ni ²⁵⁺	Ni ²⁶⁺	Ni ²⁷⁺	Ni ²⁸⁺
4.00	15.000	15.000	15.000	15.000	15.000	15.000	15.000	15.000	15.000	15.000	15.000	15.000	15.000	15.000	15.000
4.10	15.000	15.000	15.000	15.000	15.000	15.000	15.000	15.000	15.000	15.000	15.000	15.000	15.000	15.000	15.000
4.20	15.000	15.000	15.000	15.000	15.000	15.000	15.000	15.000	15.000	15.000	15.000	15.000	15.000	15.000	15.000
4.30	15.000	15.000	15.000	15.000	15.000	15.000	15.000	15.000	15.000	15.000	15.000	15.000	15.000	15.000	15.000
4.40	15.000	15.000	15.000	15.000	15.000	15.000	15.000	15.000	15.000	15.000	15.000	15.000	15.000	15.000	15.000
4.50	15.000	15.000	15.000	15.000	15.000	15.000	15.000	15.000	15.000	15.000	15.000	15.000	15.000	15.000	15.000
4.60	15.000	15.000	15.000	15.000	15.000	15.000	15.000	15.000	15.000	15.000	15.000	15.000	15.000	15.000	15.000
4.70	15.000	15.000	15.000	15.000	15.000	15.000	15.000	15.000	15.000	15.000	15.000	15.000	15.000	15.000	15.000
4.80	15.000	15.000	15.000	15.000	15.000	15.000	15.000	15.000	15.000	15.000	15.000	15.000	15.000	15.000	15.000
4.90	15.000	15.000	15.000	15.000	15.000	15.000	15.000	15.000	15.000	15.000	15.000	15.000	15.000	15.000	15.000
5.00	15.000	15.000	15.000	15.000	15.000	15.000	15.000	15.000	15.000	15.000	15.000	15.000	15.000	15.000	15.000
5.10	15.000	15.000	15.000	15.000	15.000	15.000	15.000	15.000	15.000	15.000	15.000	15.000	15.000	15.000	15.000
5.20	15.000	15.000	15.000	15.000	15.000	15.000	15.000	15.000	15.000	15.000	15.000	15.000	15.000	15.000	15.000
5.30	15.000	15.000	15.000	15.000	15.000	15.000	15.000	15.000	15.000	15.000	15.000	15.000	15.000	15.000	15.000
5.40	15.000	15.000	15.000	15.000	15.000	15.000	15.000	15.000	15.000	15.000	15.000	15.000	15.000	15.000	15.000
5.50	15.000	15.000	15.000	15.000	15.000	15.000	15.000	15.000	15.000	15.000	15.000	15.000	15.000	15.000	15.000
5.60	15.000	15.000	15.000	15.000	15.000	15.000	15.000	15.000	15.000	15.000	15.000	15.000	15.000	15.000	15.000
5.70	14.776	15.000	15.000	15.000	15.000	15.000	15.000	15.000	15.000	15.000	15.000	15.000	15.000	15.000	15.000
5.80	10.802	14.657	15.000	15.000	15.000	15.000	15.000	15.000	15.000	15.000	15.000	15.000	15.000	15.000	15.000
5.90	7.666	10.636	13.840	15.000	15.000	15.000	15.000	15.000	15.000	15.000	15.000	15.000	15.000	15.000	15.000
6.00	5.158	7.386	9.794	12.676	14.991	15.000	15.000	15.000	15.000	15.000	15.000	15.000	15.000	15.000	15.000
6.10	3.163	4.760	6.490	8.584	10.139	15.000	15.000	15.000	15.000	15.000	15.000	15.000	15.000	15.000	15.000
6.20	1.692	2.742	3.886	5.303	6.277	10.652	15.000	15.000	15.000	15.000	15.000	15.000	15.000	15.000	15.000
6.30	0.837	1.408	2.041	2.884	3.426	6.778	10.667	15.000	15.000	15.000	15.000	15.000	15.000	15.000	15.000
6.40	0.595	0.743	0.933	1.300	1.513	4.062	7.059	10.437	14.209	15.000	15.000	15.000	15.000	15.000	15.000
6.50	1.072	0.844	0.651	0.630	0.579	2.490	4.780	7.375	10.285	13.565	15.000	15.000	15.000	15.000	15.000
6.60	1.979	1.417	0.894	0.558	0.282	1.675	3.395	5.362	7.579	10.111	12.890	15.000	15.000	15.000	15.000
6.70	2.930	2.070	1.263	0.666	0.191	1.150	2.399	3.854	5.508	7.432	9.543	11.904	14.328	15.000	15.000
6.80	3.852	2.724	1.669	0.850	0.192	0.780	1.630	2.656	3.843	5.266	6.826	8.605	10.415	15.000	15.000
6.90	4.774	3.404	2.130	1.116	0.284	0.546	1.052	1.712	2.503	3.504	4.604	5.899	7.199	14.523	15.000
7.00	5.768	4.178	2.706	1.515	0.517	0.489	0.691	1.030	1.480	2.118	2.827	3.715	4.587	10.451	15.000
7.10	6.953	5.162	3.509	2.153	0.995	0.704	0.633	0.688	0.836	1.158	1.530	2.069	2.581	7.261	12.601
7.20	8.491	6.512	4.691	3.180	1.864	1.333	1.015	0.813	0.692	0.733	0.810	1.046	1.257	4.975	9.312
7.30	10.418	8.265	6.284	4.624	3.153	2.401	1.856	1.420	1.055	0.844	0.659	0.629	0.589	3.523	7.040
7.40	12.515	10.198	8.066	6.260	4.638	3.680	2.926	2.274	1.686	1.245	0.826	0.562	0.310	2.601	5.444
7.50	14.591	12.120	9.841	7.894	6.123	4.973	4.024	3.172	2.378	1.725	1.096	0.621	0.190	1.951	4.234
7.60	15.000	13.972	11.551	9.465	7.548	6.218	5.086	4.047	3.061	2.212	1.390	0.726	0.137	1.457	3.271
7.70	15.000	15.000	13.195	10.972	8.912	7.413	6.109	4.893	3.727	2.694	1.694	0.857	0.125	1.071	2.491
7.80	15.000	15.000	14.790	12.432	10.231	8.573	7.104	5.721	4.385	3.180	2.014	1.016	0.148	0.775	1.858
7.90	15.000	15.000	13.864	11.525	9.716	8.090	6.548	5.050	3.682	2.359	1.210	0.211	0.561	1.352	
8.00	15.000	15.000	15.000	12.809	10.857	9.081	7.387	5.736	4.211	2.740	1.447	0.321	0.425	0.962	
8.10	15.000	15.000	15.000	15.000	14.095	12.005	10.085	8.245	6.447	4.774	3.160	1.728	0.476	0.362	0.674
8.20	15.000	15.000	15.000	15.000	15.000	13.162	11.102	9.121	7.181	5.365	3.614	2.047	0.672	0.359	0.469
8.30	15.000	15.000	15.000	15.000	15.000	14.320	12.124	10.007	7.930	5.976	4.092	2.394	0.896	0.401	0.327
8.40	15.000	15.000	15.000	15.000	15.000	15.000	13.145	10.895	8.685	6.597	4.582	2.757	1.138	0.473	0.230
8.50	15.000	15.000	15.000	15.000	15.000	15.000	14.157	11.777	9.438	7.219	5.078	3.127	1.388	0.565	0.163
8.60	15.000	15.000	15.000	15.000	15.000	15.000	15.000	12.651	10.185	7.840	5.574	3.500	1.643	0.670	0.117
8.70	15.000	15.000	15.000	15.000	15.000	15.000	15.000	13.515	10.925	8.455	6.068	3.873	1.900	0.782	0.085
8.80	15.000	15.000	15.000	15.000	15.000	15.000	15.000	14.370	11.658	9.066	6.559	4.245	2.157	0.899	0.062
8.90	15.000	15.000	15.000	15.000	15.000	15.000	15.000	15.000	12.385	9.673	7.047	4.616	2.416	1.021	0.045
9.00	15.000	15.000	15.000	15.000	15.000	15.000	15.000	15.000	13.107	10.278	7.535	4.988	2.677	1.146	0.033

Note. — Same as Table 15 but for nickel.

Table 30. Copper CIE Fractional Abundances

Table 30—Continued

log(T)	Cu ¹⁵⁺	Cu ¹⁶⁺	Cu ¹⁷⁺	Cu ¹⁸⁺	Cu ¹⁹⁺	Cu ²⁰⁺	Cu ²¹⁺	Cu ²²⁺	Cu ²³⁺	Cu ²⁴⁺	Cu ²⁵⁺	Cu ²⁶⁺	Cu ²⁷⁺	Cu ²⁸⁺	Cu ²⁹⁺	
4.00	15.000	15.000	15.000	15.000	15.000	15.000	15.000	15.000	15.000	15.000	15.000	15.000	15.000	15.000	15.000	
4.10	15.000	15.000	15.000	15.000	15.000	15.000	15.000	15.000	15.000	15.000	15.000	15.000	15.000	15.000	15.000	
4.20	15.000	15.000	15.000	15.000	15.000	15.000	15.000	15.000	15.000	15.000	15.000	15.000	15.000	15.000	15.000	
4.30	15.000	15.000	15.000	15.000	15.000	15.000	15.000	15.000	15.000	15.000	15.000	15.000	15.000	15.000	15.000	
4.40	15.000	15.000	15.000	15.000	15.000	15.000	15.000	15.000	15.000	15.000	15.000	15.000	15.000	15.000	15.000	
4.50	15.000	15.000	15.000	15.000	15.000	15.000	15.000	15.000	15.000	15.000	15.000	15.000	15.000	15.000	15.000	
4.60	15.000	15.000	15.000	15.000	15.000	15.000	15.000	15.000	15.000	15.000	15.000	15.000	15.000	15.000	15.000	
4.70	15.000	15.000	15.000	15.000	15.000	15.000	15.000	15.000	15.000	15.000	15.000	15.000	15.000	15.000	15.000	
4.80	15.000	15.000	15.000	15.000	15.000	15.000	15.000	15.000	15.000	15.000	15.000	15.000	15.000	15.000	15.000	
4.90	15.000	15.000	15.000	15.000	15.000	15.000	15.000	15.000	15.000	15.000	15.000	15.000	15.000	15.000	15.000	
5.00	15.000	15.000	15.000	15.000	15.000	15.000	15.000	15.000	15.000	15.000	15.000	15.000	15.000	15.000	15.000	
5.10	15.000	15.000	15.000	15.000	15.000	15.000	15.000	15.000	15.000	15.000	15.000	15.000	15.000	15.000	15.000	
5.20	15.000	15.000	15.000	15.000	15.000	15.000	15.000	15.000	15.000	15.000	15.000	15.000	15.000	15.000	15.000	
5.30	15.000	15.000	15.000	15.000	15.000	15.000	15.000	15.000	15.000	15.000	15.000	15.000	15.000	15.000	15.000	
5.40	15.000	15.000	15.000	15.000	15.000	15.000	15.000	15.000	15.000	15.000	15.000	15.000	15.000	15.000	15.000	
5.50	15.000	15.000	15.000	15.000	15.000	15.000	15.000	15.000	15.000	15.000	15.000	15.000	15.000	15.000	15.000	
5.60	15.000	15.000	15.000	15.000	15.000	15.000	15.000	15.000	15.000	15.000	15.000	15.000	15.000	15.000	15.000	
5.70	15.000	15.000	15.000	15.000	15.000	15.000	15.000	15.000	15.000	15.000	15.000	15.000	15.000	15.000	15.000	
5.80	13.582	15.000	15.000	15.000	15.000	15.000	15.000	15.000	15.000	15.000	15.000	15.000	15.000	15.000	15.000	
5.90	9.827	13.263	15.000	15.000	15.000	15.000	15.000	15.000	15.000	15.000	15.000	15.000	15.000	15.000	15.000	
6.00	6.886	9.515	12.355	15.000	15.000	15.000	15.000	15.000	15.000	15.000	15.000	15.000	15.000	15.000	15.000	
6.10	4.544	6.491	8.596	11.082	13.023	15.000	15.000	15.000	15.000	15.000	15.000	15.000	15.000	15.000	15.000	
6.20	2.698	4.059	5.533	7.289	8.572	13.497	15.000	15.000	15.000	15.000	15.000	15.000	15.000	15.000	15.000	
6.30	1.386	2.236	3.161	4.298	5.087	8.885	13.270	15.000	15.000	15.000	15.000	15.000	15.000	15.000	15.000	
6.40	0.704	1.104	1.551	2.173	2.590	5.505	8.908	12.692	15.000	15.000	15.000	15.000	15.000	15.000	15.000	
6.50	0.696	0.698	0.733	0.933	1.058	3.275	5.899	8.830	12.101	15.000	15.000	15.000	15.000	15.000	15.000	
6.60	1.372	1.022	0.701	0.559	0.442	2.094	4.094	6.343	8.861	11.677	14.773	15.000	15.000	15.000	15.000	
6.70	2.289	1.625	0.999	0.576	0.247	1.432	2.920	4.615	6.523	8.686	11.065	13.695	15.000	15.000	15.000	
6.80	3.206	2.261	1.372	0.713	0.192	0.979	2.039	3.274	4.680	6.307	8.097	10.106	12.172	15.000	15.000	
6.90	4.106	2.909	1.789	0.924	0.224	0.666	1.358	2.204	3.187	4.366	5.667	7.162	8.685	15.000	15.000	
7.00	5.035	3.609	2.283	1.234	0.364	0.501	0.871	1.378	1.999	2.797	3.684	4.748	5.817	12.169	15.000	
7.10	6.083	4.448	2.935	1.716	0.683	0.545	0.629	0.837	1.141	1.608	2.140	2.835	3.523	8.611	14.364	
7.20	7.397	5.570	3.884	2.505	1.312	0.924	0.750	0.691	0.713	0.887	1.110	1.487	1.855	5.916	10.601	
7.30	9.115	7.108	5.259	3.729	2.379	1.762	1.353	1.051	0.819	0.731	0.680	0.779	0.878	4.103	7.916	
7.40	11.131	8.957	6.954	5.276	3.773	2.944	2.319	1.794	1.331	1.005	0.711	0.565	0.438	2.978	6.075	
7.50	13.208	10.876	8.724	6.903	5.249	4.223	3.397	2.666	1.991	1.447	0.934	0.571	0.252	2.227	4.732	
7.60	15.000	12.747	10.452	8.490	6.689	5.478	4.465	3.541	2.669	1.924	1.212	0.653	0.167	1.674	3.685	
7.70	15.000	14.549	12.114	10.015	8.068	6.685	5.495	4.391	3.334	2.401	1.506	0.769	0.133	1.246	2.841	
7.80	15.000	15.000	13.720	11.485	9.397	7.851	6.493	5.218	3.988	2.879	1.814	0.912	0.136	0.913	2.154	
7.90	15.000	15.000	12.918	10.691	8.991	7.474	6.037	4.642	3.366	2.142	1.085	0.176	0.662	1.599		
8.00	15.000	15.000	15.000	14.331	11.968	10.122	8.452	6.860	5.309	3.876	2.500	1.296	0.257	0.489	1.160	
8.10	15.000	15.000	15.000	15.000	13.240	11.255	9.439	7.699	5.999	4.414	2.894	1.550	0.384	0.389	0.826	
8.20	15.000	15.000	15.000	15.000	14.514	12.396	10.438	8.556	6.713	4.983	3.324	1.844	0.553	0.353	0.582	
8.30	15.000	15.000	15.000	15.000	15.000	13.541	11.447	9.427	7.445	5.576	3.782	2.170	0.756	0.369	0.409	
8.40	15.000	15.000	15.000	15.000	15.000	14.685	12.457	10.303	8.187	6.183	4.258	2.518	0.982	0.423	0.288	
8.50	15.000	15.000	15.000	15.000	15.000	15.000	13.463	11.179	8.932	6.797	4.745	2.878	1.223	0.502	0.205	
8.60	15.000	15.000	15.000	15.000	15.000	15.000	14.461	12.049	9.675	7.412	5.234	3.244	1.471	0.597	0.147	
8.70	15.000	15.000	15.000	15.000	15.000	15.000	15.000	12.911	10.412	8.024	5.724	3.612	1.723	0.703	0.106	
8.80	15.000	15.000	15.000	15.000	15.000	15.000	15.000	13.764	11.143	8.633	6.212	3.981	1.977	0.816	0.077	
8.90	15.000	15.000	15.000	15.000	15.000	15.000	15.000	15.000	14.609	11.868	9.238	6.698	4.350	2.233	0.935	0.057
9.00	15.000	15.000	15.000	15.000	15.000	15.000	15.000	15.000	12.589	9.841	7.184	4.721	2.492	1.058		

Note. — Same as Table 15 but for copper.

Table 31. Zinc CIE Fractional Abundances

Table 31—Continued

log(T)	Zn ¹⁵⁺	Zn ¹⁶⁺	Zn ¹⁷⁺	Zn ¹⁸⁺	Zn ¹⁹⁺	Zn ²⁰⁺	Zn ²¹⁺	Zn ²²⁺	Zn ²³⁺	Zn ²⁴⁺	Zn ²⁵⁺	Zn ²⁶⁺	Zn ²⁷⁺	Zn ²⁸⁺	Zn ²⁹⁺	Zn ³⁰⁺	
4.00	15.000	15.000	15.000	15.000	15.000	15.000	15.000	15.000	15.000	15.000	15.000	15.000	15.000	15.000	15.000	15.000	
4.10	15.000	15.000	15.000	15.000	15.000	15.000	15.000	15.000	15.000	15.000	15.000	15.000	15.000	15.000	15.000	15.000	
4.20	15.000	15.000	15.000	15.000	15.000	15.000	15.000	15.000	15.000	15.000	15.000	15.000	15.000	15.000	15.000	15.000	
4.30	15.000	15.000	15.000	15.000	15.000	15.000	15.000	15.000	15.000	15.000	15.000	15.000	15.000	15.000	15.000	15.000	
4.40	15.000	15.000	15.000	15.000	15.000	15.000	15.000	15.000	15.000	15.000	15.000	15.000	15.000	15.000	15.000	15.000	
4.50	15.000	15.000	15.000	15.000	15.000	15.000	15.000	15.000	15.000	15.000	15.000	15.000	15.000	15.000	15.000	15.000	
4.60	15.000	15.000	15.000	15.000	15.000	15.000	15.000	15.000	15.000	15.000	15.000	15.000	15.000	15.000	15.000	15.000	
4.70	15.000	15.000	15.000	15.000	15.000	15.000	15.000	15.000	15.000	15.000	15.000	15.000	15.000	15.000	15.000	15.000	
4.80	15.000	15.000	15.000	15.000	15.000	15.000	15.000	15.000	15.000	15.000	15.000	15.000	15.000	15.000	15.000	15.000	
4.90	15.000	15.000	15.000	15.000	15.000	15.000	15.000	15.000	15.000	15.000	15.000	15.000	15.000	15.000	15.000	15.000	
5.00	15.000	15.000	15.000	15.000	15.000	15.000	15.000	15.000	15.000	15.000	15.000	15.000	15.000	15.000	15.000	15.000	
5.10	15.000	15.000	15.000	15.000	15.000	15.000	15.000	15.000	15.000	15.000	15.000	15.000	15.000	15.000	15.000	15.000	
5.20	15.000	15.000	15.000	15.000	15.000	15.000	15.000	15.000	15.000	15.000	15.000	15.000	15.000	15.000	15.000	15.000	
5.30	15.000	15.000	15.000	15.000	15.000	15.000	15.000	15.000	15.000	15.000	15.000	15.000	15.000	15.000	15.000	15.000	
5.40	15.000	15.000	15.000	15.000	15.000	15.000	15.000	15.000	15.000	15.000	15.000	15.000	15.000	15.000	15.000	15.000	
5.50	15.000	15.000	15.000	15.000	15.000	15.000	15.000	15.000	15.000	15.000	15.000	15.000	15.000	15.000	15.000	15.000	
5.60	15.000	15.000	15.000	15.000	15.000	15.000	15.000	15.000	15.000	15.000	15.000	15.000	15.000	15.000	15.000	15.000	
5.70	15.000	15.000	15.000	15.000	15.000	15.000	15.000	15.000	15.000	15.000	15.000	15.000	15.000	15.000	15.000	15.000	
5.80	12.236	15.000	15.000	15.000	15.000	15.000	15.000	15.000	15.000	15.000	15.000	15.000	15.000	15.000	15.000	15.000	
5.90	8.707	12.264	15.000	15.000	15.000	15.000	15.000	15.000	15.000	15.000	15.000	15.000	15.000	15.000	15.000	15.000	
6.00	6.069	8.816	11.864	15.000	15.000	15.000	15.000	15.000	15.000	15.000	15.000	15.000	15.000	15.000	15.000	15.000	
6.10	4.039	6.105	8.415	10.899	13.790	15.000	15.000	15.000	15.000	15.000	15.000	15.000	15.000	15.000	15.000	15.000	
6.20	2.456	3.940	5.621	7.426	9.535	11.144	15.000	15.000	15.000	15.000	15.000	15.000	15.000	15.000	15.000	15.000	
6.30	1.276	2.254	3.389	4.605	6.048	7.099	11.358	15.000	15.000	15.000	15.000	15.000	15.000	15.000	15.000	15.000	
6.40	0.585	1.118	1.774	2.479	3.365	3.996	7.290	11.101	15.000	15.000	15.000	15.000	15.000	15.000	15.000	15.000	
6.50	0.500	0.639	0.872	1.134	1.564	1.870	4.403	7.361	10.637	14.286	15.000	15.000	15.000	15.000	15.000	15.000	
6.60	1.115	0.902	0.763	0.644	0.704	0.746	2.665	4.943	7.478	10.310	13.448	15.000	15.000	15.000	15.000	15.000	
6.70	2.223	1.695	1.225	0.781	0.539	0.355	1.768	3.493	5.431	7.602	10.035	12.695	15.000	15.000	15.000	15.000	
6.80	3.403	2.593	1.828	1.103	0.612	0.226	1.213	2.478	3.923	5.554	7.410	9.441	11.690	14.018	15.000	15.000	
6.90	4.545	3.478	2.450	1.482	0.776	0.205	0.825	1.699	2.729	3.908	5.286	6.796	8.500	10.254	15.000	15.000	
7.00	5.667	4.368	3.102	1.918	1.023	0.277	0.574	1.110	1.782	2.577	3.550	4.622	5.870	7.145	14.001	15.000	
7.10	6.837	5.324	3.841	2.464	1.396	0.482	0.493	0.728	1.087	1.548	2.172	2.870	3.731	4.601	10.109	15.000	
7.20	8.171	6.461	4.779	3.224	1.995	0.919	0.670	0.637	0.716	0.882	1.199	1.573	2.100	2.629	7.043	12.081	
7.30	9.833	7.940	6.074	4.352	2.971	1.736	1.250	0.973	0.799	0.702	0.745	0.834	1.070	1.312	4.835	8.947	
7.40	11.870	9.805	7.767	5.888	4.360	2.970	2.265	1.764	1.360	1.023	0.820	0.655	0.635	0.634	3.429	6.782	
7.50	14.073	11.846	9.647	7.617	5.947	4.404	3.497	2.789	2.172	1.616	1.188	0.795	0.549	0.340	2.537	5.264	
7.60	15.000	13.880	11.528	9.353	7.543	5.851	4.755	3.854	3.041	2.281	1.646	1.047	0.598	0.210	1.911	4.117	
7.70	15.000	15.000	13.351	11.034	9.088	7.250	5.977	4.895	3.896	2.948	2.121	1.333	0.700	0.150	1.436	3.204	
7.80	15.000	15.000	15.000	12.656	10.575	8.594	7.156	5.902	4.729	3.603	2.596	1.633	0.831	0.133	1.066	2.463	
7.90	15.000	15.000	15.000	14.232	12.018	9.897	8.302	6.885	5.548	4.254	3.077	1.950	0.990	0.151	0.781	1.860	
8.00	15.000	15.000	15.000	15.000	13.431	11.174	9.430	7.858	6.364	4.911	3.573	2.292	1.182	0.208	0.573	1.376	
8.10	15.000	15.000	15.000	15.000	14.830	12.439	10.554	8.834	7.189	5.585	4.094	2.666	1.413	0.307	0.437	0.998	
8.20	15.000	15.000	15.000	15.000	15.000	13.702	11.682	9.819	8.030	6.280	4.643	3.074	1.683	0.449	0.367	0.712	
8.30	15.000	15.000	15.000	15.000	15.000	14.965	12.816	10.815	8.886	6.997	5.218	3.513	1.989	0.629	0.355	0.505	
8.40	15.000	15.000	15.000	15.000	15.000	15.000	13.952	11.815	9.752	7.727	5.813	3.975	2.322	0.837	0.386	0.358	
8.50	15.000	15.000	15.000	15.000	15.000	15.000	15.000	15.000	12.816	10.621	8.465	6.418	4.452	2.672	1.064	0.449	0.255
8.60	15.000	15.000	15.000	15.000	15.000	15.000	15.000	15.000	13.811	11.488	9.204	7.028	4.936	3.031	1.304	0.533	0.183
8.70	15.000	15.000	15.000	15.000	15.000	15.000	15.000	15.000	14.797	12.349	9.939	7.637	5.422	3.395	1.550	0.632	0.132
8.80	15.000	15.000	15.000	15.000	15.000	15.000	15.000	15.000	15.000	13.202	10.669	8.245	5.908	3.762	1.800	0.740	0.096
8.90	15.000	15.000	15.000	15.000	15.000	15.000	15.000	15.000	15.000	14.047	11.394	8.849	6.394	4.130	2.053	0.855	0.070
9.00	15.000	15.000	15.000	15.000	15.000	15.000	15.000	15.000	15.000	14.886	12.116	9.452	6.880	4.499	2.310	0.976	0.051

Note. — Same as Table 15 but for zinc.

Table 32. Inferred FIP enhancement factors and coronal abundances used in the analysis here.

Element	FIP ¹ (eV)	Photospheric Abundance ²	FIP Enhancement Factor		Resulting Coronal Abundance	
			Current CIE Results	Mazzotta et al. (1998) CIE Results	Current CIE Results	Mazzotta et al. (1998) CIE Results
N ³	14.53	-4.08	1.00	1.00	-4.08	-4.08
O ³	13.62	-3.17	1.00	1.00	-3.17	-3.17
Ne	21.56	-3.89	1.00	1.00	-3.89	-3.89
Na ⁴	5.14	-5.67	$7.75^{+12.98}_{-4.97}$	$7.84^{+19.98}_{-6.40}$	$-4.78^{+0.42}_{-0.45}$	$-4.78^{+0.55}_{-0.73}$
Mg	7.65	-4.42	$2.78^{+2.28}_{-1.25}$	$2.91^{+0.14}_{-0.13}$	-3.98 ± 0.26	-3.96 ± 0.02
Al	5.99	-5.51	$3.58^{+1.72}_{-1.16}$	$4.51^{+1.57}_{-1.17}$	-4.96 ± 0.17	-4.86 ± 0.13
Si	8.15	-4.44	$4.94^{+2.90}_{-1.82}$	$5.18^{+3.41}_{-2.06}$	-3.75 ± 0.20	-3.73 ± 0.22
S	10.36	-4.67	$2.19^{+0.21}_{-0.19}$	$1.78^{+0.31}_{-0.33}$	-4.33 ± 0.04	-4.42 ± 0.09
Ar	15.76	-5.41	1.00	1.00	-5.41	-5.41
K ⁴	4.34	-6.87	$1.75^{+0.44}_{-0.59}$	$3.84^{+2.99}_{-1.30}$	-6.63 ± 0.35	$-6.29^{+0.25}_{-0.18}$
Ca ⁴	6.11	-5.65	$3.46^{+4.29}_{-1.93}$	$6.67^{+11.70}_{-4.25}$	$-5.11^{+0.18}_{-0.10}$	-4.83 ± 0.44
Fe	7.90	-4.50	$6.98^{+1.42}_{-1.17}$	$5.06^{+0.62}_{-0.55}$	-3.66 ± 0.08	-3.80 ± 0.05

Note. — We list here the elements used in the present analysis along with their first ionization potential. Also listed for each element is the photospheric abundance, the enhancement factor used to account for the FIP-effect, and the resulting coronal abundance. Enhancement factors and resulting coronal abundances are given for results of the GEM method using the CIE fractional abundances of the present paper and those of Mazzotta et al. (1998). All abundances are given as $\log[n(X)/n(H)]$ with $n(X)$ the abundance of element X and $n(H)$ the abundance of hydrogen.

¹Dragoset et al. (2001)

²Feldman & Laming (2000)

³As discussed in Sec. 8.4, we believe N and O to be from a cooler plasma so we do not determine their *EM* by interpolation and assume a FIP factor of 1.00 in accordance with other high-FIP elements. See also Sec. 6 and Fig. 64 for further details.

⁴Insufficient number of crossings to determine the mean *EM* so we calculate the FIP factor by using the *EM* at $\log_{10} T_e = 6.13 \pm 0.06$. See Sec. 6 and Fig. 64 for further details.

Table 33. Derived electron temperature and emission measure

Figure	Group	Step ^a	$\langle \log_{10} T_e \rangle$ (K)	$\delta \langle \log_{10} T_e \rangle$ (K)	$\langle \log_{10} EM \rangle$ (cm ⁻³)	$\delta \langle \log_{10} EM \rangle$ (cm ⁻³)
65	Ia	1	6.16	0.11	43.24	0.66
65	Ia	2	6.17	0.07	43.10	0.45
65	Ia	3	6.16	0.07	43.02	0.15
66	Ib	1	6.15	0.10	43.03	0.62
66	Ib	2	6.16	0.05	42.97	0.27
66	Ib	3	6.16	0.05	42.94	0.27
67	I	1	6.16	0.09	43.09	0.51
67	I	2	6.16	0.07	43.05	0.37
67	I	3	6.17	0.05	43.00	0.20
68	IIa	1	6.04	0.26	42.99	0.74
68	IIa	2	6.02	0.22	42.92	0.53
68	IIa	3	5.98	0.19	42.62	0.36
69	IIa ¹	1	6.13	0.20	42.97	0.56
69	IIa ¹	2	6.11	0.19	42.95	0.56
69	IIa ¹	3	6.06	0.12	42.73	0.30
70	IIa ²	1	5.79	0.30	42.50	0.91
70	IIa ²	2	5.84	0.27	42.70	0.84
70	IIa ²	3	5.44	0.00	41.44	0.00
71	IIb	1	6.14	0.12	43.25	0.75
71	IIb	2	6.11	0.06	43.05	0.32
71	IIb	3	6.11	0.04	43.00	0.21
72	II	1	6.12	0.15	43.09	0.70
72	II	2	6.11	0.09	42.98	0.39
72	II	3	6.10	0.06	42.91	0.26

Table 33—Continued

Figure	Group	Step ^a	$\langle \log_{10} T_e \rangle$ (K)	$\delta \langle \log_{10} T_e \rangle$ (K)	$\langle \log_{10} EM \rangle$ (cm ⁻³)	$\delta \langle \log_{10} EM \rangle$ (cm ⁻³)
73	III	1	6.23	0.21	43.66	1.14
73	III	2	6.17	0.10	43.40	0.59
73	III	3	6.12	0.01	43.07	0.03
74	All Lines ¹	1	6.16	0.16	43.26	0.83
74	All Lines ¹	2	6.14	0.10	43.08	0.46
74	All Lines ¹	3	6.12	0.07	42.98	0.29
75	All Lines ³	1	6.17	0.15	43.40	0.90
75	All Lines ³	2	6.14	0.08	43.15	0.46
75	All Lines ³	3	6.13	0.06	43.02	0.29

Note. — We list the geometric mean and standard deviation of the EM and T_e of each group categorization after each of the 3 steps outlined in Sec. 5. These results use the adjusted coronal elemental abundances as listed in Table 32.

^aAs defined in Sec. 5.

¹Excluding N v and O vi lines.

²Only N v and O vi lines.

³Excluding all lines from Li- and Na-like ions.

Table 34. Electron temperature and emission measure values derived using the GEM method and our current CIE fractional abundances, as well as using the GEM method with the Mazzotta et al. (1998) CIE fractional abundances. We compare with the results given in Landi et al. (2002).

Figure	Group	$\langle \log_{10} T_e \rangle$ (K)			$\langle \log_{10} EM \rangle$ (cm $^{-3}$)		
		Current CIE Results	Mazzotta et al. (1998) CIE Results	Landi et al. (2000)	Current CIE Results	Mazzotta et al. (1998) CIE Results	Landi et al. (2000)
65	Ia	6.16 ± 0.07	6.13 ± 0.06	6.13 ± 0.01	43.02 ± 0.15	43.09 ± 0.13	43.15 ± 0.10
66	Ib	6.16 ± 0.05	6.17 ± 0.03	6.17 ± 0.01	42.94 ± 0.27	42.92 ± 0.16	43.15 ± 0.05
69	IIa ¹	6.06 ± 0.12	6.03 ± 0.12	6.11 ± 0.02	42.73 ± 0.30	42.63 ± 0.26	42.90 ± 0.15
71	IIb	6.11 ± 0.04	6.10 ± 0.04	6.13 ± 0.01	43.00 ± 0.21	42.99 ± 0.22	43.30 ± 0.15
73	III	6.12 ± 0.01	6.11 ± 0.01	6.13 ± 0.01	43.07 ± 0.03	43.05 ± 0.04	43.45 ± 0.10

Note. — Here we list the mean values and errors of the $\log_{10} EM$ and $\log_{10} T_e$ derived from the GEM method using the CIE fractional abundances of the current paper and of Mazzotta et al. (1998). We also list the results reported by Landi et al. (2002). These are grouped in the same way as Table 33 but the values of the mean and standard deviation were determined in Landi et al. (2002) by eye, rather than using the more rigorous method developed and implemented here.

¹Excluding N v and O vi lines.

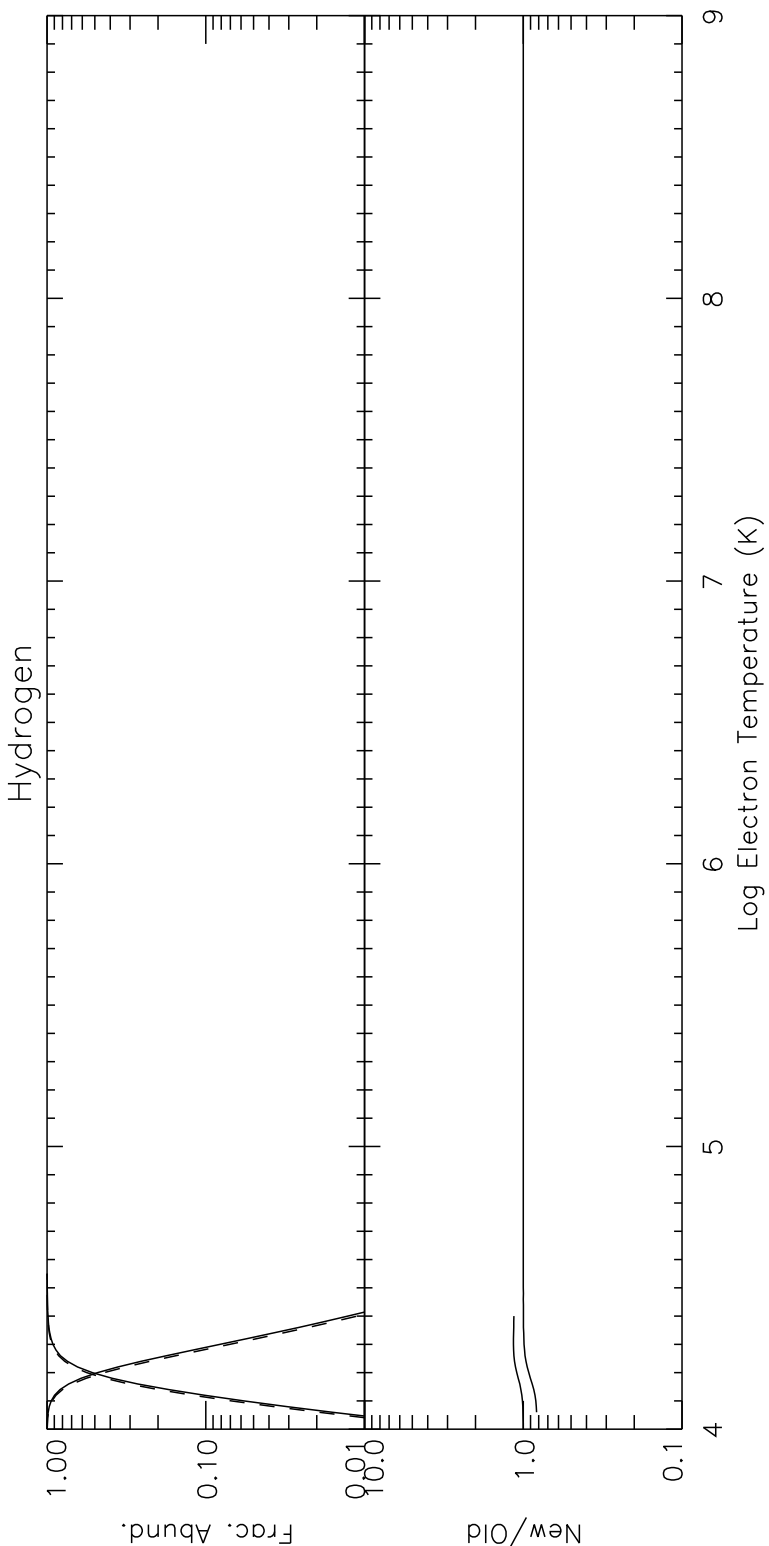


Fig. 1.— Ionization fractional abundance versus electron temperature for all ionization stages of H. The upper graph shows our results (*solid curves*) and the abundances calculated by Mazzotta et al. (1998; *dashed curves*). The lower graph shows the ratio of the calculated abundances. Comparison is made only for fractional abundances greater than 10^{-2} . We label our results as “New” and those of Mazzotta et al. (1998) as “Old”.

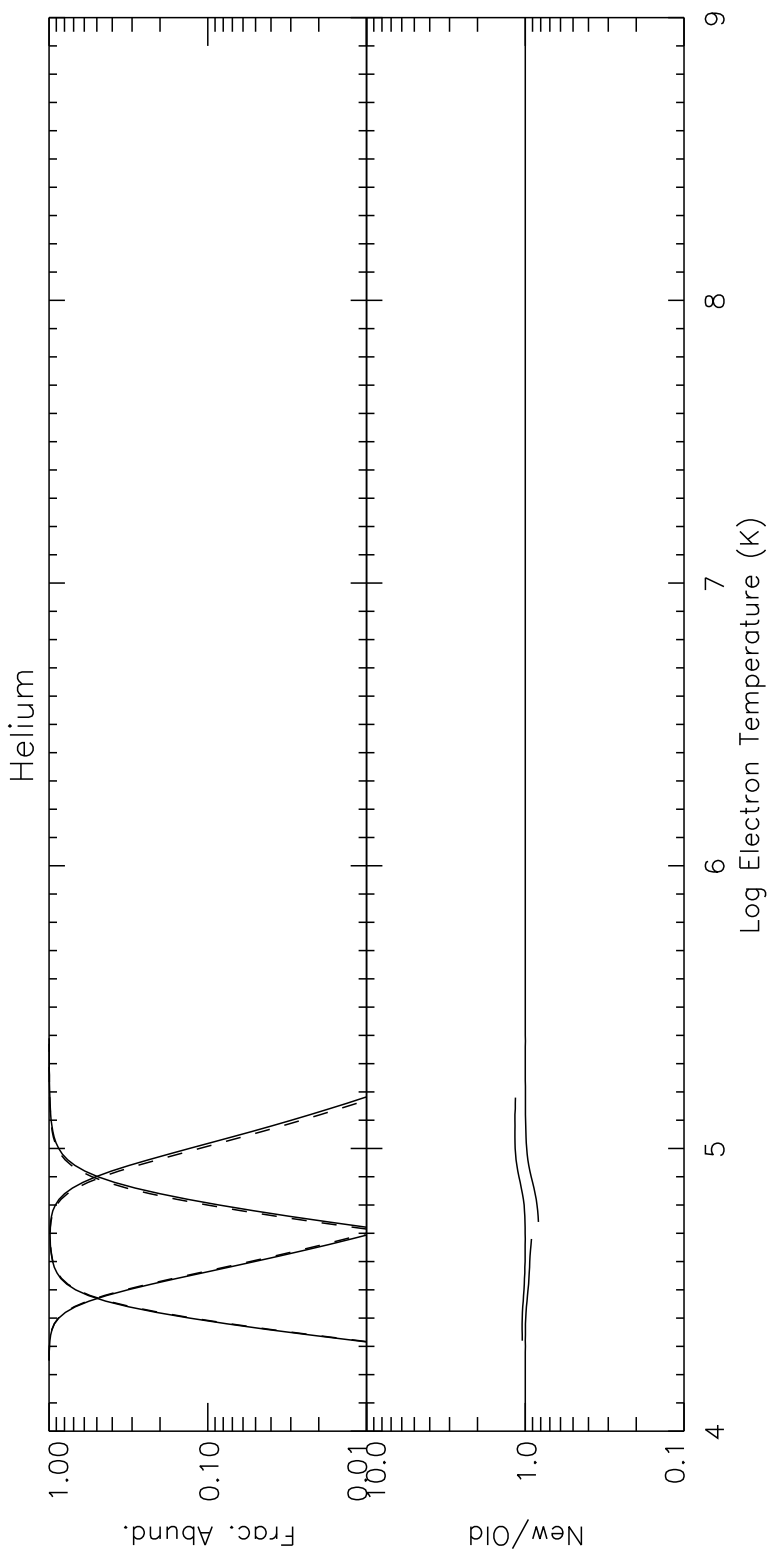


Fig. 2.— Same as Fig. 1 but for He.

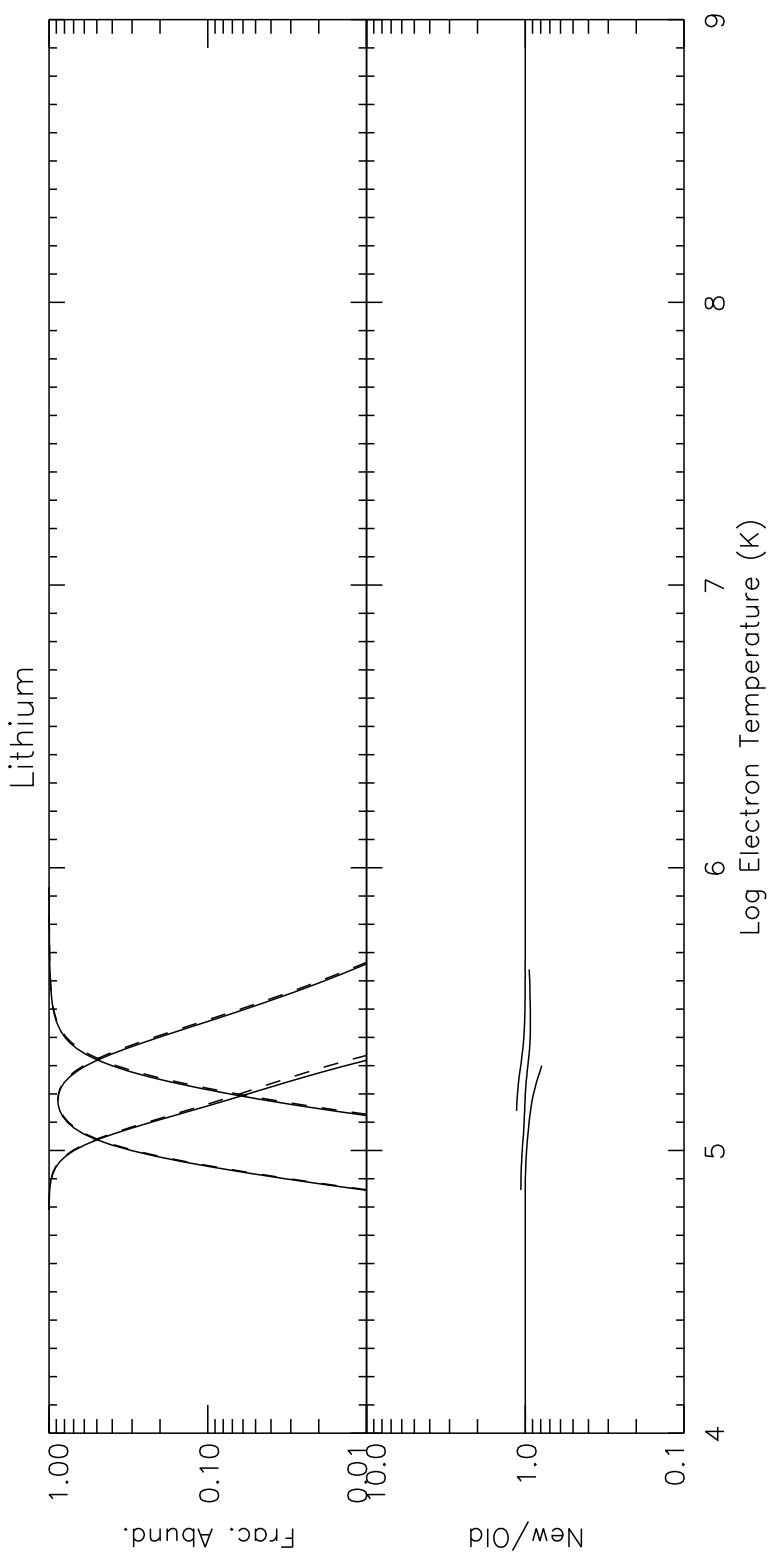


Fig. 3.— Same as Fig. 1 but for Li.

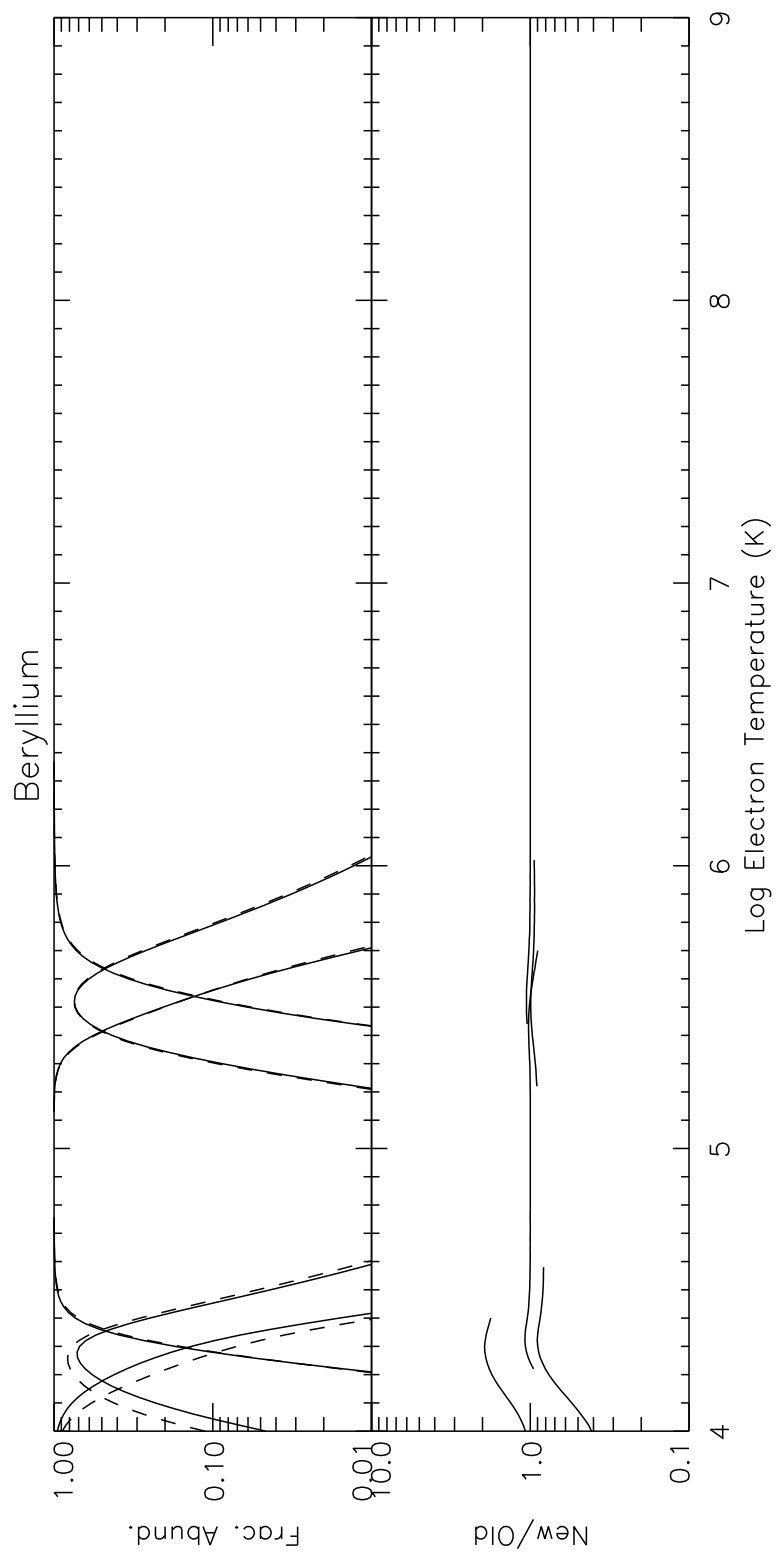


Fig. 4.— Same as Fig. 1 but for Be.

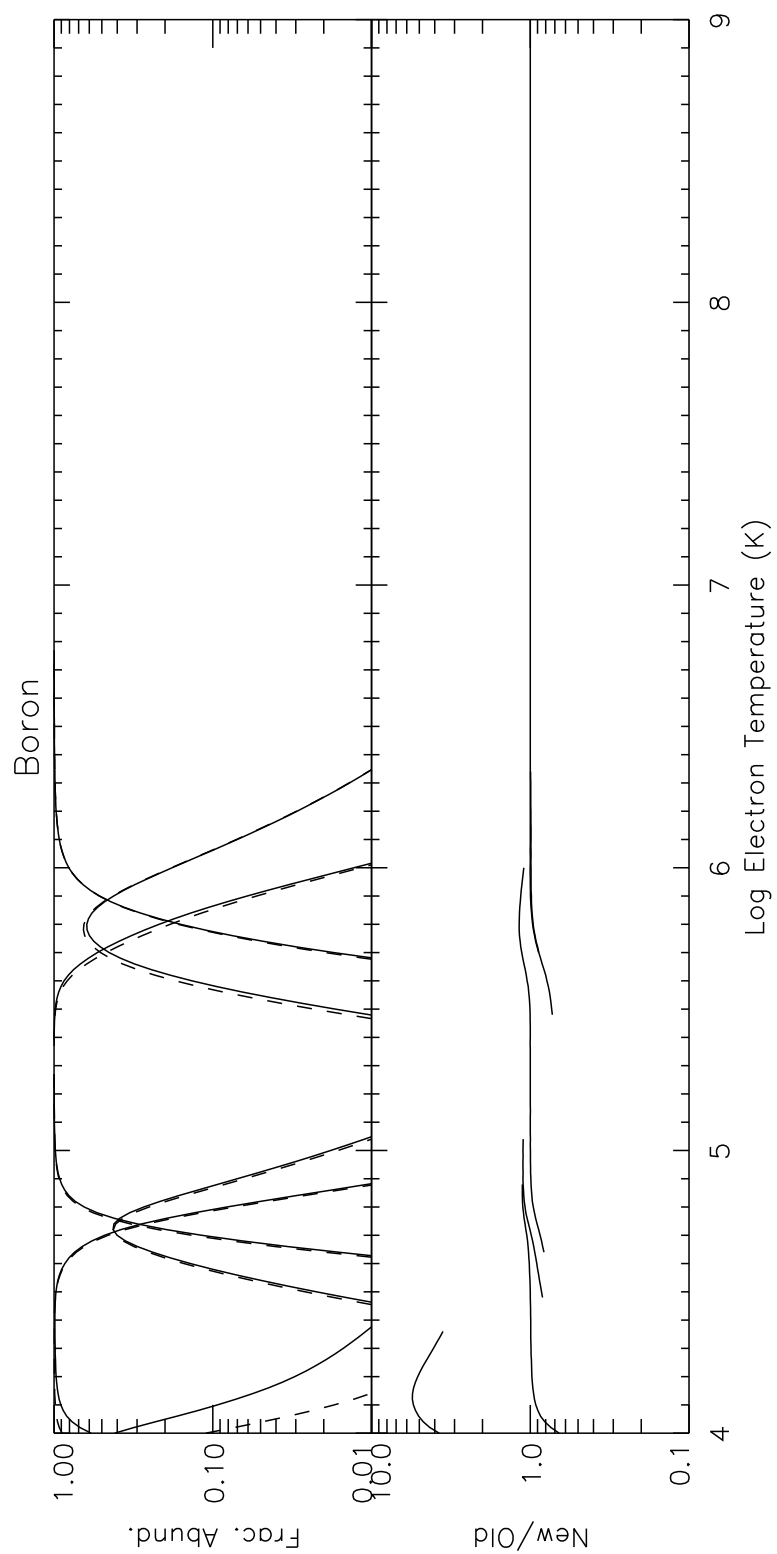


Fig. 5.— Same as Fig. 1 but for B.

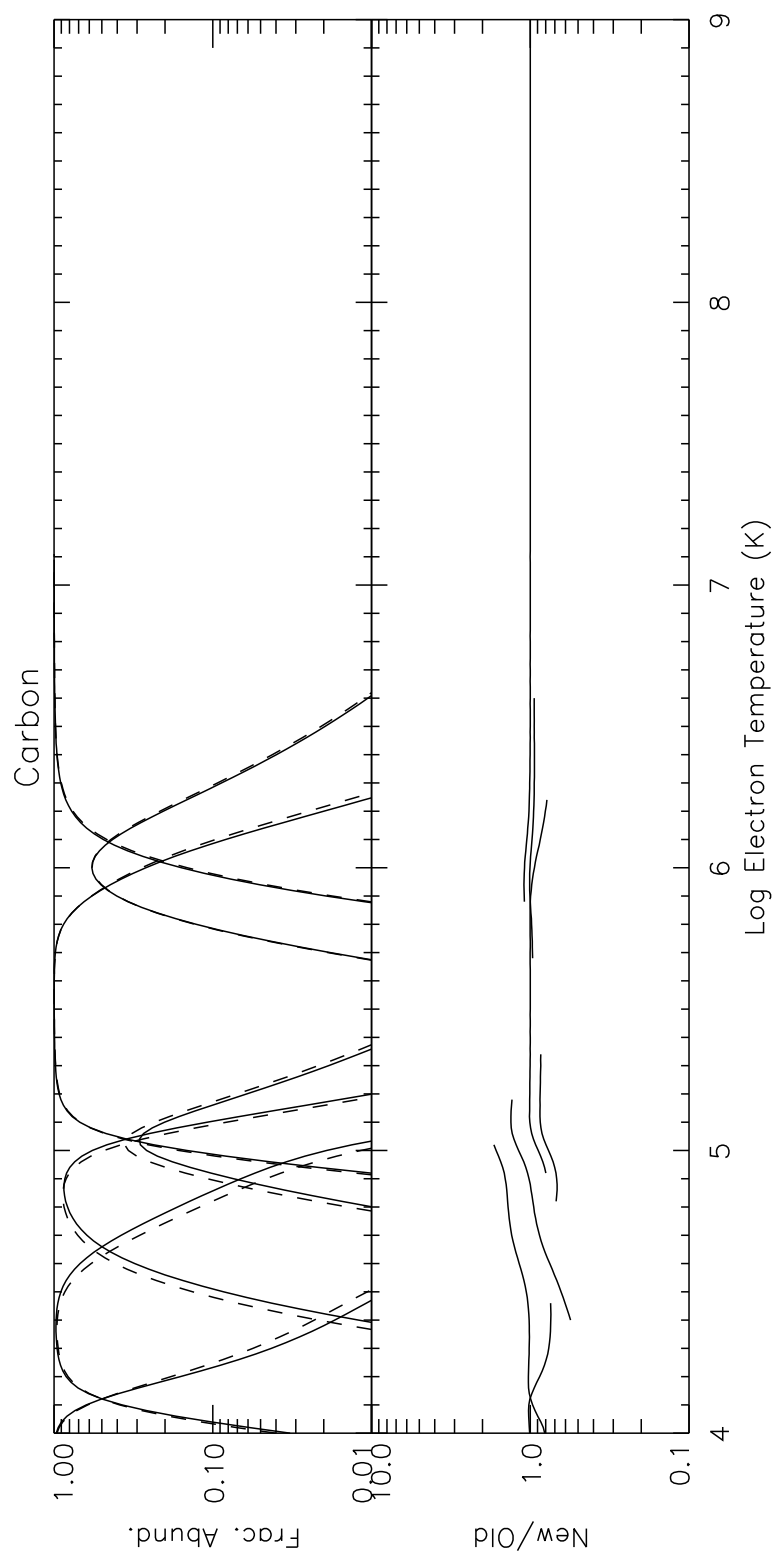


Fig. 6.— Same as Fig. 1 but for C.

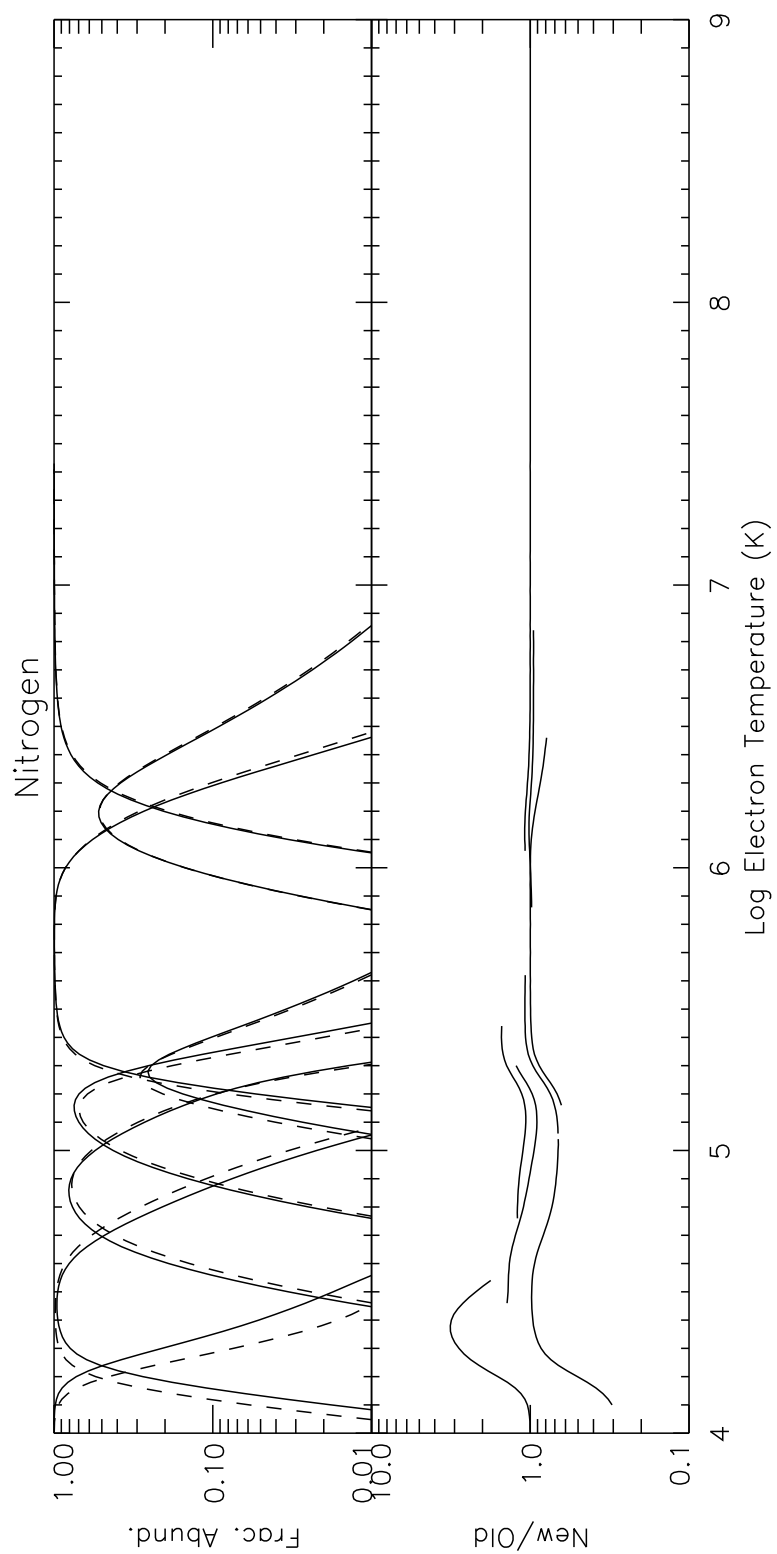


Fig. 7.— Same as Fig. 1 but for N.

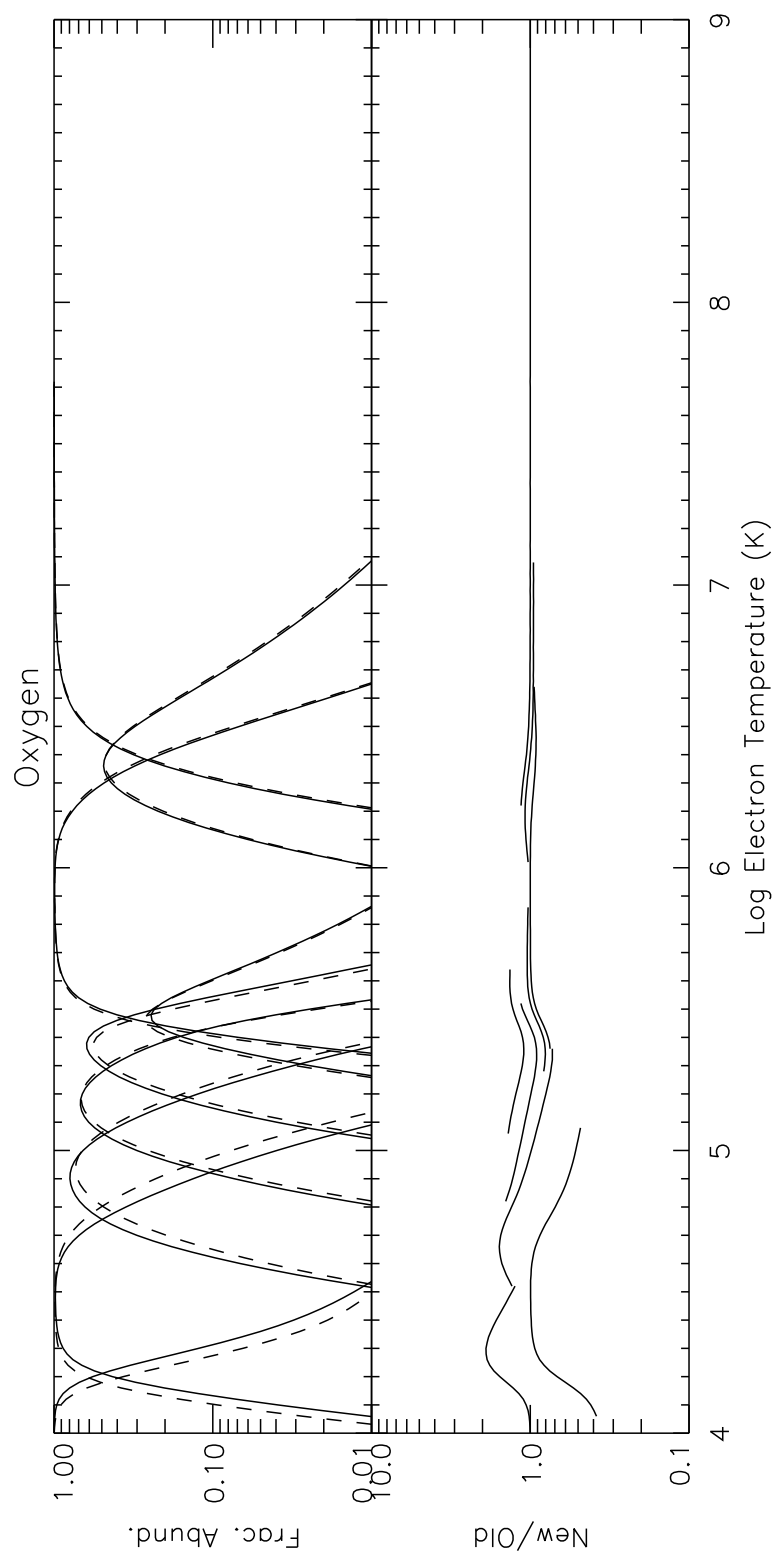


Fig. 8.— Same as Fig. 1 but for O.

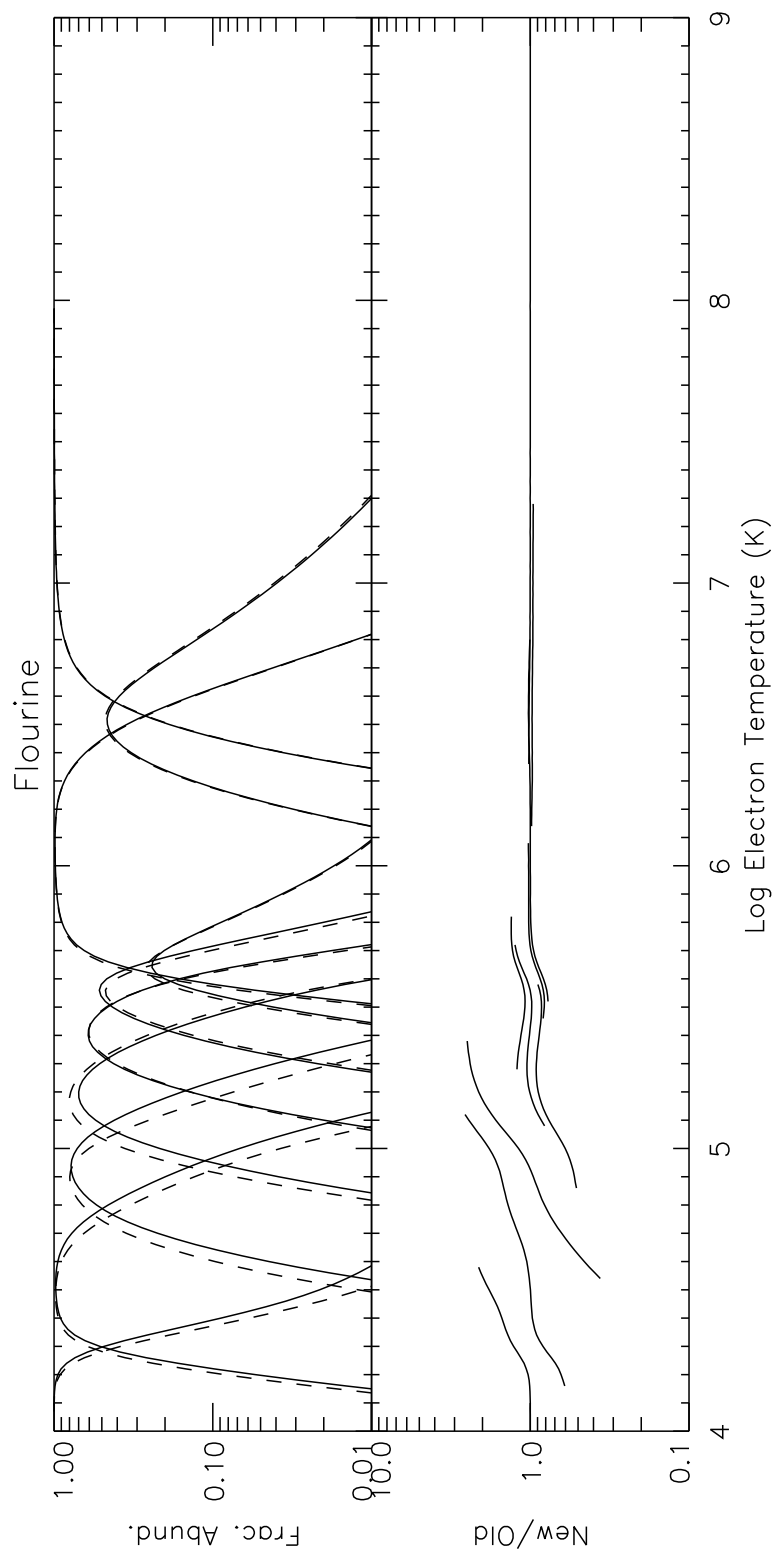


Fig. 9.— Same as Fig. 1 but for F.

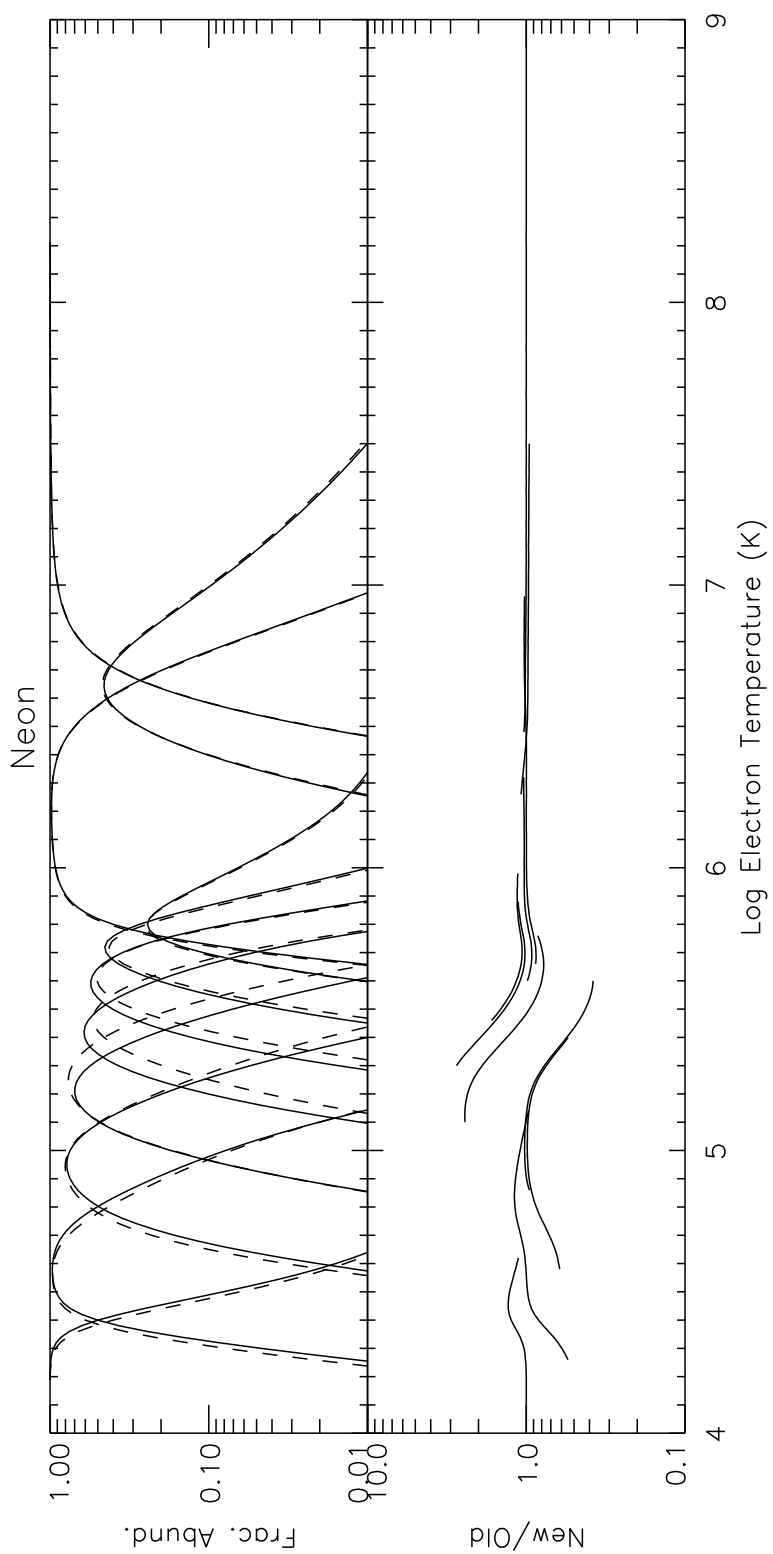


Fig. 10.— Same as Fig. 1 but for Ne.

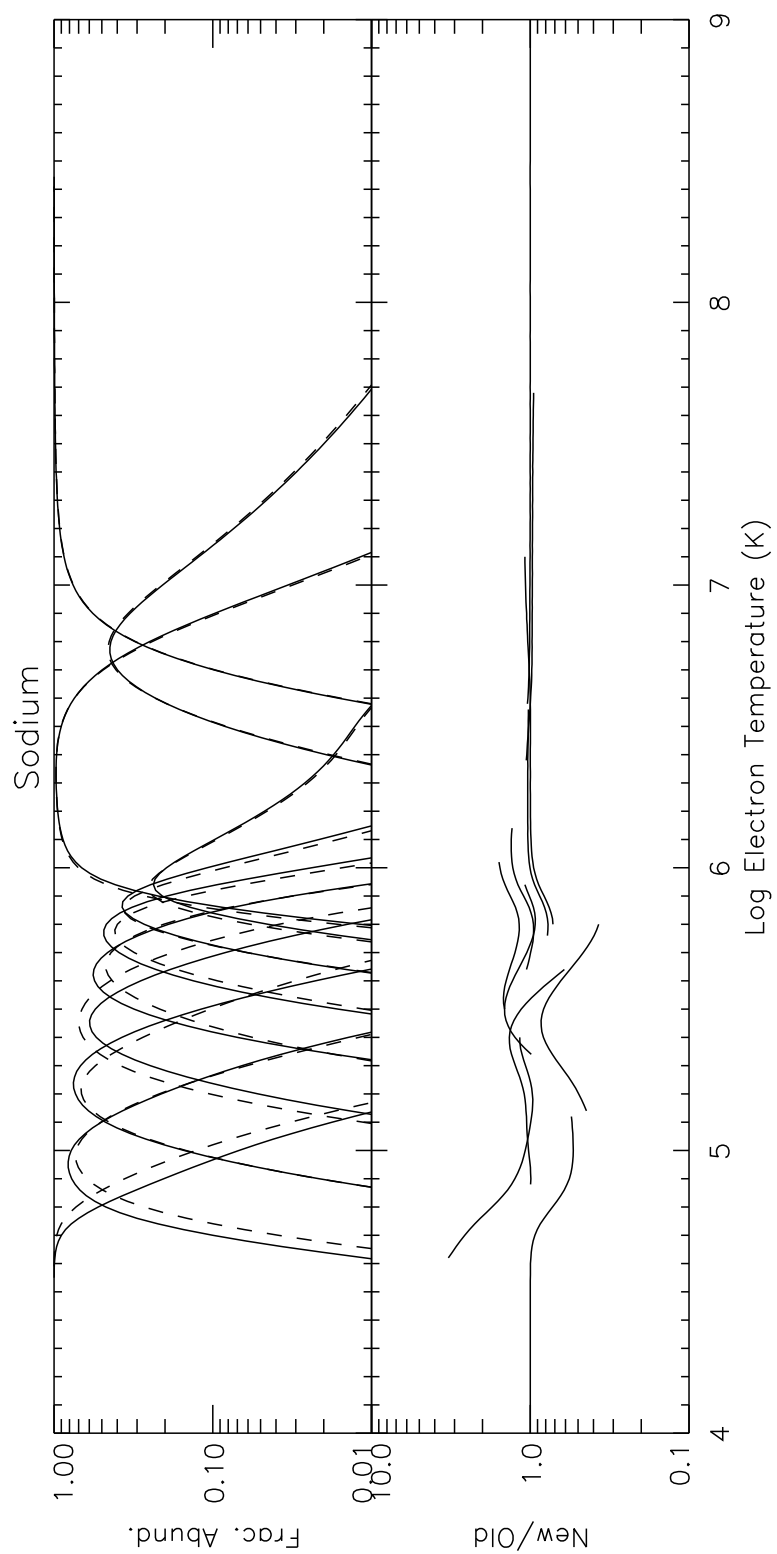


Fig. 11.— Same as Fig. 1 but for Na.

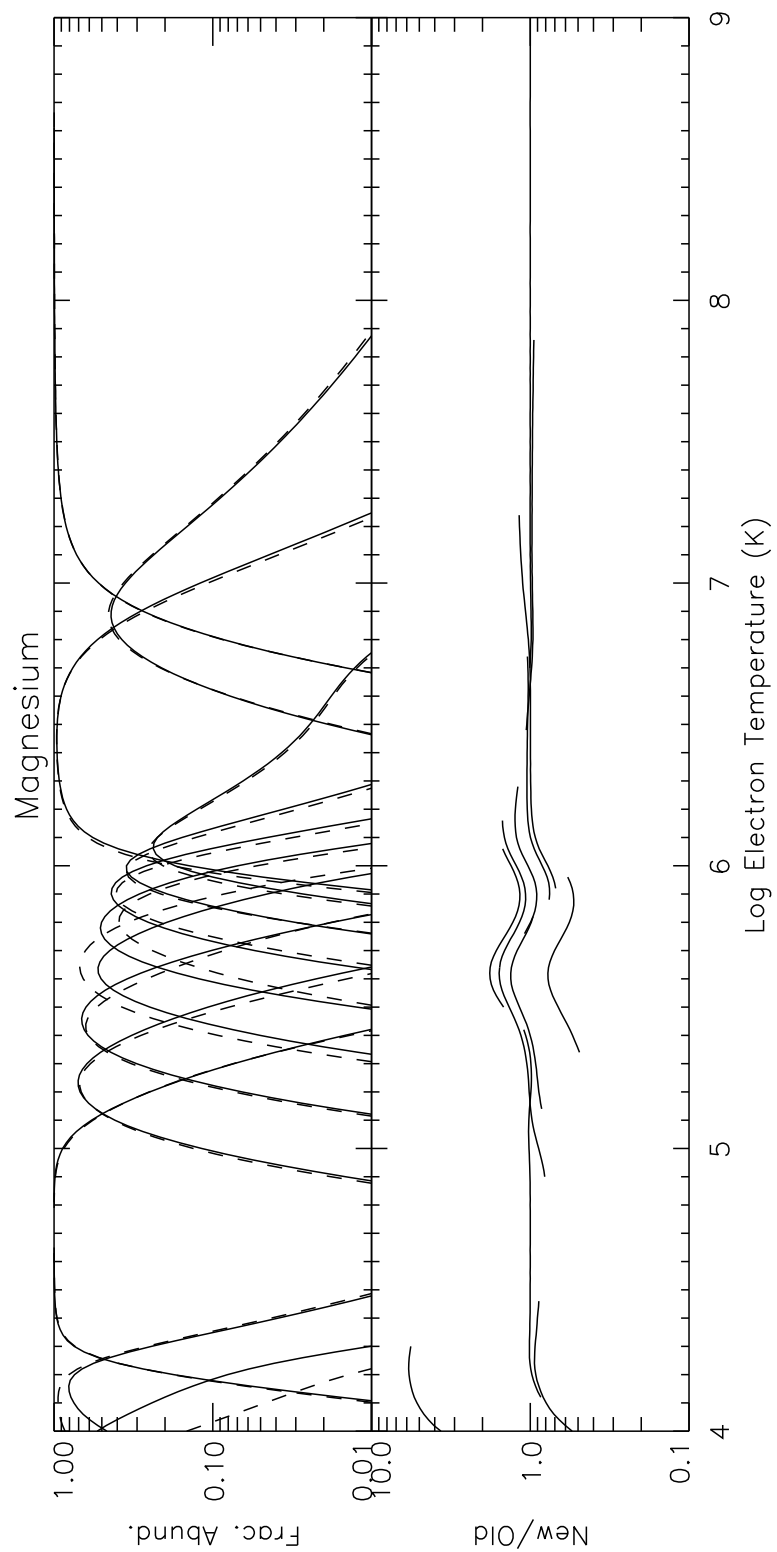


Fig. 12.— Same as Fig. 1 but for Mg.

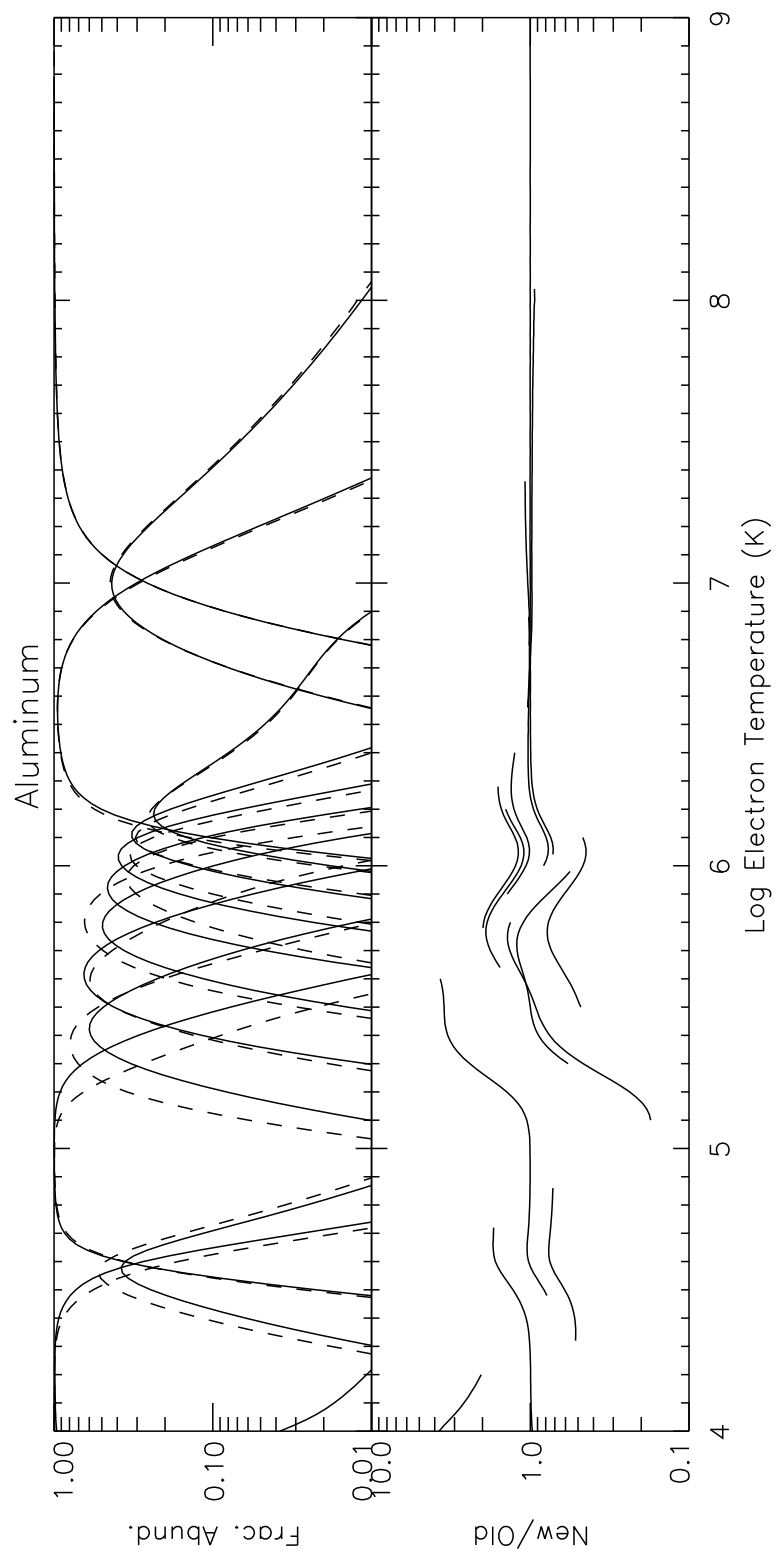


Fig. 13.— Same as Fig. 1 but for Al.

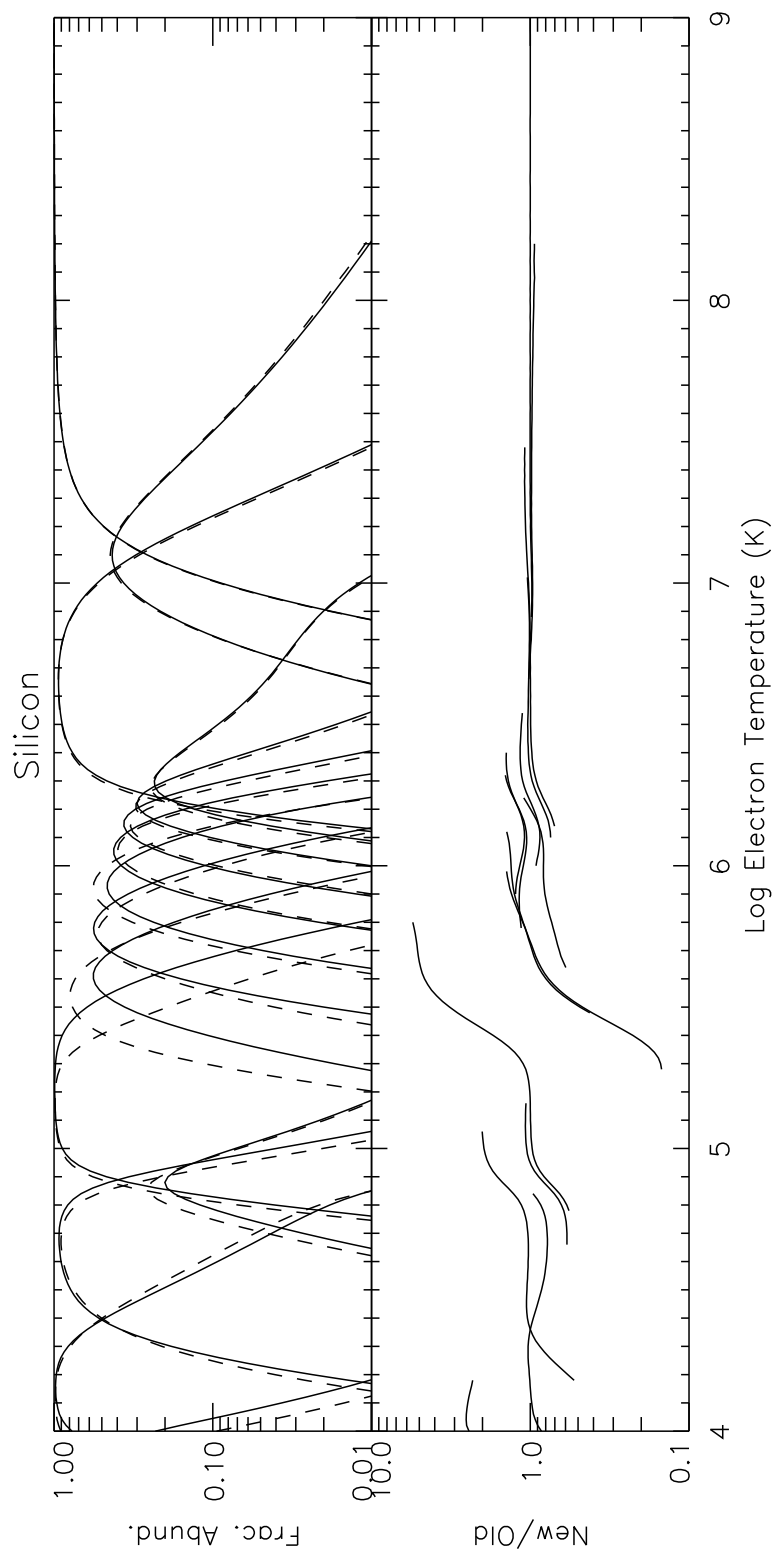


Fig. 14.— Same as Fig. 1 but for Si.

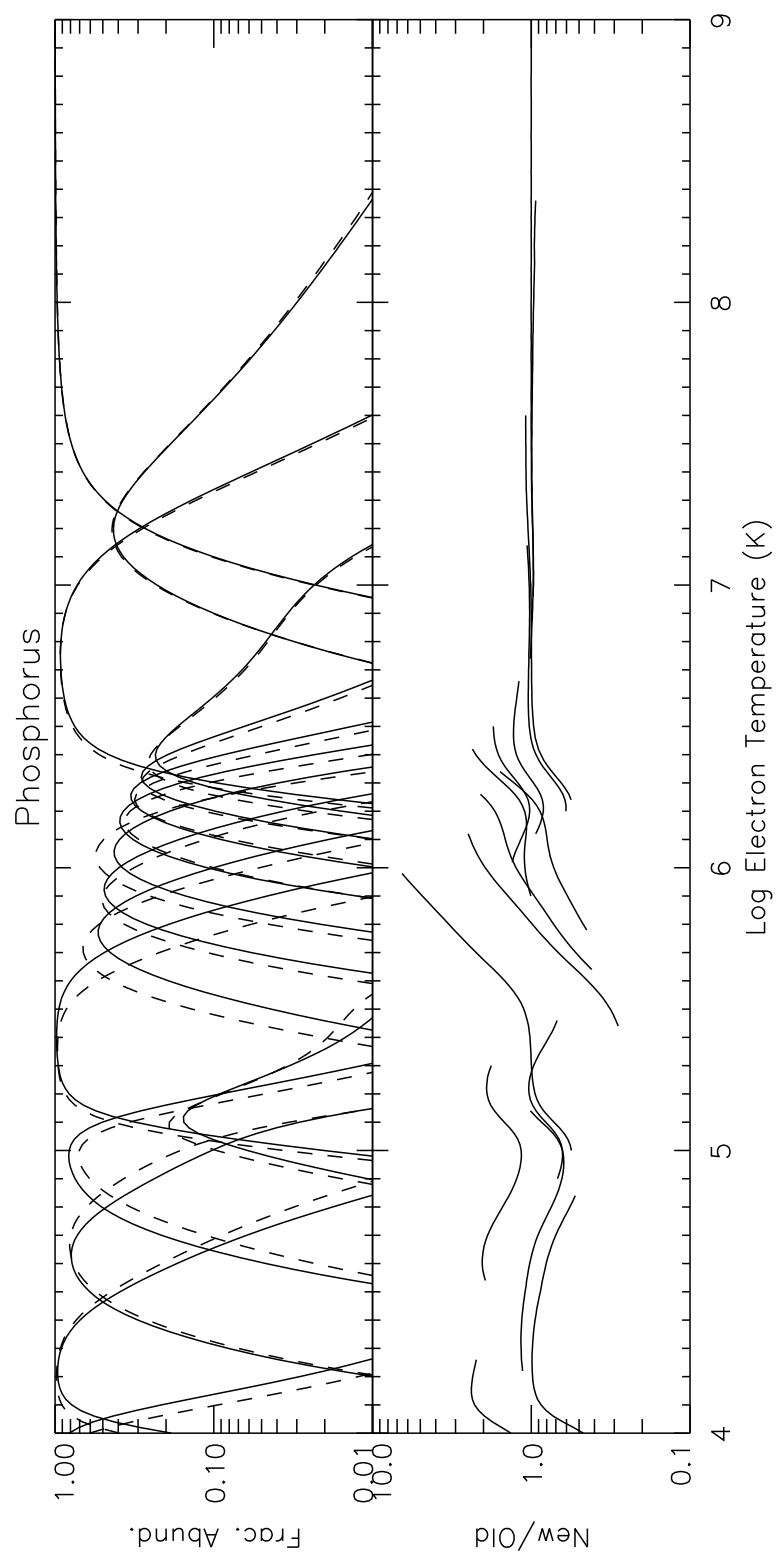


Fig. 15.— Same as Fig. 1 but for P.

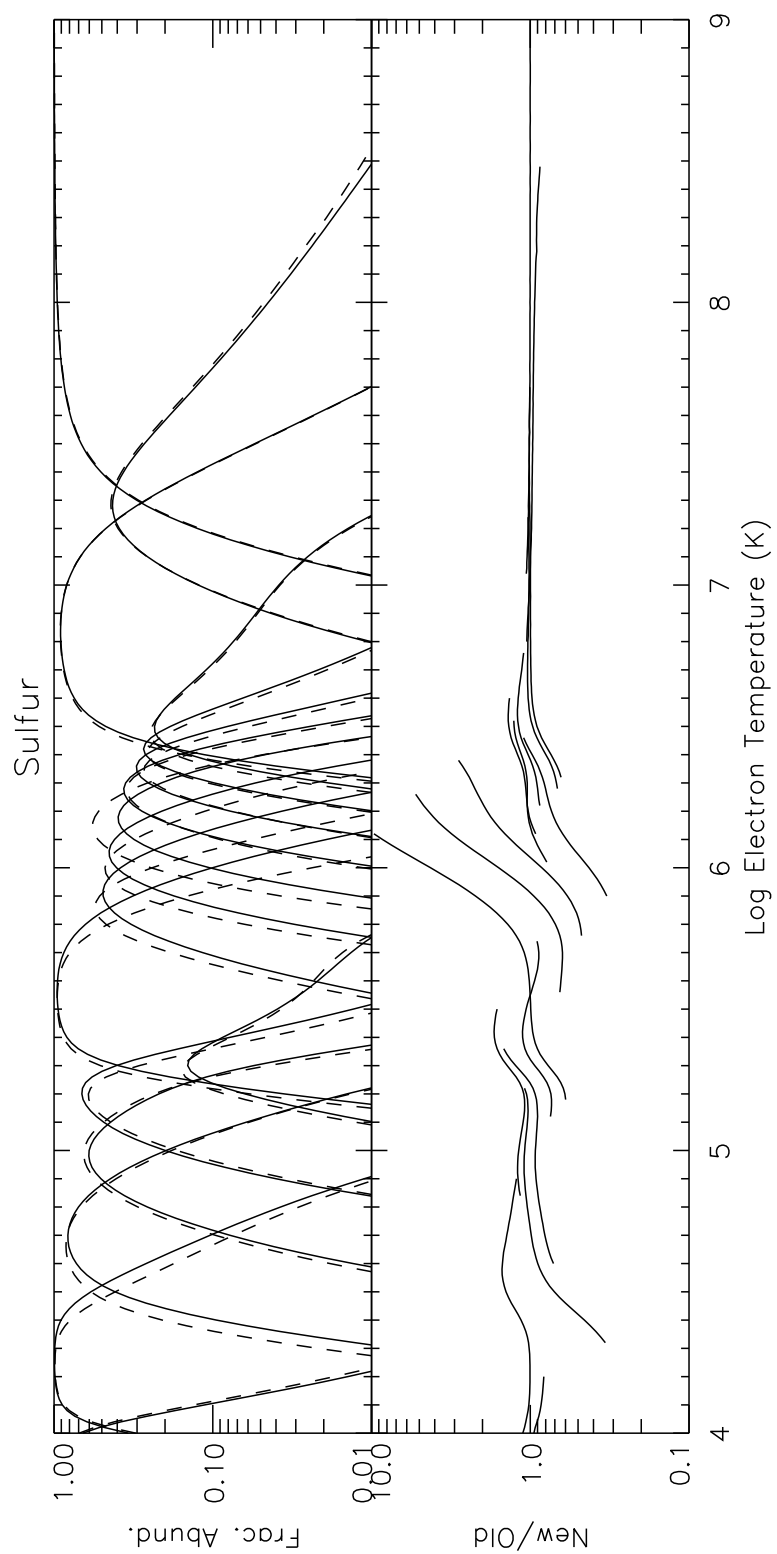


Fig. 16.— Same as Fig. 1 but for S.

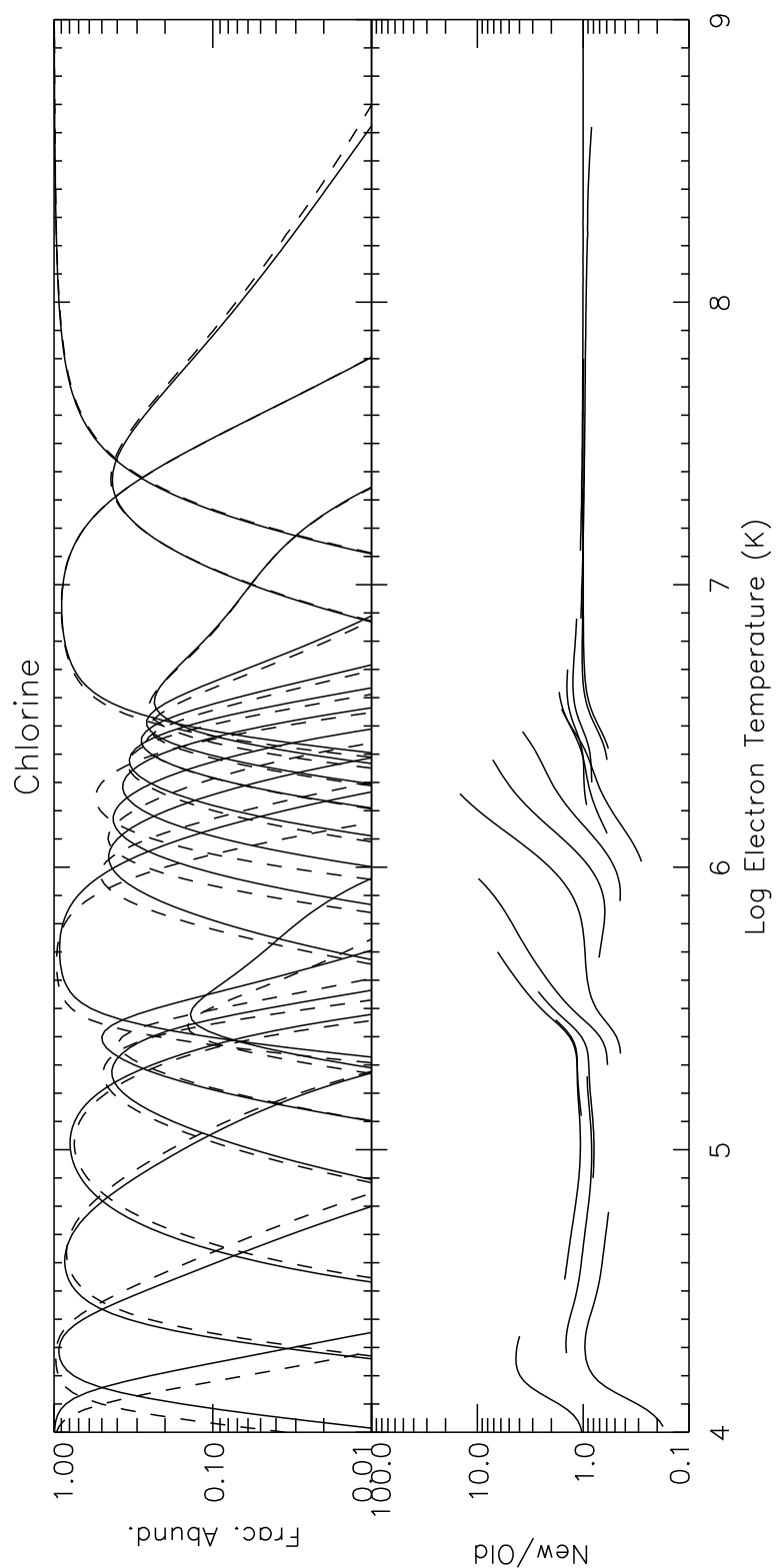


Fig. 17.— Same as Fig. 1 but for Cl.

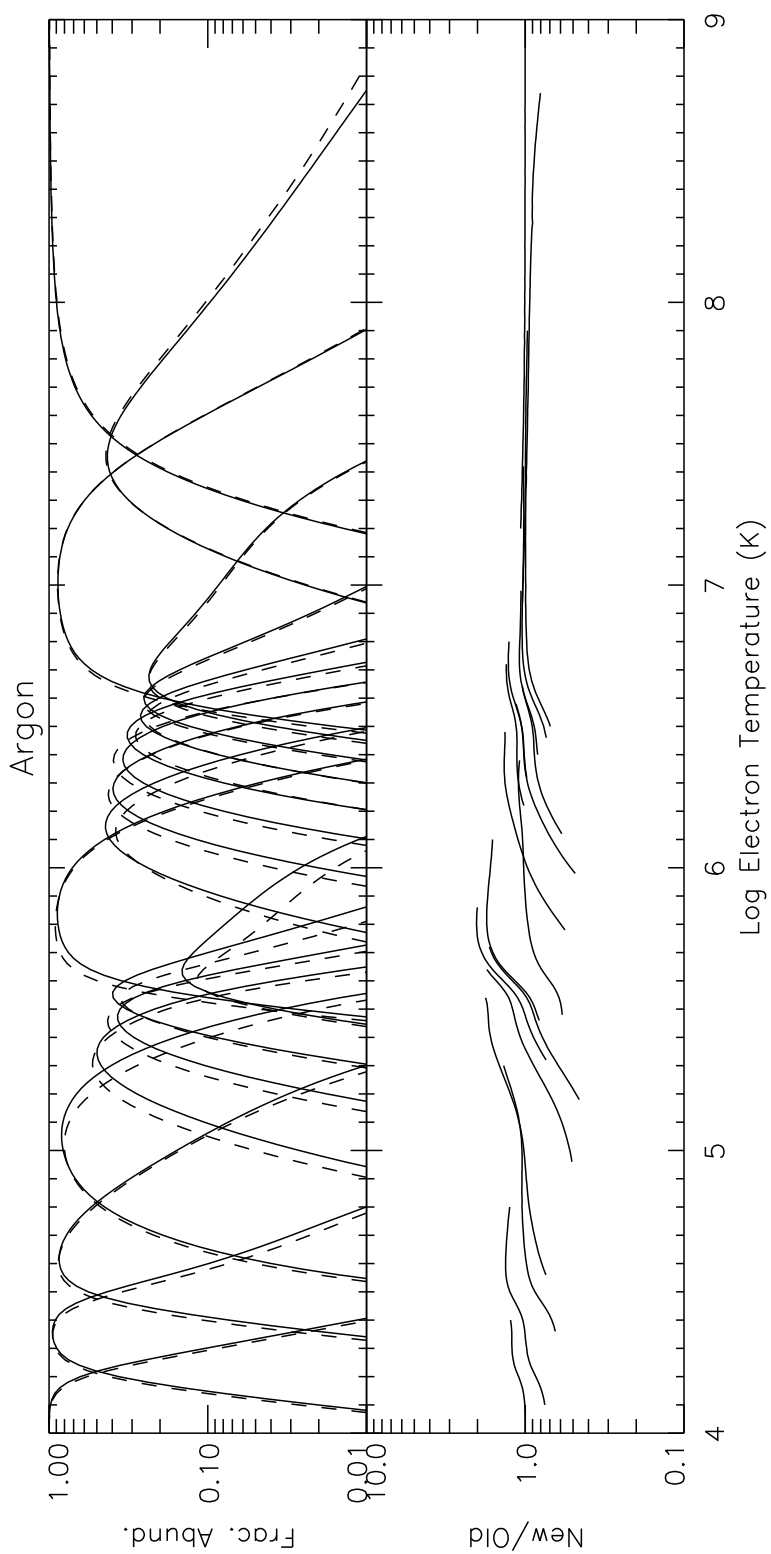


Fig. 18.— Same as Fig. 1 but for Ar.

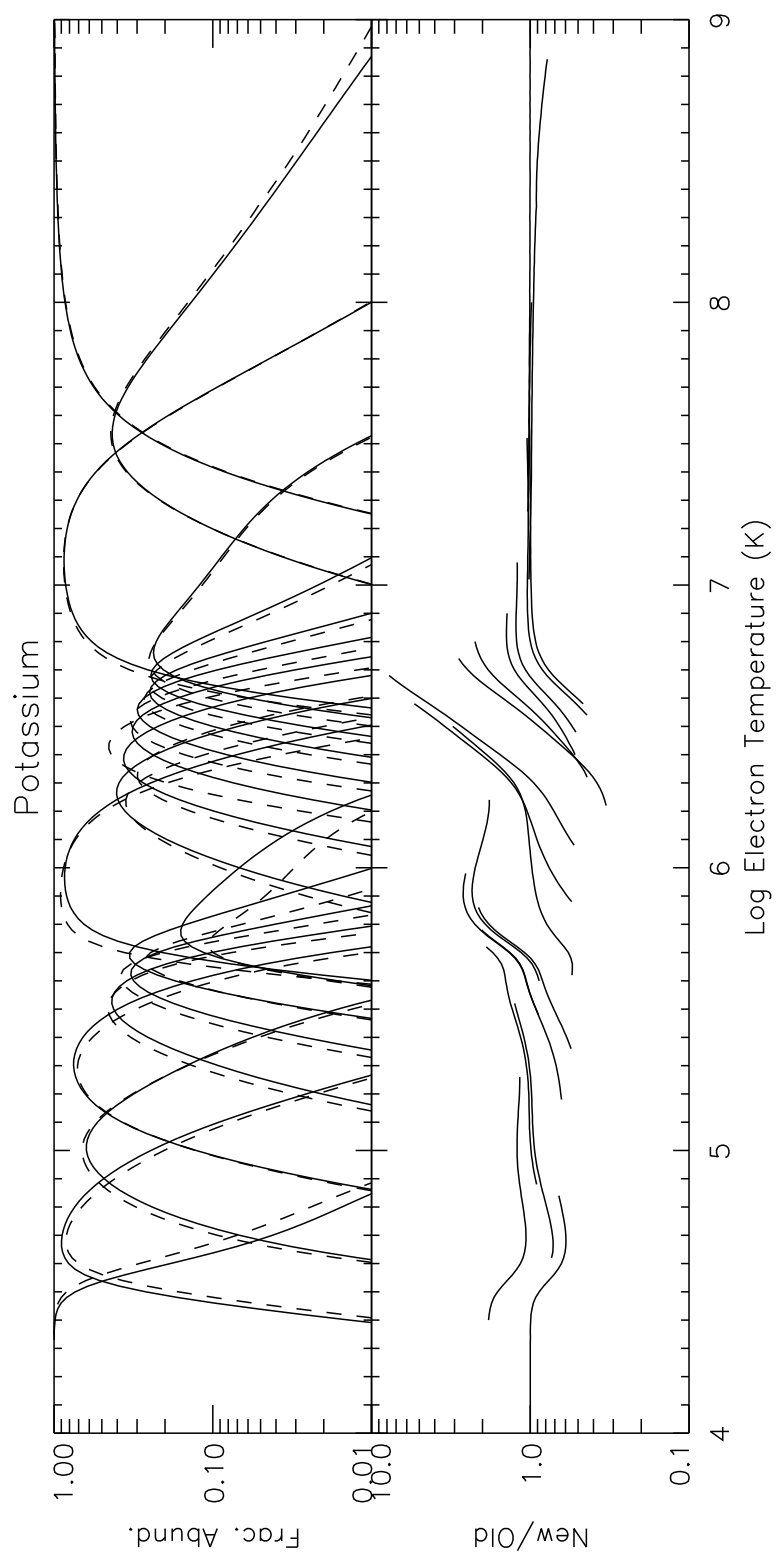


Fig. 19.— Same as Fig. 1 but for K.

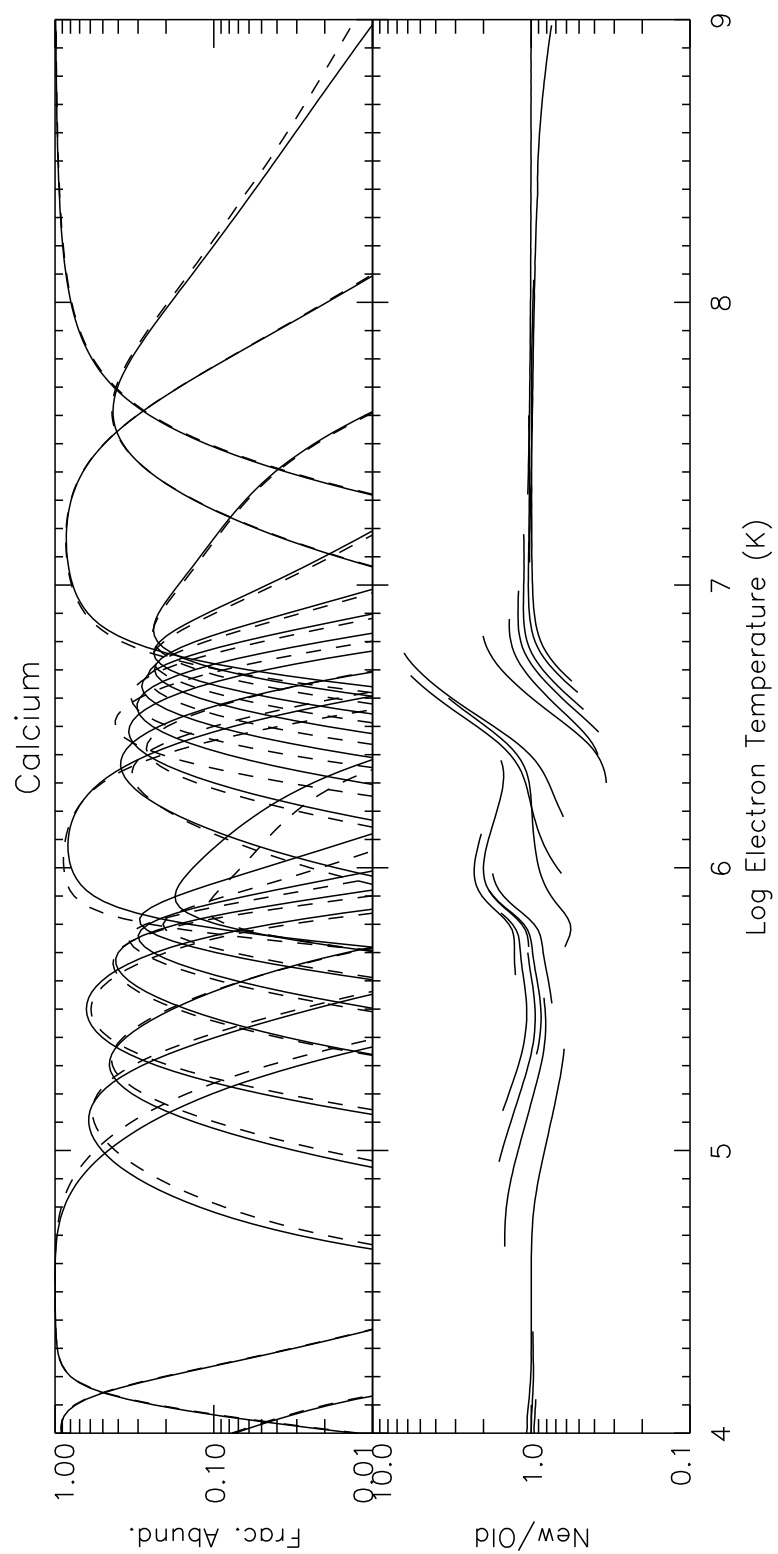


Fig. 20.— Same as Fig. 1 but for Ca.

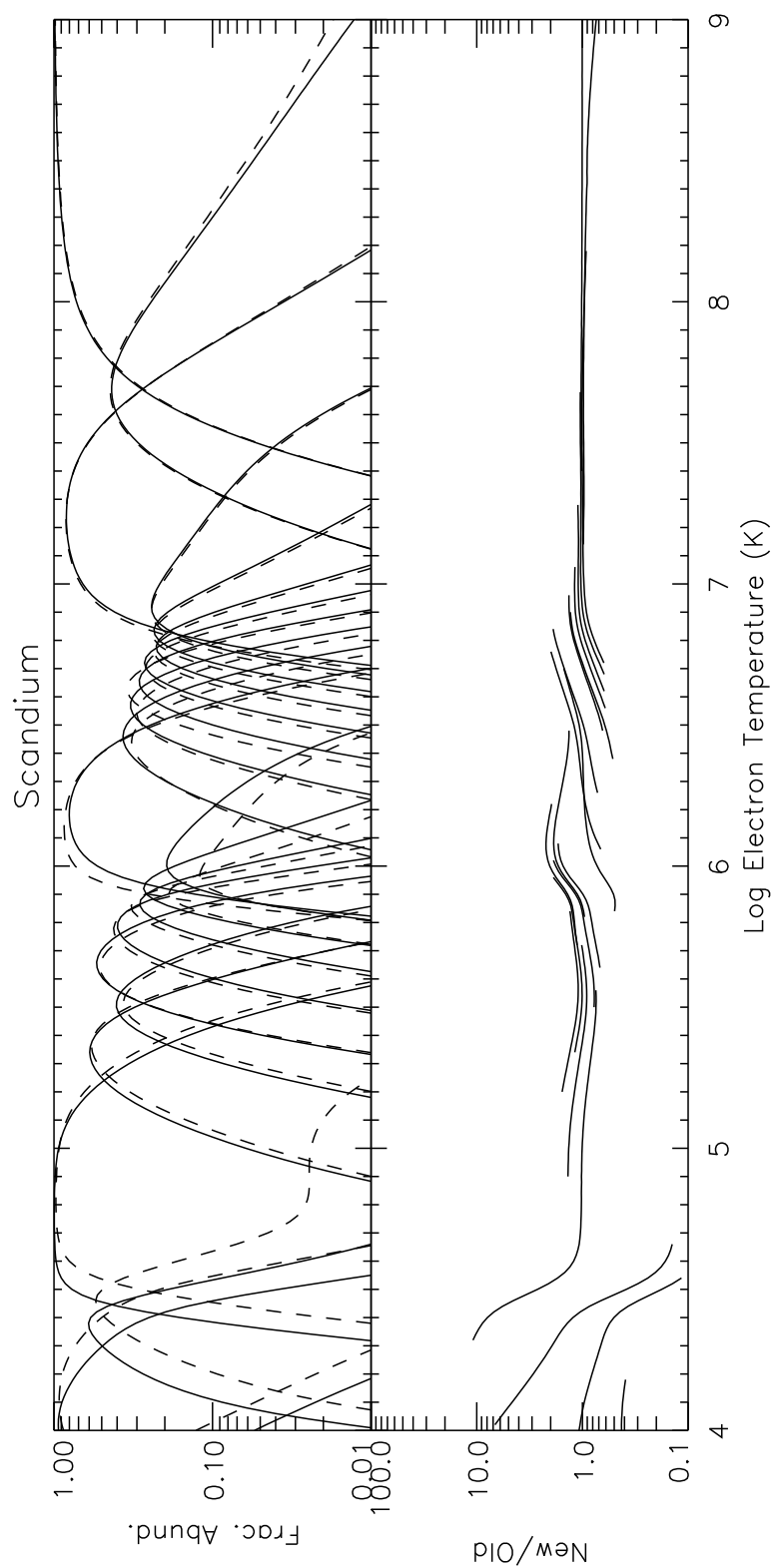


Fig. 21.— Same as Fig. 1 but for Sc.

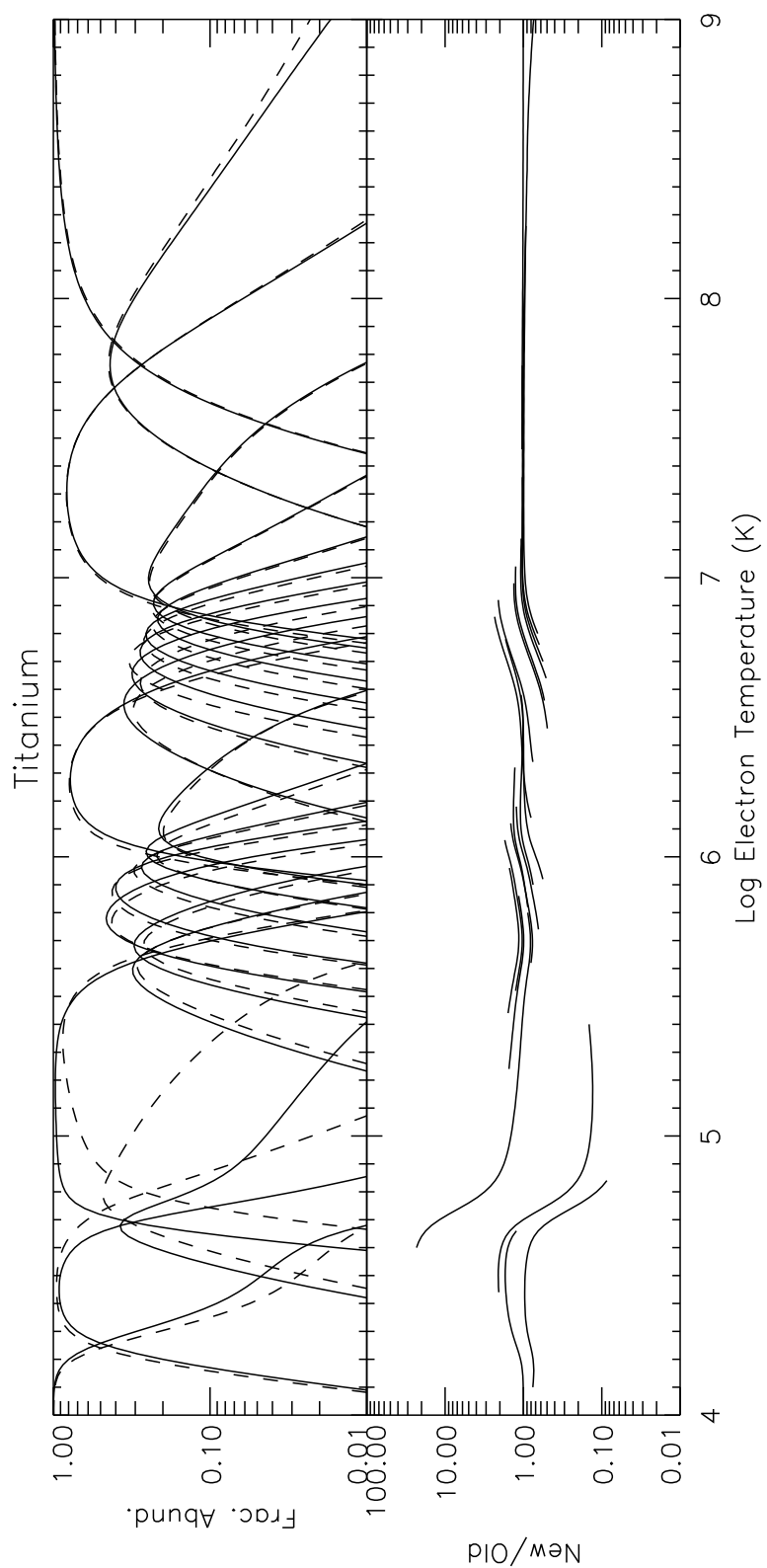


Fig. 22.— Same as Fig. 1 but for Ti.

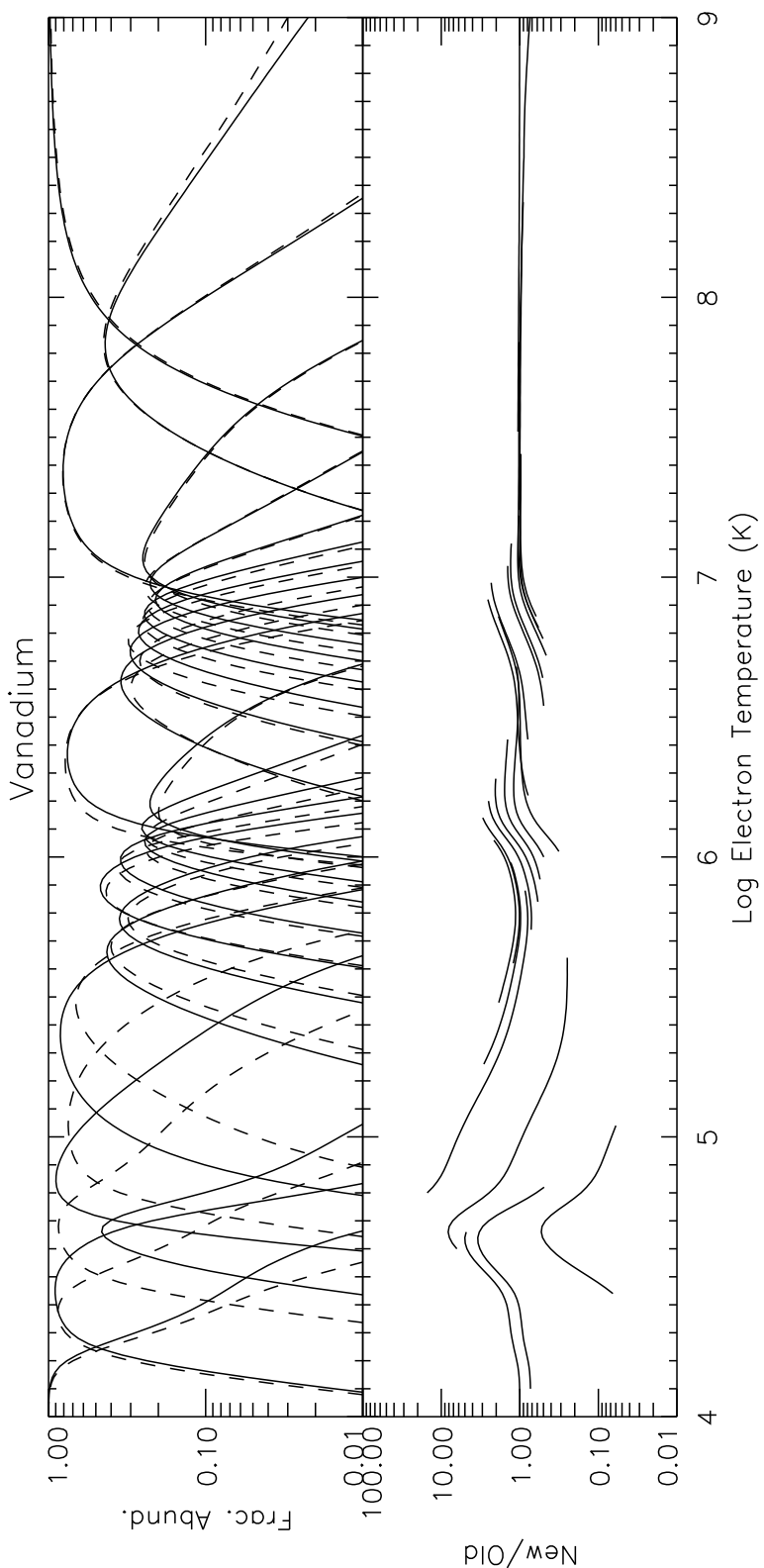


Fig. 23.— Same as Fig. 1 but for V.

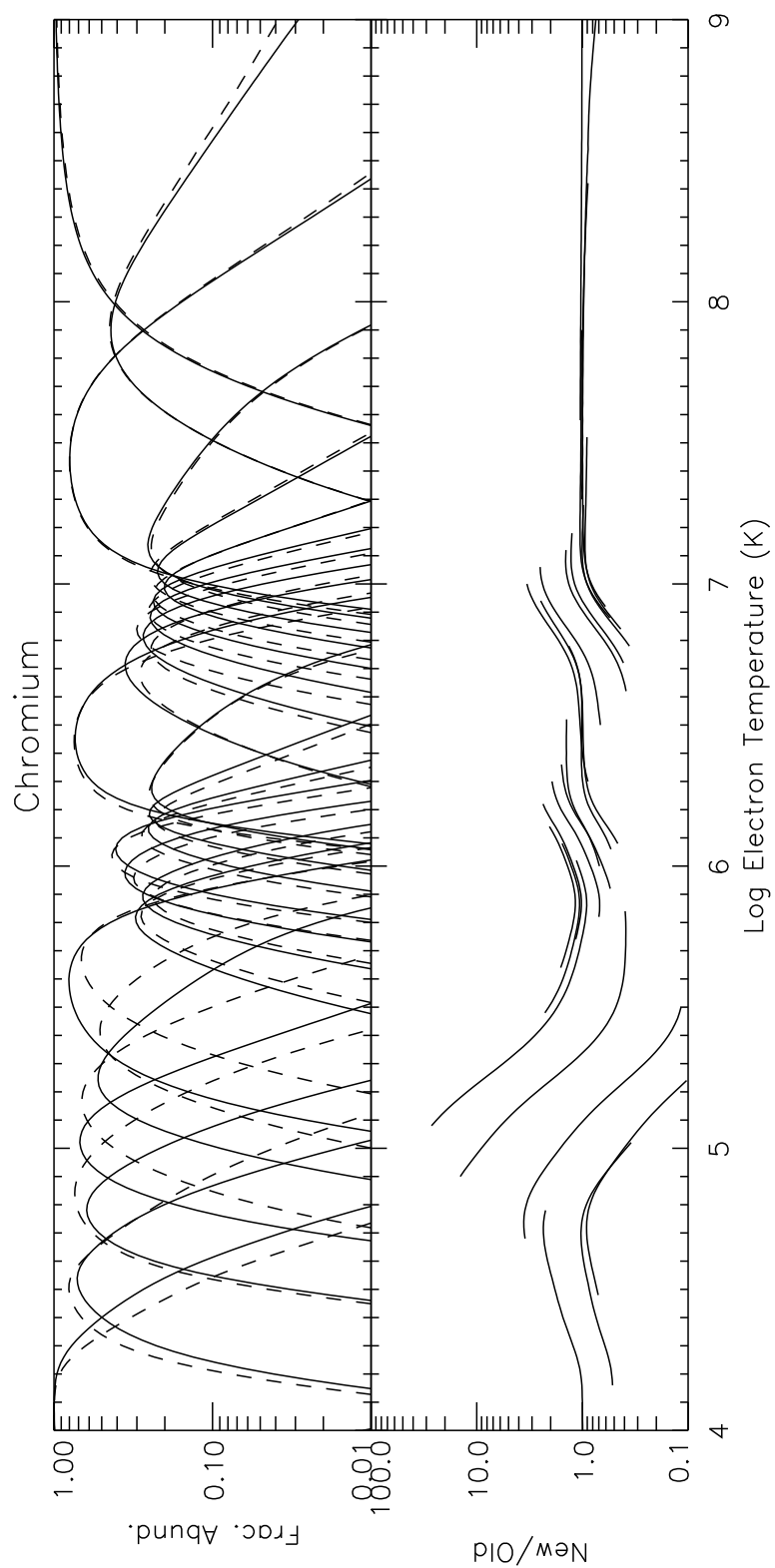


Fig. 24.— Same as Fig. 1 but for Cr.

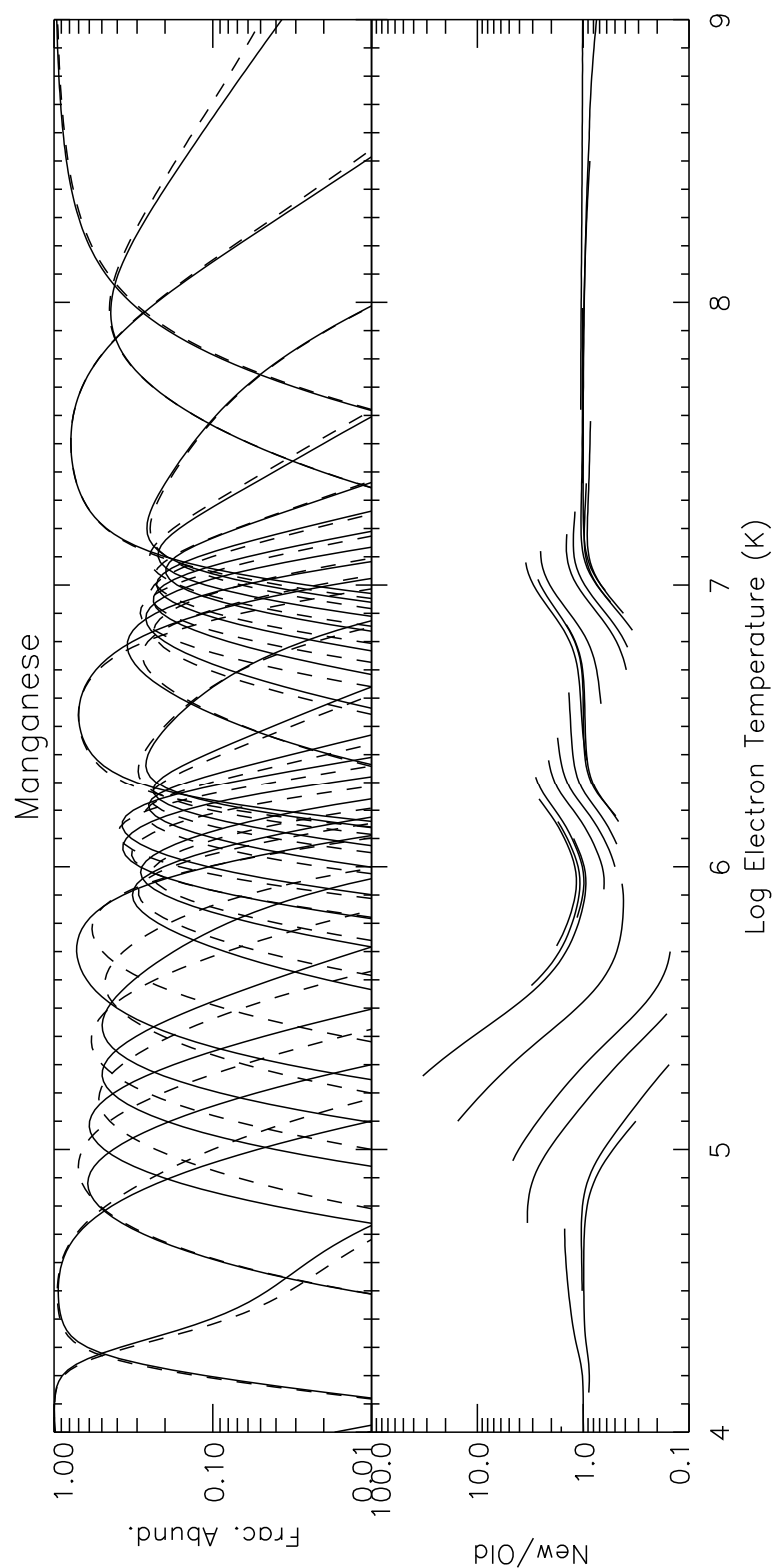


Fig. 25.— Same as Fig. 1 but for Mn.

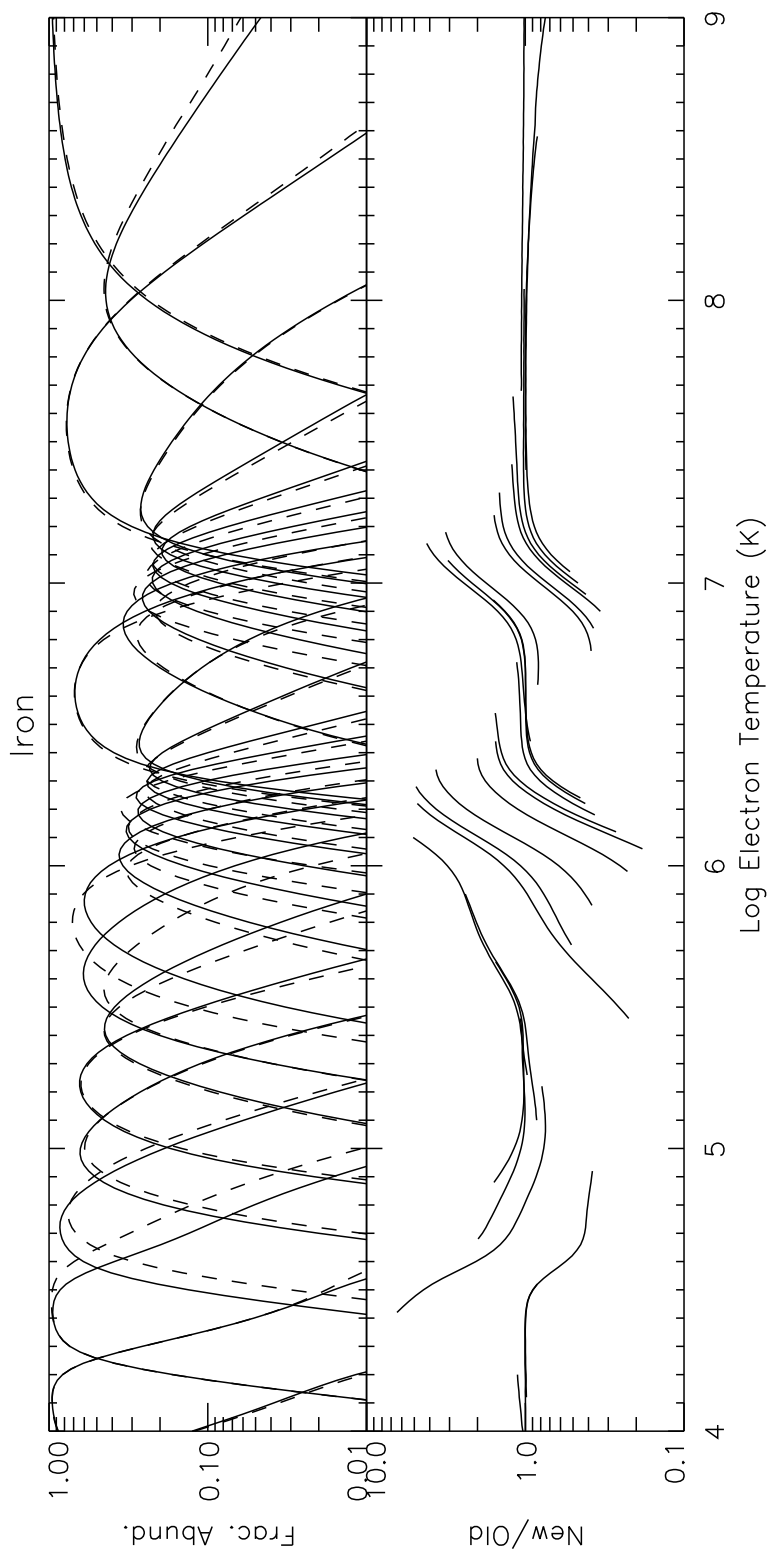


Fig. 26.— Same as Fig. 1 but for Fe.

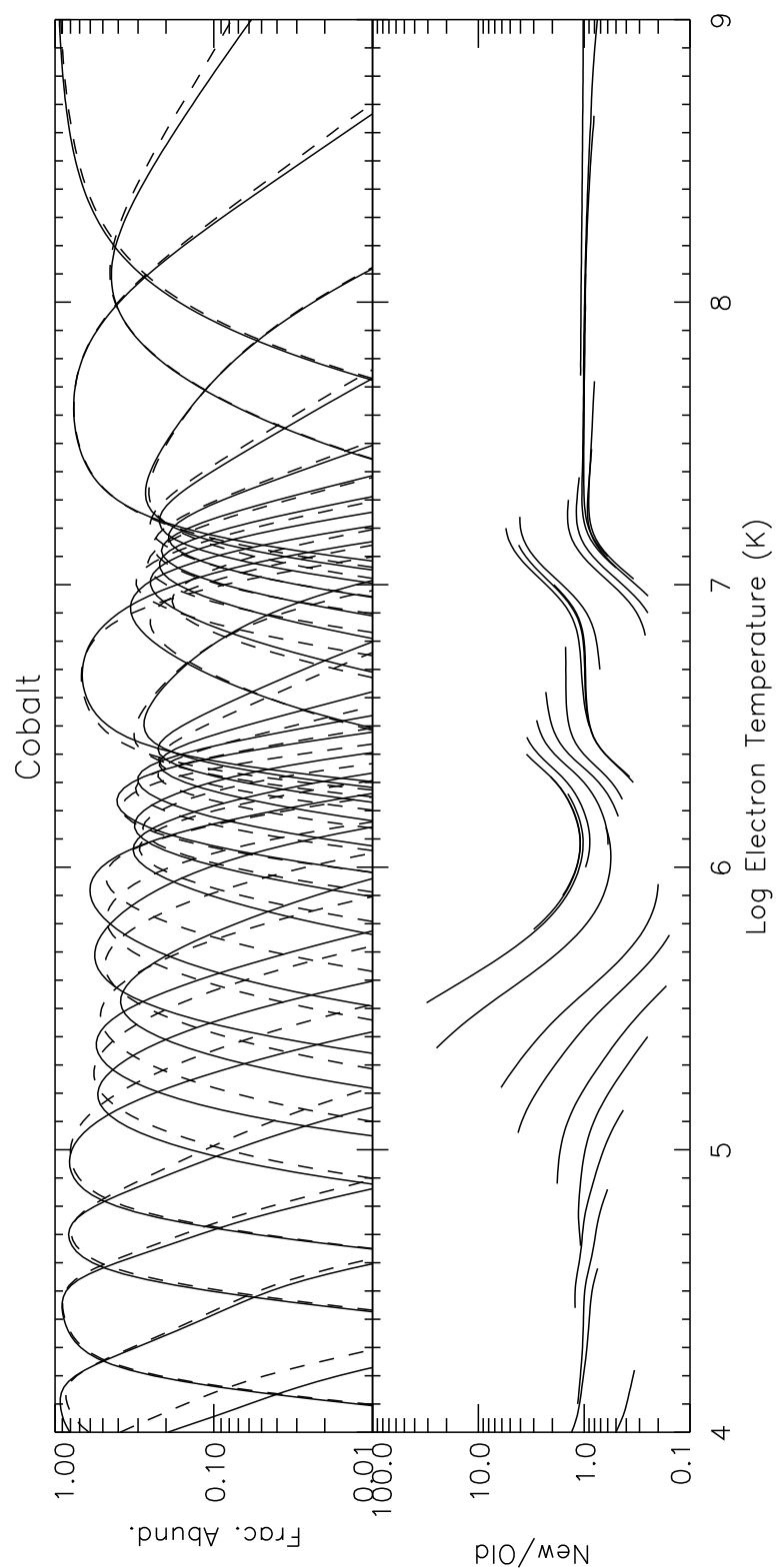


Fig. 27.— Same as Fig. 1 but for Co.

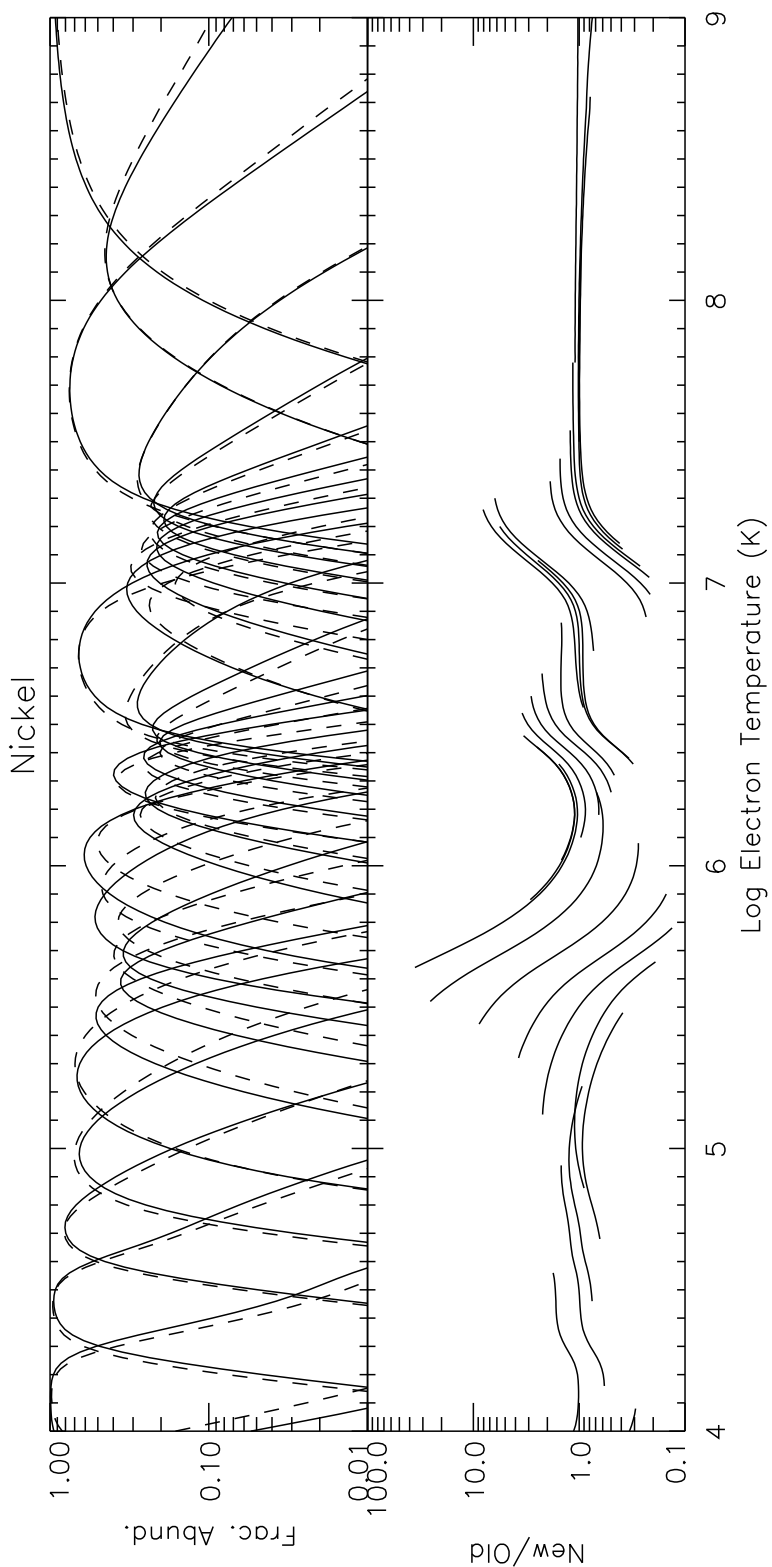


Fig. 28.— Same as Fig. 1 but for Ni.

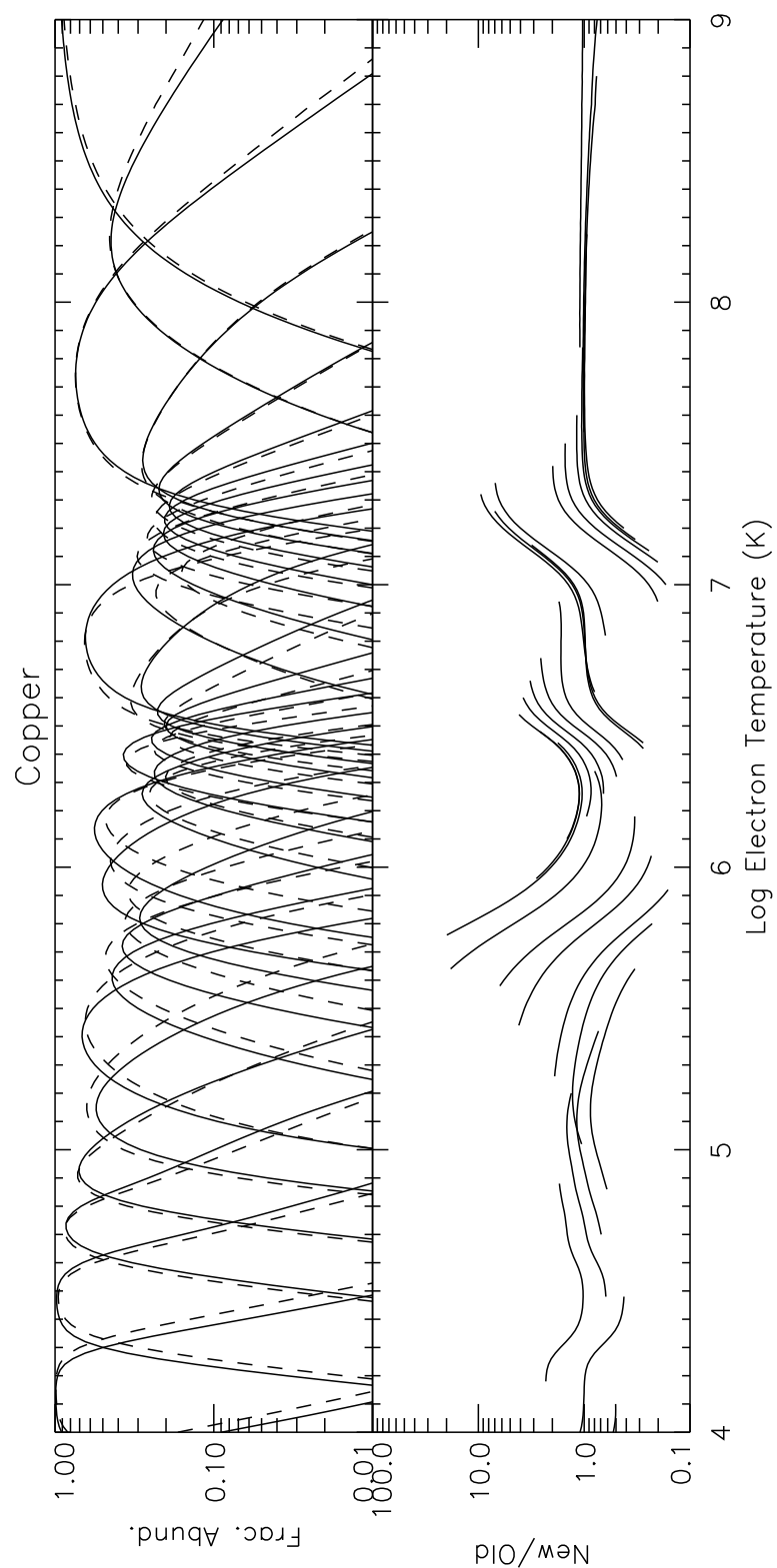


Fig. 29.— Same as Fig. 1 but for Cu.

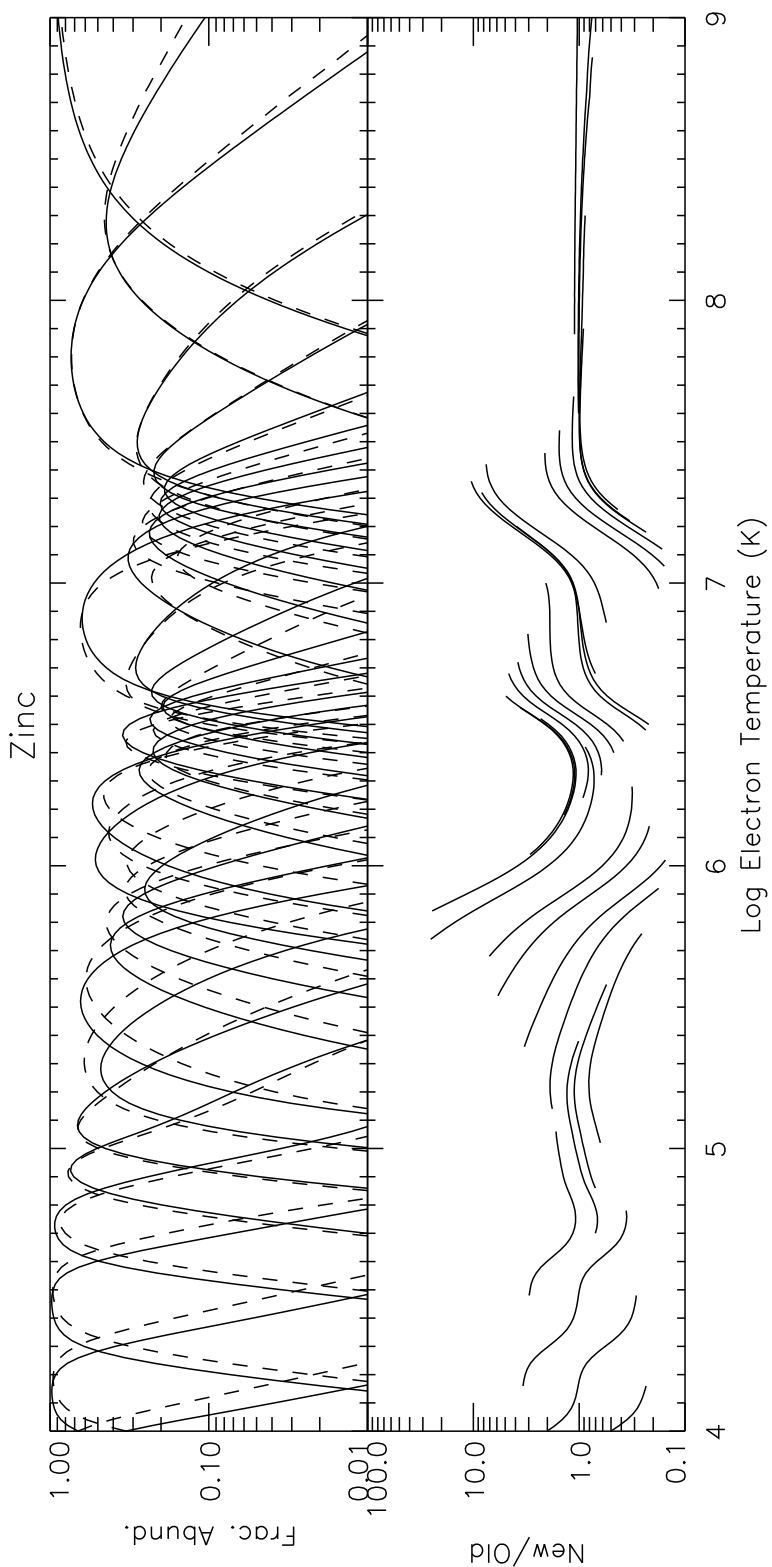


Fig. 30.— Same as Fig. 1 but for Zn.

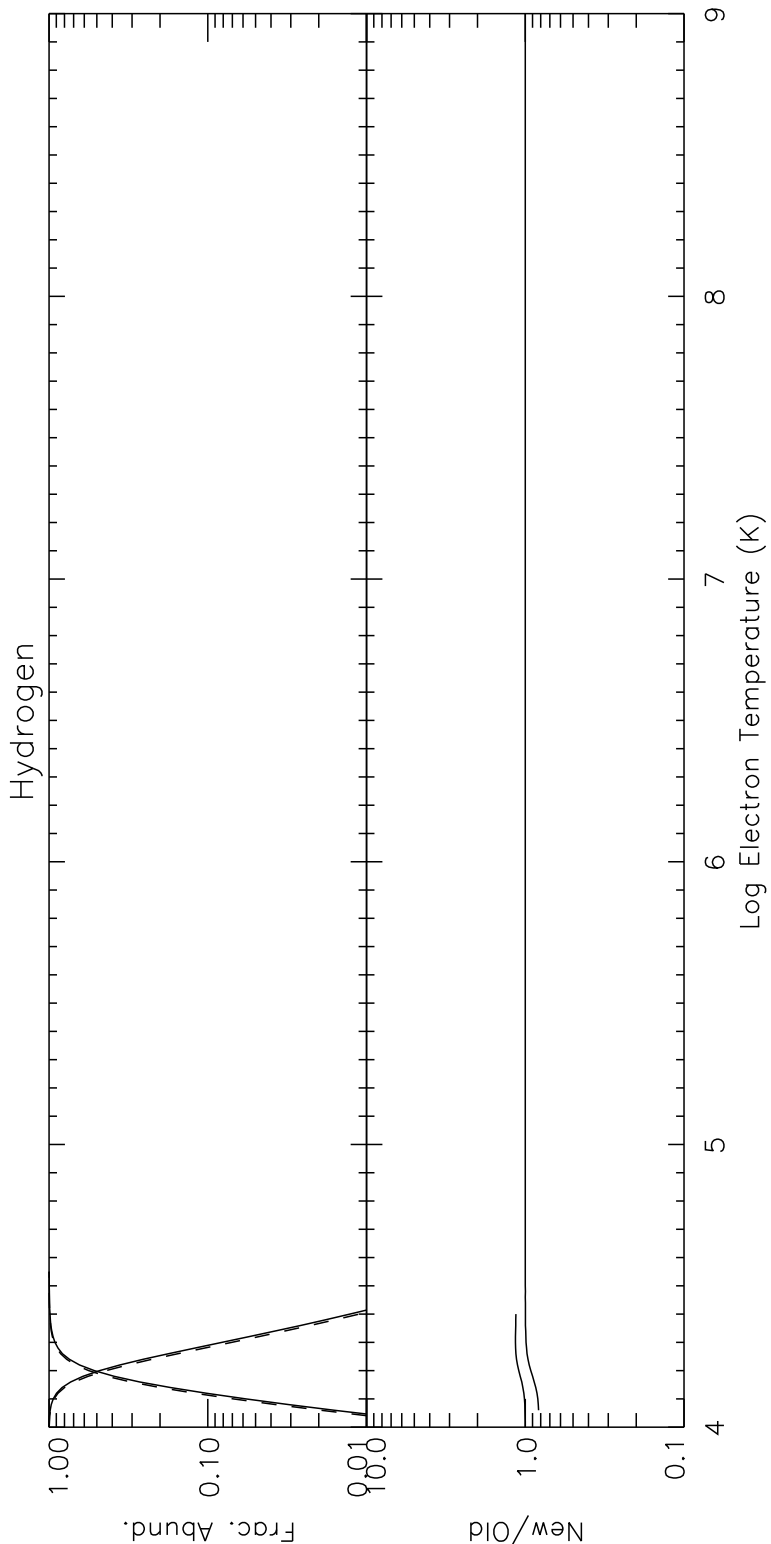


Fig. 31.— Ionization fractional abundance versus electron temperature for all ionization stages of H. The upper graph shows our results (*solid curves*) and the abundances calculated by Bryans et al. (2006; *dashed curves*). The lower graph shows the ratio of the calculated abundances. Comparison is made only for fractional abundances greater than 10^{-2} . We label our results as “New” and those of Bryans et al. (2006) as “Old”.

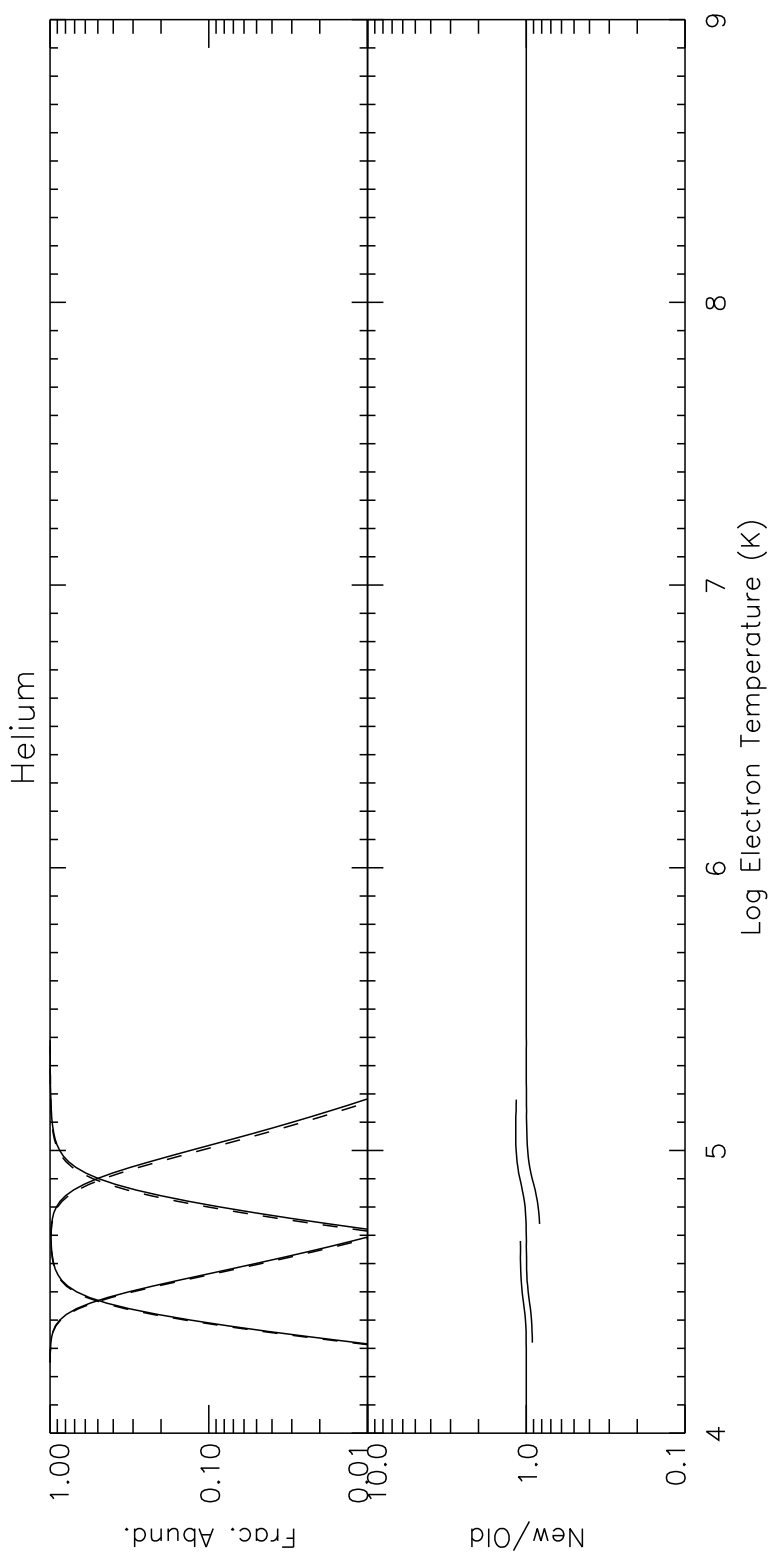


Fig. 32.— Same as Fig. 31 but for He.

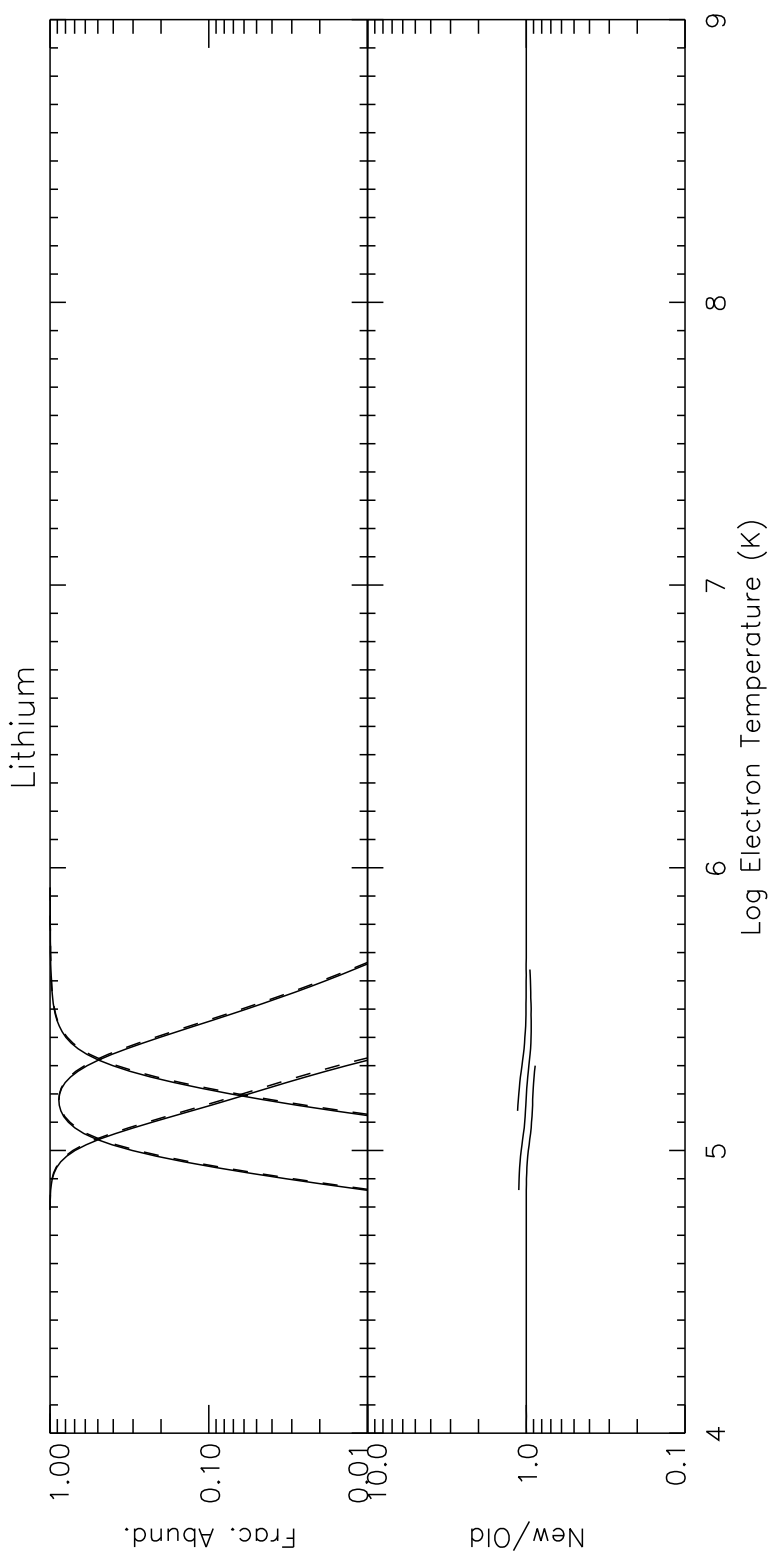


Fig. 33.— Same as Fig. 31 but for Li.

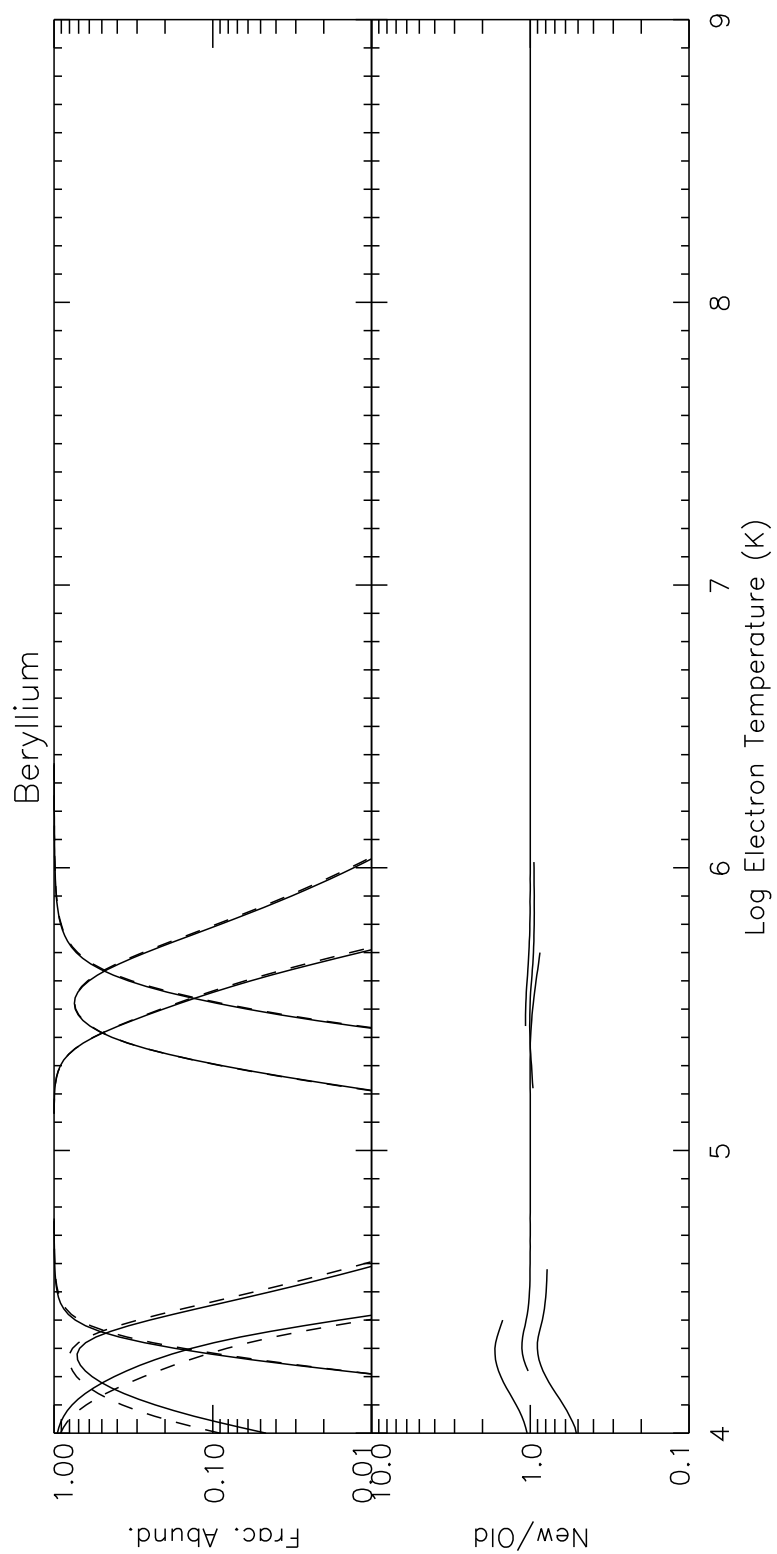


Fig. 34.— Same as Fig. 31 but for Be.

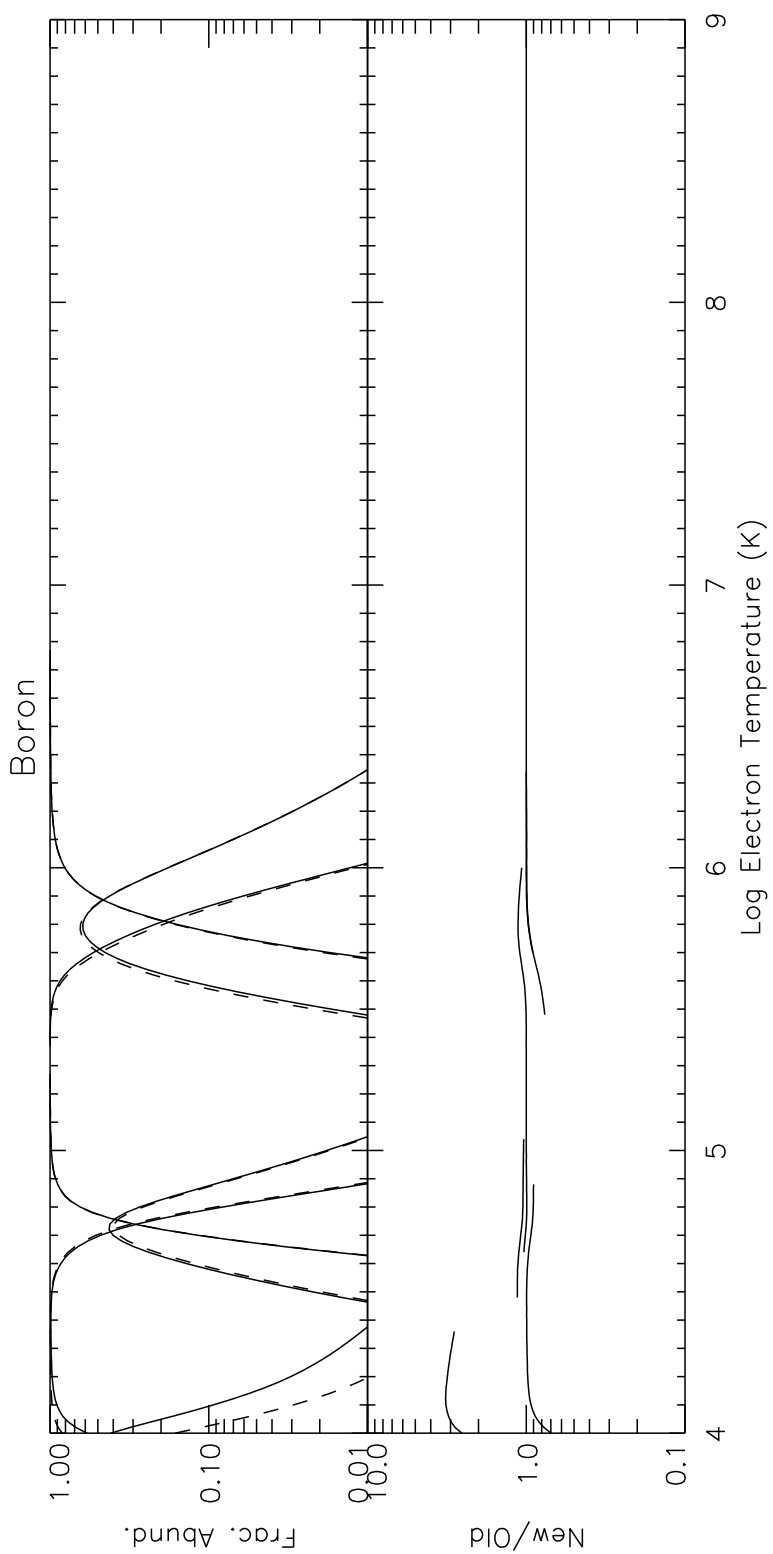


Fig. 35.— Same as Fig. 31 but for B.

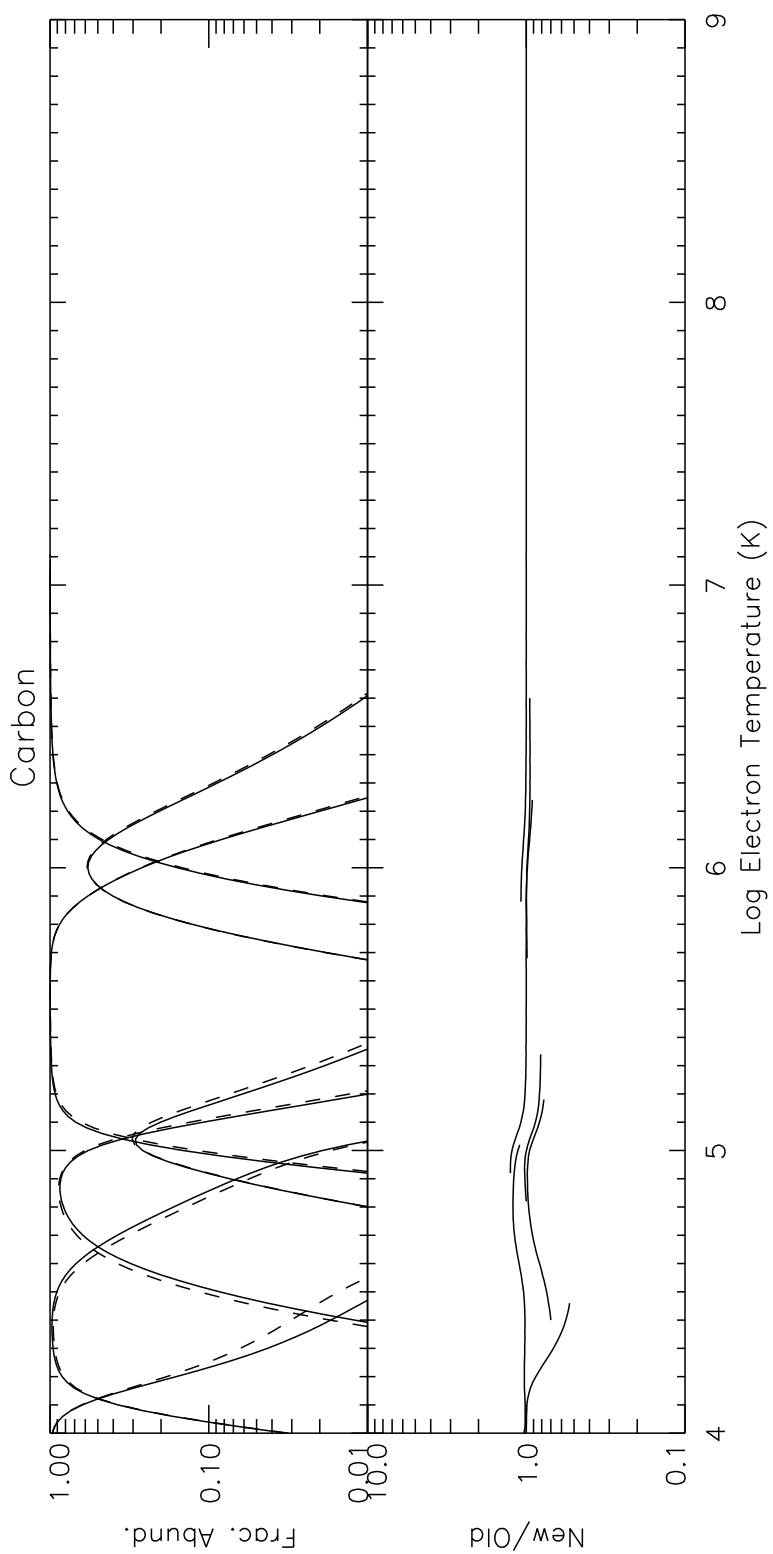


Fig. 36.— Same as Fig. 31 but for C.

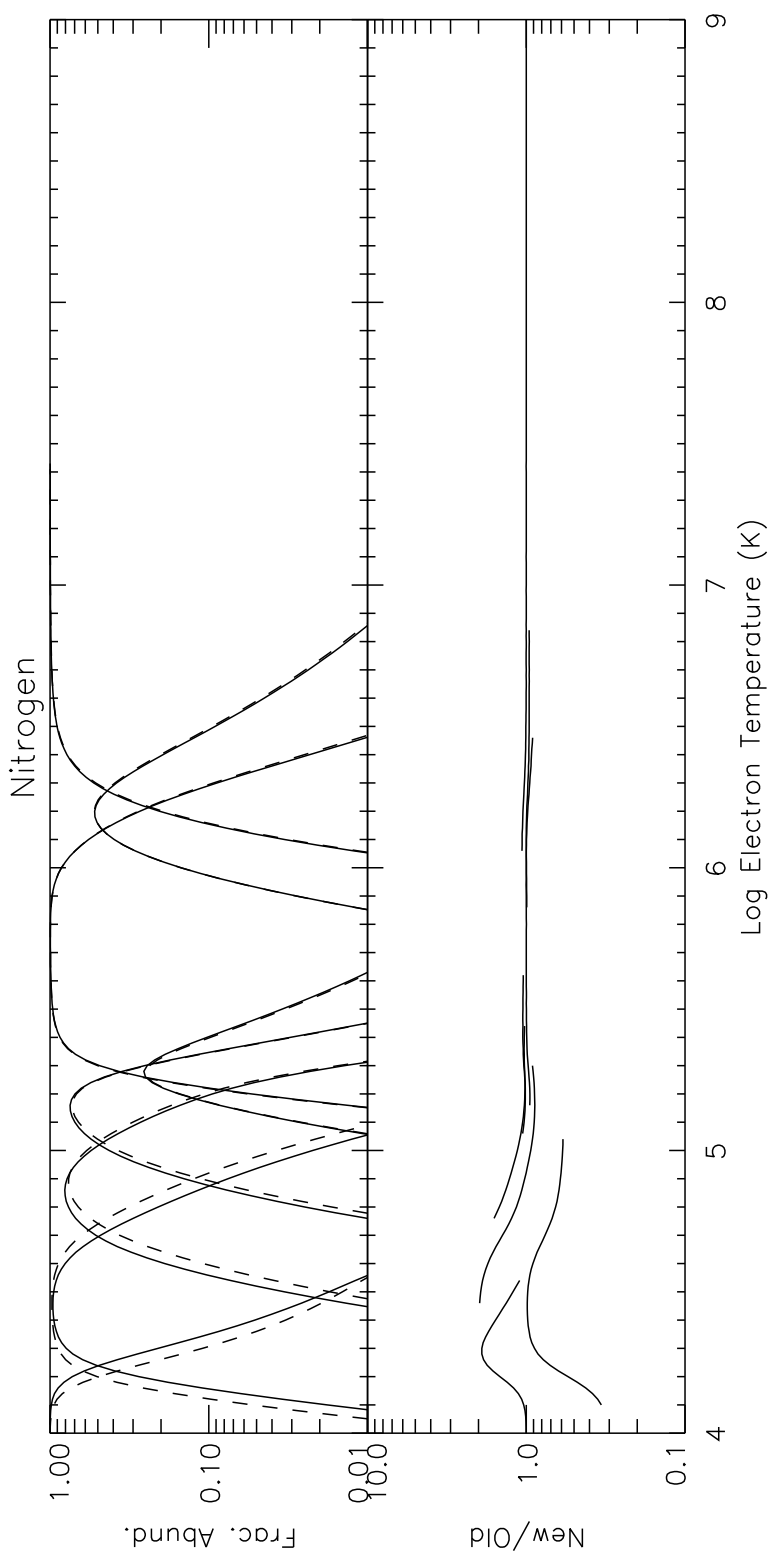


Fig. 37.— Same as Fig. 31 but for N.

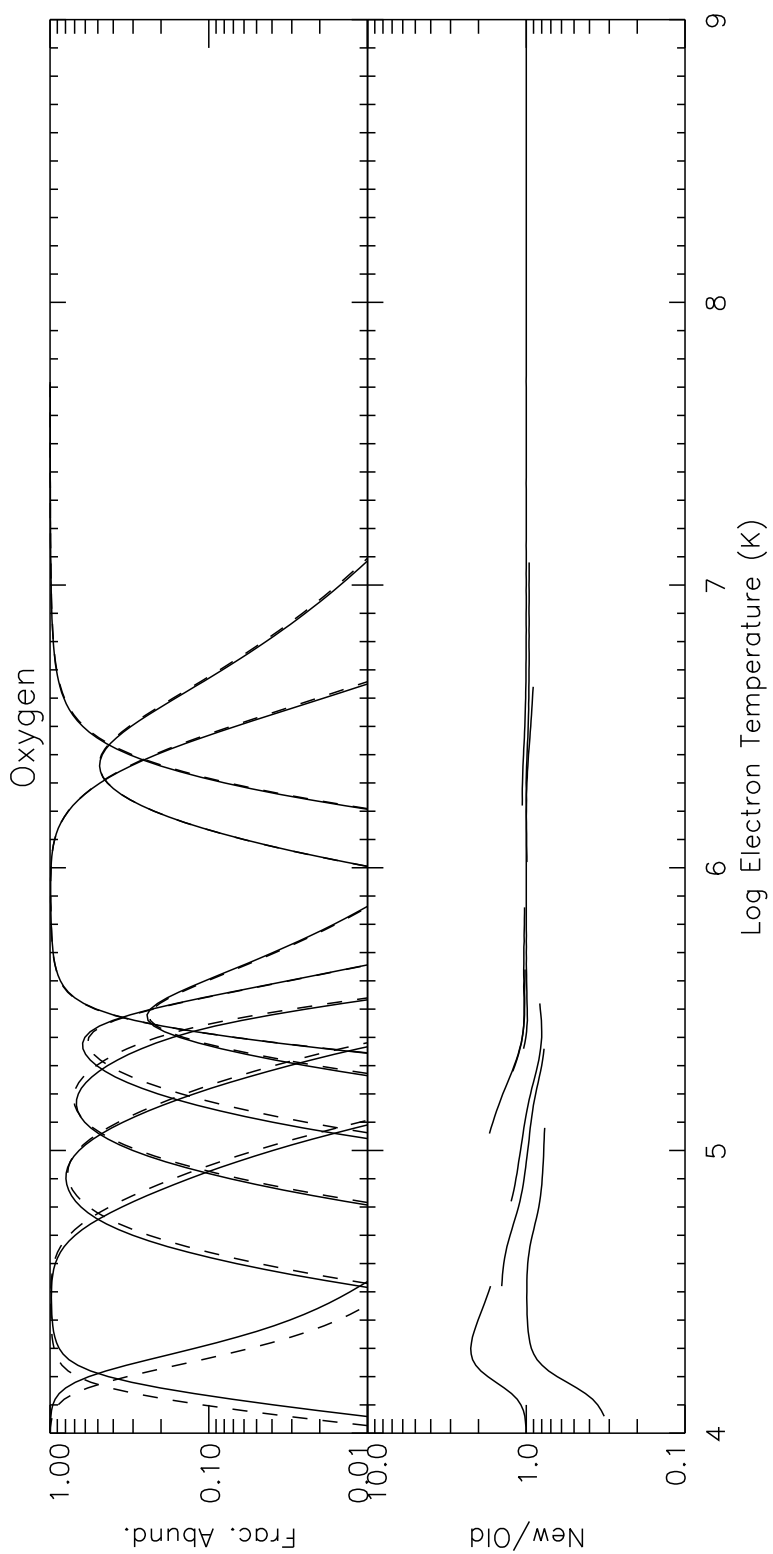


Fig. 38.— Same as Fig. 31 but for O.

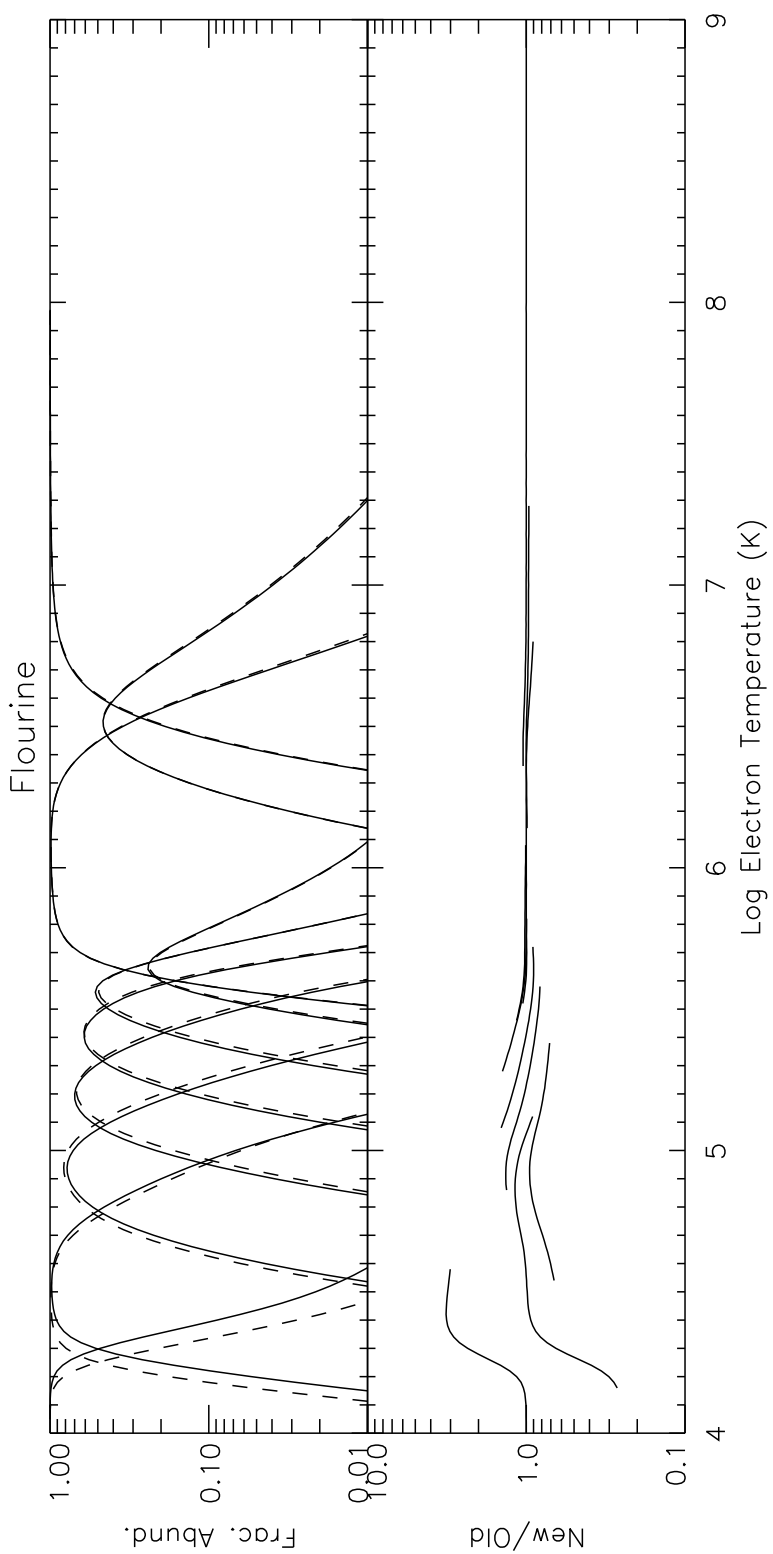


Fig. 39.— Same as Fig. 31 but for F.

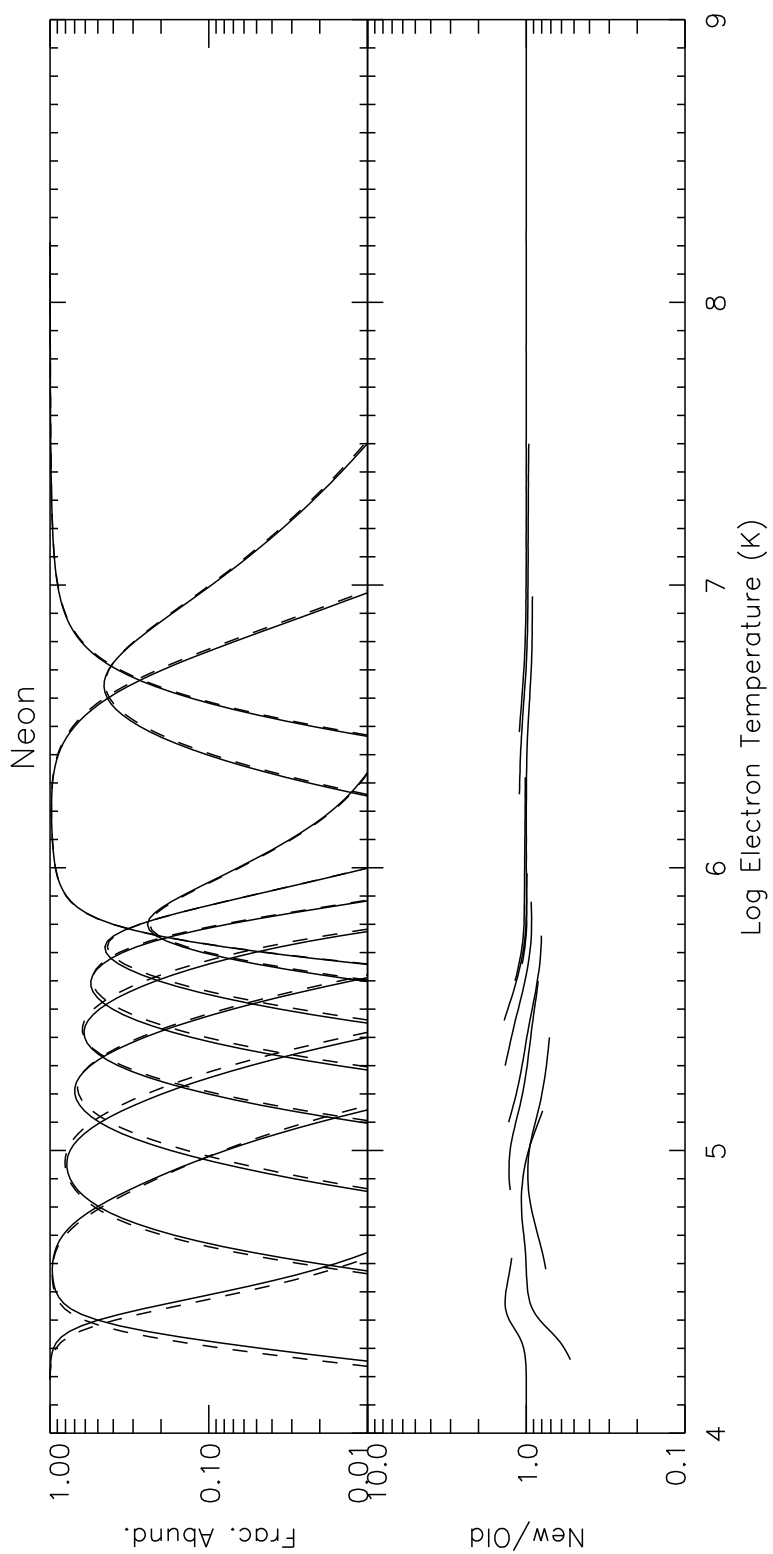


Fig. 40.— Same as Fig. 31 but for Ne.

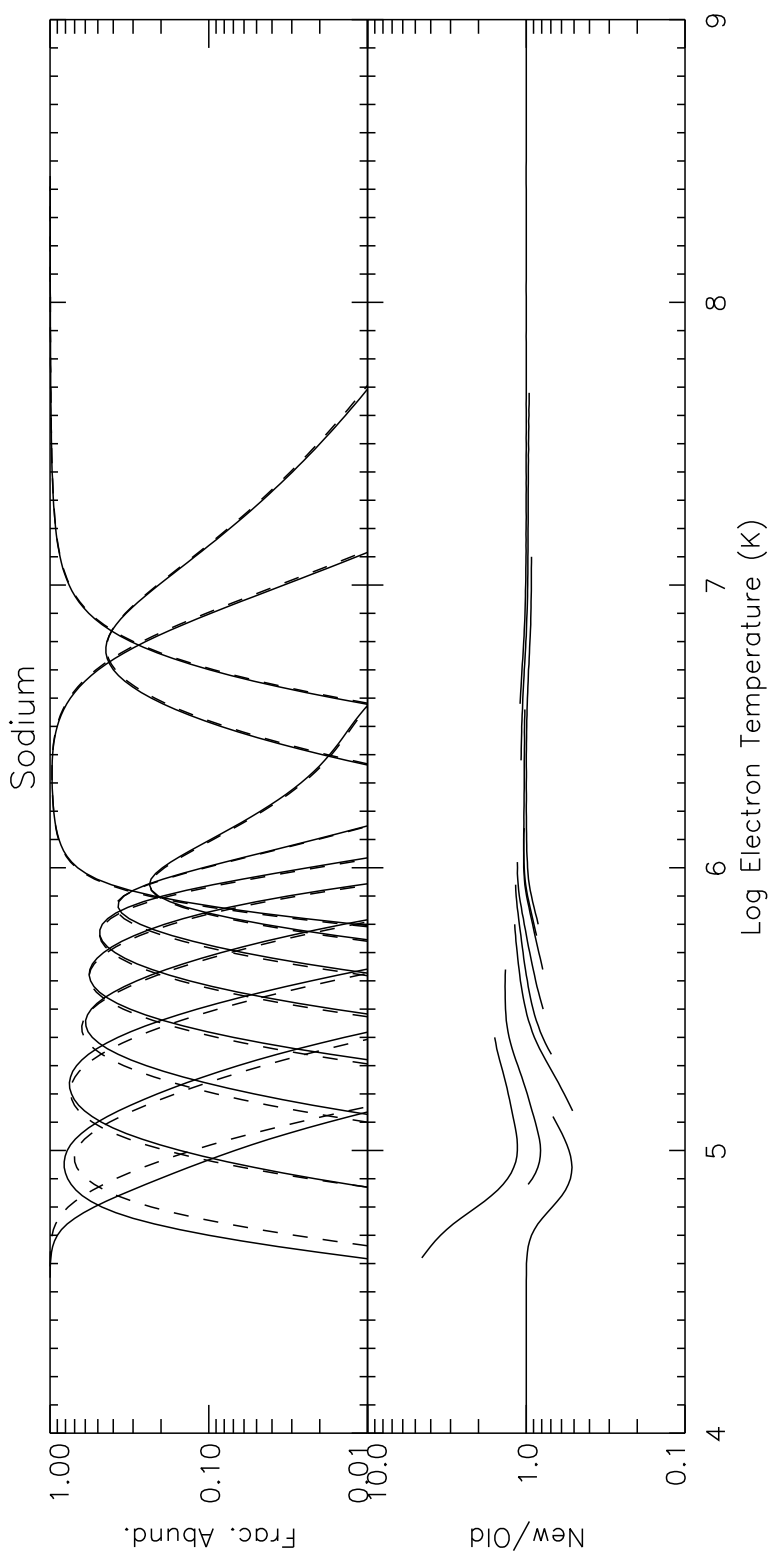


Fig. 41.— Same as Fig. 31 but for Na.

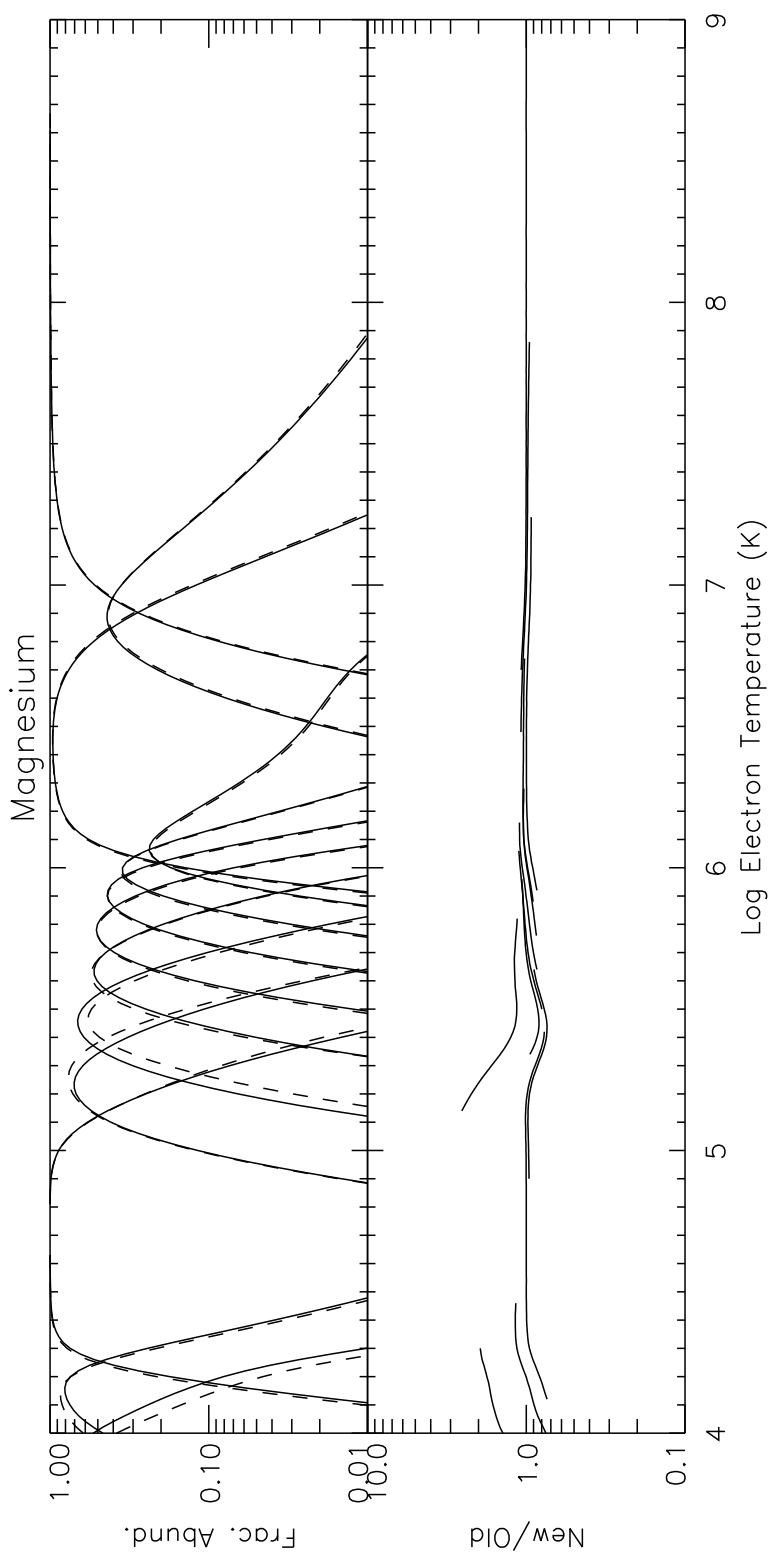


Fig. 42.— Same as Fig. 31 but for Mg.

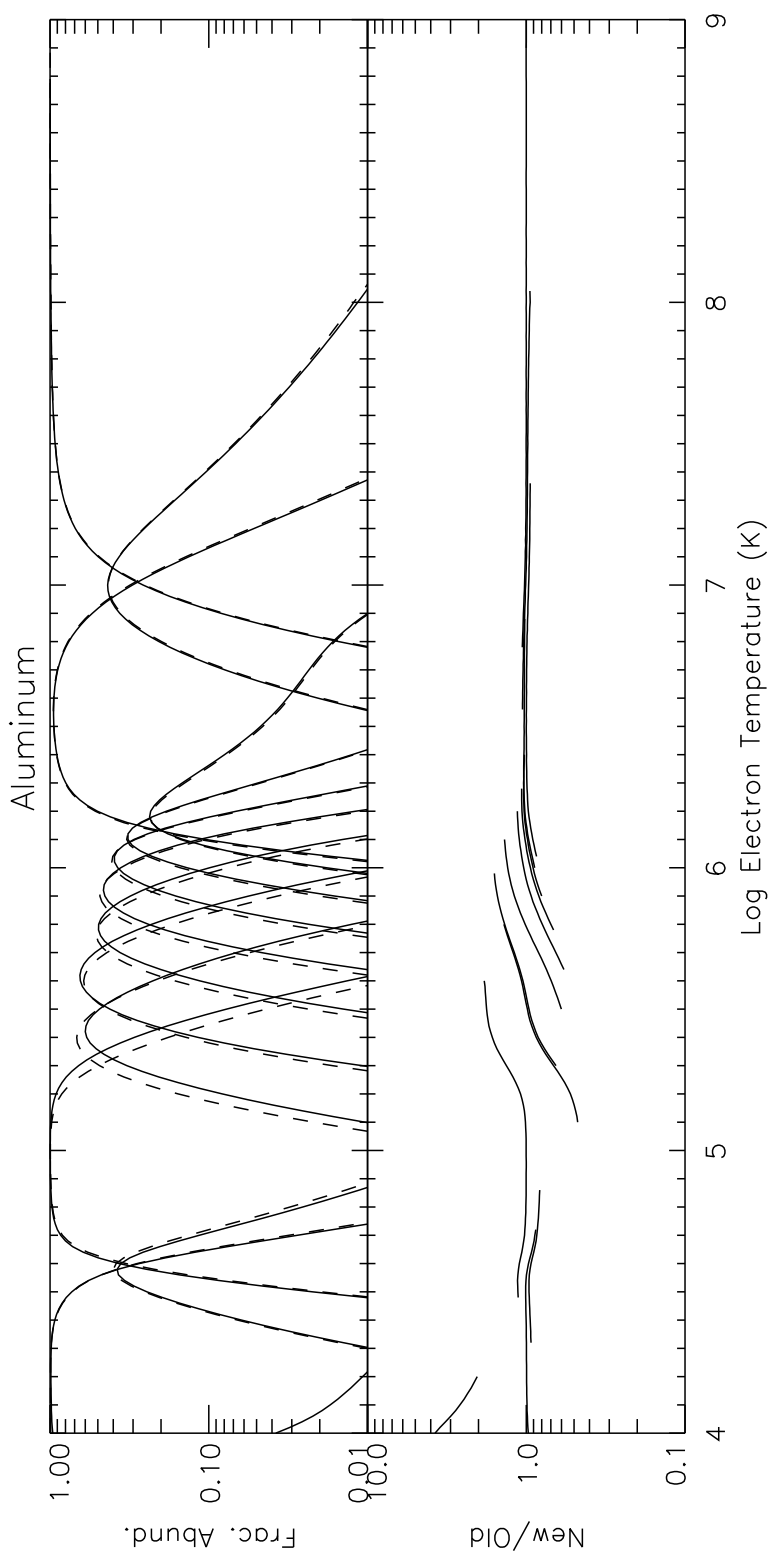


Fig. 43.— Same as Fig. 31 but for Al.

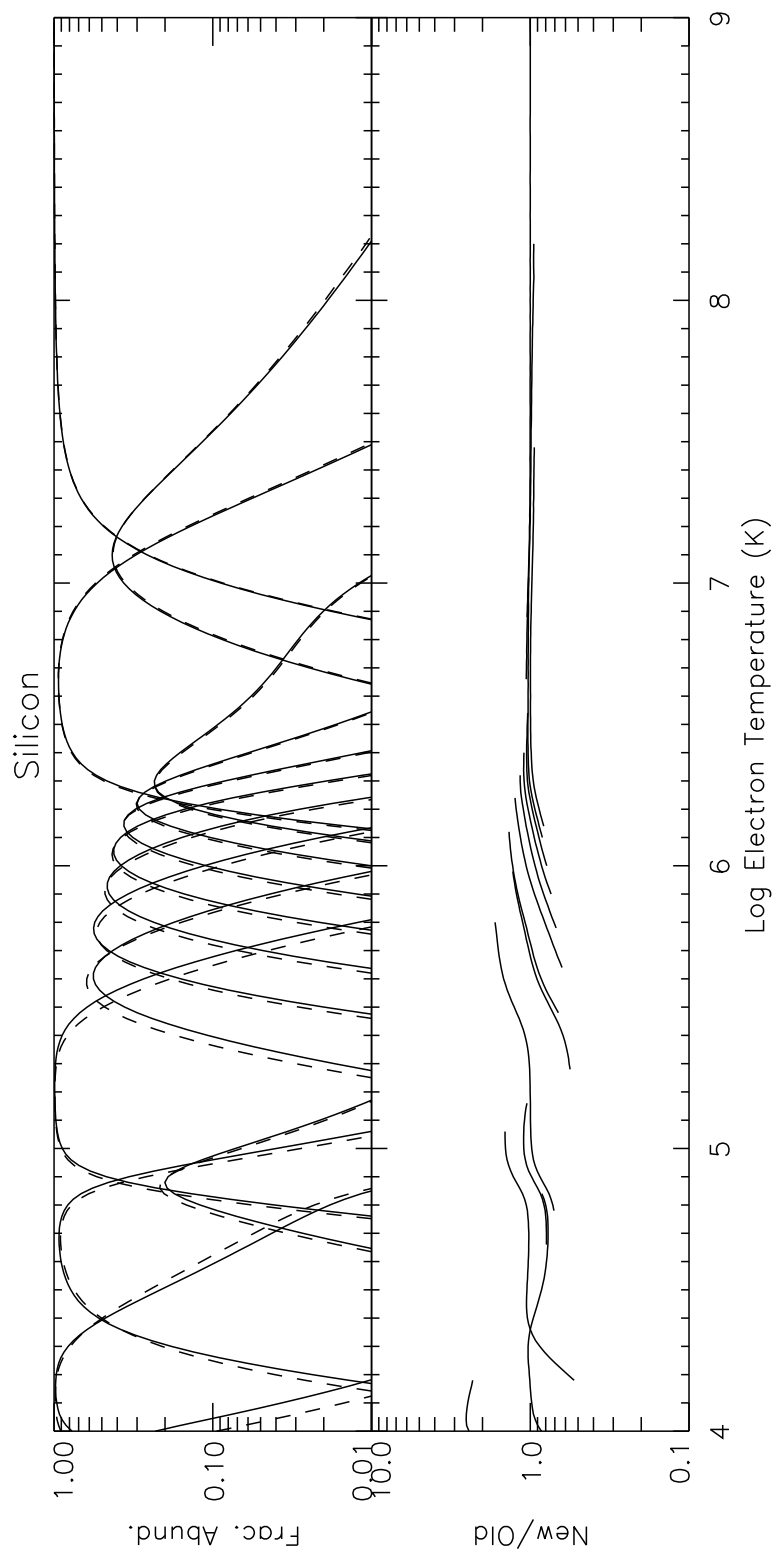


Fig. 44.— Same as Fig. 31 but for Si.

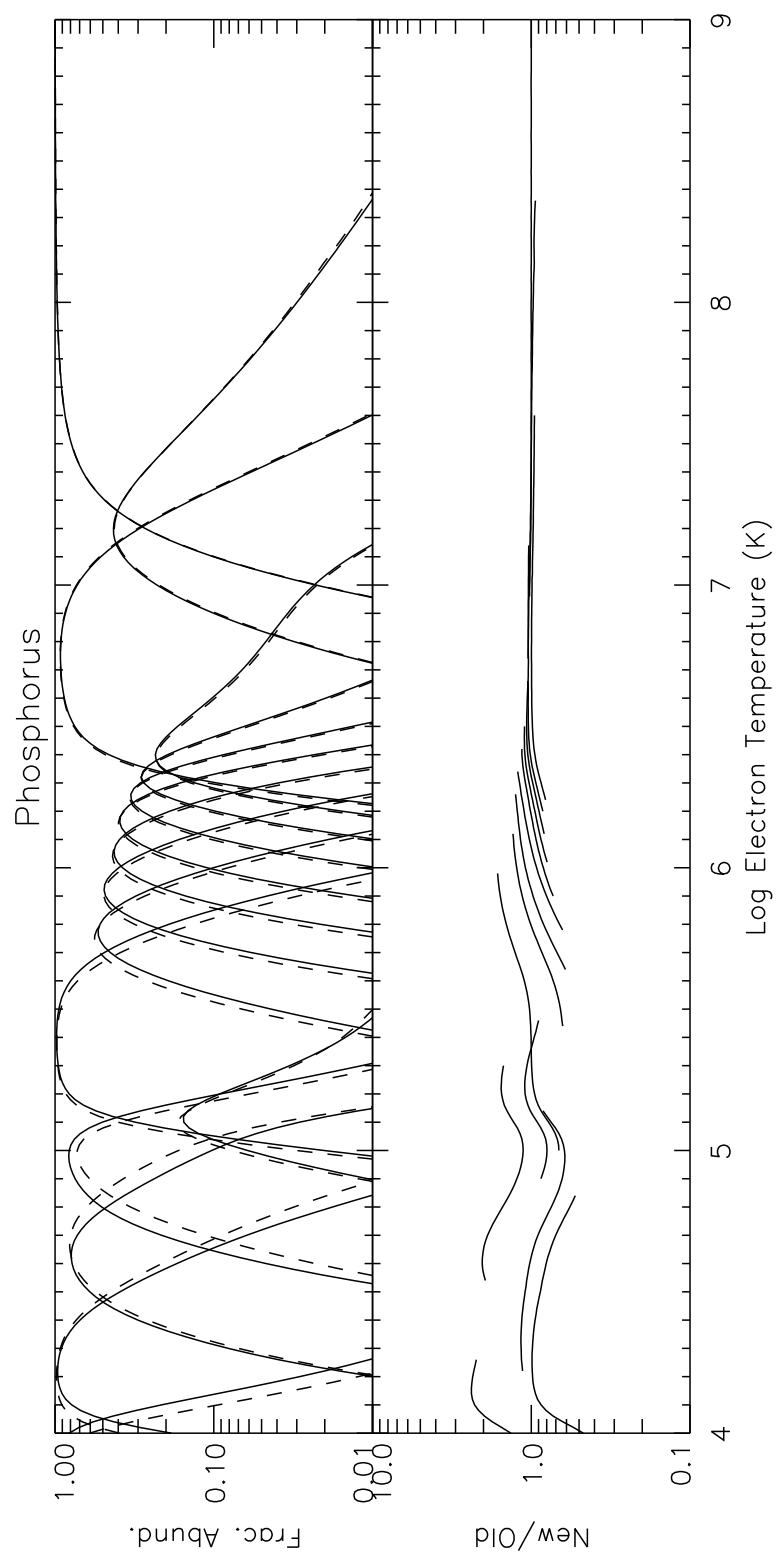


Fig. 45.— Same as Fig. 31 but for P.

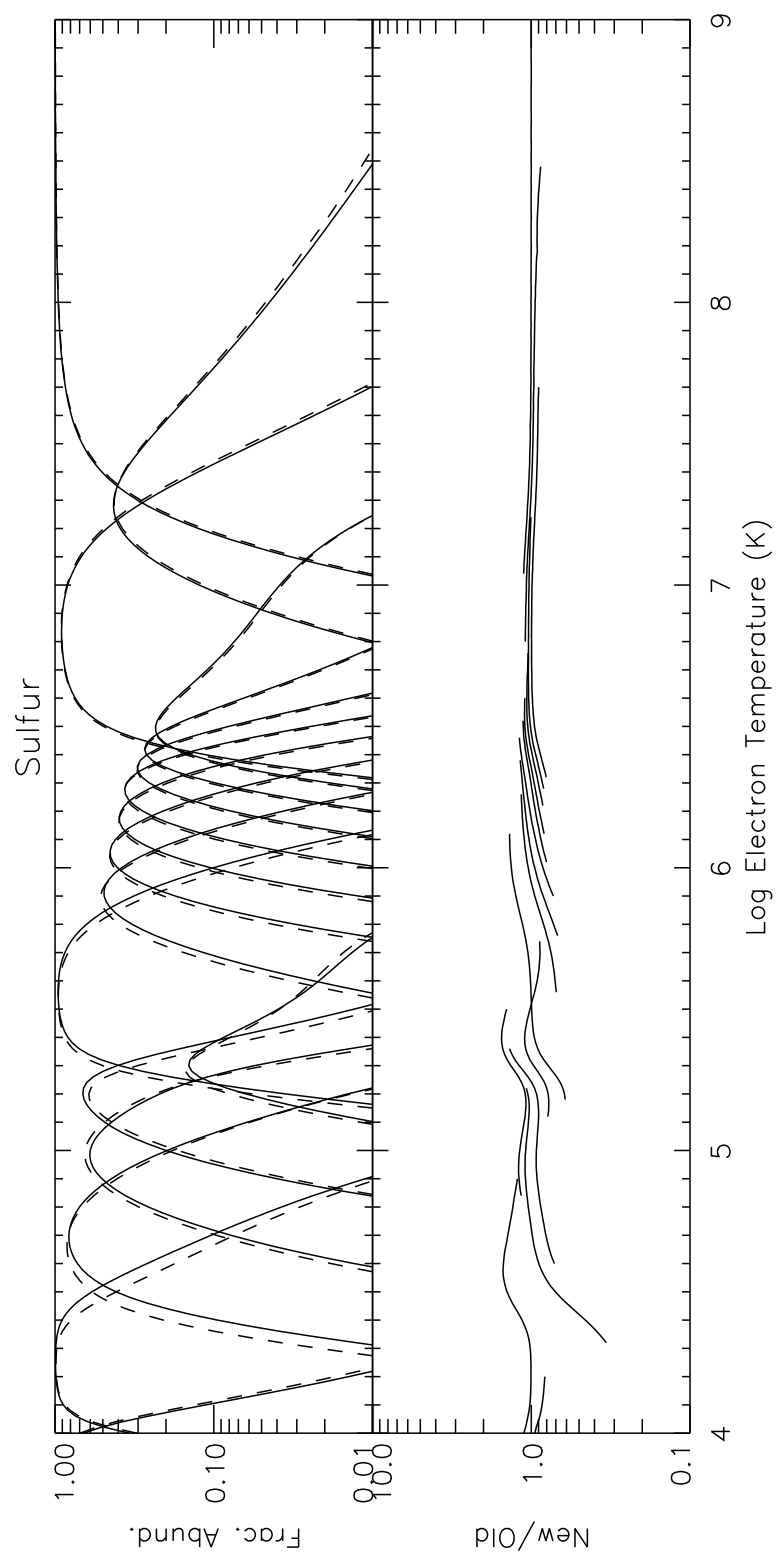


Fig. 46.— Same as Fig. 31 but for S.

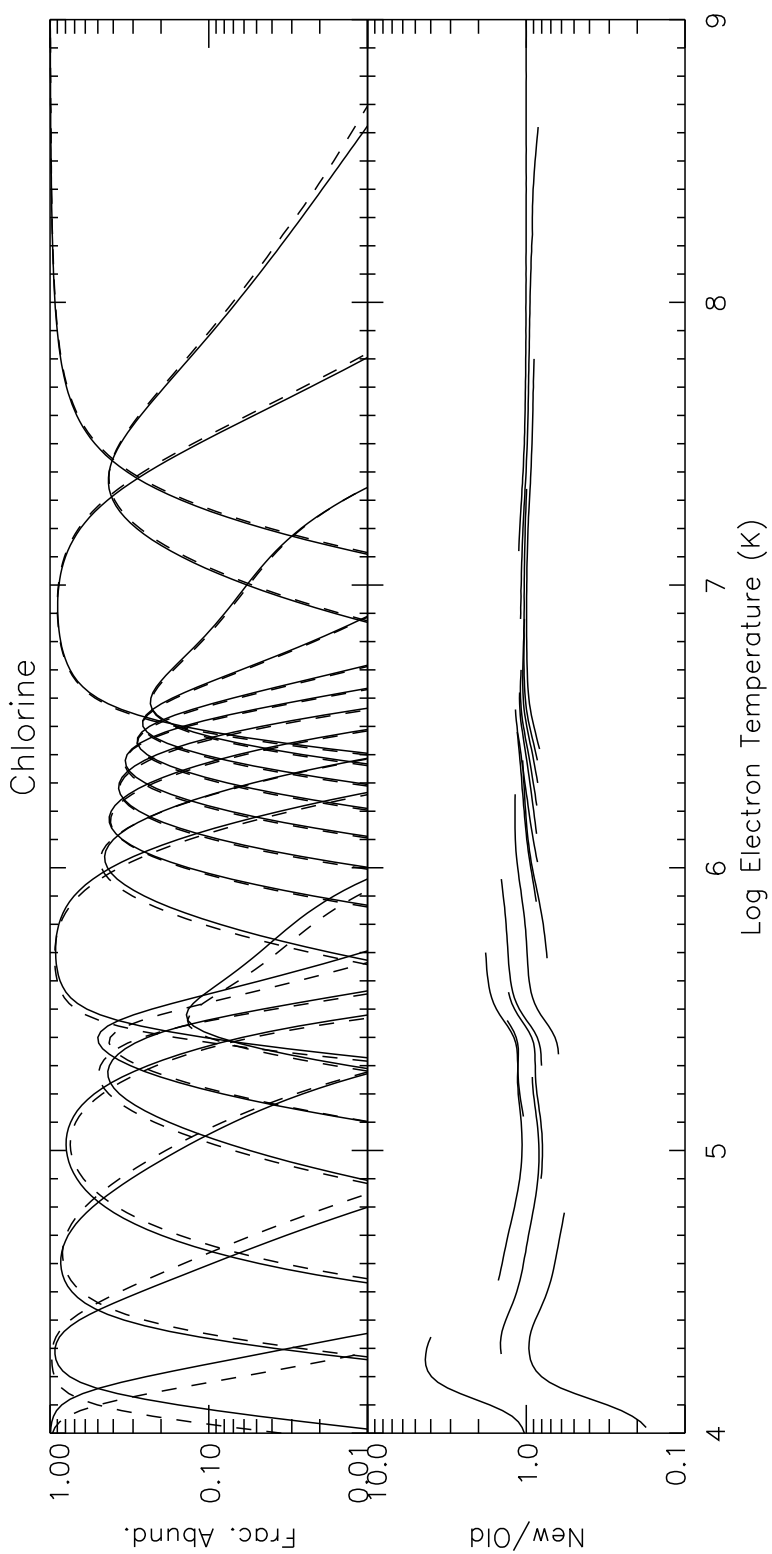


Fig. 47.— Same as Fig. 31 but for Cl.

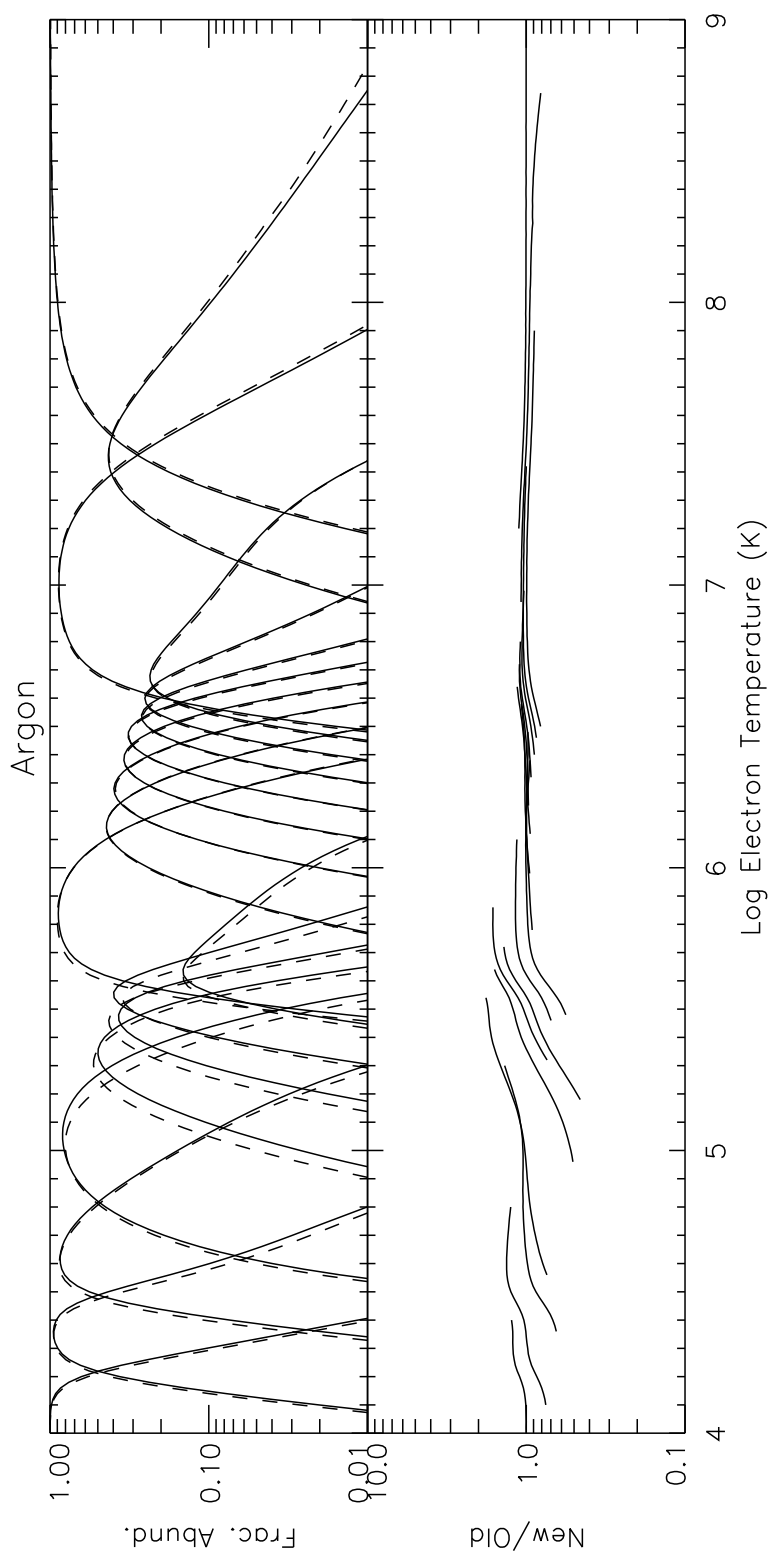


Fig. 48.— Same as Fig. 31 but for Ar.

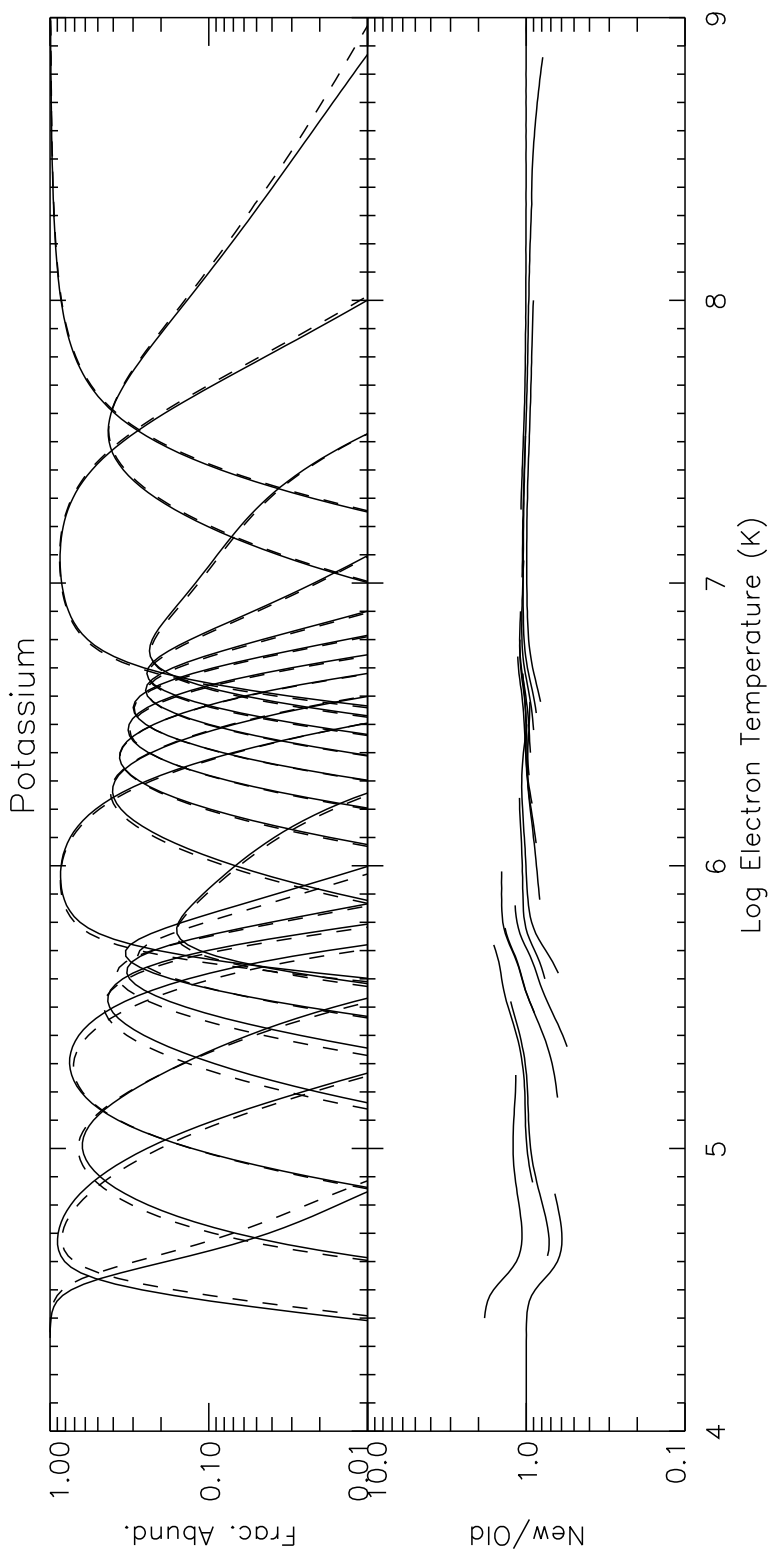


Fig. 49.— Same as Fig. 31 but for K.

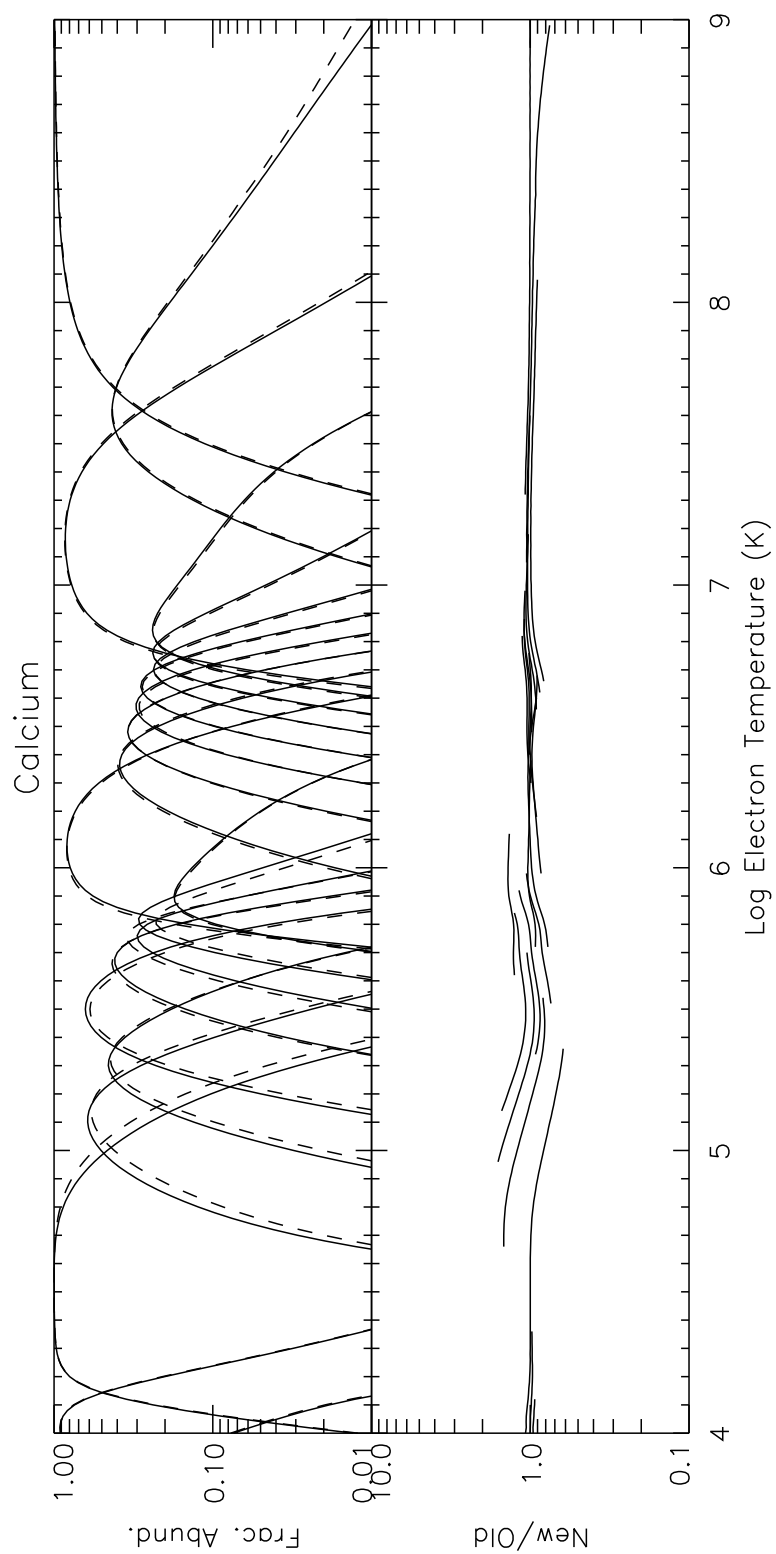


Fig. 50.— Same as Fig. 31 but for Ca.

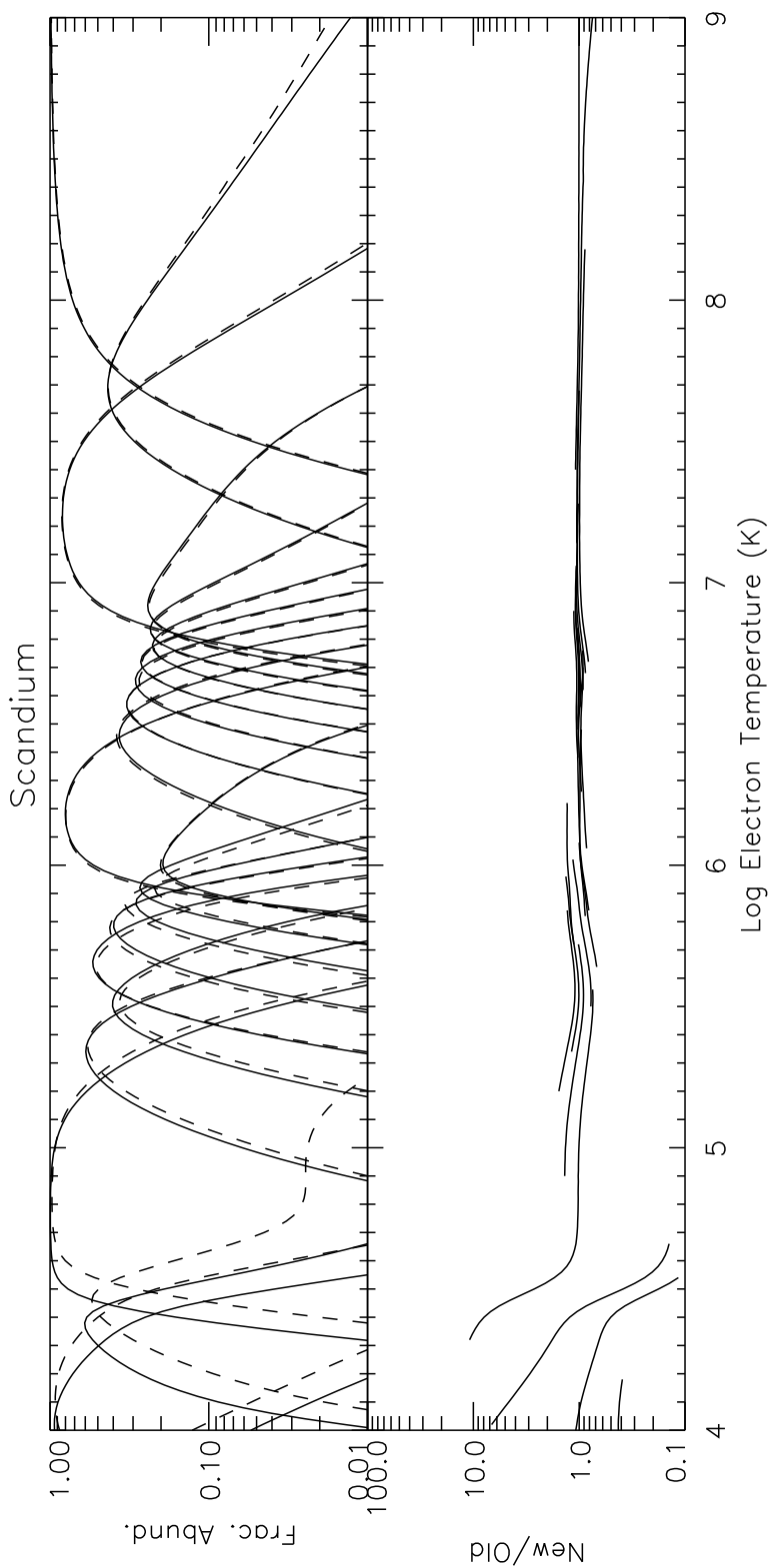


Fig. 51.— Same as Fig. 31 but for Sc.

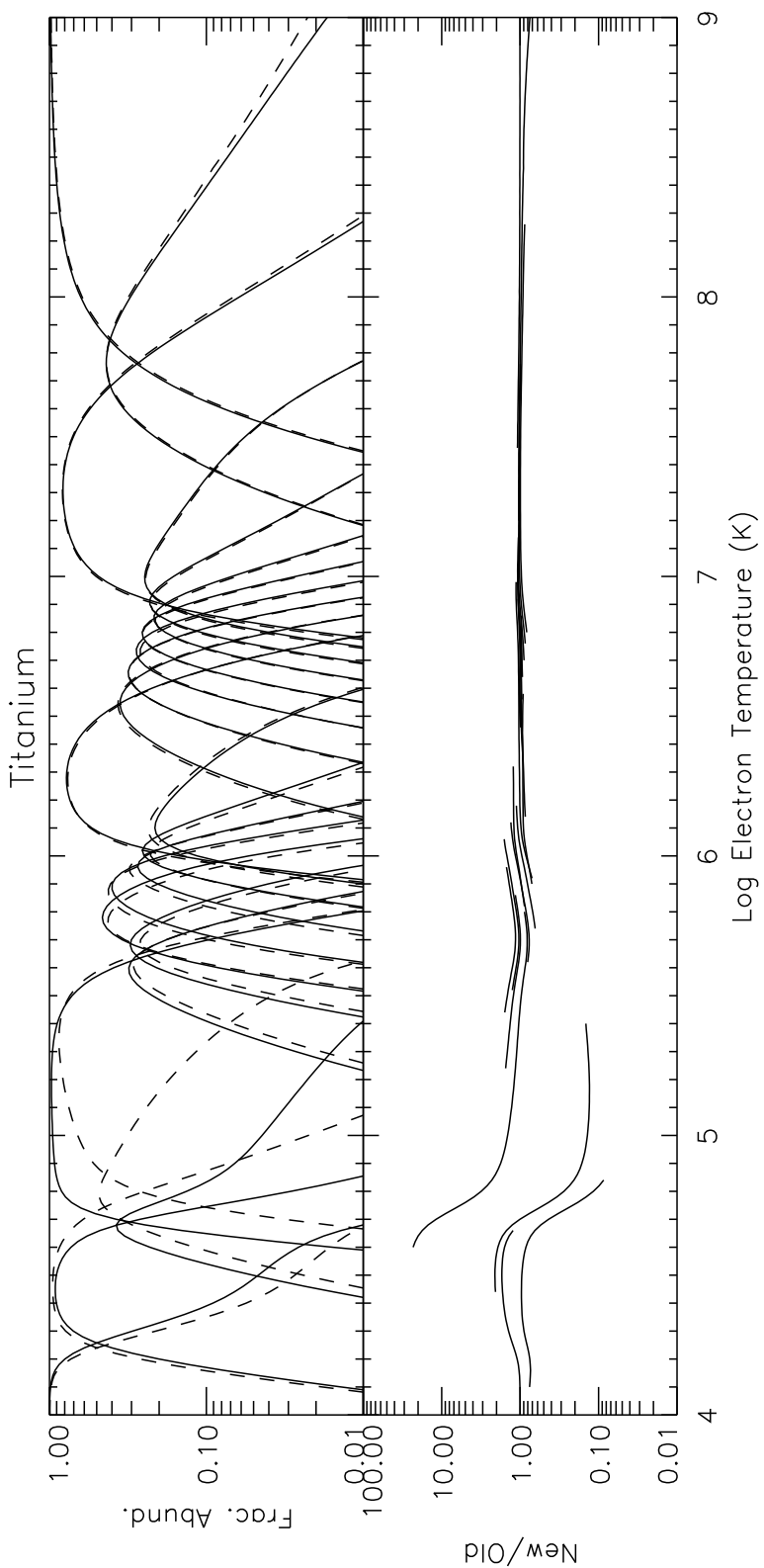


Fig. 52.— Same as Fig. 31 but for Ti.

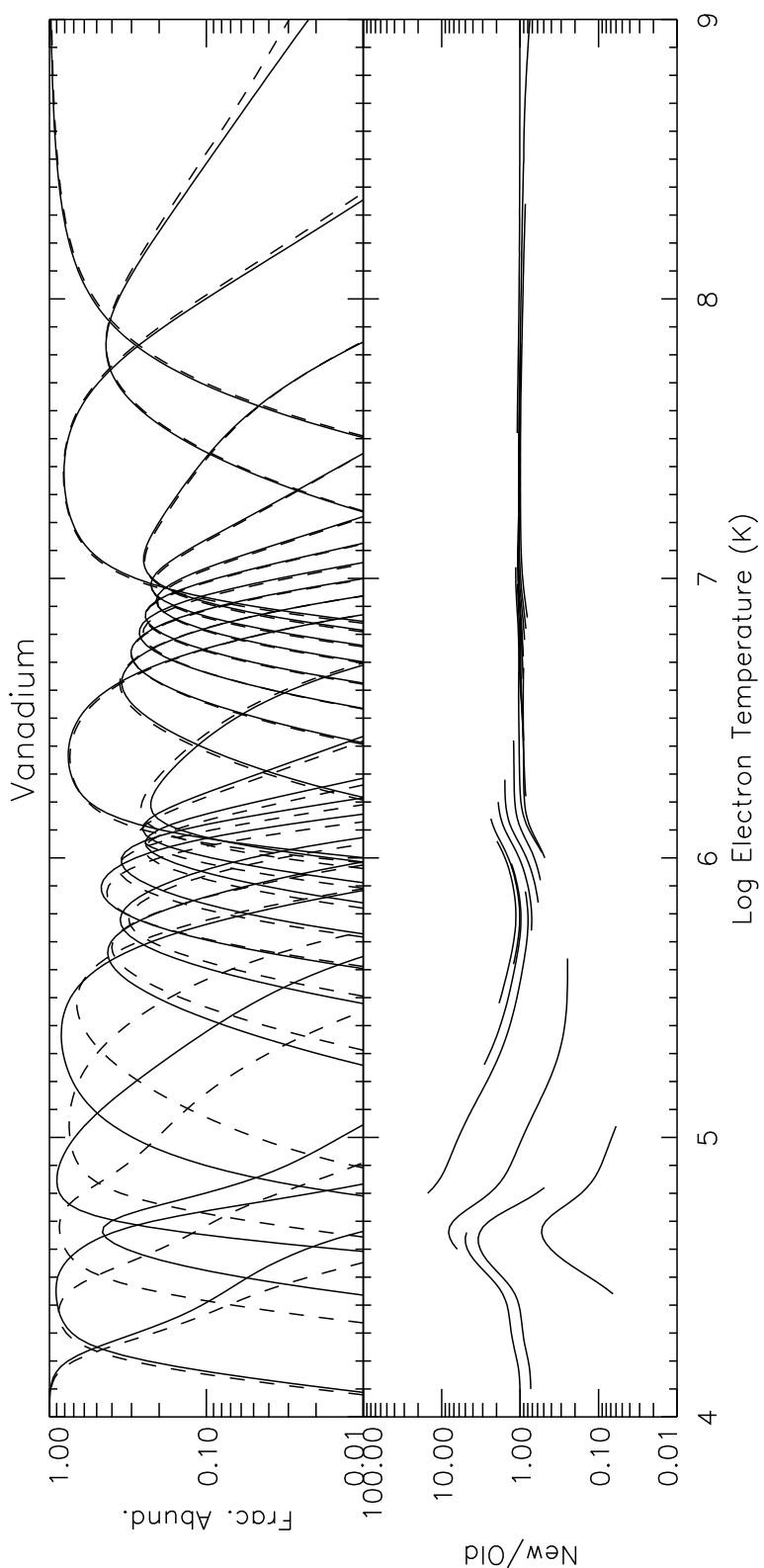


Fig. 53.— Same as Fig. 31 but for V.

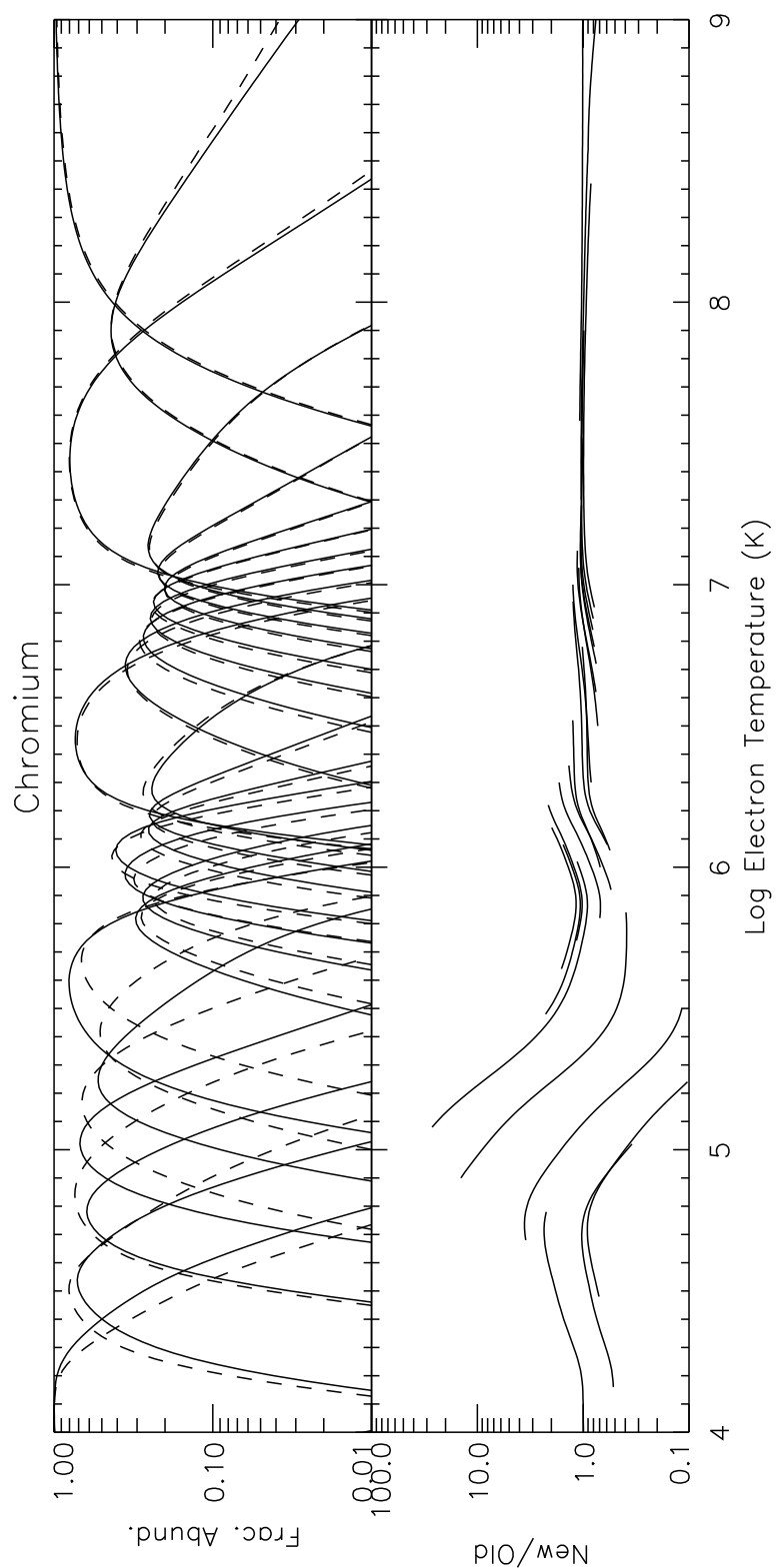


Fig. 54.— Same as Fig. 31 but for Cr.

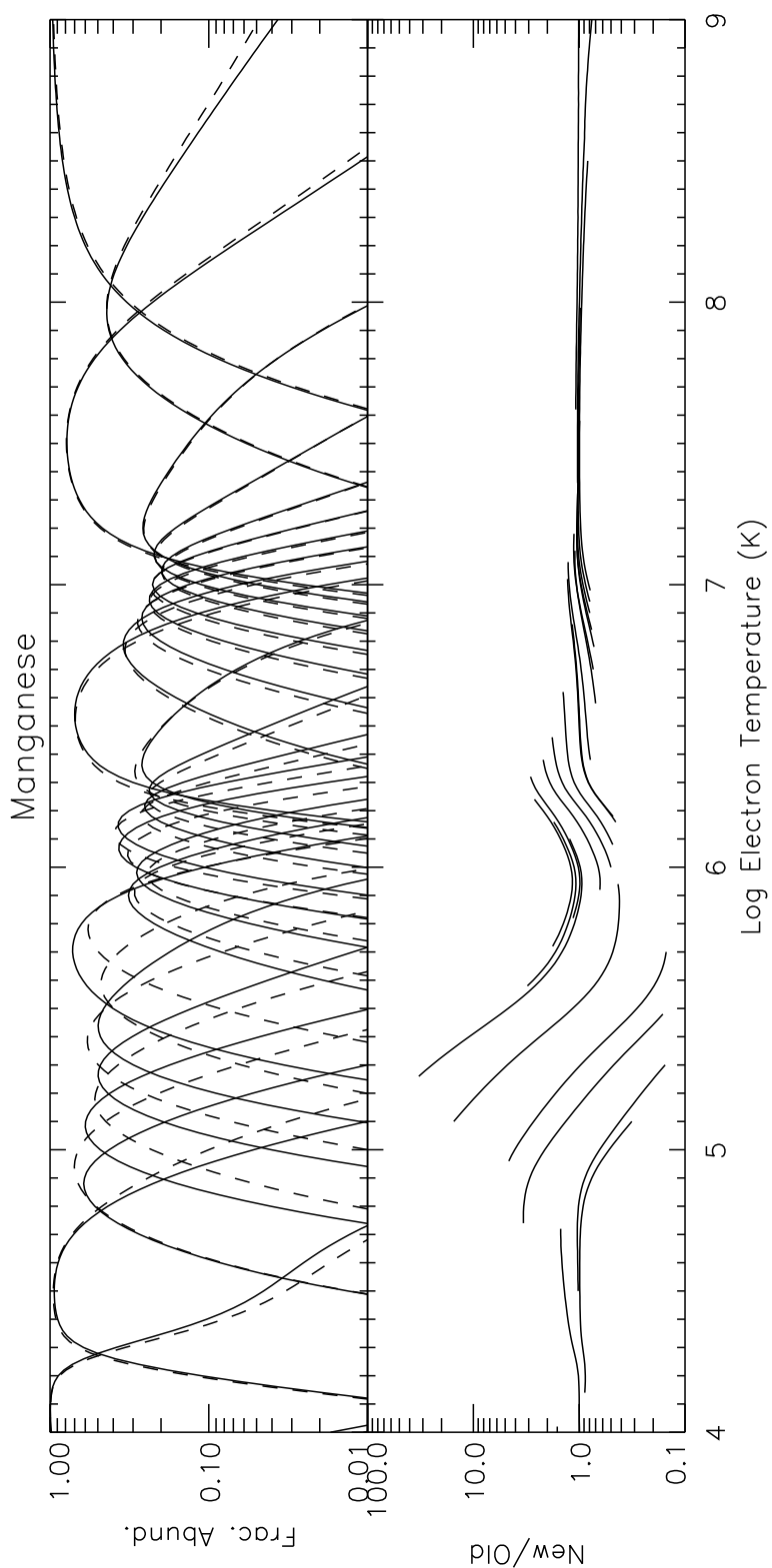


Fig. 55.— Same as Fig. 31 but for Mn.

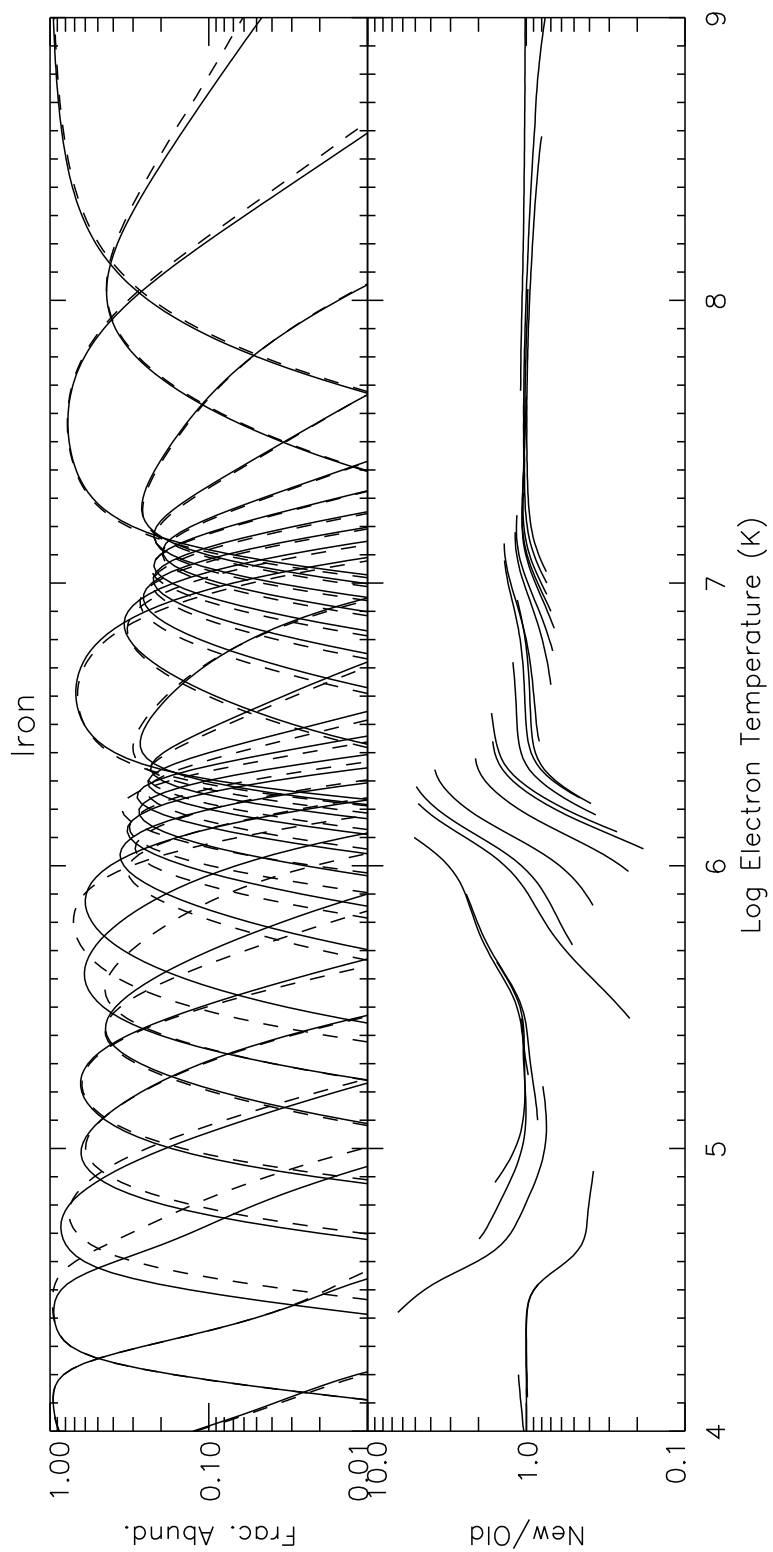


Fig. 56.— Same as Fig. 31 but for Fe.

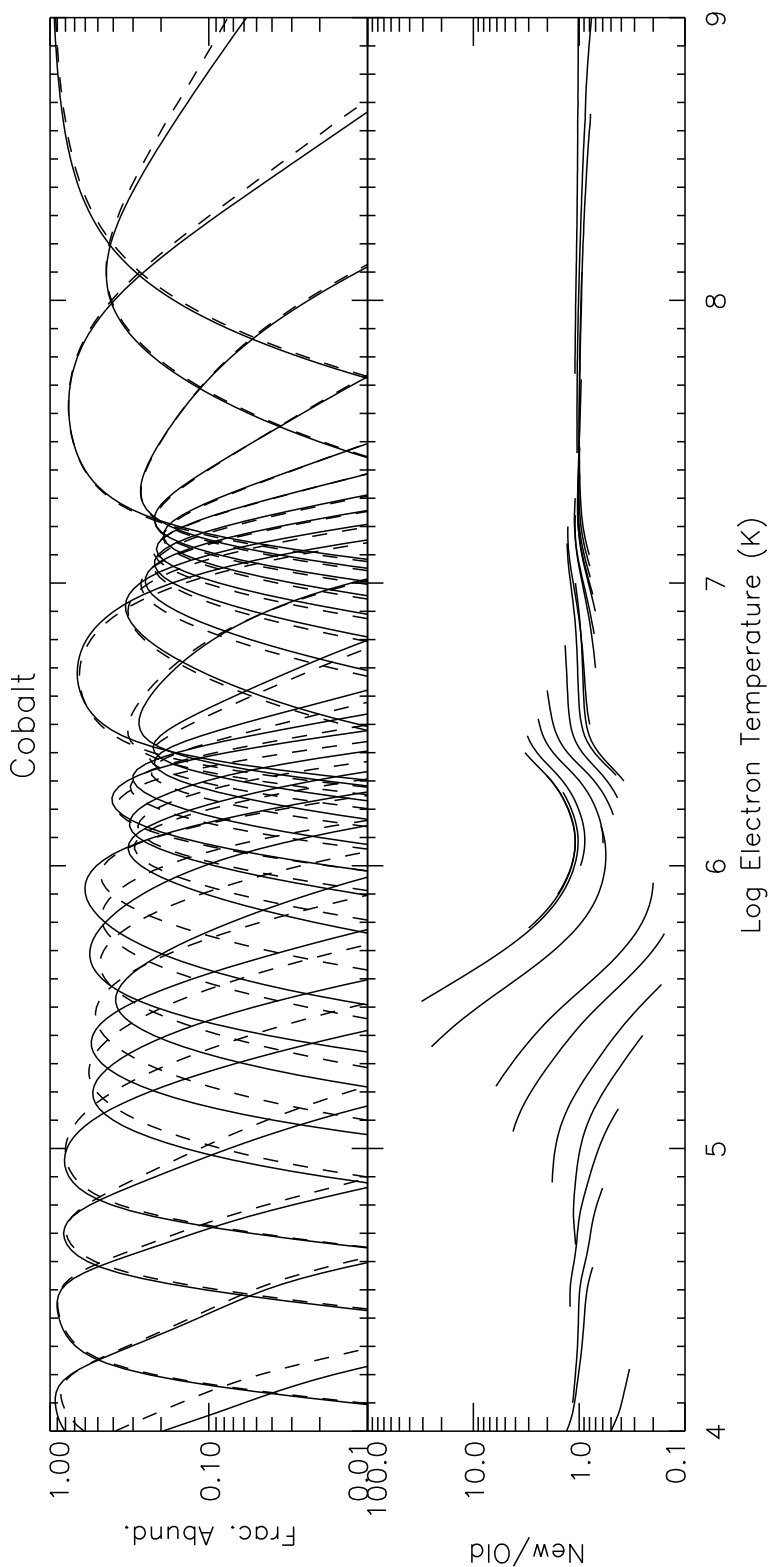


Fig. 57.— Same as Fig. 31 but for Co.

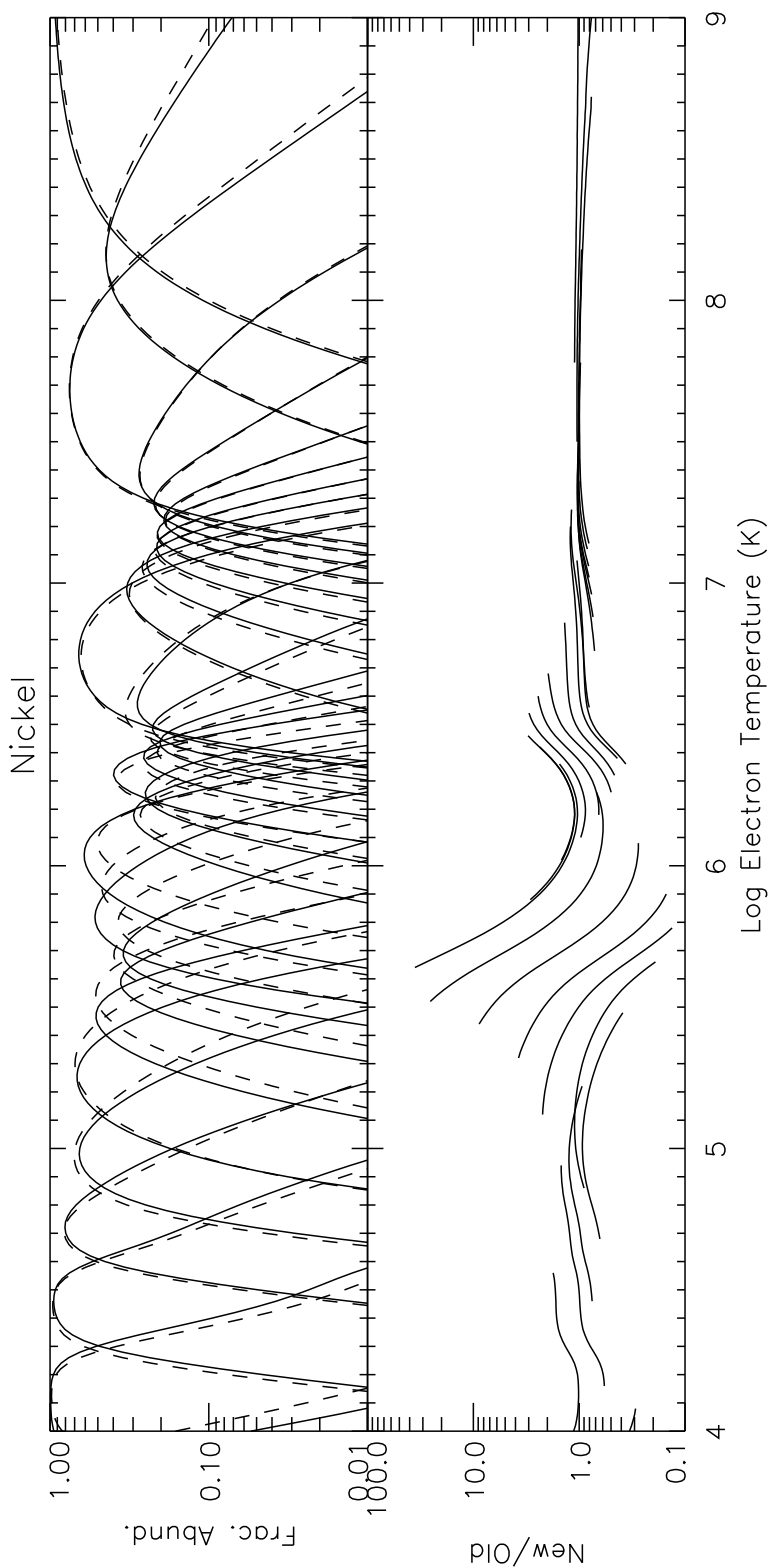


Fig. 58.— Same as Fig. 31 but for Ni.

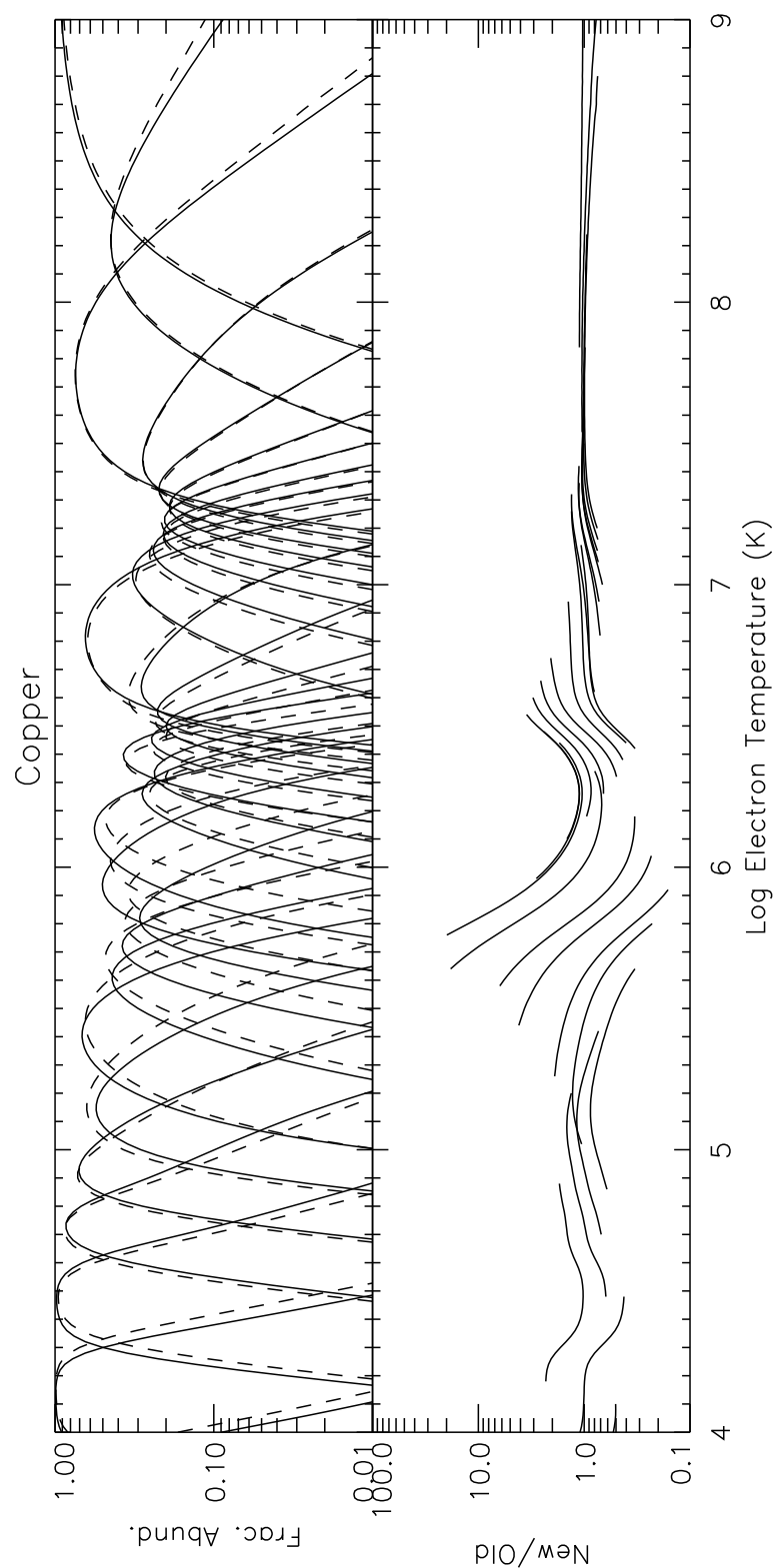


Fig. 59.— Same as Fig. 31 but for Cu.

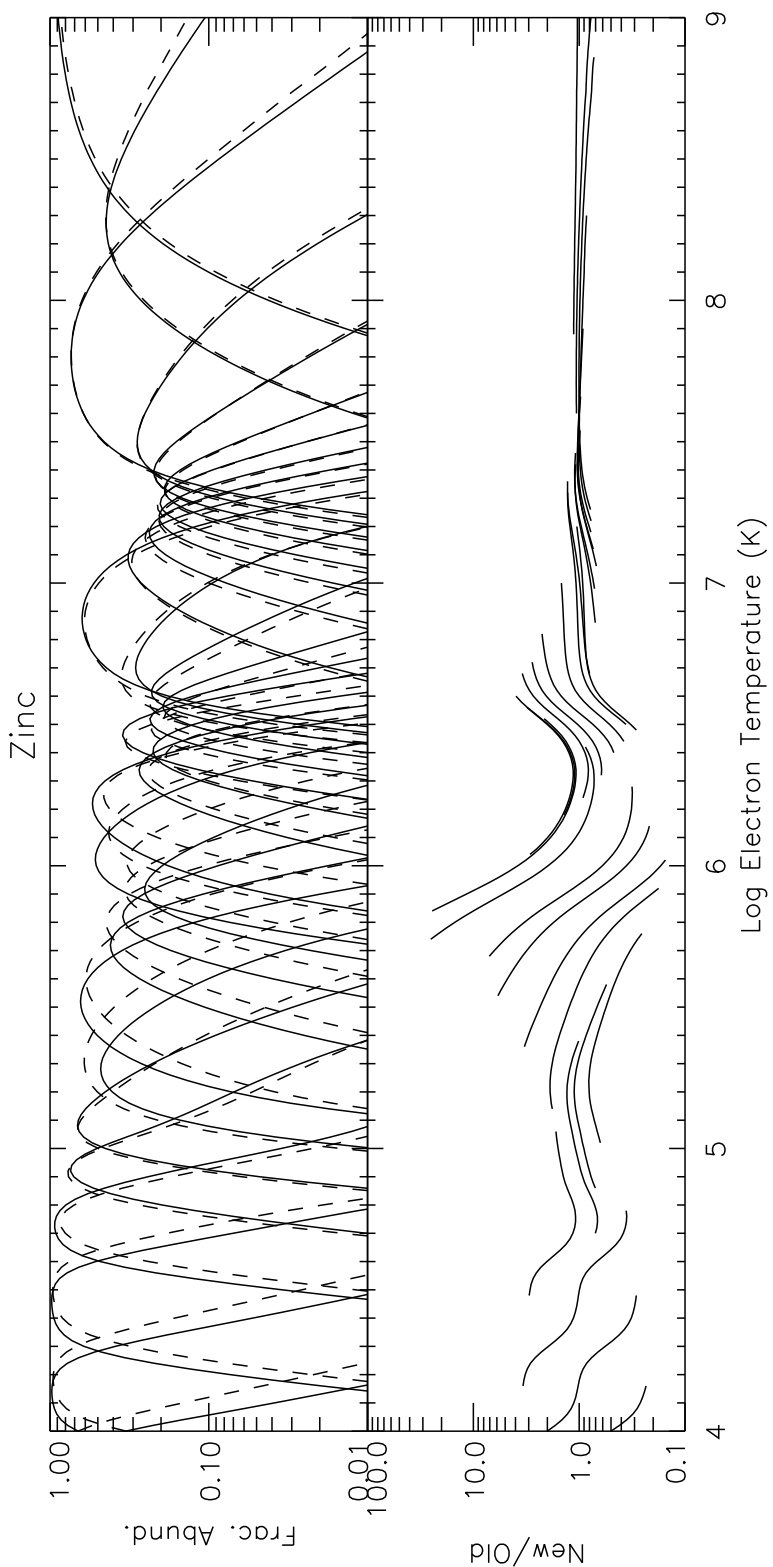


Fig. 60.— Same as Fig. 31 but for Zn.

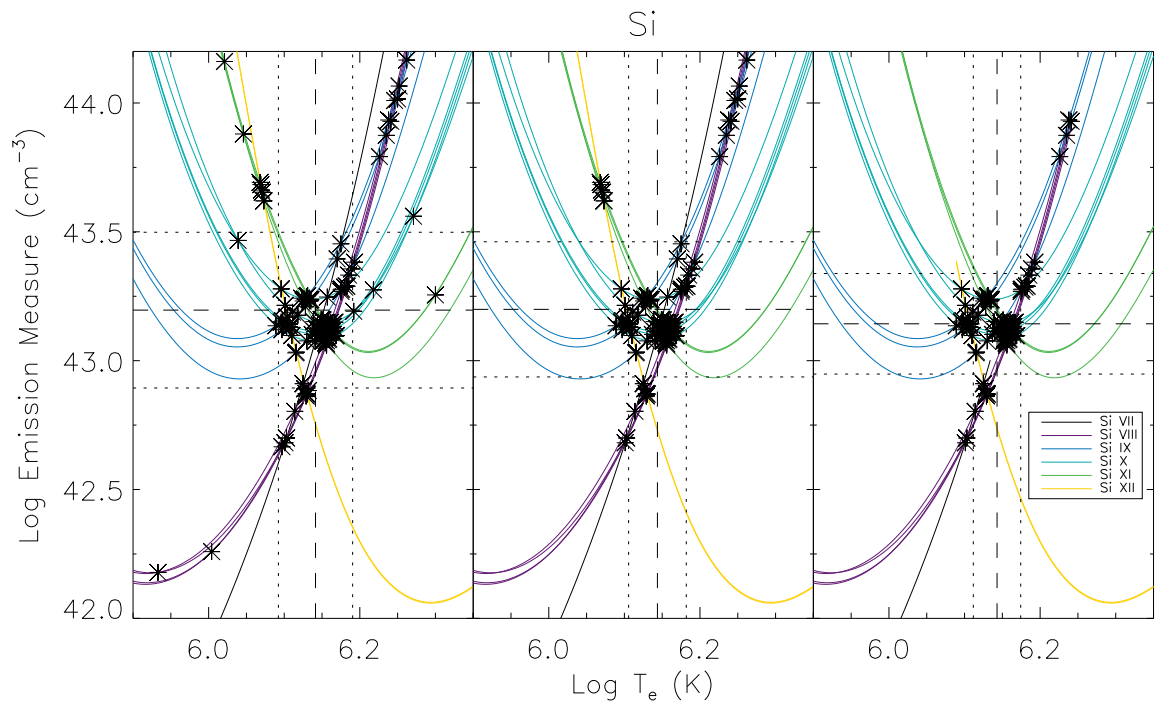


Fig. 61.— EM versus T_e curves of all emission lines observed here from Si. The dashed lines indicate the mean $\log_{10} EM$ and $\log_{10} T_e$ and the dotted lines show the standard deviations of these values. Asterisks indicate where the curves cross. The left panel shows the results after Step 1 of the analysis, the middle panel shows the results after Step 2, and the right panel shows the results after Step 3. See Sec. 5 for a description of each step.

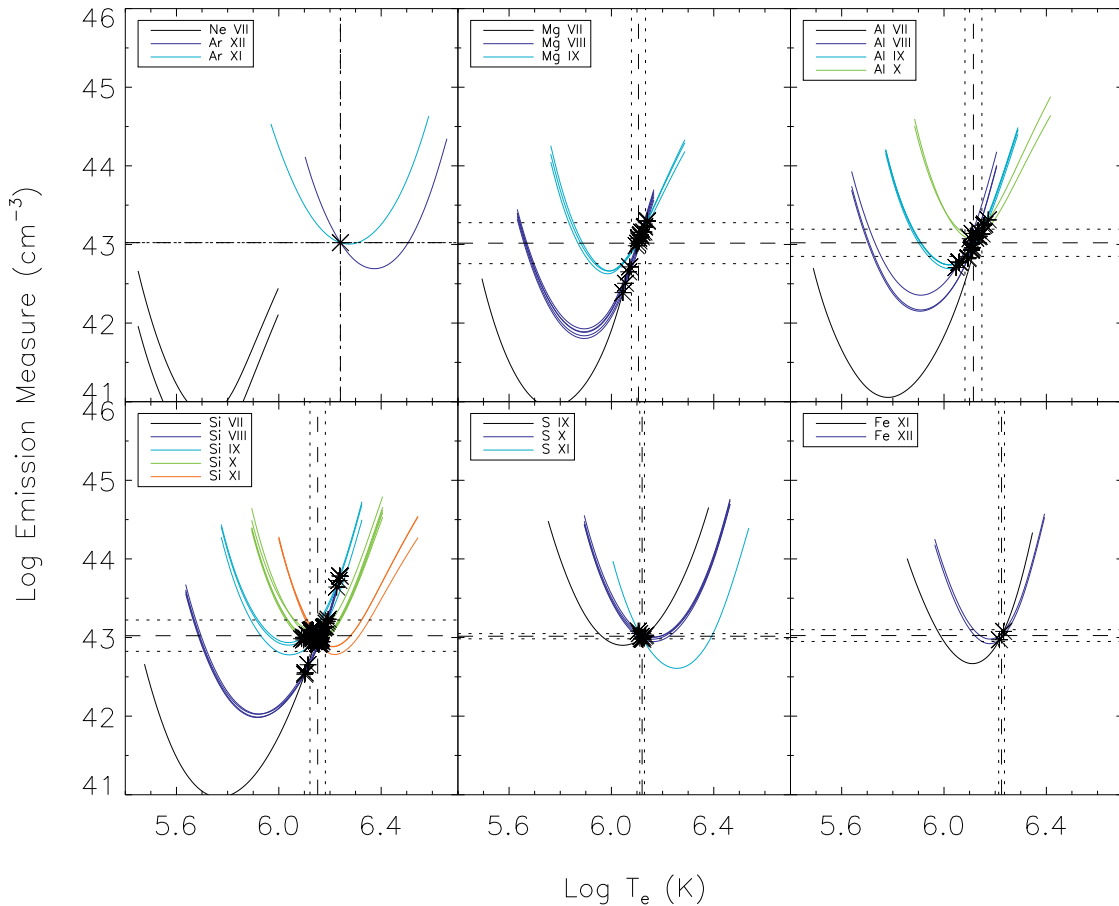


Fig. 62.— EM versus T_e curves of all the emission lines from each of the low- and moderate-FIP elements using the GEM method described in Sec. 5. Na, K and Ca are excluded as in this SUMER dataset there are not enough observed emission lines from these elements to determine a mean EM . The upper left panel shows the high-FIP elements Ne and Ar.

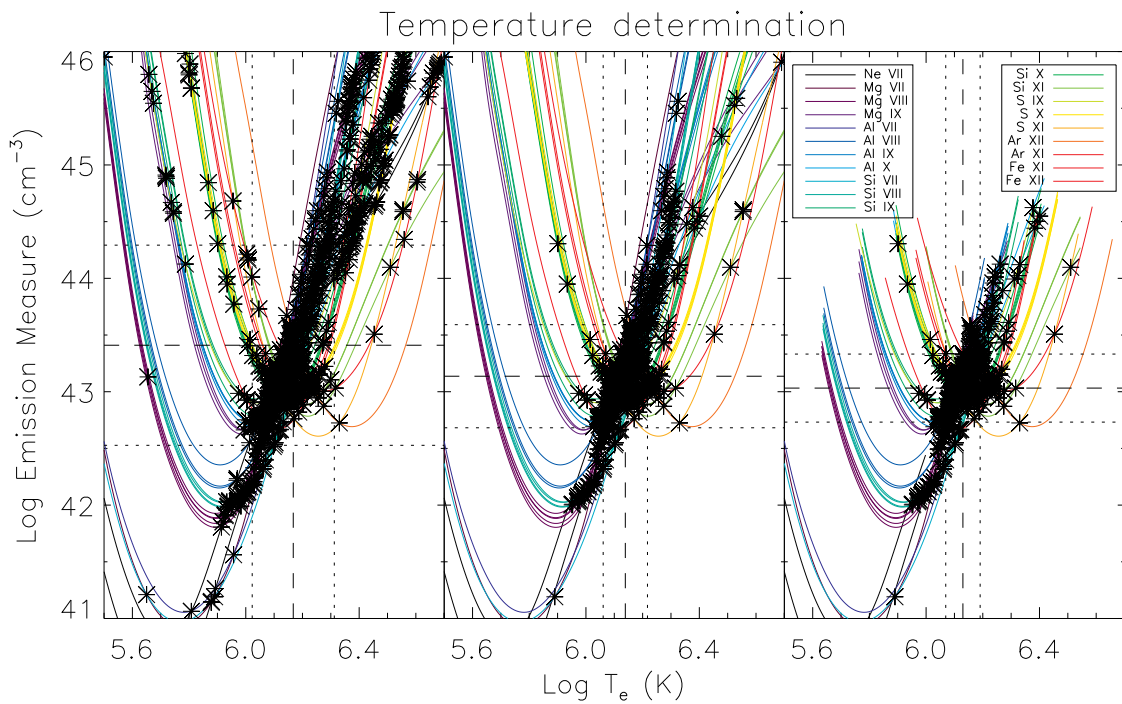


Fig. 63.— EM versus T_e curves of all the emission lines from each of the elements Ne, Mg, Al, Si, S, Ar, and Fe (excluding Li- and Na-like ions). The T_e derived from these elements were used to determine the FIP factors of Na, K and Ca. Asterisks indicate where the curves cross. The three panels show the three steps of the GEM method as in Fig. 61.

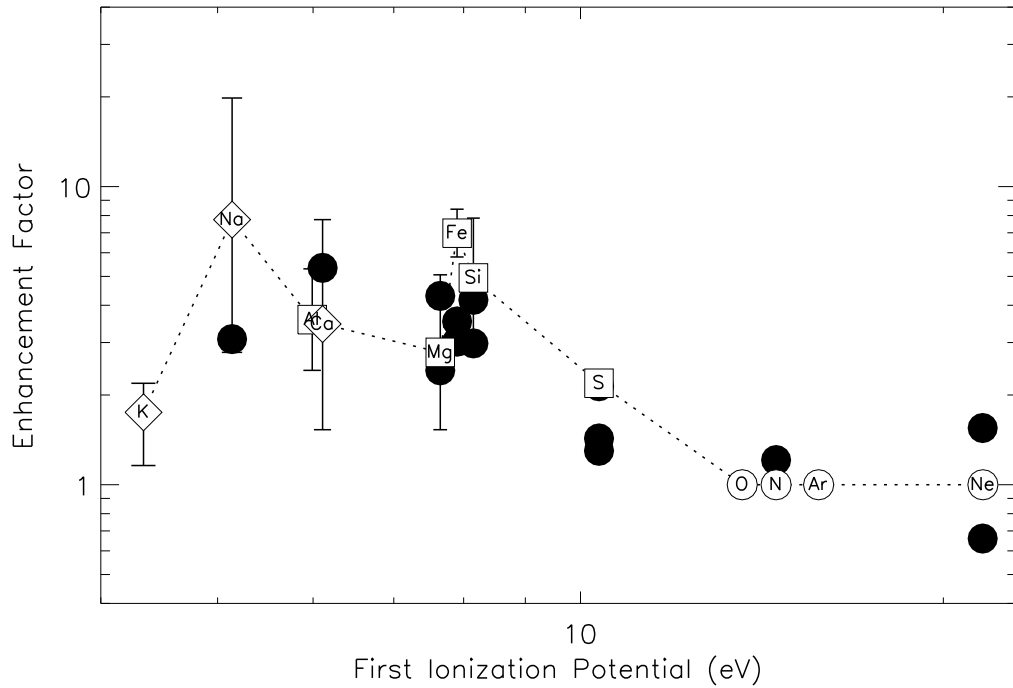


Fig. 64.— Coronal abundance enhancement factor (i.e., FIP factor) used for each of the elements versus their first ionization potential. Open circles indicate the high-FIP elements O, N, Ne and Ar where no enhancement was assumed. The elements in squares indicate those which had their enhancement factor determined by matching their mean EM with that of the high-FIP element Ar. Elements marked with diamonds are those that did not have enough crossings to determine their EM in this way (see Sec. 6 for further details). The dotted line is purely to guide the eye. The solid circles are the results of Feldman et al. (1998) for N, O, Ne, Na, Mg, Si, S, Ca, and Fe. Feldman et al. scaled their results to O and assumed a FIP factor of 1 for this element. We also set the O FIP factor to 1, so their and our FIP factors for O lie directly on top of one another in this plot.

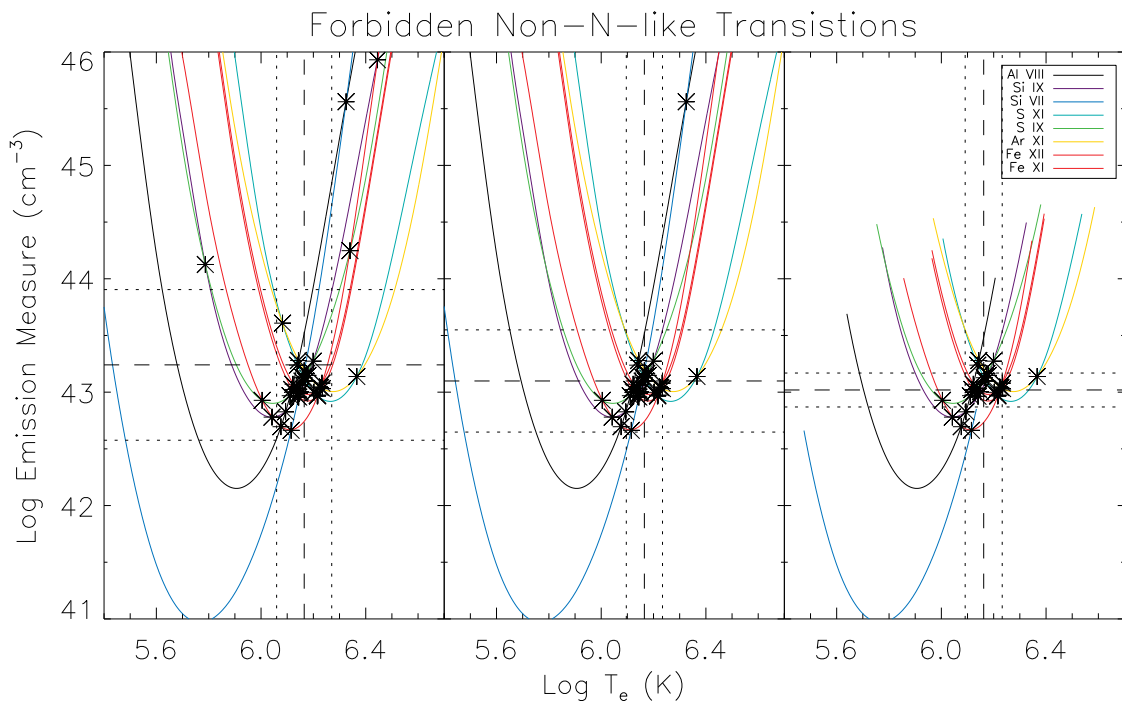


Fig. 65.— EM versus T_e curves for the emission lines of Group Ia using our inferred coronal abundances. Asterisks indicate where the curves cross. The three panels show the three steps of the GEM method as in Fig. 61.

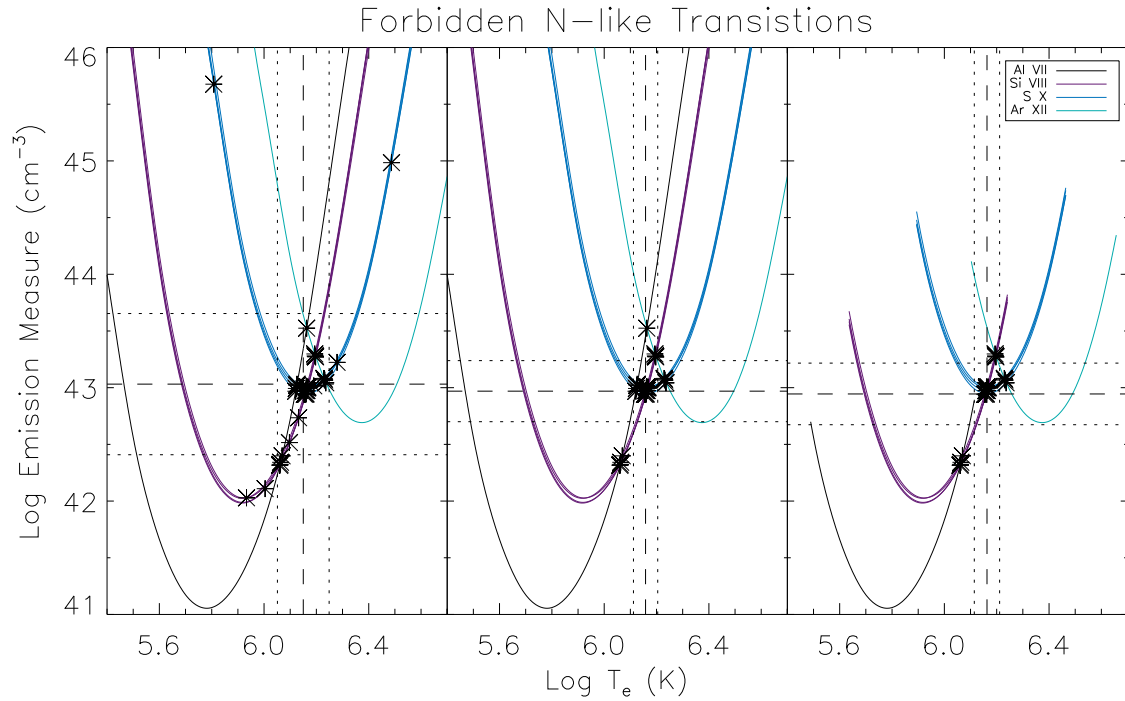


Fig. 66.— Same as Fig. 65 but for Group Ib.

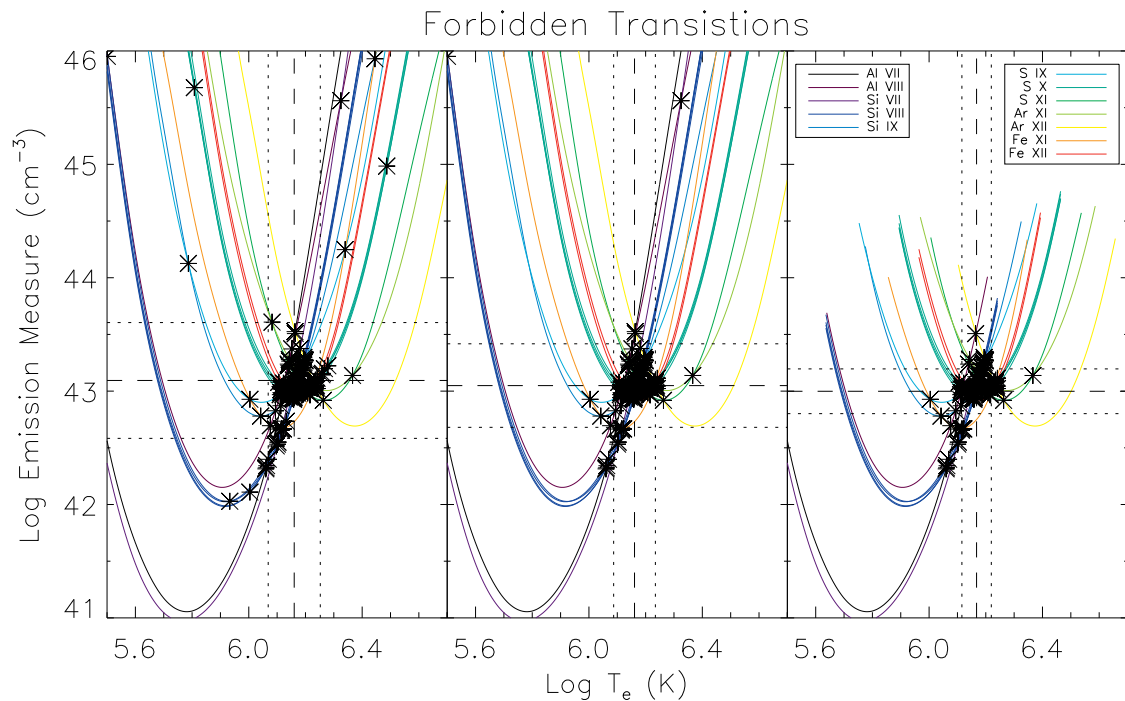


Fig. 67.— Same as Fig. 65 but for Group I as a whole.

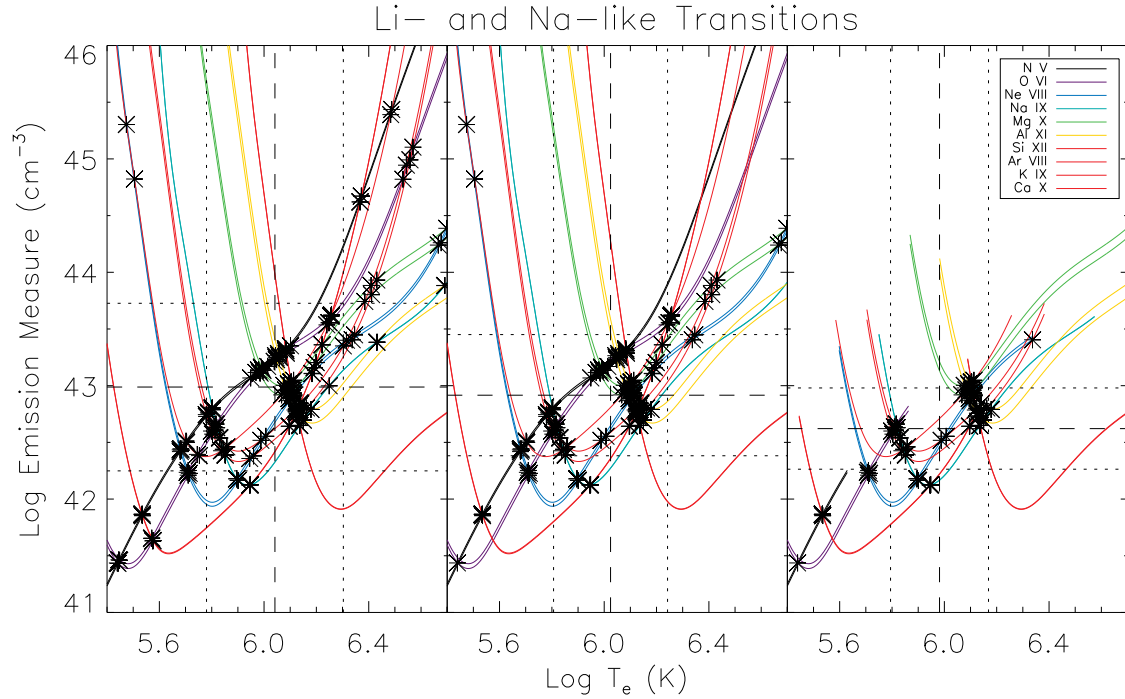


Fig. 68.— Same as Fig. 65 but for Group IIa.

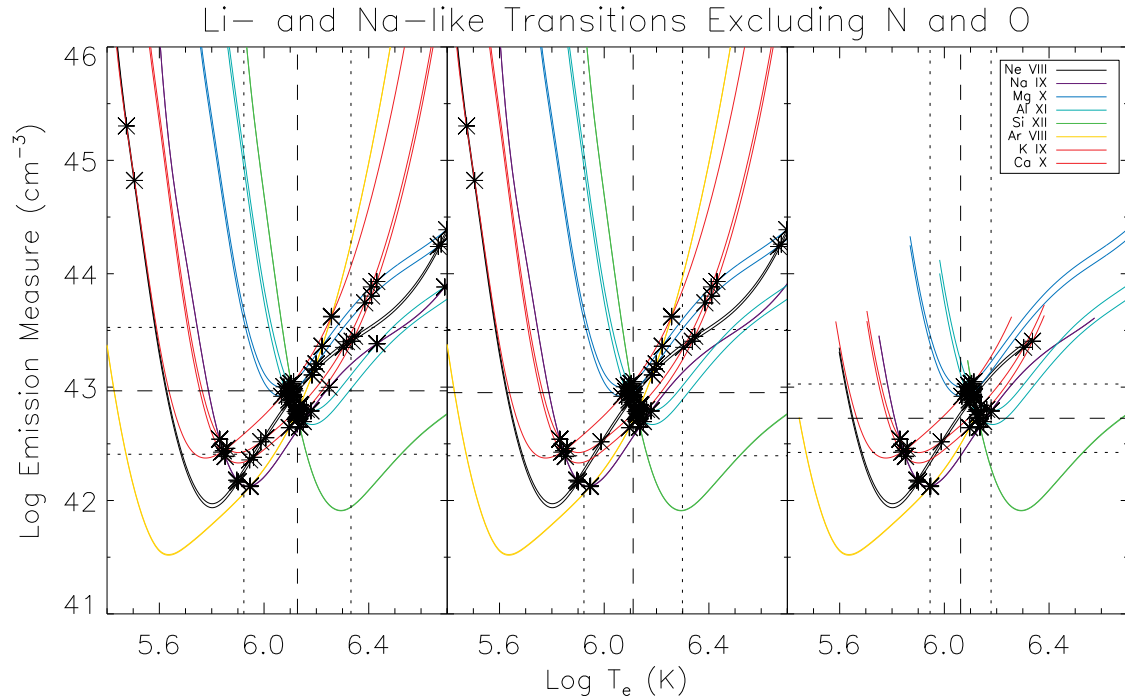


Fig. 69.— Same as Fig. 68 but excluding emission lines from N V and O VI.

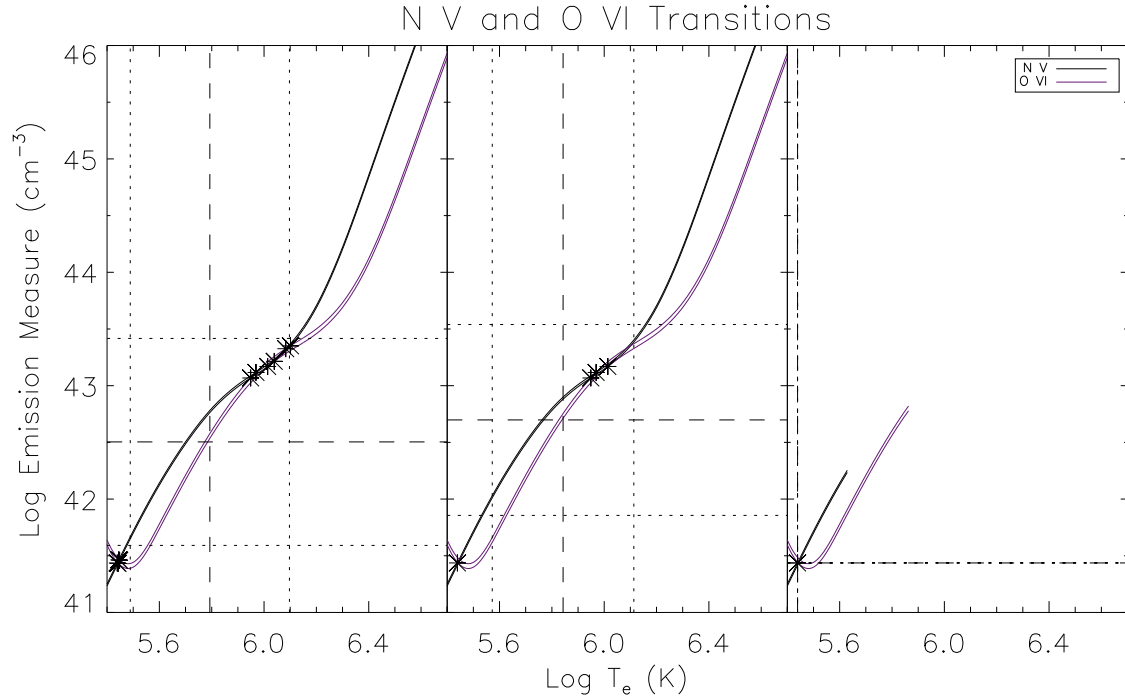


Fig. 70.— Same as Fig. 68 but showing only emission lines from N v and O vi.

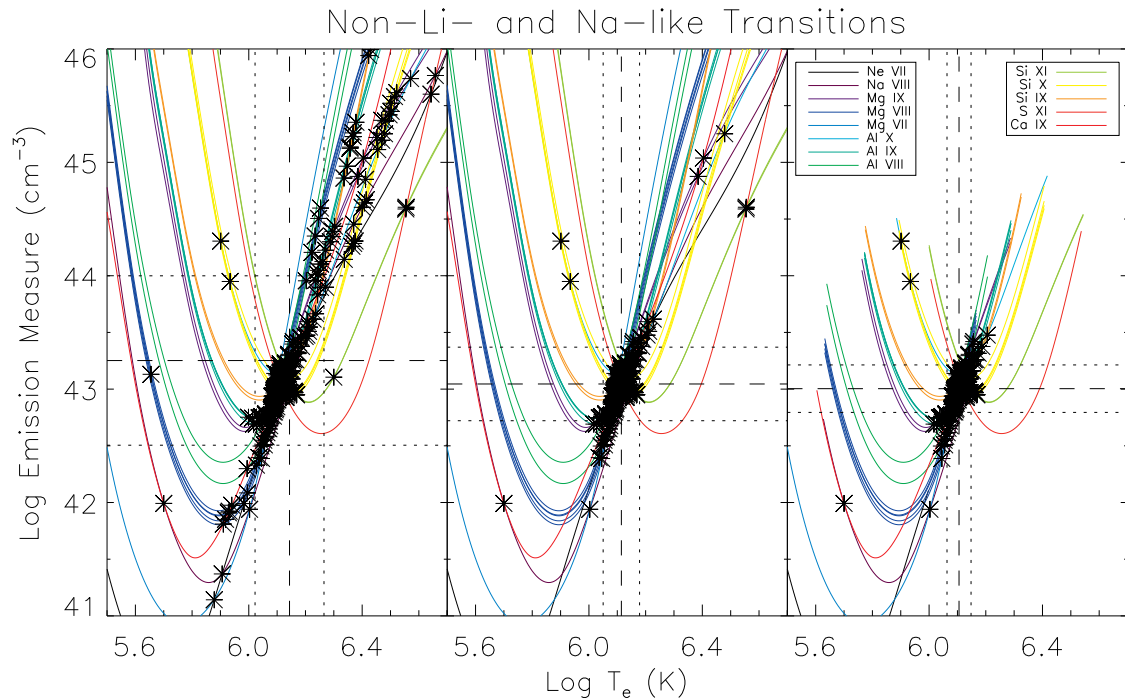


Fig. 71.— Same as Fig. 65 but for Group IIb.

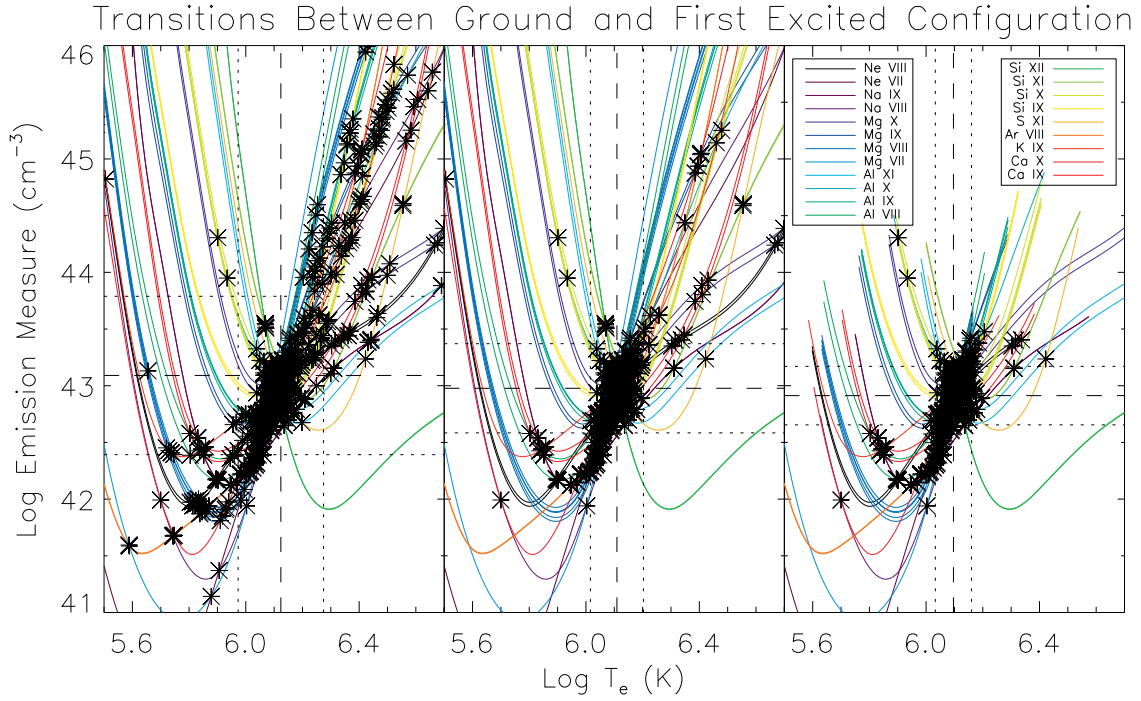


Fig. 72.— Same as Fig. 65 but for Group II as a whole, excluding emission lines from N V and O VI.

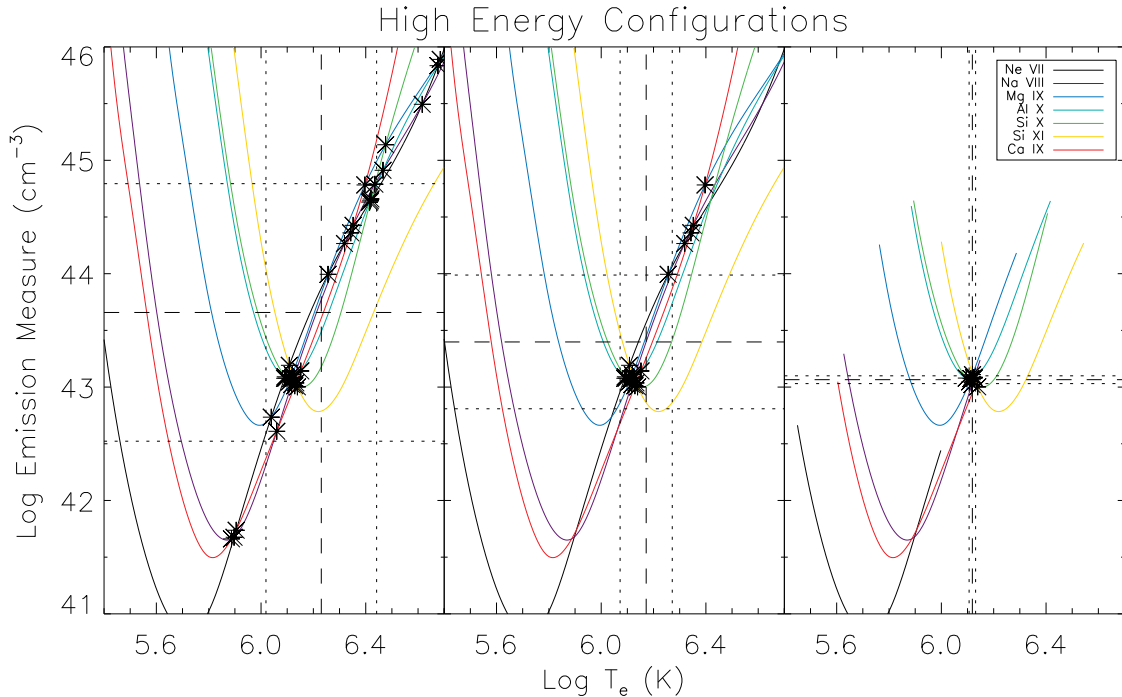


Fig. 73.— Same as Fig. 65 but for Group III.

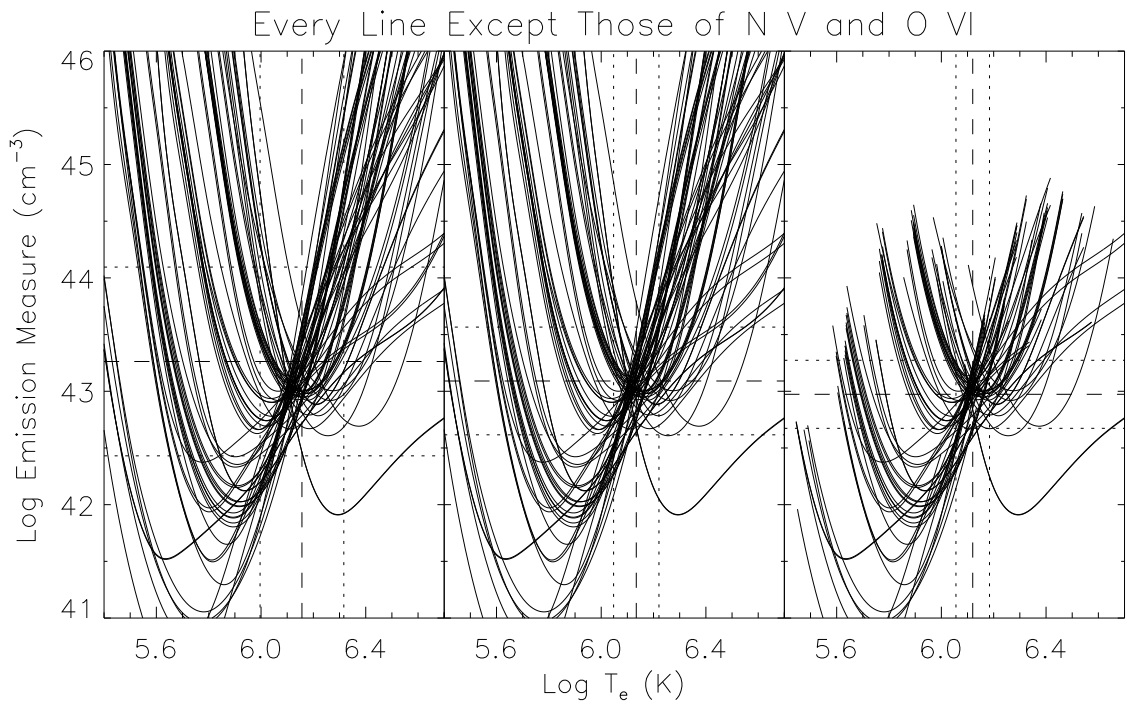


Fig. 74.— Same as Fig. 65 but for all emission lines in the observation except those from N V and O vi. Due to the large number of crossings we exclude the asterisks for clarity.

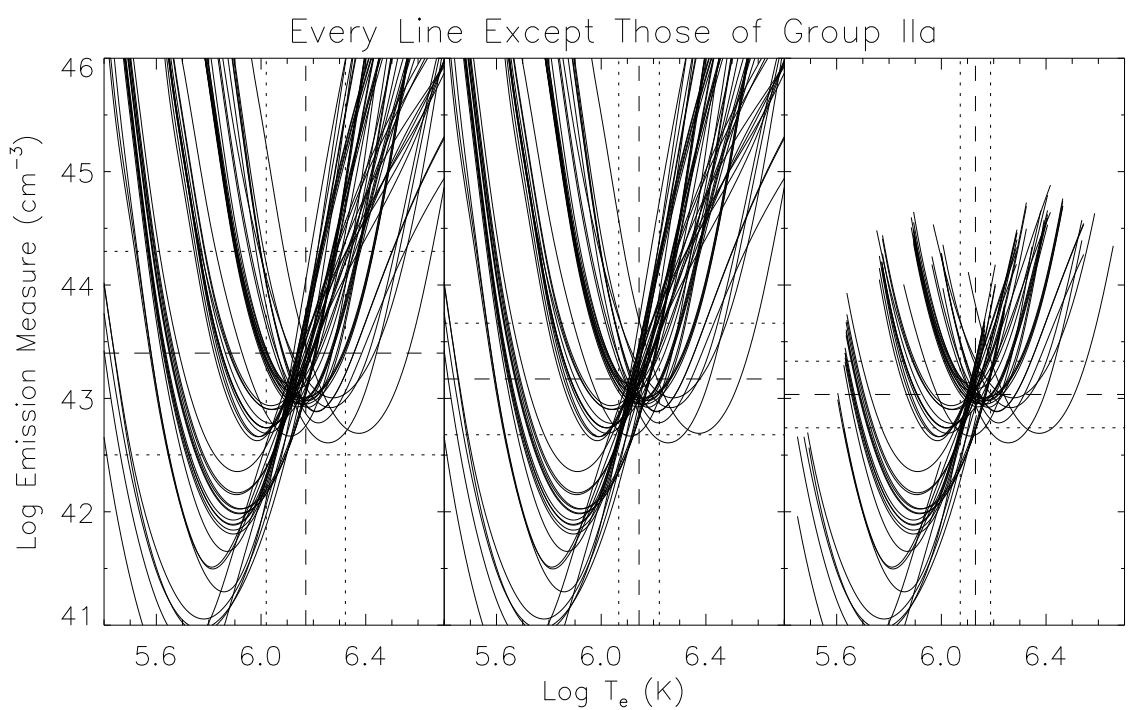


Fig. 75.— Same as Fig. 74 but excluding emission lines from all Li- and Na-like ions.

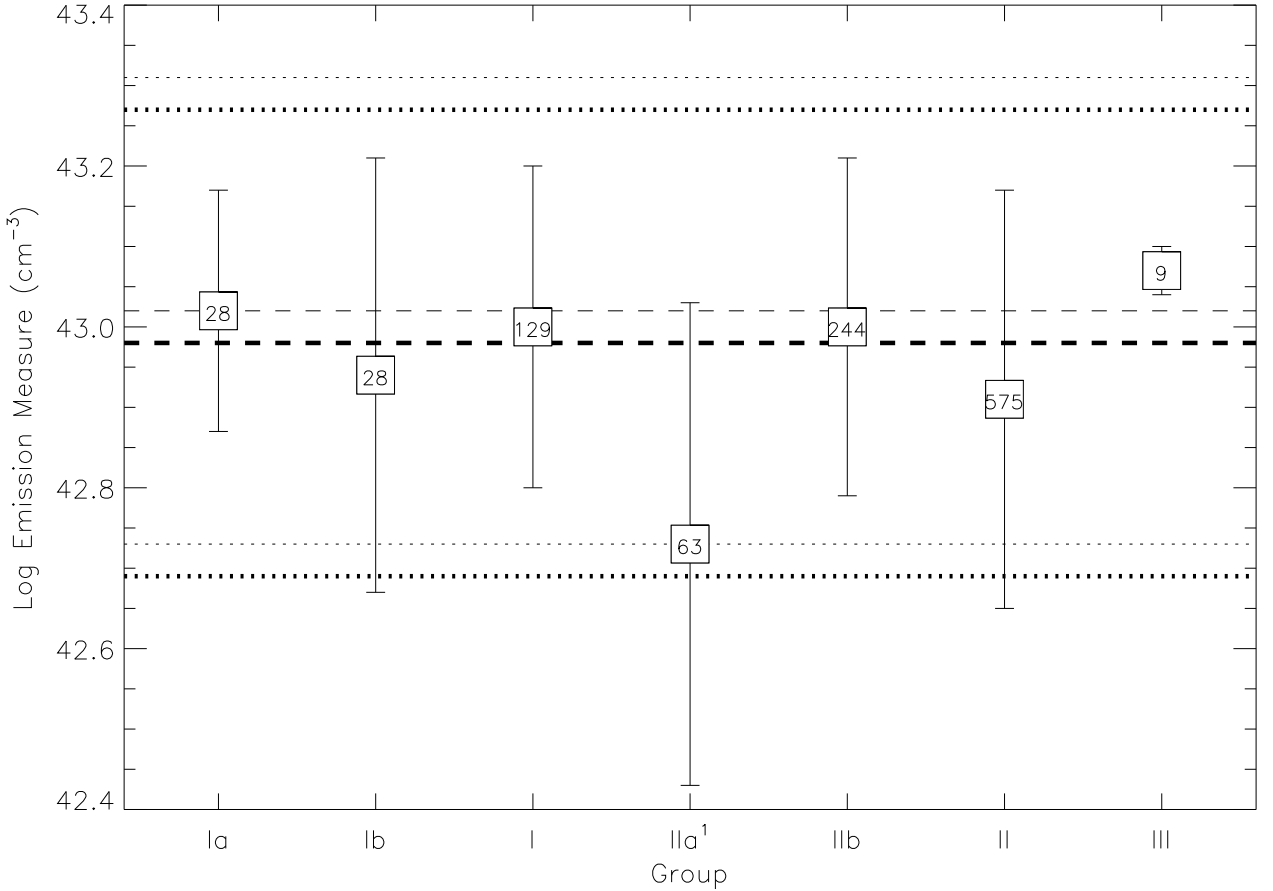


Fig. 76.— Mean $\log_{10} EM$ values for each of the groups using the GEM method (as listed in Table 33). The numbers in the data points represent the number of EM curve crossings that were used to derive the mean EM . The error bars on the points are $\pm\delta\langle\log_{10} EM\rangle$. Group IIa¹ excludes the O VI and N V lines. The dashed and dotted lines indicate the mean and standard deviation, respectively, when every emission line, except N V and O VI, is considered. The thick lines include emission lines from Li- and Na-like ions (Fig. 74) and the thin lines exclude emission lines from these ions (Fig. 75).

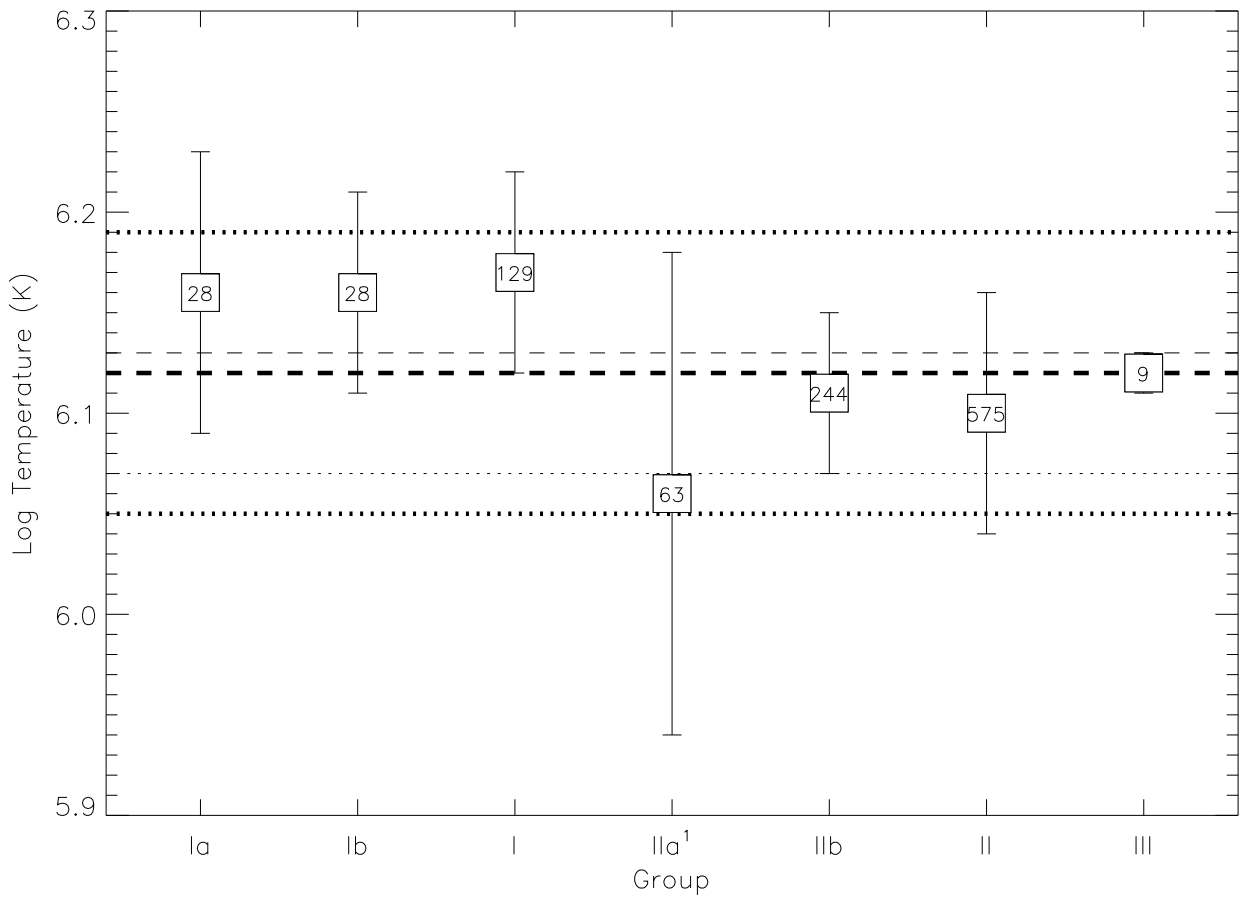


Fig. 77.— Same as Fig. 76 but for $\log_{10} T_e$. The upper values of the standard deviation for the thick and thin lines lie on top of one another.

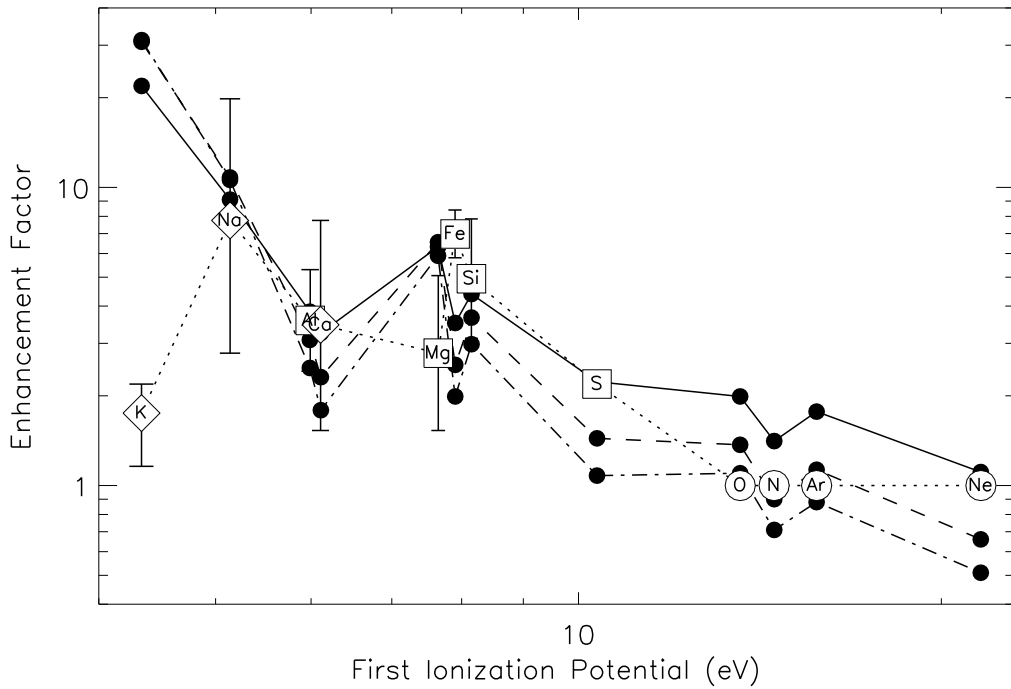


Fig. 78.— Coronal abundance enhancement factor (i.e., FIP factor) used for each of the elements versus their first ionization potential. Open symbols represent the present results; refer to Fig. 64 for details. The solid circles are the results of the model of Laming (2008) for upward Alfvén wave energy fluxes of 2, 8, and 32 (*solid, dashed, and dot-dashed lines*, respectively) in units of $10^6 \text{ ergs cm}^{-2} \text{ s}^{-1}$. Lines have been drawn between points only to guide the eye.